NF-1583.01

A DESCRIPTION AND VALIDATION OF STEADY-STATE ANALYSIS METHODS FOR BOILING WATER REACTORS

TOPICAL REPORT

FEBRUARY 1983

CP&L

Carolina Power & Light Company

NF-1583.01

A DESCRIPTION AND VALIDATION OF STEADY-STATE ANALYSIS METHODS FOR BOILING WATER REACTORS

K. E. Karcher

W. K. Cantrell

D. W. Schroeder

February 1983

APPROVED: B J Gitnick 2/16/83

B. J. Gitnick

Principal Engineer - In-Core Analysis

CAROLINA POWER & LIGHT COMPANY

411 FAYETTEVILLE STREET

RALEIGH, NORTH CAROLINA 27602

DISCLAIMER OF RESPONSIBILITY

This document was prepared by Carolina Power & Light Company and is believed to be completely true and accurate to the best of our knowledge and information. It is authorized for use specifically by Carolina Power & Light Company for the appropriate subdivisions within the U.S. Nuclear Regulatory Commission only.

With regard to any unauthorized use whatsoever, Carolina Power & Light Company and their officers, directors, agents, and employees assume no liability nor make any warranty or representation with regard to the contents of this document or its accuracy or completeness.

ACKNOWLEDGEMENTS

The authors gratefully acknowledge S. J. Ganthner, D. R. Hoskins, F. C. Jackson, and U. Shankar for their assistance in preparing this report.

The efforts of Scandpower A/S and the European FMS users group have been greatly appreciated. These organizations were instrumental in providing data for and preparation of the technical descriptions which are companions to this report.

Special appreciation is extended to R. E. Helme, who was Principal Engineer of In-Core Analysis for the majority of time during which the CP&L steady-state BWR methods were being developed. Without his help and encouragement, this work would not have been possible.

ABSTRACT

An overview of the system of codes used by Carolina Power & Light Company for nuclear design and analysis of boiling water reactors is provided. Emphasis is placed on demonstrating the use of the lattice physics code, RECORD, and the nodal simulator code, PRESTO-B. Extensive qualification of the overall analysis system is presented.

Table of Contents

List of Tables

List of Figures

1.0 Introduction

The purpose of this report is to demonstrate the capability of Carolina Power & Light Company (CP&L) to perform independent BWR simulations and to provide the statistical basis for prediction of uncertainties. This report is the controlling document that provides a description of how state-of-the-art neutronic and hydraulic computer codes are integrated into a systematic method of steady-state BWR analysis.

CP&L has employed portions of the Scandpower Fuel Management System (FMS) and portions of the Electric Power Research Institute (EPRI) code system for nuclear design and analysis of Boiling Water Reactor (BWR) cores. These methods are intended to form the bases for reload fuel evaluations and operation support of the Brunswick BWR-4 Units 1 and 2.

A flow diagram of the computer codes intended for steady-state BWR analysis application by CP&L is shown on Figure 1.0.1.

Detailed descriptions of each of the codes used by CP&L are provided in separate topical reports. A technical description of the lattice physics code, RECORD, is provided in the companion report, "Methods of Record, An LWR Fuel Assembly Code" (Reference 1). A technical description of the BWR nodal simulator code, PRESTO-B, is provided in the companion report, "Methods of PRESTO-B, A Three-Dimensional, LWR Core Simulator Code" (Reference 2). A description of the thermal-hydraulic code, FIBWR, is given in EPRI Report NP-1923 (Reference 3). In addition, the companion report "Verification of the CP&L Reference BWR Thermal-Hydraulic Methods Using the FIBWR Computer Code"

(Reference 4) describes how these thermal-hydraulic methods were established by CP&L. The auxiliary codes, THERMOS, GADPOL, MD-2, MD-1, POLRAM, and ALBMO are briefly discussed in References 1 and 2.

This report summarizes both the CP&L steady-state BWR analytical methods and the verification of the analysis approach. Sections 2 and 4 provide an overview of the methods used for lattice physics and nodal simulations, respectively. Sections 3 and 5 provide a detailed description of the verification and qualification studies performed by CP&L against higher order calculations and plant measurements from Quad-Cities Unit 1 and the Brunswick units. Section 6 summarizes the modeling uncertainties to be used in licensing calculations and conclusions as to the range of applicability.

These studies, in conjunction with the benchmarking presented by Scandpower (References 1 and 2) for other reactors, criticals, and higher order simulations provide justification for the use of CP&L steady-state BWR analysis methods for those applications listed in Table 1.0.1.

TABLE 1.0.1

APPLICATION OF CP&L

STEADY-STATE BWR ANALYSIS

I. Integral Core Simulations for Nominal and Transient Conditions

A. Development of control rod patterns.

B. Coastdown studies.

C. Xenon transient evaluations.

D. Feedwater heater derates.

E. Loss of feedwater heater transient analysis.

F. Reduced core flow analysis.

G. Increased core flow analysis.

H. Load-line analysis.

I. Rod-block monitor response.

J. Rod withdrawal error analysis.

K. APRM/LPRM projections.

L. TIP projections.

M. TIP asymmetry evaluations.

N. Analysis of misloaded bundles.

O. Bypass boiling studies.

P. On-line process monitoring

II. Fuel Management Calculations

A. Development of refueling patterns and long-term fuel cycle schedules.

B. Selection of number and enrichment of feed bundles.

C. Calculation of cycle length, exposure and isotopics.

D. Calculation of Haling EOC target power and exposure distributions.

E. Calculation of control rod absorber depletion.

F. Evaluation of fuel bundle reinsertion.

III. Calculation of Reactivities and Rod-Worths for Nominal and Transient Operations

A. Hot excess reactivity.

B. Control rod anomaly curves.

C. Evaluation of estimated critical position.

D. Integral and differential rod-worths.

E. Shutdown margin with missing control rods and/or assemblies.

F. Worth of most reactive rod.

G. Worth of standby liquid control system.

H. Benchmarking of less-sophisticated codes.

IV. Data Base for Generation of Core Effective Reactor Physics Data

A. Process computer inputs including cross-sections, reaction rates, detector responses, and isotopics.

B. Base flux and cross-section distribution for use in development of 1-D cross-sections and kinetics parameters for use with RETRAN.

C. Generation of point reactivity coefficients for hot and cold conditions.

D. Generation of core effective delayed neutron parameters.

V. Evaluation of Thermal Limits from Normal and Transient Operations

A. Power, flow, and local pin-power distributions for use in generation of critical power ratio (CPR) and sub-channel analysis.

B. Maximum fraction of limiting power density (MFLPD).

C. Maximum average planer linear heat generation rate (MAPLHGR).

D. Projection of pellet cladding interaction (PCI) ramp rate limits.

FIGURE 1.0.1

MAJOR PROGRAM MODULES
USED FOR
CP&L STEADY STATE BWR ANALYSIS

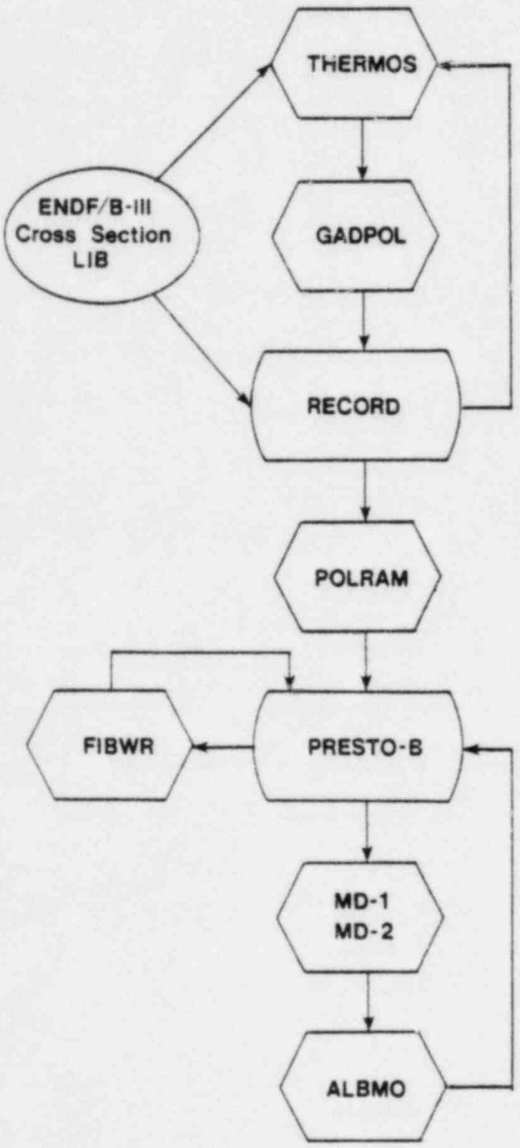

THERMOS: Transport theory code for burnable absorber cross-section generation.

GADPOL: Interface code which provides reaction rate matching between transport and diffusion theory.

RECORD: Two-dimensional multi-group code for generation of LWR lattice physics constants.

POLRAM: Interface code for generation of polynominal cross-section fits of record data for use by PRESTO-B

PRESTO-B: Three-dimensional coupled neutronic and hydraulic BWR nodal simulation code.

FIBWR: BWR Thermal-hydraulic code for generation of reference pressure and flow distributions.

MD-2: Two-dimensional multi-group fine mesh diffusion theory code for evaluation of reference flux distributions.

MD-1: One-dimensional analog of MD-2.

ALBMO: A program module within PRESTO-B for generation of core leakage parameters.

2.0 Description of RECORD

The lattice physics code RECORD determines the fast and thermal spectra, the flux distributions, and isotopic burnup in two dimensions across an LWR fuel assembly. For a given assembly, the code produces two-group diffusion parameters which incorporate effects of heterogenieties in LWR fuel designs. Variable fuel pin enrichments and dimensions, burnable and soluble poisons, water holes, gaps, and crosses, and both cruciform and cluster control rods are explicitly treated in the calculations. The basic theoretical models and experimental verification of the methods of RECORD are presented in a separate topical report, "Methods of RECORD" (Reference 1).

RECORD input consists of assembly dimensions and materials specifications. Mesh lines and atomic densities can be specified or automatically computed by the code. In addition, results of off-line calculations with THERMOS-GADPOL are required for any pins containing burnable poison.

RECORD output includes the infinite lattice multiplication factor, pin relative fission density distributions, isotopic densities, and two-group diffusion parameters as a function of exposure for nodal simulator codes. In addition, delayed neutron parameters are obtained for use in neutron kinetics calculations. The methods used to obtain these results are reviewed in the following sections. Bracketed numbers give the sections of Reference 1 which discuss the topics in detail.

2.1 Nuclear Data Library [2.3, 4.2.3, Appendix A]

A total of 51 isotopes or materials may be specified as being present in the lattice. RECORD constructs cross-section data from number densities and the microscopic cross-section and resonance integral data included in its accompanying nuclear data libraries; these are based (whenever possible) on ENDF/B-III data. Data was obtained for some fission products from Reference 18.

Thermal (up to 1.84 eV) absorption and fission for non-1/v materials are represented at 180 energy points; non-constant scattering cross-sections are given at 60 energy points. The latter were calculated using the single level Breit-Wigner formula with resonance parameters from ENDF/B-III. RECORD uses a point energy approach, with 15 points to solve the thermal spectrum equations; these points are interpolated from points given in the libraries.

In the epithermal region (1.84 eV to 10 MeV) fission, absorption, and scattering are represented in 35 groups. These were evaluated from resonance parameters and smooth cross sections from ENDF/B-III, using single or multi-level Breit-Wigner formulation to derive point cross sections; the micro-group average cross sections were calculated assuming a 1/E spectrum. Single-pin total resonance integrals and distributions are given as a function of pin cell geometry and isotopic composition. With the exception of U-238, the temperature dependence of the resonance integrals is neglected. The single-pin resonance integral for U-238 is calculated from an empirical expression normalized to Hellstrand's formula. The normalization contains a reduction of about 3 percent in the resonance integral, and is based on comparisons of calculated and measured reactivity.

2.2 Spectrum Calculations [3.1 - 4.4]

RECORD calculates the neutron spectra in the thermal region for the average homogenized pin cell in a number of assembly subregions. Using a modified Amouyal-Benoist method based on integral transport theory, the code calculates energy-dependent disadvantage factors, i.e., ratios of fluxes in fuel, clad, and moderator to flux in the homogenized pin cell. These factors are combined with two scattering models, Brown-St. John for oxygen, and Nelkin for hydrogen, to obtain region-wise neutron spectra for each pin cell in the fuel assembly. In CP&L's usage, two thermal macrogroup cross sections for each pin cell are obtained by collapsing over the microgroup spectra. Upscattering from the lowest thermal group is retained in scattering removal cross sections.

The epithermal spectrum is based on an assembly average pin cell, because the mean-free path of epithermal neutrons is comparable to assembly dimensions. A multi-group Fourier transform technique with a B-1 approximation to the Boltzmann equation is used for the calculation. A Greuling-Goertzel slowing-down model is applied for light isotopes and Fermi age for heavy isotopes. Resonance absorption and fission reactions are based on total lattice resonance integrals obtained from the library, and mutual shielding factors computed at run time. Mutual shielding factors are functions of the Dancoff factor, which is computed by Sauer's method. A correction is applied for corner and edge pins, and for pins adjacent to water holes.

A fast advantage factor, defined as the ratio of average flux in fuel to average flux in clad and moderator, is applied in the high energy range to correct absorption, fission, and scattering rates in fuel.

Epithermal cross-sections are collapsed to three macrogroups for each pin cell.

2.3 Treatment of Burnable Poisons [5.1 - 5.3]

Burnable poisons (BP) are treated off-line by a burnup version of the transport theory code, THERMOS, and an auxiliary code, GADPOL. In THERMOS (Reference 19), the BP cell is represented in cylindrical geometry with pin, clad, and moderator; it is surrounded by a homogenized source region representing the eight neighboring cells and an outer scattering ring of water. The thickness of this scattering ring is adjusted so that the BP cell sees approximately the same thermal spectrum it will see in RECORD. Spatially dependent spectra are determined by the transport calculation and used to collapse two thermal macro-group cross-sections for the BP and fissionable isotopes. For each reference void, the BP pin is depleted in steps of flux-time, with the spectra calculations repeated at each step. Restarts for off-nominal conditions are routinely made. Reaction rates from the THERMOS depletion are input to GADPOL, which performs a two thermal group diffusion calculation of the THERMOS problem in 2-D RECORD mesh. Conversion of transport to diffusion parameters is by a prescription which forces agreement in reaction rates:

$$\left[\frac{\phi_p^x}{\phi_h} \quad \frac{\Sigma_p^x}{\Sigma_h}\right]_{\text{Diffusion}} = \left[\frac{\phi_p}{\phi_h} \quad \frac{\Sigma_p}{\Sigma_h}\right]_{\text{THERMOS}} \qquad \text{Eq. 2.3.1}$$

where p refers to BP cell.

h refers to homogenized region.

x refers to converted parameter and resultant flux that produces equivalent reaction rates.

The THERMOS-GADPOL treatment provides to RECORD the following quantities: thermal microscopic fission and absorption cross-sections for U and Pu isotopes, thermal macroscopic absorption cross-sections for the poison, removal cross sections and diffusion coefficients for the BP cell. These are used in RECORD until absorption in the poison reaches a constant, residual level. Thereafter, RECORD-generated cross-sections are used; however, the residual absorption of the poison as determined by THERMOS is retained.

2.4 Control Rods [6.1 - 6.2]

Control rods are treated in RECORD as non-diffusion sub-regions defined by albedo boundary conditions which are functions of current-to-flux-ratios normalized to transport corrected ratios for a black slab. Effective boundary conditions are obtained for each microgroup and subsequently collapsed into the five-group RECORD structure. Empirical and semi-empirical corrections to slab transmission and reflection coefficients are made for rod cluster control elements and blades composed of equally spaced cylindrical rods.

2.5 Two-dimensional Flux and Power Calculations [7.1 - 7.4]

Having obtained few group diffusion parameters for all elements in the assembly, the flux distribution and eigenvalue of the system are determined from two-dimensional, five-group diffusion theory, which is approximated by a set of five-point difference equations at the mesh points. The diffusion calculation is the same as in MD-2. The five-group flux solution is used to collapse assembly macroscopic cross sections to two groups. The solution is also used to generate fission density distribution, local peaking factor, and neutron detector response. The local peaking factor (LPF) calculation at present assumes all fission energy is deposited at its origin, neglecting gamma smearing effects. Detector response is computed as the ratio of (dilute) U-235 reaction rate at the detector location to assembly power density.

2.6 Burnup Calculations [8.1 - 8.3]

RECORD assumes that flux and cross sections are constant during a burnup step and that isotope chains can be resolved into single paths with no branching. Within each macro-burnup step, the burnup equations (Bateman solution) are first solved for each fuel pin. The five-group fluxes from the diffusion calculation and microscopic cross sections from the spectra calculation are used. The step is iterated to ensure the pin burnups are collectively within one-half MWD/MTU of the specified assembly average. The isotopics file created during burnup steps may be used for restart cases at off-nominal conditions.

Two options are provided for following fission products. The first follows only xenon and samarium explicitly, with the rest represented by a number of pseudo elements. The second option, used by CP&L, has explicit treatment of eleven fission products and four pseudo elements.

3.0 Verification of Lattice Physics Calculations

Reference 1, Section 10, gives the results of 55 cold, clean criticals modeled with RECORD cross sections. A wide range of uranium and plutonium lattices measured at different laboratories were included. The overall agreement between RECORD and experiment was within the uncertainty in modeling leakage. Some bias was noted between calculated reactivities of plutonium and uranium lattices.

RECORD calculated uranium and plutonium isotopics have been compared to measurements made during the Yankee-Rowe Core Evaluation Program and reported in the above reference. The comparisons were generally quite good, with noted trends of Pu-239 to be overestimated and Pu-240 to be underestimated at higher burnups.

Finally, the above referenced report shows the local fission density distributions determined by RECORD compared with experimental data from the 1976 Quad Cities 1 gamma-scan measurements. Results for the three uranium assemblies pin-wise gamma-scanned showed agreement that was comparable to the measurement uncertainty. Similar results were obtained for comparisons with Dodewaard and Muhleberg.

To augment the results reported above, CP&L has performed calculations to compare burnup-dependent reactivity of RECORD with CPM (Reference 5). Isotopics comparisons have been made with measurements for both a PWR, CP&L's own H. B. Robinson Unit 2, and a BWR assembly from Quad-Cities Unit 1. Finally, CP&L has repeated the comparisons of RECORD pin powers with the 1976

Quad Cities 1 gamma scan measurements, adding comparisons with the center mixed oxide assembly. Void history and local exposure were obtained from PRESTO simulations using RECORD cross sections. Results of comparisons performed by CP&L are given in the following sections.

3.1 Assembly Reactivity Comparisons with CPM

The quality of BWR nodal simulator reactivity predictions is directly dependent on the few group nodal equivalent cross sections generated by lattice physics codes such as RECORD. No convenient method exists to compare nodal equivalent cross sections against measured data. Quantitative benchmarking of these parameters must therefore be inferred from the results of integral simulations, which will be presented in Section 5.0. The following section presents qualitative comparisons of the lattice K infinity, a good figure of merit to represent the few group cross sections and the flux spectrum upon which they were generated. These comparisons were made with CPM (Reference 5), an established code for lattice physics calculations. CPM was chosen for this study as it uses an alternate methodology (Collision Probability Method) and cross section library. The comparisons shown in Figures 3.1.1 through 3.1.9 show reactivity trends at 0-, 40-, and 70-percent voids for three gadolinia loadings (1 pin at 2.5 w/o, 3 pins at 4.0 w/o, and 4 pins at 4.0 w/o) in otherwise identical assemblies. These comparisons are generally very close for low exposure and low gadolinia loading. However, it is apparent in the higher loadings that RECORD burns the poison faster,

causing some divergence in reactivity. Also, at higher exposures, RECORD shows a reactivity loss compared to CPM in the low void, low gadolinia cases; the high exposure comparisons, however, converge in the high void, high gadolinia cases.

Overall, RECORD results are comparable to CPM's. A closer assessment of reactivity accuracy depends on comparison with measurements; i.e., using RECORD cross sections in reactor simulator codes. Results obtained by CP&L using PRESTO are presented in Sections 5.3 and 5.4 of this report.

It should be stressed that reactivity accuracy in reactor analyses does not preclude eigenvalue bias; the accuracy requirements are that the bias be steady (i.e., have small standard deviation) over the expected range of reactor conditions, and that calculated changes in reactivity (e.g., control rod worth) be well correlated with measured values.

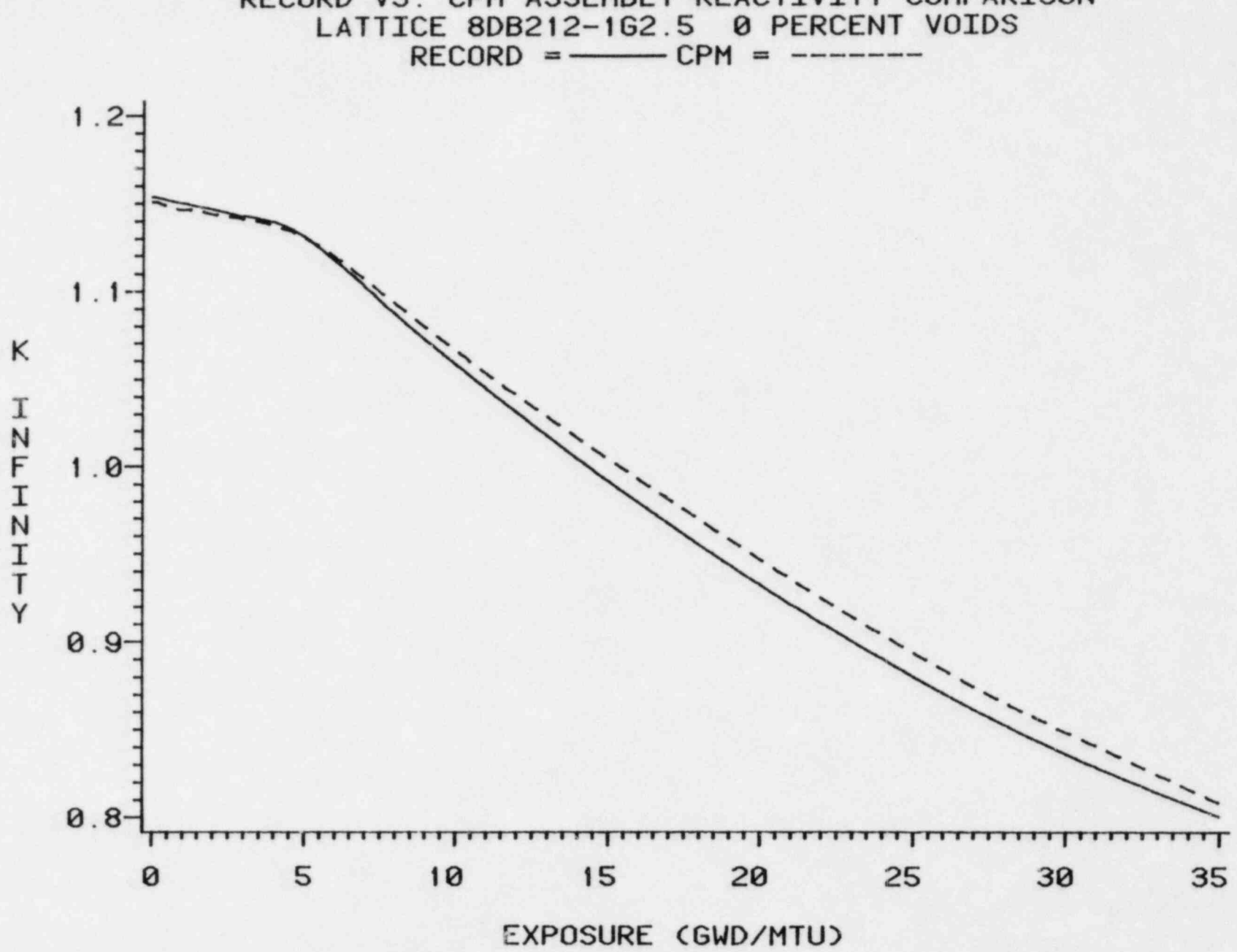
RECORD VS. CPM ASSEMBLY REACTIVITY COMPARISON
LATTICE 8DB212-1G2.5 0 PERCENT VOIDS
RECORD = ——— CPM = -------
K INFINITY
1.2
1.1
1.0
0.9
0.8
0
5
10
15
20
25
30
35
EXPOSURE (GWD/MTU)

FIGURE 3.1.1

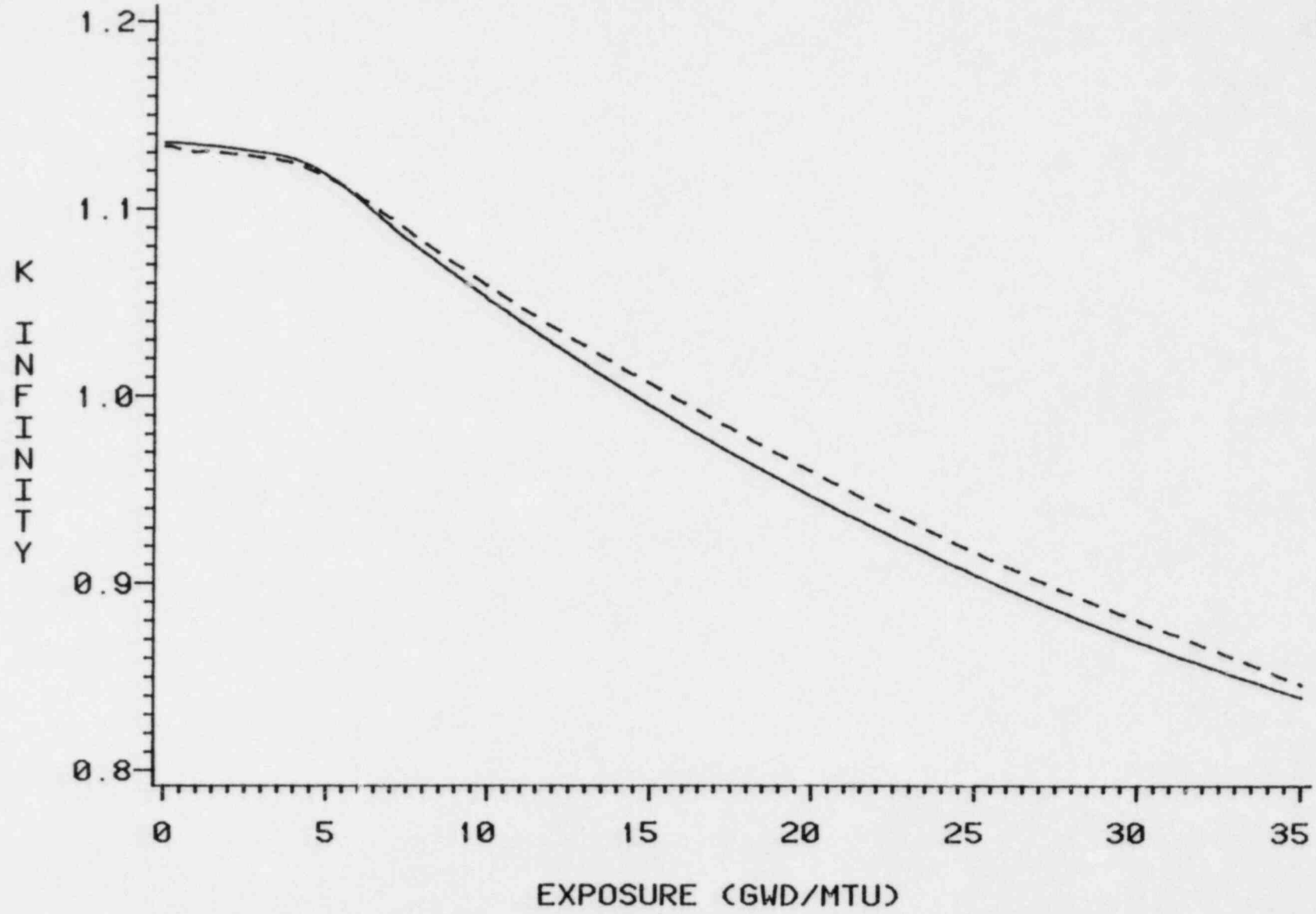
RECORD VS. CPM ASSEMBLY REACTIVITY COMPARISON
LATTICE 8DB212-1G2.5 40 PERCENT VOIDS
RECORD = ——— CPM = -------
K INFINITY
1.2
1.1
1.0
0.9
0.8
0
5
10
15
20
25
30
35
EXPOSURE (GWD/MTU)

FIGURE 3.1.2

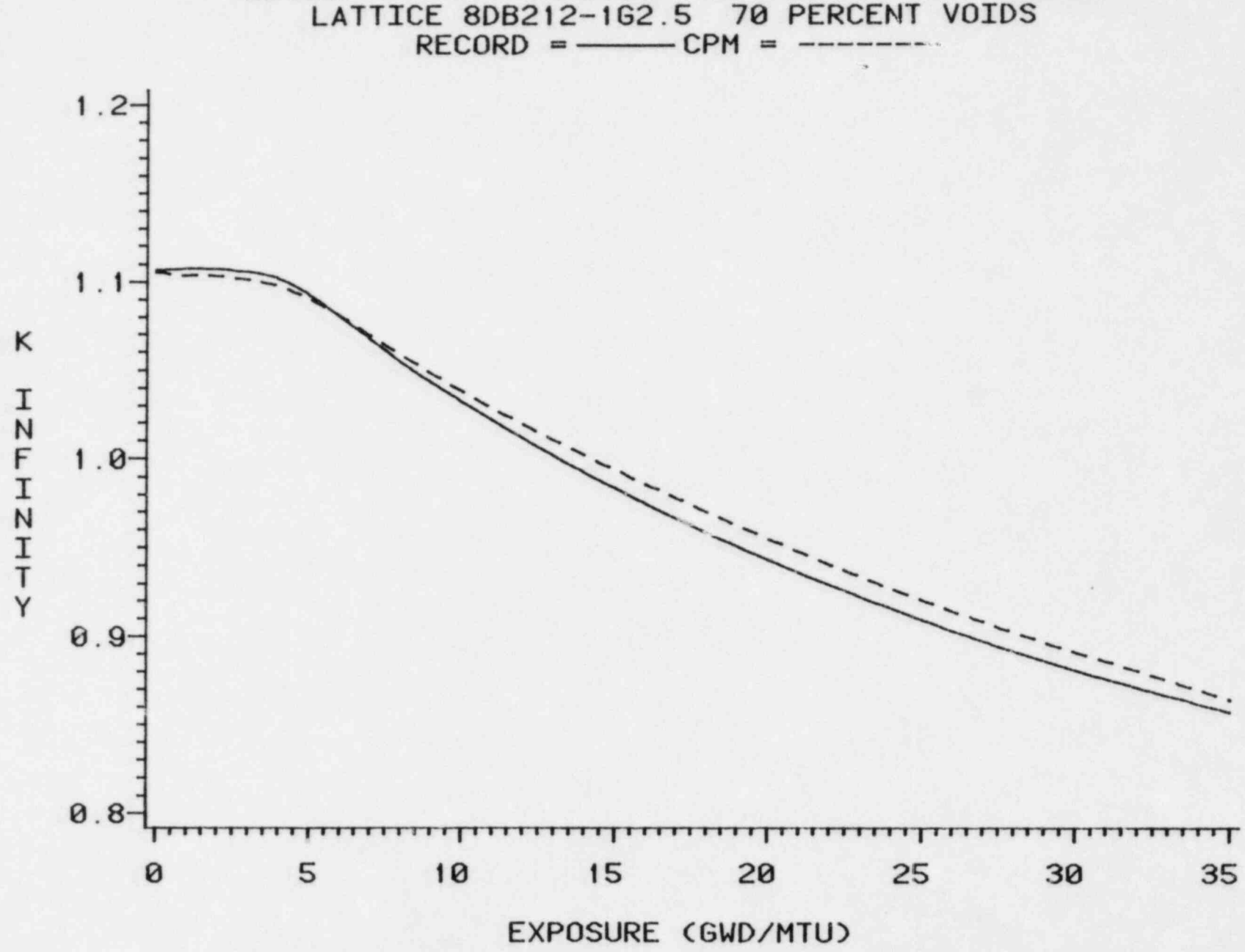
RECORD VS. CPM ASSEMBLY REACTIVITY COMPARISON
LATTICE 8DB212-1G2.5 70 PERCENT VOIDS
RECORD = ——— CPM = - - - - - - -
K INFINITY
1.2
1.1
1.0
0.9
0.8
0
5
10
15
20
25
30
35
EXPOSURE (GWD/MTU)

FIGURE 3.1.3

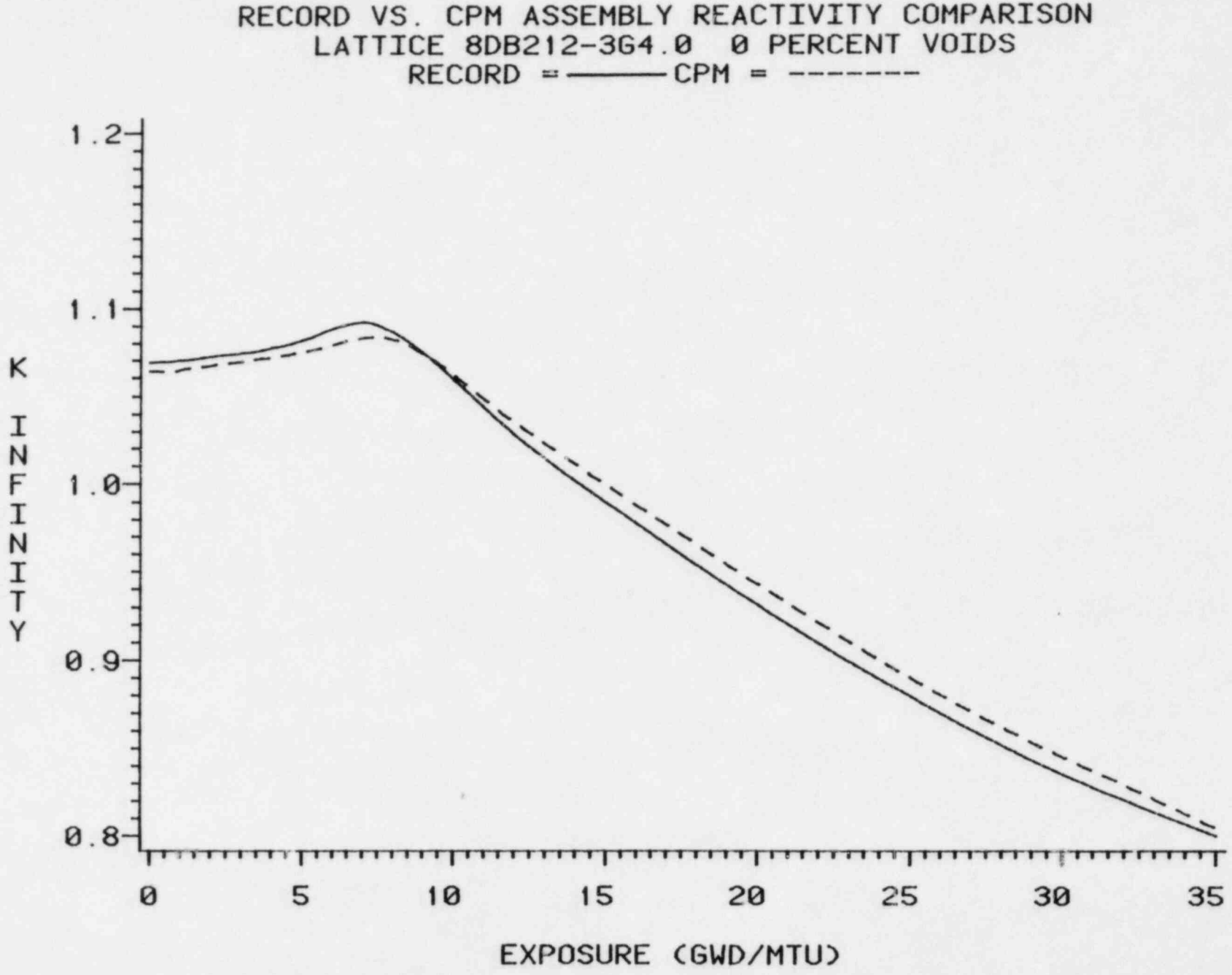
RECORD VS. CPM ASSEMBLY REACTIVITY COMPARISON
LATTICE 8DB212-3G4.0 0 PERCENT VOIDS
RECORD = ——— CPM = -------
K INFINITY
1.2
1.1
1.0
0.9
0.8
0
5
10
15
20
25
30
35
EXPOSURE (GWD/MTU)

FIGURE 3.1.4

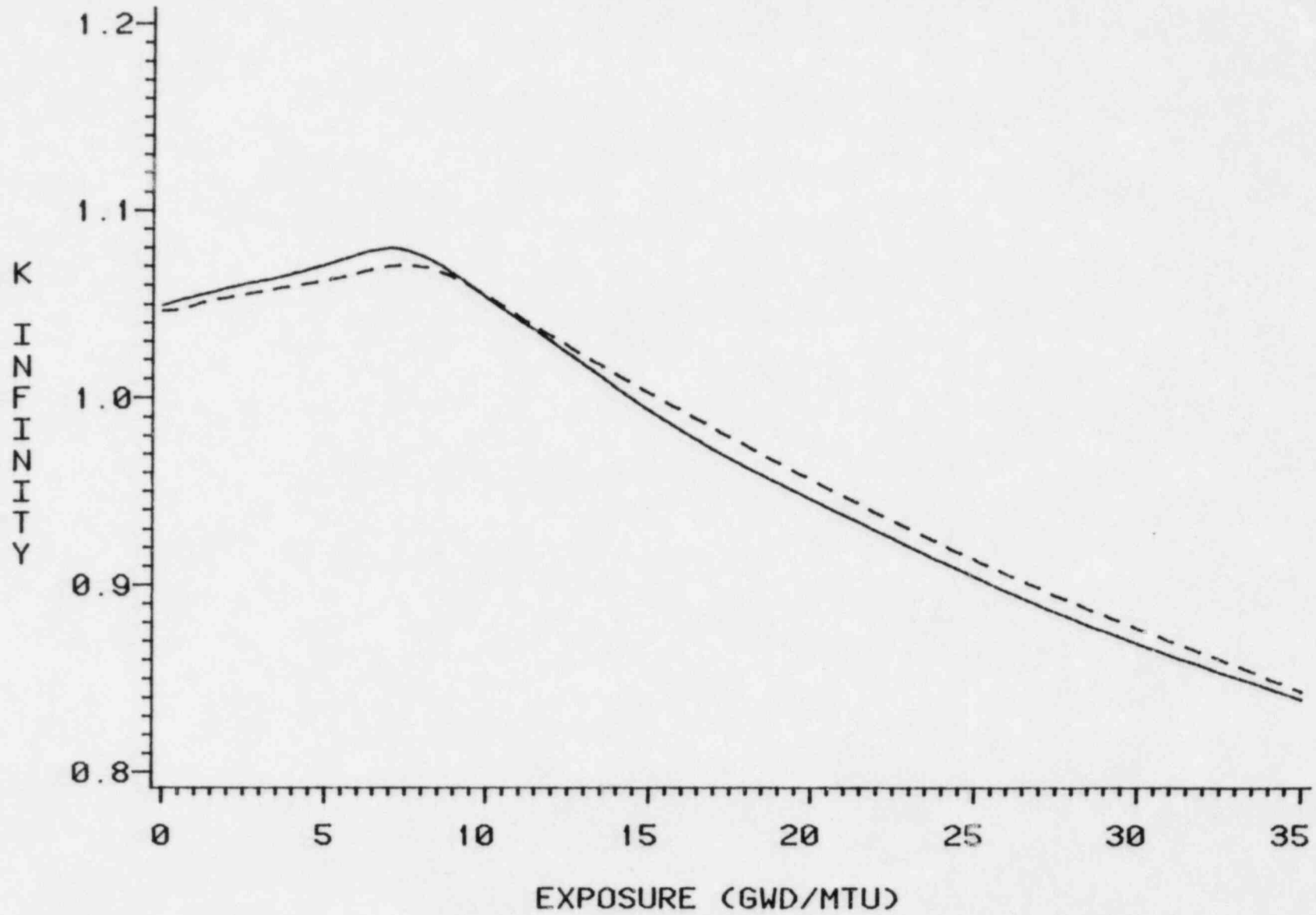
RECORD VS. CPM ASSEMBLY REACTIVITY COMPARISON
LATTICE 8DB212-3G4.0 40 PERCENT VOIDS
RECORD = ——— CPM = -------
K INFINITY
1.2
1.1
1.0
0.9
0.8
0
5
10
15
20
25
30
35
EXPOSURE (GWD/MTU)

FIGURE 3.1.5

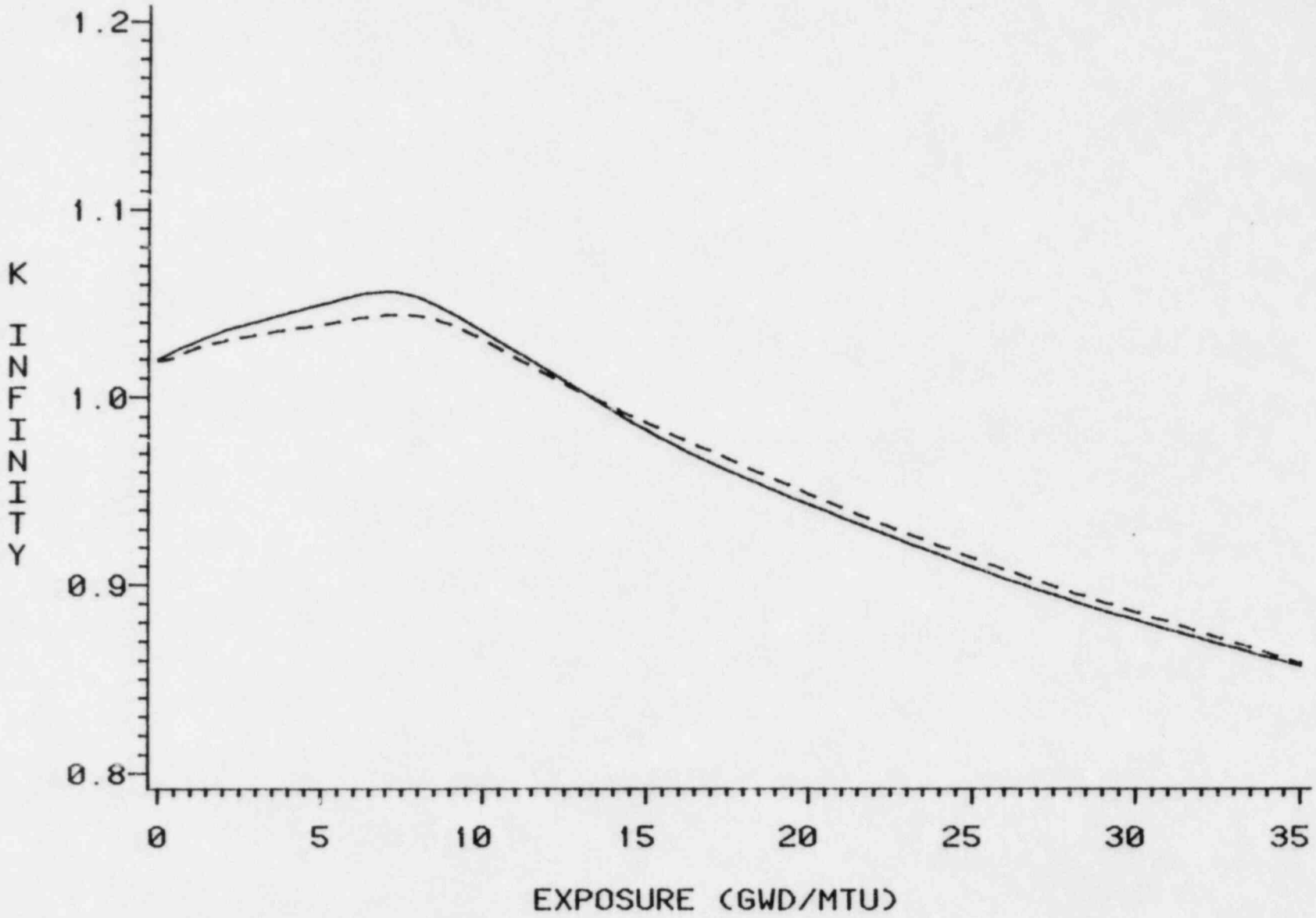
RECORD VS. CPM ASSEMBLY REACTIVITY COMPARISON
LATTICE 8DB212-3G4.0 70 PERCENT VOIDS
RECORD = ——— CPM = -------
K INFINITY
1.2
1.1
1.0
0.9
0.8
0
5
10
15
20
25
30
35
EXPOSURE (GWD/MTU)

FIGURE 3.1.8

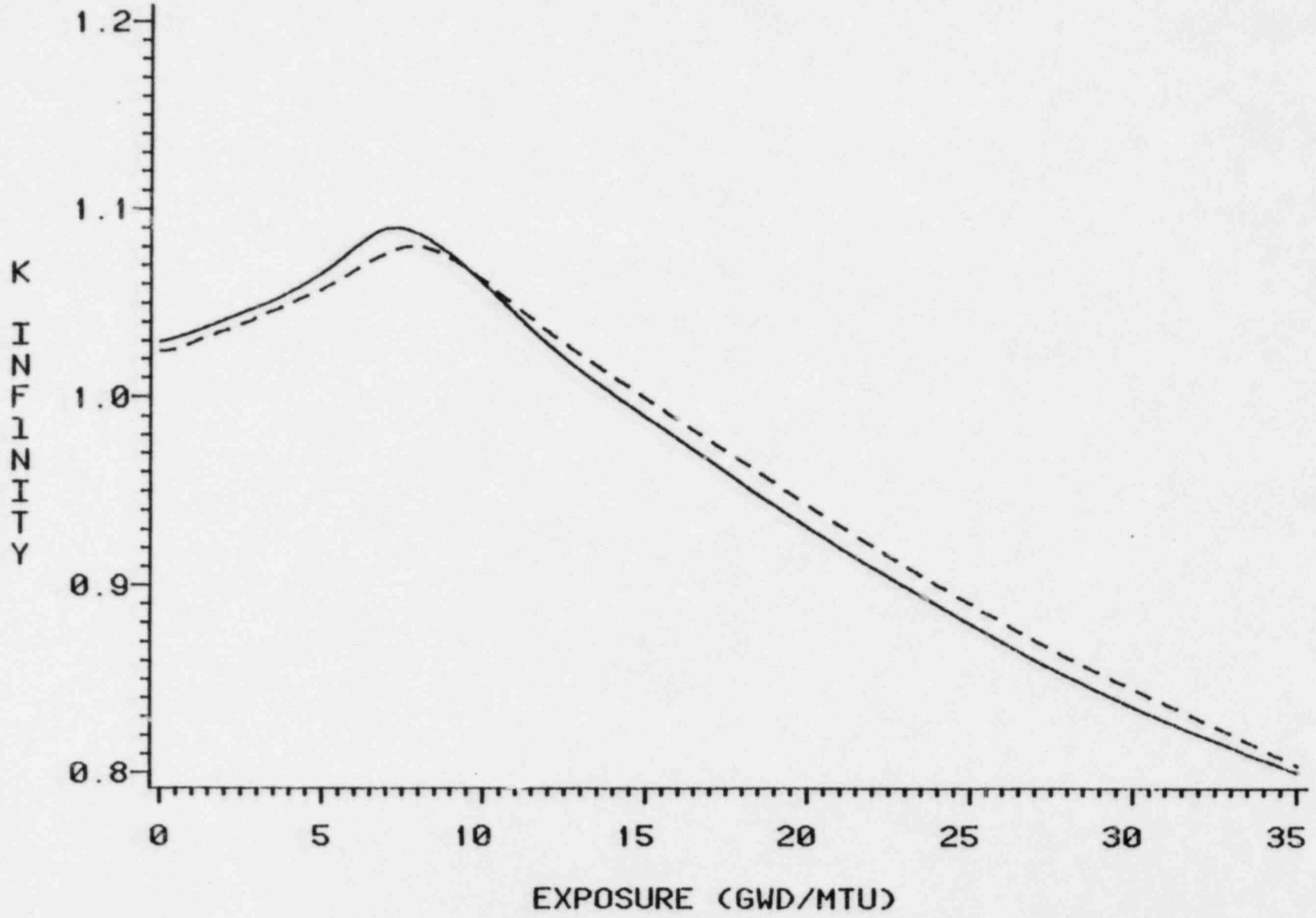
RECORD VS. CPM ASSEMBLY REACTIVITY COMPARISON
LATTICE 8DB212-4G4.0 0 PERCENT VOIDS
RECORD = ——— CPM = - - - - - - -
K INFINITY
1.2
1.1
1.0
0.9
0.8
0
5
10
15
20
25
30
35
EXPOSURE (GWD/MTU)

FIGURE 3.1.7

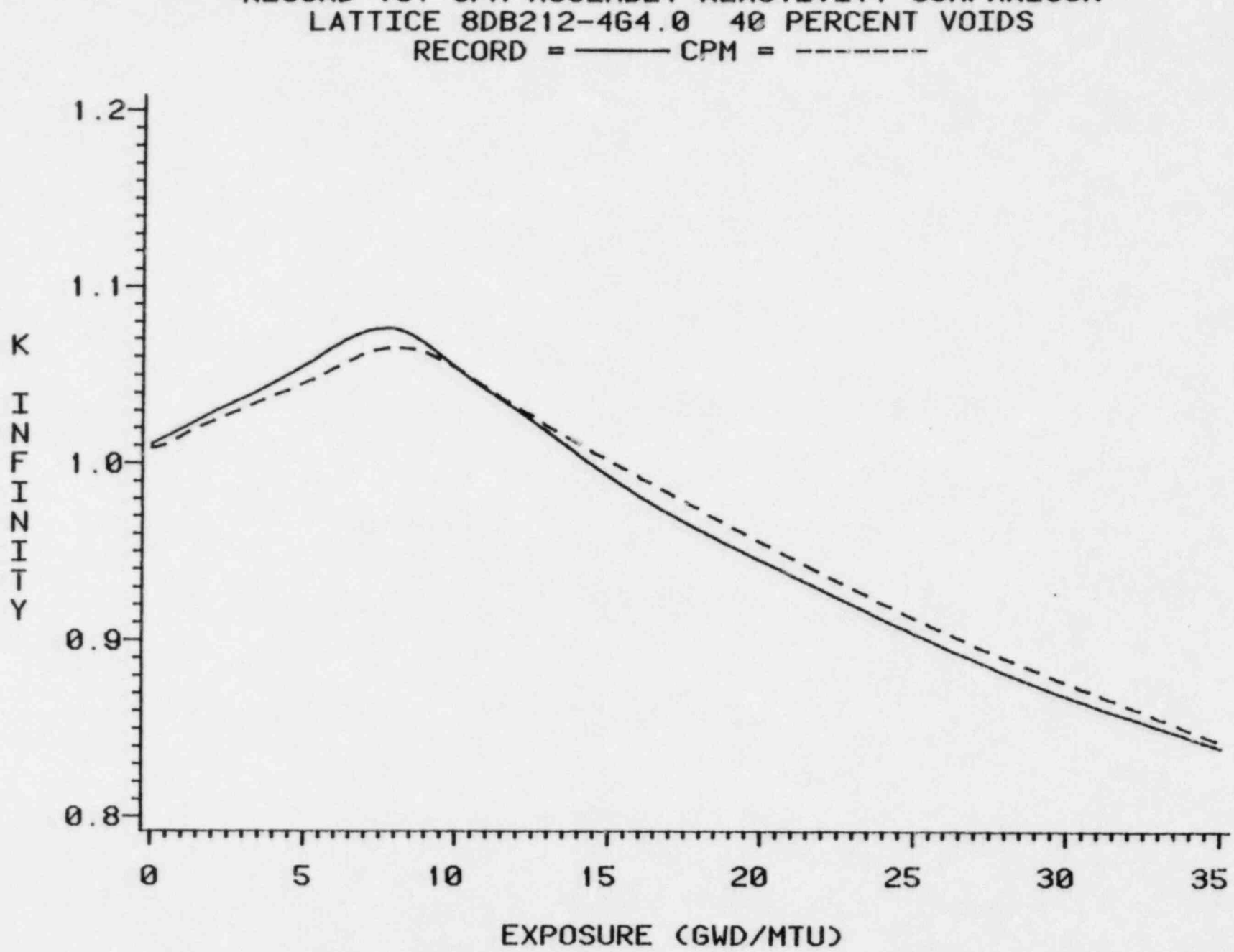
RECORD VS. CPM ASSEMBLY REACTIVITY COMPARISON
LATTICE 8DB212-4G4.0 40 PERCENT VOIDS
RECORD = ——— CPM = - - - - - -
K INFINITY
1.2
1.1
1.0
0.9
0.8
0
5
10
15
20
25
30
35
EXPOSURE (GWD/MTU)

FIGURE 3.1.8

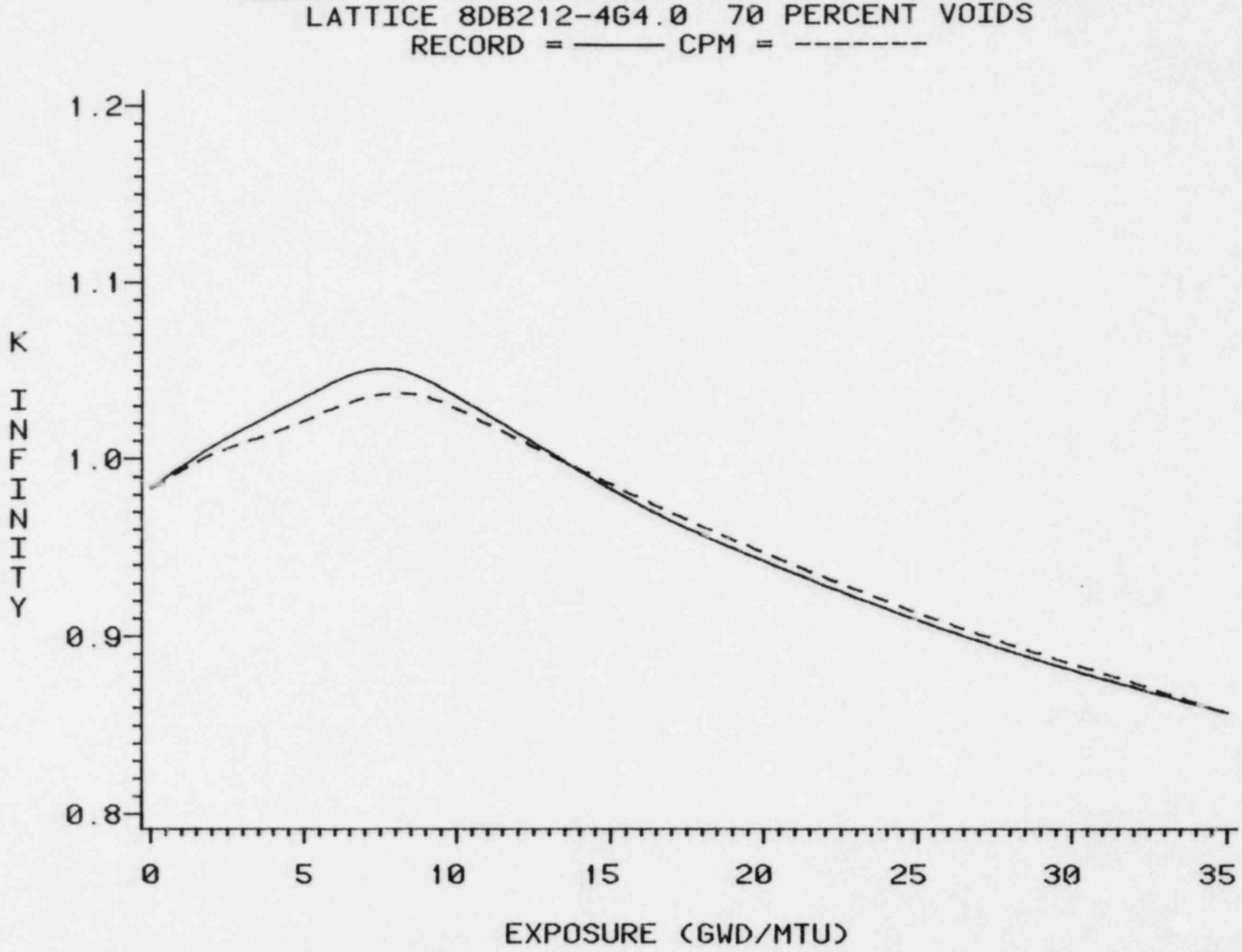
RECORD VS. CPM ASSEMBLY REACTIVITY COMPARISON
LATTICE 8DB212-4G4.0 70 PERCENT VOIDS
RECORD = ——— CPM = -------
K INFINITY
1.2
1.1
1.0
0.9
0.8
0
5
10
15
20
25
30
35
EXPOSURE (GWD/MTU)

FIGURE 3.1.9

3.2 Comparison with H. B. Robinson Isotopics

Table 3.2.1 presents the results of comparisons of isotopics, with RECORD calculations, measured by Battelle Columbus (Reference 6) for three pin samples exposed in Cycles 1 and 2 of H. B. Robinson Unit 2. A quarter-assembly was depleted in RECORD, with symmetric boundary conditions and a constant soluable boron concentration. The calculation was restarted at the EOC1 exposure to simulate removal of glass BP rods at that point. Pin isotopics were edited from the calculation at the burnups measured for the three samples.

The comparisons indicate some bias in RECORD calculation of the higher isotopes; but for the three samples, standard deviations of ratios of measurements to calculations were small.

Table 3.2.1

SUMMARY

COMPARISON OF MEASURED VS. RECORD CALCULATED ISOTOPICS

H. B. ROBINSON UNIT 2 REGION 2 (W 2.55%)

MEASURED/CALCULATED RATIOS

	N	AVERAGE	STD.DEV.
U235/U	3	1.0160	.044
U238/U	3	.9996	.000
PU39/U	3	.9941	.039
PU40/U	3	1.1326	.023
PU41/U	3	.9403	.046
PU42/U	3	.9283	.005

SAMPLE BURNUPS: 24,570 - 30,920 MWD/MTU

STD.DEV. = SQRT (SUMMATION (X(I)**2 - AVERAGE**2) / N)

3.3 Comparisons with Measured Quad-Cities Isotopics

Table 3.3.1 compares measured and RECORD-calculated isotopics for samples from a mixed oxide assembly exposed in Quad-Cities Unit 1, Cycle 2 (Reference 7). The table divides these samples according to the axial level from which they were taken. Eight pins were measured at each level, four were initially UO_2, and four were initially mixed oxide. Initial enrichments varied from 1.69 to 4.3 w/o fissile.

Pin isotopics were edited from 0-, 40-, and 70-percent void RECORD depletions of the nominal assembly design for these comparisons. Edits were interpolated to the nodal average exposure and exposure-weighted void given by PRESTO simulation of the cycle; the PRESTO values are shown on the table. The samples included exposures in the range of 7,000 to 12,000 MWD/MTU, and exposure-weighted voids (VH) from 5 to 65 percent.

Again, the results show some bias in the higher isotopes, as was seen in the PWR pin, as well as an increase in standard deviation with isotope atomic mass number. However, the results are consistent from bottom to top of fuel, indicating void history does not contribute to the bias.

The RECORD depletions modeled the nominal center bundle design. During the destructive testing, it was discovered that in the actual bundle, a 2.5 w/o Gd_2O_3 pin had been inadvertently substituted for a 3.0 w/o Gd_2O_3 pin. This pin was not included in the comparisons, but the overall consistency between results for this bundle and the H. B. Robinson pin show the small loading errors had no significant effect on neighboring pins.

Table 3.3.1

COMPARISON OF MEASURED VS. RECORD CALCULATED ISOTOPICS

QUAD CITIES UNIT 1 ASSEMBLY GEB161

MEASURED/CALCULATED RATIOS

	N	AVERAGE	STD.DEV.
22.5 in. From Bottom	11290 MWD/MTM	VH=0.10	
U235/U	8	1.0041	.016
U238/U	8	1.0000	.000
PU39/U	8	1.0120	.022
PU40/U	8	1.1533	.044
PU41/U	8	.9510	.172
PU42/U	8	.9842	.200
57.5 in. From Bottom	9204 MWD/MTM	VH=0.405	
U235/U	8	1.0001	.008
U238/U	8	1.0000	.000
PU39/U	8	1.0080	.034
PU40/U	8	1.1502	.052
PU41/U	8	.9585	.231
PU42/U	8	1.0177	.250
94.5 in. From Bottom	9248 MWD/MTM	VH=0.578	
U235/U	8	1.0041	.010
U238/U	8	1.0000	.000
PU39/U	8	1.0028	.034
PU40/U	8	1.1582	.045
PU41/U	8	.9558	.223
PU42/U	8	1.0151	.232
130.5 in. From Bottom	7086 MWD/MTM	VH=0.662	
U235/U	8	1.0160	.013
U238/U	8	.9998	.000
PU39/U	8	.9874	.030
PU40/U	8	1.1108	.036
PU41/U	8	.9081	.235
PU42/U	8	1.0015	.254

STD.DEV. = SQRT (SUMMATION (X(I)**2 - AVERAGE**2) / N)

3.4 Comparison with Quad-Cities Pin Gamma Scans

Figures 3.4.1 through 3.4.16 compare RECORD calculated pin fission rates with four of the five Quad Cities Unit 1 assemblies whose individual pins were scanned at EOC2 for relative La-140 concentration (Reference 8). Because the reactor operated at a stabilized power distribution for the last two months of the cycle, the La-140 distribution can be equated with the fission distribution at EOC. The measured values in Figures 3.4.1 through 3.4.16 are the average of two measurements taken six inches apart, and the stated axial location is half-way between the measured locations. The measured values for mixed oxide pins were corrected to account for the different La-140 yields of Pu-239 and U-235. All measurements were normalized to a planar average of one. Pins initially containing Gd_2O_3 are marked with slashes. The RECORD-calculated values are interpolated from depletions at 0-, 40-, and 70-percent voids to the nodal exposure and exposure-weighted void given by PRESTO simulation of the cycle. The RECORD depletions were done with symmetric boundary conditions, so the percent differences include differences induced by gradients in the core. In the case of the fifth assembly that was scanned, a peripheral assembly, the core gradiant was too severe to allow comparison with a symmetric depletion. The assemblies in these comparisons include 7x7, 8x8 and MO_2 designs. Nodal exposures ranged from 7500 to 19380 MWD/MTU, and exposure-weighted voids ranged from 4 percent to 65 percent. Gd_2O_3 loadings ranged from 1.5 to 3.0 weight percent per pin, and two to five pins per assembly.

Results of these comparisons are summarized in Table 3.4.1. The average standard deviation for all pins was 2.6 percent; for all Gd_2O_3 pins, 2.8 percent; and for all pins excluding the MO_2 assembly, 2.4 percent. The local peaking factors (LPF) for all assemblies were predicted by RECORD an average of 1.7 percent high with a standard deviation of 4.1 percent; for UO_2 assemblies only, RECORD was an average of 0.2 percent low with a standard deviation of 1.6 percent.

Pin power distributions are three to four percent less peaked than the fission rate distributions compared here; this is due to gamma smearing, the effect by which a net transfer of energy from high to low gamma intensity areas occurs. A model of this effect is being developed for RECORD calculations of pin powers. For the present, however, the calculated fission rate distribution is being equated to pin power distribution for calculation of peaking factors, MLHGR, etc.

Table 3.4.1

RECORD - QC1 GAMMA SCANS COMPARISONS

ASSEMBLY	TYPE	INCHES FROM BOT	PRESTO MWD/MTU	PRESTO VOID HIST	STD.DEV. %	* LOCAL PEAKING FACTOR % DIFF (M-C)
CX 214	7X7	18.0	16,310	0.04	3.3	0.5
		53.5	19,300	0.27	2.1	0.7
		90.0	18,600	0.50	2.5	3.5
		126.0	14,940	0.61	2.4	0.4
CX 672	7X7	18.0	16,000	0.04	3.9	0.6
		53.5	19,380	0.27	2.4	2.0
		90.0	18,650	0.50	2.3	-1.4
		126.0	15,510	0.61	2.5	-2.8
GEB159	7X7,MO2	18.0	11,425	0.08	4.7	-12.0
		53.5	9,219	0.38	3.1	-10.0
		90.0	9,025	0.56	2.5	-6.0
		126.0	7,500	0.65	2.7	-1.3
GEH002	8X8	18.0	11,320	0.08	1.8	-1.9
		53.5	9,550	0.38	1.9	-0.2
		90.0	9,325	0.57	2.3	1.0
		126.0	7,665	0.65	1.9	0.0
AVERAGE					2.7	-1.7±4.1
AVERAGE (GD203 PINS)					2.8	
AVERAGE (UO2 ASSEMBLIES ONLY)					2.4	0.2±1.6

* Detailed distributions given in Figures 3.4.1 thru 3.4.16

Figure 3.4.1

QUAD CITIES 1 EOC2 GAMMA SCANS

ASSEMBLY CX 214 18.0 IN. FROM BOTTOM

COMPARISON TO RECORD 16310.MWD/MTU VOID HIST.= .04

.955	1.079	*****	1.048	*****	.966	.955	MEAS.
.988	1.085	*****	1.057	*****	.964	.943	CALC.
-3.2	-.7	*****	-.9	*****	.2	1.2	DIFF.%
			///////				
1.059	.968	.942	/1.015/	.987	1.045	1.037	
1.085	1.045	1.012	/1.021/	1.032	1.049	.992	
-2.7	-7.7	-7.0	/ -.7/	-4.5	-.5	4.5	
			///////				
*****	.993	.968	.936	.986	1.075	*****	
*****	1.012	.972	.967	.993	1.056	*****	
*****	-1.9	-.5	-3.1	-.7	1.9	*****	
	///////						
1.044	/ .991/	.961	*****	.988	1.090	1.010	
1.057	/1.021/	.967	*****	.987	1.051	.969	
-1.3	/ -3.1/	-.6	*****	.1	3.9	4.1	
	///////						
*****	1.007	.984	.974	1.023	.913	*****	
*****	1.032	.993	.987	1.013	.922	*****	
*****	-2.5	-.9	-1.3	.9	-.9	*****	
.919	1.051	1.055	1.070	.925	.991	.972	
.964	1.049	1.056	1.051	.922	.963	.919	
-4.5	.1	-.1	1.9	.3	2.8	5.3	
.933	1.024	*****	1.042	*****	.984	1.041	
.944	.992	*****	.969	*****	.919	.979	
-1.1	3.2	*****	7.3	*****	6.5	6.1	

***** Tie rods (Not measured) WIDE

///// Pins initially containing Gd2O3 WIDE GAP

STANDARD DEVIATION 3.3% (40 PINS)

Figure 3.4.2

QUAD CITIES 1 EOC2 GAMMA SCANS

ASSEMBLY CX 214 53.5 IN. FROM BOTTOM

COMPARISON TO RECORD 19300.MWD/MTU VOID HIST.= .27

.953	1.059	*****	1.058	*****	.946	.972	MEAS.
1.000	1.067	*****	1.042	*****	.978	.986	CALC.
-4.7	-.9	*****	1.5	*****	-3.2	-1.3	DIFF,%
			///////				
1.074	1.012	.958	/ .993/	.989	1.030	.996	
1.067	1.025	.994	/ .994/	1.019	1.036	1.008	
.7	-1.3	-3.6	/ -.1/	-2.9	-.5	-1.2	
			///////				
*****	.954	.942	.980	.980	1.031	*****	
*****	.994	.957	.953	.982	1.044	*****	
*****	-4.0	-1.5	2.7	-.2	-1.3	*****	
	///////						
1.022	/1.009/	.951	*****	.984	1.055	1.005	
1.042	/ .995/	.953	*****	.976	1.040	.987	
-2.0	/ 1.5/	-.2	*****	.7	1.5	1.8	
	///////						
				///////			
*****	1.007	.980	.995	/1.021/	.940	*****	
*****	1.019	.982	.976	/1.009/	.935	*****	
*****	-1.1	-.2	1.9	/ 1.3/	.5	*****	
				///////			
.948	1.056	1.051	1.060	.933	.990	.985	
.978	1.036	1.044	1.040	.935	.977	.960	
-3.0	2.0	.7	2.0	-.2	1.3	2.4	
.984	1.025	*****	1.027	*****	.991	1.057	
.986	1.008	*****	.987	*****	.960	1.031	
-.1	1.7	*****	4.0	*****	3.1	2.6	

***** Tie rods (Not measured) WIDE

///// Pins initially containing Gd2O3 WIDE GAP

STANDARD DEVIATION 2.1% (40 PINS)

Figure 3.4.3

QUAD CITIES 1 EOC2 GAMMA SCANS

ASSEMBLY CX 214 90.0 IN. FROM BOTTOM

COMPARISON TO RECORD 18600.MWD/MTU VOID HIST.= .50

.975	1.064	*****	1.068	*****	.967	1.017	MEAS.
1.011	1.059	*****	1.032	*****	.994	1.024	CALC.
-3.6	.5	*****	3.6	*****	-2.6	-.7	DIFF,%
			///////				
1.037	.974	.968	/ .965/	.965	1.033	1.030	
1.059	1.001	.966	/ .94°/	1.003	1.036	1.036	
-2.2	-2.6	.2	/ 1.6/	-3.8	-.4	-.6	
			///////				
*****	.936	.907	.920	.949	1.054	*****	
*****	.966	.925	.925	.963	1.041	*****	
*****	-3.1	-1.8	-.4	-1.3	1.3	*****	
	///////						
.997	/ .956/	.908	*****	.961	1.064	1.064	
1.032	/ .949/	.925	*****	.961	1.040	1.014	
-3.5	/ .8/	-1.7	*****	.1	2.4	5.0	
	///////						
				///////			
*****	.963	.954	.991	/1.012/	.943	*****	
*****	1.003	.963	.961	/ .994/	.947	*****	
*****	-4.0	-.8	3.0	/ 1.8/	-.4	*****	
				///////			
.959	1.027	1.063	1.082	.949	.986	1.023	
.994	1.036	1.041	1.040	.947	1.000	1.001	
-3.4	-1.0	2.2	4.3	.2	-1.4	2.2	
1.018	1.031	*****	1.063	*****	1.031	1.125	
1.024	1.036	*****	1.014	*****	1.001	1.090	
-.6	-.5	*****	4.9	*****	3.0	3.5	

***** Tie rods (Not measured) WIDE

///// Pins initially containing Gd203 WIDE GAP

STANDARD DEVIATION 2.5% (40 PINS)

Figure 3.4.4

QUAD CITIES 1 EOC2 GAMMA SCANS

ASSEMBLY CX 214 126.0 IN. FROM BOTTOM

COMPARISON TO RECORD 14940.MWD/MTU VOID HIST.= .61

.960	1.012	*****	1.064	*****	.984	1.041	MEAS.
1.006	1.058	*****	1.028	*****	.997	1.032	CALC.
-4.6	-4.6	*****	3.5	*****	-1.3	.9	DIFF.%
			///////				
1.005	.965	.930	/ .963/	.941	1.038	1.074	
1.058	.985	.947	/ .949/	.994	1.046	1.052	
-5.3	-2.1	-1.7	/ 1.4/	-5.4	-.8	2.2	
			///////				
*****	.924	.894	.912	.944	1.048	*****	
*****	.947	.902	.904	.949	1.045	*****	
*****	-2.3	-.8	.8	-.5	.3	*****	
	///////						
1.046	/ .955/	.905	*****	.946	1.066	1.075	
1.028	/ .949/	.904	*****	.950	1.047	1.028	
1.8	/ .6/	.1	*****	-.4	1.9	4.7	
	///////						
*****	.977	.940	.939	1.000	.969	*****	
*****	.994	.949	.950	.996	.948	*****	
*****	-1.7	-.9	-1.1	.5	2.1	*****	
.996	1.056	1.051	1.062	.932	1.031	1.023	
.997	1.046	1.045	1.047	.948	1.015	1.015	
-.2	1.0	.6	1.5	-1.6	1.6	.8	
1.032	1.056	*****	1.083	*****	1.041	1.122	
1.032	1.052	*****	1.028	*****	1.015	1.118	
.0	.3	*****	5.5	*****	2.6	.4	

***** Tie rods (Not measured) WIDE

///// Pins initially containing Gd2O3 WIDE GAP

STANDARD DEVIATION 2.4% (40 PINS)

Figure 3.4.5

QUAD CITIES 1 EOC2 GAMMA SCANS

ASSEMBLY CX 672 18.0 IN. FROM BOTTOM

COMPARISON TO RECORD 16000.MWD/MTU VOID HIST.= .04

.920	1.015	*****	1.009	*****	.915	.911	MEAS.
.987	1.087	*****	1.058	*****	.963	.942	CALC.
-7.0	-6.8	*****	-4.7	*****	-5.2	-3.3	DIFF.%
			///////				
1.045	1.005	.969	/ .995/	1.027	1.072	1.031	
1.087	1.045	1.012	/1.022/	1.032	1.051	.992	
-3.9	-3.9	-4.3	/ -2.6/	-.5	2.1	3.8	
			///////				
*****	1.012	.919	.968	.969	1.093	*****	
*****	1.012	.972	.966	.993	1.056	*****	
*****	-.0	-5.6	.2	-2.4	3.4	*****	
	///////						
.990	/1.022/	.972	*****	.989	1.060	1.048	
1.058	/1.022/	.966	*****	.987	1.052	.969	
-6.6	/ .0/	.6	*****	.3	.8	7.8	
	///////						
*****	1.023	.982	.989	1.046	.943	*****	
*****	1.032	.993	.987	1.014	.921	*****	
*****	-.9	-1.0	.2	3.2	2.4	*****	
.990	1.043	1.063	1.074	.904	.998	.982	
.963	1.051	1.056	1.052	.921	.963	.917	
2.8	-.7	.6	2.1	-1.8	3.6	6.8	
.933	1.049	*****	1.004	*****	.982	1.032	
.942	.992	*****	.969	*****	.917	.978	
-.9	5.6	*****	3.5	*****	6.9	5.4	

***** Tie rods (Not measured) WIDE WIDE GAP

///// Pins initially containing Gd203

STANDARD DEVIATION 3.9% (40 PINS)

Figure 3.4.6

QUAD CITIES 1 EOC2 GAMMA SCANS

ASSEMBLY CX 672 53.5 IN. FROM BOTTOM

COMPARISON TO RECORD 19380.MWD/MTU VOID HIST.= .27

1.001	1.016	*****	1.013	*****	.967	1.009	MEAS.
1.000	1.066	*****	1.042	*****	.977	.985	CALC.
.1	-4.8	*****	-2.8	*****	-1.0	2.4	DIFF.%
			///////				
1.056	1.012	.958	/ .996/	1.032	1.084	1.004	
1.067	1.025	.994	/ .994/	1.018	1.035	1.008	
-1.0	-1.2	-3.7	/ .2/	1.3	4.6	-.4	
			///////				
*****	.990	.929	.982	.974	1.087	*****	
*****	.994	.956	.953	.982	1.044	*****	
*****	-.4	-2.9	3.0	-.9	4.1	*****	
	///////						
1.018	/1.021/	.977	*****	.992	1.075	1.015	
1.042	/ .994/	.953	*****	.978	1.040	.987	
-2.3	/ 2.6/	2.5	*****	1.4	3.3	2.8	
	///////						
*****	1.038	.999	1.011	1.035	.917	*****	
*****	1.018	.982	.978	1.005	.937	*****	
*****	1.9	1.7	3.4	2.9	-2.2	*****	
.943	1.040	1.038	1.068	.919	.958	.934	
.977	1.035	1.044	1.040	.937	.978	.961	
-3.6	.4	-.6	2.6	-2.0	-2.0	-2.8	
.958	.994	*****	.977	*****	.95^	1.015	
.986	1.008	*****	.987	*****	.96[illegible]	1.031	
-2.8	-1.4	*****	-1.1	*****	-1.1	-1.6	

***** Tie rods (Not measured) WIDE

///// Pins initially containing Gd203 WIDE GAP

STANDARD DEVIATION 2.4% (40 PINS)

Figure 3.4.7

QUAD CITIES 1 EOC2 GAMMA SCANS

ASSEMBLY CX 672 90.0 IN. FROM BOTTOM

COMPARISON TO RECORD 18650.MWD/MTU VOID HIST.= .50

1.022	1.017	*****	1.022	*****	.931	.986	MEAS.
1.010	1.058	*****	1.031	*****	.993	1.024	CALC.
1.2	-4.0	*****	-.9	*****	-4.4	-3.7	DIFF,%
			///////				
1.076	.998	.957	/ .974/	.997	1.038	1.022	
1.058	1.000	.966	/ .948/	1.002	1.036	1.036	
1.6	-.2	-.9	/ 2.7/	-.5	.2	-1.4	
			///////				
*****	1.001	.892	.946	.940	1.070	*****	
*****	.966	.925	.925	.963	1.041	*****	
*****	3.5	-3.6	2.3	-2.4	2.7	*****	
	///////						
1.042	/ .995/	.954	*****	.973	1.052	1.017	
1.032	/ .948/	.925	*****	.961	1.040	1.014	
1.0	/ 4.8/	3.1	*****	1.2	1.2	.3	
	///////						
*****	1.020	.977	.971	1.029	.937	*****	
*****	1.002	.963	.961	.998	.948	*****	
*****	1.7	1.4	.9	3.1	-1.2	*****	
.992	1.027	1.057	1.067	.917	.984	1.009	
.993	1.036	1.041	1.040	.948	1.001	1.001	
-.1	-.9	1.5	2.6	-3.3	-1.7	.8	
.998	1.041	*****	.988	*****	.989	1.063	
1.024	1.036	*****	1.014	*****	1.001	1.090	
-2.5	.5	*****	-2.7	*****	-1.3	-2.6	

***** Tie rods (Not measured) WIDE

///// Pins initially containing Gd2O3 WIDE GAP

STANDARD DEVIATION 2.3% (40 PINS)

Figure 3.4.8

QUAD CITIES 1 EOC2 GAMMA SCANS

ASSEMBLY CX 672 126.0 IN. FROM BOTTOM

COMPARISON TO RECORD 15510.MWD/MTU VOID HIST.= .61

1.045	1.050	*****	1.041	*****	.960	.995	MEAS.
1.008	1.058	*****	1.028	*****	.999	1.035	CALC.
3.5	-.7	*****	1.2	*****	-4.0	-3.9	DIFF,%
			///////				
1.091	.980	.927	/ .962/	1.015	1.076	1.056	
1.057	.986	.948	/ .945/	.995	1.045	1.052	
3.1	-.6	-2.3	/ 1.8/	2.0	2.9	.3	
			///////				
*****	.979	.880	.905	.941	1.056	*****	
*****	.948	.904	.905	.950	1.044	*****	
*****	3.2	-2.7	-.1	-1.0	1.1	*****	
	///////						
1.054	/ .983/	.903	*****	.951	1.053	1.034	
1.028	/ .945/	.905	*****	.951	1.045	1.028	
2.4	/ 3.9/	-.3	*****	-.0	.7	.5	
	///////						
*****	1.018	.947	.959	1.018	.943	*****	
*****	.995	.950	.951	.981	.948	*****	
*****	2.3	-.3	.9	3.7	-.6	*****	
1.008	1.068	1.046	1.073	.897	.985	.974	
.999	1.045	1.044	1.045	.948	1.014	1.016	
.9	2.2	.2	2.6	-5.6	-2.9	-4.3	
1.015	1.047	*****	1.004	*****	1.015	1.054	
1.035	1.052	*****	1.029	*****	1.016	1.119	
-1.9	-.5	*****	-2.4	*****	-.2	-6.1	

***** Tie rods (Not measured) WIDE

///// Pins initially containing Gd2O3 WIDE GAP

STANDARD DEVIATION 2.5% (40 PINS)

Figure 3.4.9

QUAD CITIES 1 EOC2 GAMMA SCANS

ASSEMBLY GEB159 18.0 IN. FROM BOTTOM

COMPARISON TO RECORD 11425.MWD/MTU VOID HIST.= .08

.990	1.066	*****	1.046	*****	.926	.976	MEAS.
1.036	1.094	*****	1.039	*****	.908	.962	CALC.
-4.6	-2.8	*****	.7	*****	1.8	1.4	DIFF,%
	///////			///////			
1.067	/ .821/	1.183	1.147	/ .882/	.983	.988	
1.095	/ .811/	1.301	1.226	/ .855/	.954	.964	
-2.8	/ 1.0/	-11.8	-7.9	/ 2.7/	2.8	2.4	
	///////			///////			
		///////					
*****	1.171	/ .588/	1.094	1.000	1.041	*****	
*****	1.303	/ .649/	1.205	1.022	1.032	*****	
*****	-13.2	/ -6.1/	-11.1	-2.1	.9	*****	
		///////					
1.051	1.154	1.099	*****	.999	1.086	.963	
1.040	1.229	1.133	*****	.998	1.035	.935	
1.1	-7.5	-3.4	*****	.1	5.1	2.8	
	///////			///////			
*****	/ .880/	1.011	1.020	/ .895/	1.007	*****	
*****	/ .856/	1.024	1.000	/ .858/	.956	*****	
*****	/ 2.4/	-1.3	2.1	/ 3.7/	5.1	*****	
	///////			///////			
.950	.975	1.057	1.076	1.005	.933	.980	
.909	.955	1.033	1.035	.956	.899	.949	
4.1	2.0	2.4	4.0	4.9	3.4	3.1	
.996	.993	*****	.949	*****	.979	.973	
.963	.965	*****	.935	*****	.949	.934	
3.4	2.8	*****	1.4	*****	3.0	3.9	

***** Tie rods (Not measured) WIDE

///// Pins initially containing Gd2O3 WIDE GAP

STANDARD DEVIATION 4.7% (40 PINS)

Figure 3.4.10

QUAD CITIES 1 EOC2 GAMMA SCANS

ASSEMBLY GE8159 53.5 IN. FROM BOTTOM

COMPARISON TO RECORD 9219.MWD/MTU VOID HIST.= .38

1.023	1.054	*****	1.040	*****	.962	1.026	MEAS.
1.034	1.068	*****	1.018	*****	.928	1.019	CALC.
-1.1	-1.4	*****	2.2	*****	3.4	.7	DIFF,%
	///////			///////			
1.036	/ .728/	1.144	1.150	/ .825/	.981	1.019	
1.069	/ .706/	1.248	1.203	/ .809/	.963	1.009	
-3.3	/ 2.2/	-10.4	-5.2	/ 1.6/	1.8	1.0	
	///////			///////			
		///////					
*****	1.149	/ .487/	1.091	.992	1.049	*****	
*****	1.250	/ .511/	1.152	1.023	1.032	*****	
*****	-10.1	/ -2.4/	-6.1	-3.1	1.6	*****	
		///////					
1.059	1.114	1.061	*****	1.016	1.070	1.000	
1.019	1.206	1.085	*****	1.010	1.041	.977	
4.0	-9.2	-2.4	*****	.6	2.9	2.3	
	///////			///////			
*****	/ .831/	.995	1.014	/ .857/	.991	*****	
*****	/ .811/	1.026	1.011	/ .843/	.979	*****	
*****	/ 2.1/	-3.0	.3	/ 1.4/	1.3	*****	
	///////			///////			
.981	.997	1.044	1.081	1.007	.946	1.037	
.929	.964	1.033	1.041	.979	.940	1.019	
5.3	3.3	1.1	4.0	2.8	.6	1.7	
1.055	1.021	*****	.997	*****	1.036	1.032	
1.019	1.009	*****	.977	*****	1.019	1.020	
3.6	1.2	*****	1.9	*****	1.6	1.2	

***** Tie rods (Not measured)

///// Pins initially containing Gd2O3

WIDE
WIDE
GAP

STANDARD DEVIATION 3.7% (40 PINS)

Figure 3.4.11

QUAD CITIES 1 EOC2 GAMMA SCANS

ASSEMBLY GEB159 90.0 IN. FROM BOTTOM

COMPARISON TO RECORD 9025.MWD/MTU VOID HIST.= .56

1.020	1.031	*****	1.042	*****	.980	1.065	MEAS.
1.029	1.051	*****	1.006	*****	.936	1.047	CALC.
-.9	-2.0	*****	3.6	*****	4.3	1.9	DIFF,%
	///////			///////			
1.062	/ .721/	1.140	1.124	/ .809/	.967	1.030	
1.051	/ .689/	1.211	1.175	/ .803/	.965	1.026	
1.1	/ 3.2/	-7.1	-5.2	/ .5/	.3	.4	
	///////			///////			
		///////					
*****	1.151	/ .491/	1.068	.987	1.033	*****	
*****	1.213	/ .504/	1.121	1.016	1.032	*****	
*****	-6.2	/ -1.3/	-5.3	-2.9	.2	*****	
		///////					
1.059	1.153	1.047	*****	1.011	1.061	.998	
1.006	1.178	1.055	*****	1.005	1.043	.996	
5.3	-2.6	-.8	*****	.6	1.8	.2	
	///////			///////			
*****	/ .875/	.998	.988	/ .840/	.986	*****	
*****	/ .805/	1.018	1.006	/ .851/	.989	*****	
*****	/ 7.0/	-1.9	-1.8	/ -1.1/	-.3	*****	
	///////			///////			
.974	.977	1.057	1.072	1.010	.944	1.041	
.937	.965	1.032	1.044	.989	.960	1.053	
3.8	1.2	2.5	2.9	2.2	-1.6	-1.2	
1.067	1.033	*****	1.008	*****	1.032	1.048	
1.047	1.027	*****	.996	*****	1.053	1.070	
2.0	.7	*****	1.1	*****	-2.1	-2.3	

***** Tie rods (Not measured) WIDE

///// Pins initially containing Gd203 WIDE GAP

STANDARD DEVIATION 3.0% (40 PINS)

Figure 3.4.12

QUAD CITIES 1 EOC2 GAMMA SCANS

ASSEMBLY GEB159 126.0 IN. FROM BOTTOM

COMPARISON TO RECORD 7500.MWD/MTU VOID HIST.= .65

1.043	1.052	*****	1.060	*****	.981	1.109	MEAS.
1.029	1.044	*****	.999	*****	.945	1.073	CALC.
1.3	.8	*****	6.1	*****	3.5	3.6	DIFF.%
	///////			///////			
1.068	/ .640/	1.134	1.141	/ .716/	.976	1.061	
1.044	/ .618/	1.187	1.165	/ .749/	.973	1.048	
2.4	/ 2.1/	-5.4	-2.4	/ -3.2/	.3	1.2	
	///////			///////			
		///////					
*****	1.144	/ .428/	1.037	.973	1.037	*****	
*****	1.189	/ .454/	1.096	1.017	1.040	*****	
*****	-4.5	/ -2.6/	-5.9	-4.4	-.3	*****	
		///////					
1.061	1.176	1.026	*****	.997	1.068	1.016	
1.000	1.168	1.031	*****	1.013	1.055	1.017	
6.1	.9	-.5	*****	-1.7	1.3	-.2	
	///////			///////			
*****	/ .739/	.971	.996	/ .765/	.989	*****	
*****	/ .750/	1.019	1.014	/ .816/	1.006	*****	
*****	/ -1.1/	-4.8	-1.8	/ -5.2/	-1.7	*****	
	///////			///////			
1.017	.999	1.055	1.073	1.020	.955	1.083	
.946	.974	1.041	1.055	1.006	.984	1.090	
7.1	2.5	1.5	1.8	1.4	-2.9	-.7	
1.120	1.061	*****	1.039	*****	1.073	1.104	
1.074	1.049	*****	1.018	*****	1.090	1.113	
4.7	1.2	*****	2.1	*****	-1.7	-1.0	

***** Tie rods (Not measured)

///// Pins initially containing Gd2O3

WIDE
WIDE
GAP

STANDARD DEVIATION 3.2% (40 PINS)

Figure 3.4.13

QUAD CITIES 1 EOC2 GAMMA SCANS

ASSEMBLY GEH002 18.0 IN. FROM BOTTOM

COMPARISON TO RECORD 11320.MWD/MTU VOID HIST.= .08

.962	1.080	*****	1.007	1.039	*****	.998	1.035	MEAS.
1.026	1.114	*****	1.054	1.063	*****	1.006	1.040	CALC.
-6.4	-3.4	*****	-4.7	-2.4	*****	-.7	-.4	DIFF,%
	///////				///////			
1.095	/ .989/	.939	.929	.955	/ .997/	1.085	1.052	
1.114	/ .995/	.967	.952	.958	/ .989/	1.073	1.047	
-1.9	/ -.5/	-2.8	-2.2	-.3	/ .8/	1.2	.5	
	///////				///////			
*****	.955	.922	.929	.924	.956	1.042	*****	
*****	.967	.943	.943	.935	.951	1.029	*****	
*****	-1.2	-2.1	-1.4	-1.1	.6	1.3	*****	
1.053	.944	.934	*****	.945	.937	1.035	1.032	
1.054	.952	.943	*****	.936	.938	1.014	1.007	
-.1	-.7	-.9	*****	.9	-.1	2.1	2.5	
1.060	.965	.927	.931	.918	.947	1.034	1.036	
1.063	.959	.935	.936	.931	.947	1.025	1.014	
-.3	.6	-.8	-.4	-1.3	.0	.9	2.2	
	///////				///////			
*****	/1.002/	.959	.931	.954	/ .998/	1.086	*****	
*****	/ .989/	.951	.938	.947	/ .952/	1.063	*****	
*****	/ 1.3/	.9	-.7	.7	/ 4.6/	2.3	*****	
	///////				///////			
1.000	1.094	1.028	1.016	1.039	1.073	.992	1.023	
1.006	1.073	1.029	1.014	1.025	1.063	.979	1.024	
-.6	2.1	-.1	.2	1.4	1.0	1.3	-.1	
1.043	1.051	*****	1.030	1.037	*****	1.043	1.002	
1.040	1.047	*****	1.007	1.014	*****	1.024	.992	
.3	.5	*****	2.3	2.3	*****	1.9	1.0	

***** Tie rods or Water hole (Not measured) WIDE

///// Pins initially containing Gd2O3 WIDE GAP

STANDARD DEVIATION 1.8% (55 PINS)

Figure 3.4.14

QUAD CITIES 1 EOC2 GAMMA SCANS

ASSEMBLY GEH002 53.5 IN. FROM BOTTOM

COMPARISON TO RECORD 9550.MWD/MTU VOID HIST.= .38

.987	1.052	*****	.999	1.027	*****	.983	1.075	MEAS.
1.032	1.103	*****	1.038	1.054	*****	1.026	1.085	CALC.
-4.5	-5.2	*****	-3.9	-2.7	*****	-4.3	-.9	DIFF,%
	///////				///////			
1.097	/ .950/	.915	.906	.933	/ .972/	1.079	1.073	
1.103	/ .985/	.936	.922	.936	/ .982/	1.081	1.079	
-.6	/ -3.5/	-2.2	-1.6	-.3	/ -1.0/	-.2	-.6	
	///////				///////			
*****	.930	.898	.912	.896	.939	1.031	*****	
*****	.936	.910	.908	.908	.934	1.030	*****	
*****	-.6	-1.1	.4	-1.2	.4	.1	*****	
1.052	.919	.931	*****	.934	.916	1.012	1.037	
1.038	.922	.908	*****	.906	.920	1.014	1.031	
1.3	-.3	2.3	*****	2.8	-.4	-.2	.6	
1.080	.933	.912	.933	.917	.942	1.035	1.052	
1.054	.935	.907	.906	.905	.934	1.031	1.043	
2.6	-.2	.4	2.7	1.2	.8	.4	.9	
	///////				///////			
*****	/ .989/	.942	.921	.967	/1.010/	1.082	*****	
*****	/ .982/	.934	.920	.934	/ .976/	1.085	*****	
*****	/ .7/	.8	.2	3.3	/ 3.4/	-.2	*****	
	///////				///////			
1.009	1.089	1.061	1.030	1.048	1.101	1.010	1.070	
1.025	1.081	1.030	1.014	1.031	1.085	1.013	1.077	
-1.7	.8	3.1	1.6	1.7	1.7	-.3	-.7	
1.091	1.080	*****	1.057	1.055	*****	1.066	1.061	
1.084	1.079	*****	1.031	1.043	*****	1.077	1.057	
.7	.2	*****	2.6	1.2	*****	-1.0	.4	

***** Tie rods or Water hole (Not measured) WIDE

///// Pins initially containing Gd203 WIDE GAP

STANDARD DEVIATION 1.9% (55 PINS)

Figure 3.4.15

QUAD CITIES 1 EOC2 GAMMA SCANS

ASSEMBLY GEH002 90.0 IN. FROM BOTTOM

COMPARISON TO RECORD 9325.MWD/MTU VOID HIST.= .57

.956	1.038	*****	1.001	1.029	*****	1.001	1.092	MEAS.
1.030	1.087	*****	1.022	1.042	*****	1.033	1.110	CALC.
-7.4	-4.9	*****	-2.2	-1.3	*****	-3.3	-1.9	DIFF.%
	///////				///////			
1.041	/ .922/	.900	.884	.905	/ .966/	1.071	1.092	
1.087	/ .978/	.916	.903	.920	/ .987/	1.080	1.094	
-4.6	/ -5.7/	-1.6	-1.9	-1.5	/ -2.1/	-1.0	-.2	
	///////				///////			
*****	.910	.875	.912	.901	.937	1.047	*****	
*****	.916	.890	.889	.894	.926	1.029	*****	
*****	-.6	-1.5	2.4	.7	1.1	1.7	*****	
1.016	.914	.905	*****	.912	.914	1.008	1.049	
1.022	.903	.888	*****	.892	.913	1.015	1.046	
-.7	1.1	1.7	*****	2.0	.1	-.7	.3	
1.061	.938	.914	.917	.913	.946	1.058	1.074	
1.042	.920	.893	.892	.896	.931	1.037	1.061	
1.9	1.8	2.1	2.5	1.6	1.5	2.1	1.3	
	///////				///////			
*****	/ .986/	.937	.935	.960	/1.010/	1.100	*****	
*****	/ .987/	.926	.913	.931	/1.000/	1.098	*****	
*****	/ -.2/	1.1	2.2	2.9	/ 1.0/	.2	*****	
	///////				///////			
1.026	1.086	1.053	1.048	1.068	1.120	1.022	1.097	
1.033	1.080	1.029	1.015	1.037	1.098	1.035	1.109	
-.8	.5	2.4	3.3	3.2	2.2	-1.4	-1.2	
1.110	1.107	*****	1.061	1.090	*****	1.100	1.074	
1.110	1.094	*****	1.046	1.061	*****	1.109	1.105	
-.0	1.3	*****	1.5	2.9	*****	-1.0	-3.0	

***** Tie rods or Water hole (Not measured)

///// Pins initially containing Gd2O3

STANDARD DEVIATION 2.3% (55 PINS)

WIDE
WIDE
GAP

Figure 3.4.16

QUAD CITIES 1 EOC2 GAMMA SCANS

ASSEMBLY GEH002 126.0 IN. FROM BOTTOM

COMPARISON TO RECORD 7665.MWD/MTU VOID HIST.= .65

.975	1.037	*****	1.010	1.043	*****	1.022	1.122	MEAS.
1.024	1.080	*****	1.013	1.035	*****	1.036	1.124	CALC.
-4.9	-4.3	*****	-.3	.7	*****	-1.4	-.2	DIFF,%
	///////				///////			
1.047	/ .926/	.884	.883	.911	/ .969/	1.097	1.109	
1.080	/ .982/	.902	.889	.909	/ .998/	1.084	1.104	
-3.3	/ -5.5/	-1.8	-.6	.2	/ -2.9/	1.3	.5	
	///////				///////			
*****	.894	.854	.892	.881	.928	1.051	*****	
*****	.902	.876	.874	.882	.918	1.030	*****	
*****	-.8	-2.2	1.8	-.1	1.0	2.1	*****	
1.007	.932	.886	*****	.895	.908	1.020	1.058	
1.013	.889	.874	*****	.881	.906	1.017	1.052	
-.6	4.3	1.1	*****	1.4	.2	.3	.5	
1.044	.924	.890	.898	.902	.940	1.053	1.082	
1.035	.909	.882	.881	.888	.927	1.041	1.071	
.8	1.5	.8	1.7	1.4	1.3	1.2	1.1	
	///////				///////			
*****	/ .979/	.921	.908	.943	/ .998/	1.122	*****	
*****	/ .998/	.918	.906	.927	/1.022/	1.110	*****	
*****	/ -1.9/	.3	.2	1.5	/ -2.4/	1.2	*****	
	///////				///////			
1.021	1.116	1.037	1.037	1.057	1.124	1.044	1.132	
1.036	1.084	1.030	1.016	1.041	1.110	1.049	1.131	
-1.5	3.2	.6	2.0	1.5	1.3	-.5	.0	
1.102	1.121	*****	1.058	1.087	*****	1.120	1.103	
1.124	1.104	*****	1.052	1.071	*****	1.131	1.128	
-2.2	1.6	*****	.5	1.6	*****	-1.1	-2.5	

***** Tie rods or Water hole (Not measured)

///// Pins initially containing Gd203

STANDARD DEVIATION 1.9% (55 PINS)

WIDE
WIDE
GAP

4.0 Description of PRESTO-B

PRESTO-B is the primary tool used by Carolina Power & Light Company (CP&L) for BWR neutronic evaluations. A detailed description of the technical aspects of PRESTO-B is provided in a companion report: "Methods of PRESTO-B, A Three-Dimensional, LWR Core Simulation Code" (Reference 2). The purpose of Section 4 of this report is to provide additional background concerning the use of PRESTO-B by CP&L.

4.1 Neutronic Models

The basic PRESTO neutron balance equations are described in Reference 2, Section 5. The nodal algorithm used in this analysis is fundamentally the same as was first introduced in 1971 (Reference 21). PRESTO-B uses standard two-group cross-section data to solve for fast flux in a node. The thermal flux can be determined in two ways. The original approach assumed that the thermal flux could be found by using the ratio of fast to thermal flux which was given by the infinite lattice calculation. This usage of the so-called "asymptotic" thermal flux approximation is the basis of PRESTO-B benchmarking performed prior to 1982.

Recently, a new approach to thermal flux modeling was developed which makes a leakage correction to the asymptotic thermal flux. This revised approach is most useful in cases where large discontinuities in nodal flux are expected to occur. A typical example of such a case is single rod-out criticality such as shutdown margin calculations. All of the analyses presented in this report make use of thermal flux leakage correction. The benchmarking presented in

Reference 2, for the most part, is based on the asymptotic thermal flux approximation. These two methods show very little difference in power shape and eigenvalue for normal core follow studies. Typically, application of the thermal flux leakage correction makes a slight reduction in nodal peaking and about 0.003 reduction in eigenvalue as compared to previous methods. These are not considered to be significant differences and do not invalidate any of the general conclusions presented in Reference 2.

CP&L has adopted the use of the thermal leakage correction method because it provides greater consistency between the cold critical and hot operating models.

4.2 Boundary Conditions

A description of the mathematical representation of the PRESTO two-group boundary conditions is given in Reference 2, Section 5.2. Physically, these terms are analogous to a fast extrapolation distance and an incoming thermal to outgoing fast current ratio. PRESTO permits the user to define leakage correction terms (boundary conditions) for each node in the problem. It is standard practice, however, to apply leakage correction terms to only those fuel nodes with one or more reflector faces or corners.

Characteristic cycle dependent radial and fuel type dependent axial boundary conditions are generated using the ALBMO option in PRESTO. This approach starts with a distribution of PRESTO two-group cross sections and reference fine mesh two-group fluxes calculated by MD-1 or MD-2. The basic PRESTO nodal algorithm is then reformed to solve for a set of leakage parameters which will

yield the reference fine mesh flux distribution when using the reference two-group cross-sections.

A flow diagram for the boundary condition generation process is given in Figure 4.2.1. Typically, a unique set of boundary conditions is generated for each reactor cycle and for various different combinations of power and temperature. The analyses reported here made use of boundary conditions generated for hot nominal, warm zero power, and cold zero power conditions. The following is a brief discussion pertaining to the axial and radial boundary condition generation procedure.

4.2.1 Axial Boundary Condition Generation

The axial boundary condition calculation process starts with the generation of representative two-group nodal cross sections. These are produced by running PRESTO at the specified operating conditions and editing a set of axial cross sections for the bundle of choice.

The cross sections are then transferred to the MD-1 program where a fine mesh axial calculation is performed. MD-1 is a one-dimensional analog of the MD-2 program described in Reference 1, Section 7. The MD-1 axial representation consists of two lower reflector regions, the 24-node core region, and three upper reflector regions. Two-group constants for the reflector regions are generated using a special RECORD calculation which preserves the structural detail and generates flux weighted cross sections using a dilute fission source. The end product of the MD-1 calculations is a set of two-group fluxes and an eigenvalue for the reference one-dimensional problem. Finally,

the ALBMO option in PRESTO is exercised using the previously generated two-group cross sections and flux files.

The PRESTO axial boundary conditions are dependent on overall thermal-hydraulic state and lattice structural design. The top reflector boundary conditions tend to be relatively insensitive to void content in the upper fuel region. A major difference in reflector treatment is observed, however, when comparing fuel with and without axial blankets and of different axial heights. Very little difference in reflector parameters is observed when comparing the GE 7x7 and 8x8 fuel designs. Comparisons of GE 8x8 and 8x8R fuel, on the other hand, show a marked difference.

Nodal simulator codes are not designed for evaluations of fuel with different axial heights. As a result, some amount of approximation is required for evaluating cores in transition between 144- and 150-inch fuel. The assumption made by CP&L is that the top 6-inch blanket of 150-inch fuel produces no power. As a result, the natural blanket region can be evaluated as a reflector region rather than a fuel region. This conservative approximation has proven to be a very good one and permits analysis of an axial stack of 24 equal length nodes. The only correction required by ignoring the power generation in the top reflector is to adjust exposure accounting to represent the fact that the longer fuel is modeled with less total fuel weight. Future evaluations will be performed using an axial stack of 25 nodes when the Brunswick cores are completely loaded with 150-inch fuel.

4.2.2 Radial Boundary Condition Generation

The process of calculating radial boundary conditions is analogous to that used for the axials. The most notable difference is the choice of the reference two-group cross section set. The cross sections used for the radial evaluation are intended to typify the average leakage condition during the cycle. The Haling power and burnup distribution is the most appropriate to use for reload cores. The hot nominal operations cross sections are generated by editing out two-group constants at the core mid-plane from PRESTO. The basic two-group constants for warm and cold critical conditions are generated using an all-rods-in restart of the Haling EOC calculation for an axial plane near the top of the core. This approach is intended to weight the radial leakage at the axial flux peak.

The cross sections are then transferred to the MD-2 program where the fine mesh 2-D radial calculation is performed. The MD-2 method is described in Reference 2, Section 7. This evaluation can also be performed using PDQ07 instead of MD-2. Side-by-side runs of MD-2 and PDQ07 show virtually identical results when used for this type of reference calculation. MD-2 is normally used, however, because of its automated handling of PRESTO data. Finally, the ALBMO option in PRESTO is exercised as in the 1-D axial problem. The 2-D ALBMO option, in PRESTO, provides additional adjustment to the radial boundary conditions to match the core radial power distribution as well as the radial leakage. This is needed because leakage parameters are only supplied at the core periphery.

Figure 4.2.2 shows a comparison of the PRESTO coarse mesh and MD-2 fine mesh 2-D evaluations for Brunswick 2, Cycle 5, hot operations. Experience has shown that cycle specific radial boundary conditions are needed only when a substantial change in radial leakage is anticipated, such as between the first and second cycle of operations. It is standard practice, however, to generate radial boundary conditions uniquely for each cycle at the various operating conditions.

FIGURE 4.2.1

FLOW DIAGRAM FOR PRESTO-B BOUNDARY CONDITION GENERATION

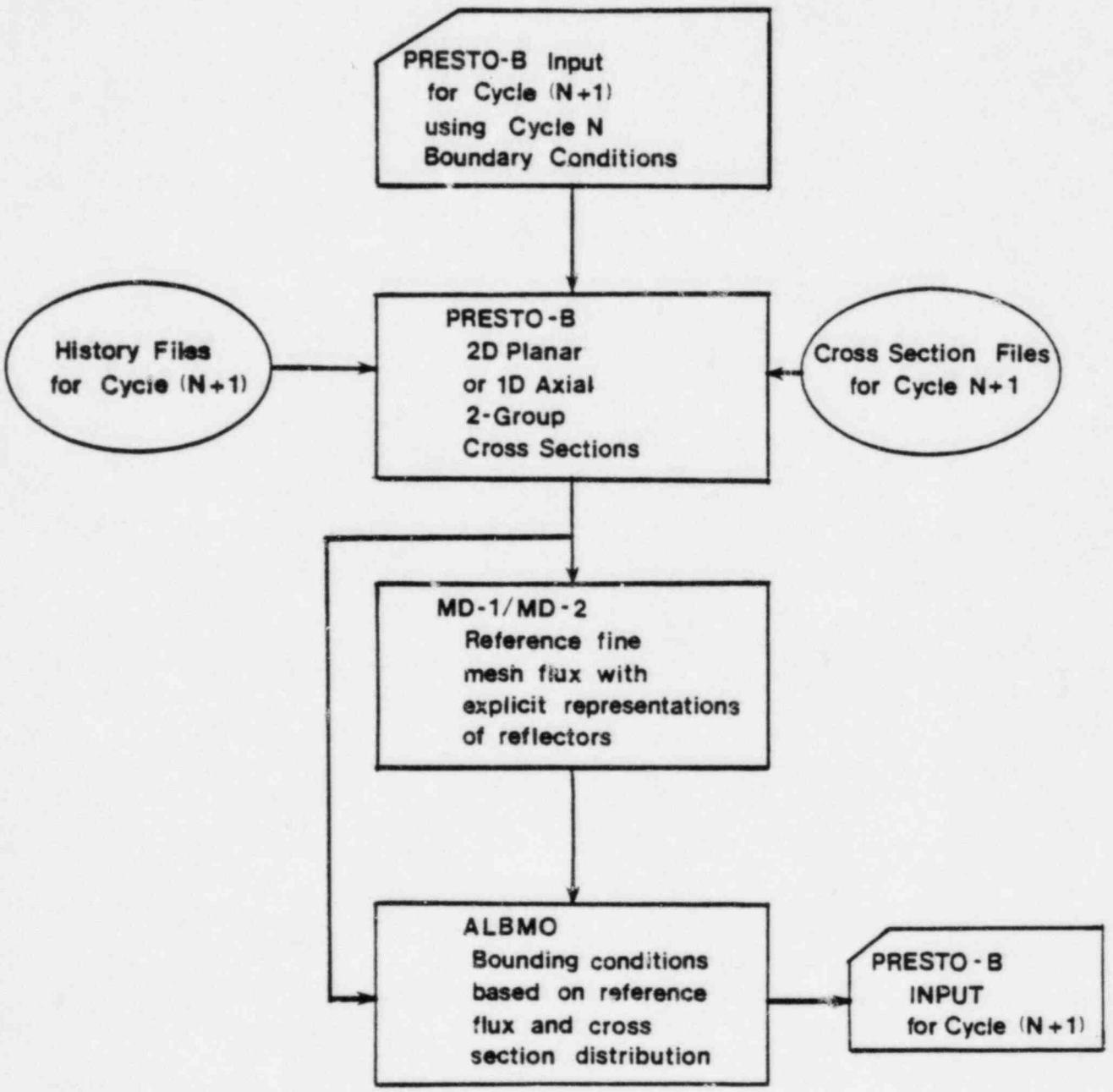

FIGURE 4.2.2
COMPARISON OF PRESTO-B NODAL TO
MD-2 FINE MESH CALCULATION FOR
HOT BOUNDARY CONDITION GENERATION
B2C5 PLANE 12

	27	29	31	33	35	37	39	41	43	45	47	49	51
26	.96 .99 -3.0	1.06 1.07 -0.9	1.29 1.31 -1.5	1.03 1.04 -1.0	1.02 1.04 -1.9	1.13 1.12 0.9	1.34 1.36 -1.5	1.04 1.05 -1.0	1.08 1.08 0.0	1.11 1.10 0.9	1.17 1.17 0.0	.87 .84 3.6	.50 .50 0.0
24	1.07 1.08 -0.9	1.30 1.31 -0.8	1.15 1.14 0.9	1.31 1.32 -0.8	1.14 1.14 0.0	1.33 1.33 0.0	1.17 1.16 0.9	1.30 1.31 -0.8	1.15 1.15 0.0	1.26 1.27 -0.8	1.06 1.04 1.9	.84 .82 2.4	.48 .48 0.0
22	1.30 1.31 -0.8	1.18 1.18 0.0	1.33 1.33 0.0	1.17 1.17 0.0	1.32 1.34 -1.5	1.17 1.16 0.9	1.33 1.33 0.0	1.17 1.16 0.9	1.26 1.27 -0.8	1.11 1.09 1.8	1.12 1.12 0.0	.84 .82 2.4	.47 .47 0.0
20	1.03 1.04 -1.0	1.31 1.32 -0.8	1.17 1.17 0.0	1.04 1.06 -1.9	1.13 1.13 0.0	1.32 1.34 -1.5	1.18 1.18 0.0	1.01 1.02 -1.0	.97 .98 -1.0	1.18 1.18 0.0	.99 .98 1.0	.77 .76 1.3	.42 .42 0.0
18	1.02 1.04 -1.9	1.14 1.14 0.0	1.32 1.34 -1.5	1.14 1.14 0.0	1.04 1.06 -1.9	1.14 1.14 0.0	1.30 1.31 -0.8	1.10 1.10 0.0	1.05 1.05 0.0	1.02 1.02 0.0	.99 .99 0.0	.61 .62 -1.6	.37 .37 0.0
16	1.13 1.13 0.0	1.32 1.33 -0.8	1.16 1.15 0.9	1.32 1.34 -1.5	1.14 1.14 0.0	1.31 1.32 -0.8	1.12 1.11 0.9	1.25 1.26 -0.8	1.07 1.07 0.0	1.07 1.06 0.9	.74 .73 1.4	.49 .49 0.0	
14	1.34 1.35 -0.7	1.16 1.15 0.9	1.33 1.33 0.0	1.18 1.17 0.9	1.30 1.31 -0.8	1.12 1.10 1.8	1.26 1.27 -0.8	1.09 1.09 0.0	1.12 1.13 -0.9	.90 .88 2.3	.56 .55 1.8		
12	1.04 1.04 0.0	1.30 1.31 -0.8	1.17 1.16 0.9	1.00 1.01 -1.0	1.09 1.09 0.0	1.24 1.25 -0.8	1.08 1.08 0.0	.95 .96 -1.0	.88 .89 -1.1	.76 .76 0.0	.45 .45 0.0		
10	1.07 1.07 0.0	1.16 1.15 0.9	1.26 1.27 -0.8	.97 .98 -1.0	1.04 1.04 0.0	1.06 1.06 0.0	1.12 1.12 0.0	.88 .88 0.0	.80 .81 -1.2	.64 .64 0.0	.37 .37 0.0		
08	1.12 1.11 0.9	1.26 1.27 -0.8	1.10 1.08 1.9	1.17 1.18 -0.8	1.01 1.00 1.0	1.06 1.06 0.0	.90 .88 2.3	.74 .74 0.0	.64 .64 0.0	.42 .42 0.0			
06	1.18 1.17 0.9	1.06 1.04 1.9	1.13 1.12 0.9	.99 .98 1.0	.98 .99 -1.0	.75 .75 0.0	.56 .55 1.8	.45 .45 0.0	.36 .37 -2.7				
04	.87 .85 2.4	.86 .84 2.4	.84 .82 2.4	.77 .76 1.3	.59 .59 0.0	.48 .48 0.0							
02	.50 .50 0.0	.49 .49 0.0	.47 .47 0.0	.42 .43 -2.3	.37 .37 0.0								

PRESTO
MD-2
% DIFF

KEFF(PRESTO-B) = 1.00503
KEFF(MD-2) = 1.00521

4.3 Thermal-Hydraulics Models

The reactivity feedback caused by moderator boiling in a BWR is significant and plays a principal role in the calculation of the power distribution. To a lesser extent, the fuel temperature also provides neutronic feedback through the Doppler effect. Moderator boiling and Doppler broadening are negative power reactivity feedbacks. These effects, coupled with xenon poisoning, result in a system of equations which are highly nonlinear in local power. The thermal hydraulics and neutronics must be coupled in order to determine a unique equilibrium power distribution solution.

The end products of the thermal-hydraulic and neutronic iteration processes are state variables which can be used to describe the condition of the fuel. The parameters of greatest concern, for thermal limit evaluations, are the bundle power and flow distributions. These parameters are of primary importance in establishing margin to maximum average planer linear heat generation rate (MAPLHGR) and critical power ratio (CPR).

Reference 2, Section 6, provides a summary of the system of equations used for the thermal-hydraulic and fuel-temperature analyses in PRESTO. The orientation of the following section will be to describe how input to the PRESTO equation sets is developed in order to generate the end product thermal analysis and also to highlight those areas which are not covered in detail in Reference 2.

4.3.1 Fuel Temperature Modeling

Under normal operating conditions, the effect of fuel temperature feedback (Doppler broadening) is weak compared with that of moderator voiding. This is fortunate, because a precise evaluation of BWR fuel temperature is highly dependent on previous operating history as well as present conditions. The approach taken in PRESTO is to specify an average fuel temperature at rated conditions and then make an adjustment for local power density based on a linear power dependency.

The average fuel temperature as a function of exposure, for each lattice type, is evaluated using a detailed fuel performance code such as COMETHE (Reference 9).

4.3.2 Core and Bypass Flow Distributions

PRESTO models the core flow distribution by assuming many parallel flow channels with equal pressure drop between the core inlet and exit. The momentum equations cited in Reference 2, Section 6, are first solved for a simplified system consisting of a few large hydraulic regions and the core bypass. After the overall pressure drop has been evaluated in the few region problem, individual bundle flows are allocated.

The various flow paths for a typical BWR geometry are shown in Figure 4.3.1. One can observe that there is a complex interplay between bypass flow and in-channel flow. For nodal simulation purposes, the exact specification of

the flow through each of the unique bypass paths is not as important as the overall split between in-channel and bypass flow. PRESTO simplifies the flow geometry to represent single-path communication, for each channel, with the upper and lower plenums. The detailed distribution of flow given by any unique combination of orifice, fuel support piece, and fuel design is only important in developing effective form loss coefficients for specifying the inlet pressure losses. The actual flow splits are provided by reference FIBWR calculations.

The bundle flow calculated by PRESTO represents the total coolant flow which is subject to conductive heat transfer from the fuel. All other coolant flows, such as water tubes or channels, and inter-channel bypass are considered as part of the bypass fraction.

Pressure dissipation by form losses are assumed to be proportional to the momentum flow given in Reference 2, Section 6. This results in a pressure drop equation given by:

$$\Delta P = K_x[(1-\alpha_x)\,\rho_f V_f^2 + \alpha_x\,\rho_g V_g^2] \qquad \text{Eq. 4.3.1}$$

where "x" represents inlet or outlet.

ρ_f, ρ_g = Saturated fluid and gas densities respectively,

V_f, V_g = Saturated fluid and gas velocities respectively,

and

α_x = void fraction.

The axial distribution of grid spacer pressure losses is represented by lumping the first two grids into the entrance loss and the remaining grids

into the exit loss. The effective entrance loss coefficient for each hydraulic region is generated using standard pressure loss data as follows:

$$K_{IN} = \left[\frac{\rho_{sat}}{\rho_{in}}\left(F_o \cdot W_T^2 + F_{ip}(W_T - W_6 - W_9)^2 + \frac{(A_o^2 W_T^2 - A_c^2 W_c^2)}{A_o^2 \cdot A_c^2}\right) + 2F_g \cdot W_c^2\right] \frac{A_c^2}{2W_c^2} \qquad \text{Eq. 4.3.2}$$

where:

F_o = The form loss coefficient per unit area squared for the inlet orifice (K/A^2)

F_{ip} = The form loss coefficient per unit area squared for the fuel inlet plenum (K/A^2)

F_g = Form loss coefficient per unit area squared for one grid spacer (K/A^2)

W_T = The total coolant flow entering the orifice region per bundle.

W_6 = The coolant flow per bundle which flows through bypass path 6 (see Figure 4.3.1)

W_9 = The coolant flow per bundle which flows through bypass path 9.

W_c = In-channel coolant flow per bundle which is subject to convective and conductive heat transfer from the fuel.

ρ_{sat}, ρ_{in} = Saturation and inlet densities, respectively.

A_c = In-channel flow area per bundle.

A_o = Lower plenum flow area per bundle.

In a similar manner, the channel outlet form loss coefficient is calculated by:

$$K_{OUT} = \frac{A_c^2}{2}\left[(NG - 2) \cdot F_g + F_{up} \right] \quad \text{Eq. 4.3.3}$$

where:

F_{up} = The form loss coefficient per unit area squared for the channel upper structure (K/A^2)

and

NG = Total number of grids per channel.

Typical values for all pressure loss data can be found in References 3 and 4.

The bypass flow can be represented in two ways. The first approach represents the bypass region as a single flow channel. The effective form loss coefficient for this region is normally adjusted to give a total bypass fraction consistent with FIBWR reference calculations. The second approach is to input the bypass fraction as a function of core flow. This functional dependence is determined from FIBWR calculations at various points on the 100 percent rod line of the power-flow map. The single bypass path includes all flows that are not subject to heat transfer from the fuel.

It is general practice to evaluate all pressure loss coefficients at conditions representative of 100 percent power and flow. The flow splits between in-channel and bypass for other combinations of power and flow tend to be sufficiently proportional to those evaluated at rated conditions that no modifications to the effective form loss coefficients are required. This is not true, however, for very low flow conditions which approach natural circulation. At this point, the effective form loss coefficients are regenerated with new reference data.

4.3.3 In-Channel Void Distribution

Section 6 of Reference 2 provides a detailed description of the PRESTO-B void correlation. Detailed comparisons with FRIGG Loop data are presented in Section 11. The PRESTO-B comparisons with the FRIGG Loop measurements were generated with the input constants provided in Reference 2, Table 11.4. The CP&L steady-state BWR analysis model uses the slightly modified set of input constants shown in Reference 2, Table 6.1. The modified void parameters used by CP&L provide better agreement with plant data at low-flow conditions.

The low-flow modification of the PRESTO-B void model still shows good agreement with the FRIGG data. Analysis of the 31 cases shows an average bias of -1.13 percent void and a standard deviation of 2.2 percent void. The FRIGG Loop measurement uncertainty was estimated to be 2 percent void.

FIGURE 4.3.1

COOLANT FLOW PATHS FOR BWR GEOMETRY

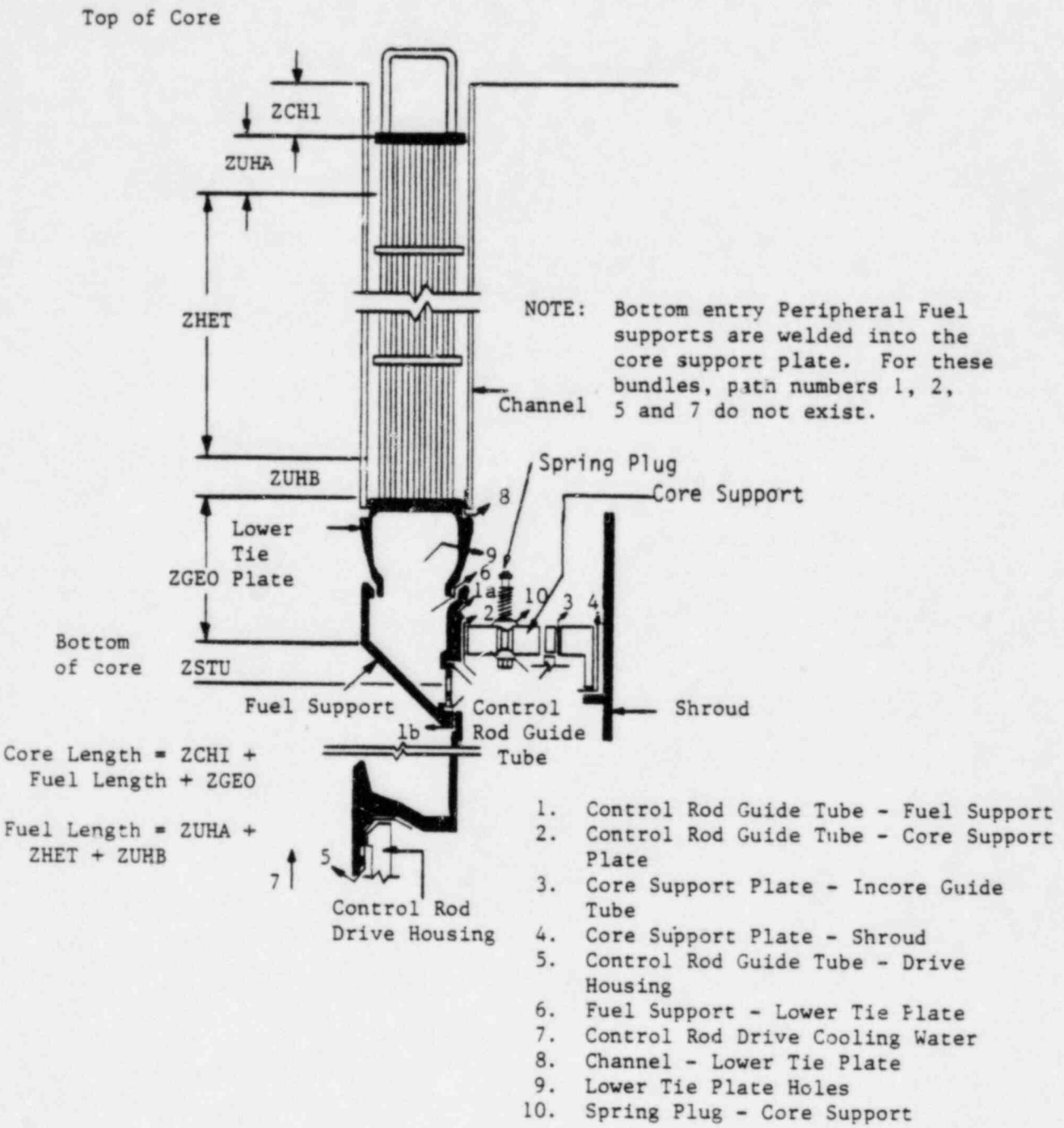

Figure 1-2. Fuel Bundle Geometry and Various Leakage Flow Paths

(From Reference 3)

4.4 Exposure Accounting

The exposure accounting techniques used in PRESTO are integral methods which are used to track cross sections based on the following independent variables:

1. Exposure
2. Void history
3. Control rod history
4. Control rod exposure

Representative two-group cross sections are generated by interpolation between conditions represented by the instantaneous state and the historical states of the fuel. A complete description of the integration process employed and cross section functional dependence is given in Reference 2.

PRESTO makes use of four exposure accounting methods which are used for different applications. A brief description of each of these follows.

4.4.1 Fixed Power Distribution Exposure Accounting

For exposure intervals of less than 500 MWD/MTU, the power distribution calculated at the beginning of the exposure interval is used to accumulate exposure during the interval. The previously cited variables are assumed constant during the interval. Beginning-of-step initial conditions are obtained from a previously generated PRESTO restart file. Updated values of the variables at the end of the exposure interval can be used to calculate the

power distribution at the final exposure. This method is typically employed when actual operating data is available at frequent exposures. The exposure accounting for the Brunswick Units 1 and 2 benchmark calculations was performed in this manner as are operations support and core follow calculations.

4.4.2 Iterative Power Distribution Exposure Accounting

For exposure intervals between 500 and 1500 MWD/MTU or when the power distribution is changing rapidly with exposure, an iterative exposure accounting method is used. This approach uses a weighted average of the power distribution at the beginning and the end of the step to establish average properties for exposure accounting. The first prediction of the power distribution at the end-of-step is based on a depletion using constant properties from beginning-of-step. A new exposure accounting is then generated using an average of the beginning of step and the predicted end-of-step power distributions. This provides the historical basis for a new power distribution calculation at the end of the interval. This method does not require that the control rod pattern or the thermal-hydraulic state of the reactor be the same at the beginning and end of the interval. The iterative exposure acccunting method can also be used with the various critical search options such as power, flow, and control rod pattern searches. This approach is very useful for studying coast-down operations where the power magnitude and distribution is changing rapidly with exposure, and is recommended for cycle management analysis where exposure steps of approximately 1000 MWD/MTU are used. The Quad-Cities benchmark analysis uses this method of exposure accounting.

4.4.3 Exposure Accounting Using Haling's Principle

PRESTO can perform exposure accounting according to the Haling principle (Reference 10) using either a fixed exposure interval or in conjunction with a critical eigenvalue search. The Haling principle is applied when it is desirable to define a representative cycle average power distribution or typical end-of-cycle conditions. The following are uses of the Haling power and exposure accounting principle:

1. Cycle length projections
2. Target end-of-cycle conditions for design and safety analysis
3. Characteristic hydraulic conditions for establishing PRESTO hydraulic input
4. Characteristic neutron leakage conditions for generation of cycle dependent boundary conditions
5. Evaluation of cycle average thermal limits for loading pattern development

4.4.4 Exposure Accounting Using Haling Backburns

Often it is desirable to develop approximate exposure accounting which would be independent of cycle specific control rod patterns. To do this, the Haling backburn method is employed. This approach uses an end-of-cycle Haling restart file and applies a single negative exposure interval towards beginning of cycle. In each case, the distribution of power and voids is given by the Haling principle at EOC conditions and is used to represent the average

properties over a burnup interval. Assuming that the base Haling iteration has completely converged, a negative burn back to beginning of cycle (BOC) would exactly reproduce the BOC historical state.

The exposure accounting which results from this method is most appropriate at the beginning and the end-of-cycle, with the greatest uncertainty at mid-cycle. For the Brunswick units, this method overpredicts the mid-cycle reactivity. This is because BWR's are recommended to operate with a power peak lower in the core for the first half of the cycle than is calculated using the Haling distribution. As a result, burning with a Haling power shape depletes the gadolinia at the top of the core more quickly than occurs in practice. The net result is a conservative estimate of mid-cycle reactivity for both hot operating and cold critical conditions.

This approach is useful in establishing the exposure accounting bases for the following:

1. First estimate of control rod patterns and control density
2. Shut-down margin bounding analysis
3. Rod drop and rod withdrawal error bounding analyses
4. Initial conditions for mid-cycle transient analysis
5. Standby liquid control system worth as a function of cycle exposure

5.0 Verification of PRESTO-B Core Simulations

The companion report, "Methods of PRESTO-B, A Three-Dimensional LWR Core Simulation Code" (Reference 2), provides a detailed evaluation of the performance verification which was conducted by Scandpower A/S. This evaluation includes the following:

A. Comparisons with IAEA standard neutronic problems.

B. Evaluation of the EOC-1 gamma scan measurements at Edwin I. Hatch BWR.

C. Results of core follow calculations for Cycle 1 of Edwin I. Hatch 1.

D. The results of European core follow calculations and gamma scan measurements.

E. Qualification of the hydraulic model against FRIGG loop data.

The purpose of Section 5 of this report is to provide supplementary justification in those areas not covered by the companion report and to demonstrate the ability of CP&L to provide high-quality simulations with PRESTO-B.

5.1 Description of Cores Modeled for the Benchmarking Report

The primary method of determining the accuracy of the PRESTO-B nodal simulator code (Reference 2) in BWR analysis is by comparison of its predictions to observed data from operating reactors. The two Brunswick BWR-4 units provide a large data base for comparison. These two units are sister plants with an identical geometry and power rating. The major differences involve flow orificing and fuel designs (i.e., mix of GE 7x7, 8x8, 8x8R). The third plant which was analyzed is Quad Cities Unit 1. This plant differs markedly in size and power density from the Brunswick units, and was chosen to allow comparison between PRESTO-B calculated and Quad Cities measured gamma scan data. Quad-Cities Unit 1 benchmarking has been presented as a standard problem in References 11, 12, and 13. Comparisons of calculated-to-measured reactor data provide additional insight into the quality of the overall BWR analysis (including lattice physics methods and analysis procedures).

PRESTO nodal simulation calculations will be compared to data recorded for the following reactor cores:

1. Brunswick Unit 1, Cycles 1, 2, and 3
2. Brunswick Unit 2, Cycles 4 and 5
3. Quad-Cities Unit 1, Cycles 1 and 2

The Quad-Cities Unit 1 reactor is substantially larger than the Brunswick units (724 versus 560 fuel assemblies); however, the power density is approximately 20 percent lower. Figure 5.1.1 and Figure 5.1.2 show the geometry of Brunswick and Quad-Cities cores, respectively. Table 5.1.1 contrasts the major features of the two reactor designs.

The three cycles of Brunswick Unit 1 operation have utilized GE 8x8, 8x8R, and P8x8R fuel. The Brunswick Unit 1 data base is well documented and contains a variety of off-nominal and test conditions as well as normal operations. This report will rely heavily on results from Brunswick 1 and will demonstrate Brunswick 2 results in order to show that a similar quality of projection is obtained.

Brunswick Unit 2 began operations before Brunswick Unit 1. The five cycles of Brunswick Unit 2 operation have utilized GE 7x7, 8x8, 8x8R, and P8x8R fuel. Cycle 4 includes a mixture of all of the previous fuel designs with gadolinia burnable poison. The Brunswick 2, Cycle 4, benchmarking will be reported in detail. Comparisons for Cycle 5 are included but limited to the available data. The exposure accounting used as the starting point for the Brunswick Unit 2, Cycle 4, benchmarking was taken from a preliminary PRESTO-B evaluation. The beginning data base is considered to be a good one, but was not subject to current design practices.

The Quad-Cities Unit 1, Cycle 1, core consisted of GE 7x7 fuel with gadolinia used as a burnable poison. Quad-Cities, Cycle 2, appears to have been an extension of Cycle 1 because only nine percent of the initial core was discharged. Reload 1 contains a mixture of 59 GE 7x7 and 8x8 fuel assemblies, with gadolinia burnable poison, and five mixed oxide test assemblies. Quad-Cities Unit 1, Cycles 1 and 2, made much more extensive use of control rods than has been observed in any cycle of Brunswick operations. In general, the Quad-Cities data base presents nuclear conditions which are not typical of Brunswick nominal conditions. The design information used for Quad-Cities

modeling was obtained from a variety of EPRI reports and private communications (References 14, 15, and 16).

TABLE 5.1.1

COMPARISON OF THE MAJOR FEATURES OF THE
BRUNSWICK AND QUAD CITIES REACTORS

	BRUNSWICK	QUAD CITIES
CORE DESCRIPTION		
NUMBER OF ASSEMBLIES	560	724
NUMBER BOTTOM ENTRY CONTROL RODS	137	177
EQUIVALENT CORE DIAMETER (IN.)	160.2	182.2
CORE POWER DENSITY (KW/L)	50.5	40.8
NUMBER OF ORIFICED PERIPHERAL ASSEMBLIES	76	84
NOMINAL OPERATING CONDITIONS		
CORE THERMAL POWER	2436 (MWth)	2511 (MWth)
RATED CORE FLOW	77 (Mlb/HR) 9.70E+3 (Kg/SEC)	98 (Mlb/HR) 1.23E+4 (Kg/SEC)
DOME PRESSURE	1035 (PSIA) 7.14 (MPA)	1050 (PSIA) 7.24 (MPA)

FIGURE 5.1.1

BRUNSWICK UNITS 1, 2 CORE GEOMETRY

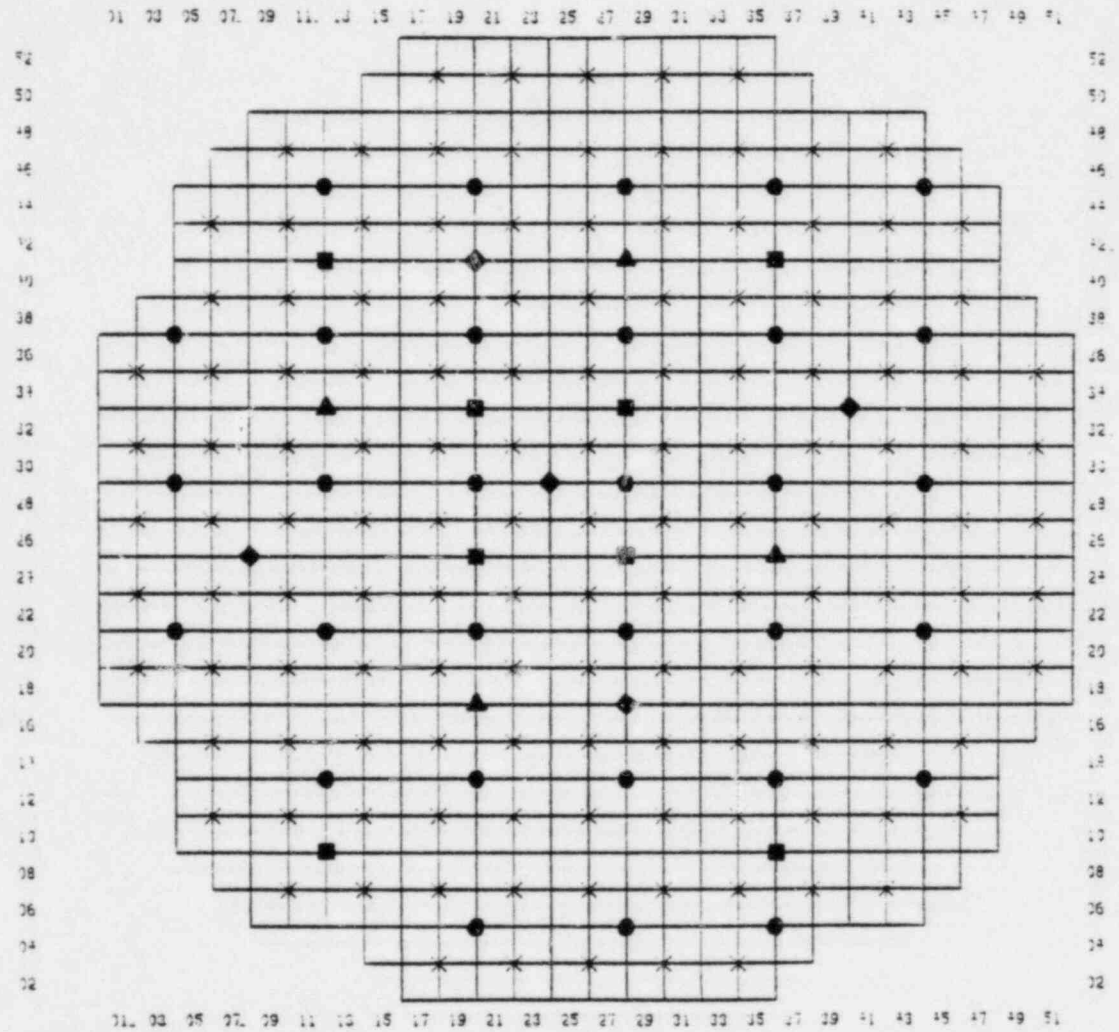

NUMBER OF FUEL ASSEMBLIES - 560

LOCAL POWER-RANGE MONITORS (31) ●

INTERMEDIATE-RANGE MONITORS (8) ■

SOURCE-RANGE MONITORS (4) ▲

NEUTRON SOURCES (5) ◆

CONTROL RODS (137) ×

FIGURE 5.1.2

QUAD CITIES UNIT 1 CORE GEOMETRY

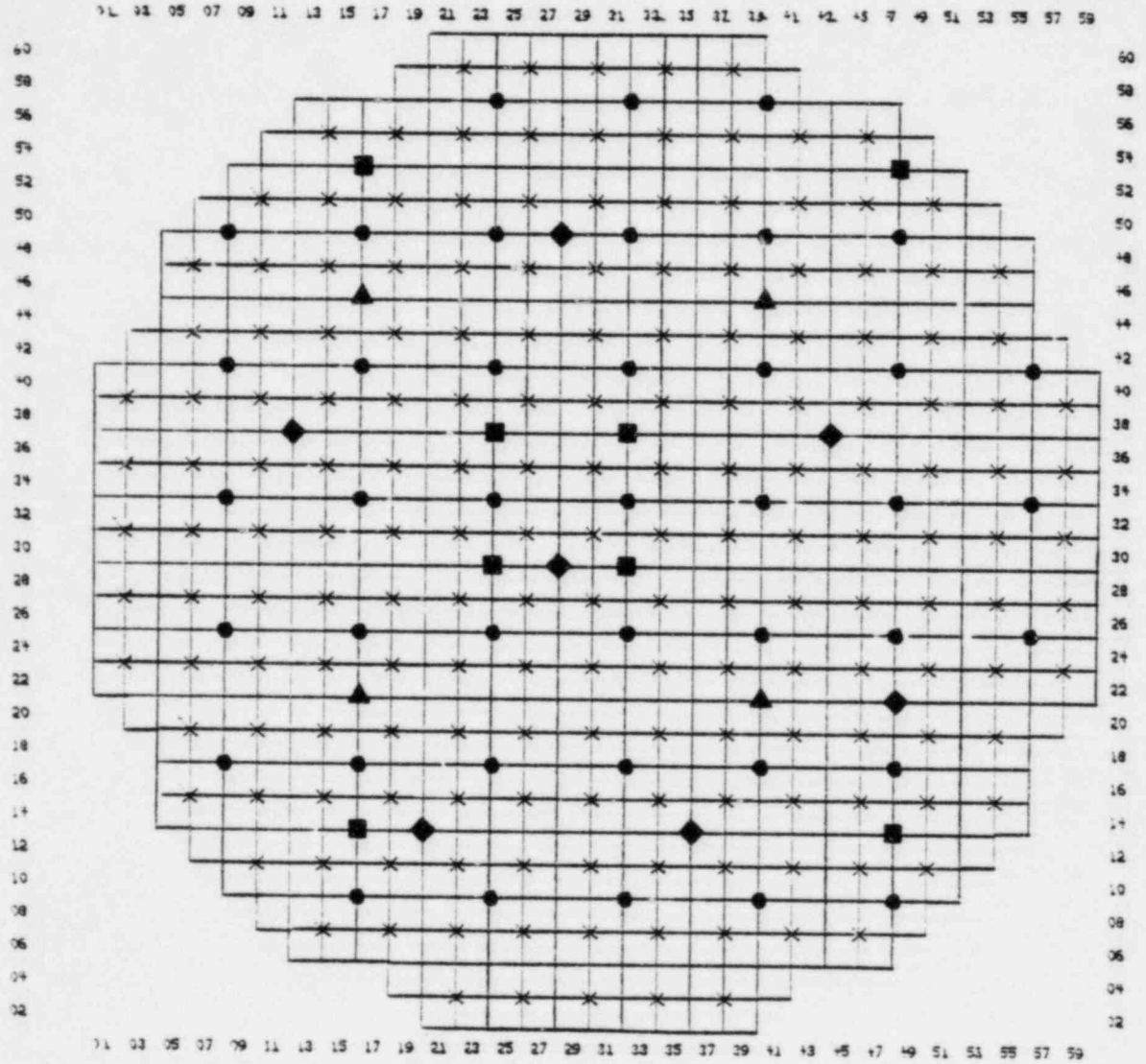

Number of Fuel Assemblies - 724

Local Power-Range Monitors (41) ●

Intermediate-Range Monitors (8) ■

Source-Range Monitors (4) ▲

Neutron Sources (7) ◆

Control Rods (177) ×

5.2 Comparison With Fine Mesh Calculations

Comparisons with fine-mesh, two-group calculations have been generated in order to determine the overall performance of the PRESTO-B neutron diffusion algorithm. The results of PRESTO-B benchmarking against 2-D and 3-D IAEA standard problems are shown in Reference 2, Section 11.

Additional studies were conducted which compare the results of PRESTO-B and PDQ-07 simulations against a series of two-group, two-dimensional problems. For each of these cases, a quarter-core, 2-D distribution of cross-sections was extracted from previous 3-D PRESTO-B calculations. PDQ-07 was then run using an 8x8 fine mesh for each PRESTO-B coarse-mesh node. The boundary region in the PDQ-07 problem was evaluated explicitly by using a large reflector region around the core. The PRESTO-B simulation used boundary conditions generated previously for core follow studies.

Table 5.2.1 presents a comparison of nodal and fine-mesh simulations for five different rod pattern configurations based on the Brunswick 2, Beginning-Of-Cycle 5, Control Cell Core loading. The following cases were run at cold conditions:

1. Single rod out near the core periphery (SR01).
2. Single rod out of the core interior (SR02).
3. Fifty percent control rod density in A sequence (A50).
4. Twenty-five percent control rod density in A sequence (A25).
5. All rods in (ARI).

For each case, a comparison between PRESTO-B and PDQ-07 eigenvalue and rod worth were made. Figures 5.2.1 through 5.2.5 also show the PDQ-07 and PRESTO-B predicted power distributions for each of these five cases. The purpose of this study was to demonstrate the PRESTO-B nodal method for a range of conditions which would be typical of cold critical configurations. Good overall agreement in eigenvalue and rod worth were obtained. It was observed that PRESTO-B overpredicted the power peaking and eigenvalue for those cases where large local flux gradients exist. Previous comparisons against fine mesh, five-group, four-bundle cell calculations (Reference 20) indicate that this is the correct trend.

Table 5.2.2 presents a comparison of nodal and fine mesh simulations for 11 different cold critical configurations analyzed for Brunswick 1, at End-Of-Cycle 3. The purpose of this study was to demonstrate PRESTO-B predictive capability for the analysis of shutdown margin with one or more fuel assemblies removed from the core, such as during fuel shuffle. For each of these cases, a comparison between PRESTO-B and PDQ-07 eigenvalue and rod worth was made. These calculations exhibited the same trends as those noted in the previous study. PRESTO conservatively overestimates rod worth by approximately $0.003\Delta K$.

Figures 5.2.6 through 5.2.8 present the comparisons of nodal and fine mesh simulations for three different hot-power configurations based on a Brunswick 2 Beginning-Of-Cycle-5 rod pattern. The purpose of this study was to demonstrate PRESTO-B predictive capability for conditions with a combination of voiding and control rods. The three cases are representative

of three different axial levels within the core, hence, three different void distributions. This is considered to be a severe test of the PRESTO-B nodal method for prediction of nominal operations. These results show excellent overall agreement on power distribution and eigenvalue, with a slight underprediction of the power in rodded assemblies.

TABLE 5.2.1

COMPARISON of PRESTO-B and PDQ07 TWO-DIMENSIONAL CALCULATIONS

for SELECT BRUNSWICK 2, CYCLE 5 COLD ZERO-POWER ROD PATTERNS

CASE	KEFF (PDQ07)	KEFF (PRESTO-B)	DIFFERENCE (PRESTO-PDQ)	RODWORTH* (PDQ07)	RODWORTH* (PRESTO-B)	DIFFERENCE (PRESTO-PDQ)
SR01	1.00906	1.01280	0.00374	0.03110	0.03454	0.00344
SR02	1.00170	1.00450	0.00280	0.02378	0.02632	0.00254
A50	1.06455	1.06710	0.00255	0.08463	0.08677	0.00214
A25	1.02808	1.03160	0.00352	0.04978	0.05294	0.00316
ARI	0.97816	0.97841	0.00025	-------	-------	-------
AVERAGE			0.00257			0.00282

*RODWORTH = ln(K-ROD / K-ARI)

TABLE 5.2.2

PRESTO-B VS. PDQ07 KEFF RESULTS FOR 11 PARTIAL CORE COLD CALCULATIONS IN BRUNSWICK 1 CYCLE 3

CASE	DESCRIPTION	PRESTO-2D	PDQ07	DIFFERENCE (PRESTO-PDQ)
1	ALL RODS IN (ARI)	0.96065	0.96069	-.00004
2	ALL RODS OUT (ARO)	1.12010	1.12014	-.00004
	TOTAL ROD WORTH	0.15945	0.15945	-.00000
3	ARI, H2O @ 29-24	0.95762	0.95767	-.00005
4	ARI, H2O @ 27-26	0.93781	0.95785	-.00004
5	ARI, H2O @ 41-26,27-12	0.95469	0.95545	-.00076
6	ARI, H2O @ 41-26,27-12 43-26,27-10	0.95330	0.95368	-.00038
7	STRONGEST ROD OUT (SRO) H2O @ 29-24	0.99335	0.99066	.00269
	SRO ROD WORTH	0.03573	0.03299	.00274
8	SRO, H2O @ 27-26	0.99336	0.99067	.00269
	SRO ROD WORTH	0.03555	0.03282	.00273
9	SRO, H2O @ 41-26,27-12	0.99330	0.99061	.00269
	SRO ROD WORTH	0.03861	0.03516	.00345
10	SRO, H2O @ 41-26,27-12 43-26,27-10	0.99327	0.99057	.00270
	SRO ROD WORTH	0.03997	0.03689	.00308
11	SRO, H2O @ 27-26 (CENTER ROD IN)	0.99336	0.99067	.00269

FIGURE 5.2.1
COMPARISON OF PRESTO-B NODAL AND
PDQ07 FINE MESH POWER DISTRIBUTION
FOR B2C5 COLD CRITICAL CASE SR01

	27	29	31	33	35	37	39	41	43	45	47	49	51
26	.06 .08 -2	.08 .10 -2	.10 .12 -2	.12 .15 -3	.16 .19 -3	.21 .24 -3	.20 .24 -4	.22 .24 -2	.25 .28 -3	.21 .24 -3	.14 .17 -3	.11 .13 -2	.05 .06 -1
24	.08 .10 -2	.10 .12 -2	.12 .15 -3	.16 .19 -3	.21 .25 -4	.24 .27 -3	.28 .32 -4	.29 .32 -3	.30 .33 -3	.23 .26 -3	.18 .20 -2	.14 .15 -1	.08 .07 -1
22	.10 .13 -3	.14 .17 -3	.17 .20 -3	.25 .29 -4	.28 .32 -4	.36 .40 -4	.41 .45 -3	.48 .51 -3	.41 .44 -3	.36 .39 -3	.25 .28 -3	.18 .20 -2	.08 .09 -1
20	.12 .15 -3	.16 .20 -4	.25 .29 -4	.30 .35 -5	.45 .50 -5	.53 .58 -5	.70 .75 -5	.72 .75 -3	.67 .70 -3	.54 .58 -4	.39 .43 -4	.25 .28 -3	.10 .12 -2
18	.17 .20 -3	.22 .26 -4	.29 .33 -4	.45 .50 -5	.58 .64 -6	.86 .93 -7	1.05 1.09 -4	1.39 1.38 1	1.33 1.31 2	.99 1.01 -2	.57 .62 -5	.30 .34 -4	.11 .14 -3
16	.22 .25 -3	.24 .28 -4	.36 .41 -5	.52 .58 -6	.84 .91 -7	1.16 1.24 -8	1.75 1.80 -5	2.10 2.07 3	2.14 2.11 3	1.44 1.47 -3	.91 .95 -4	.41 .48 -7	
14	.21 .24 -3	.29 .32 -3	.40 .44 -4	.69 .73 -4	1.03 1.08 -5	1.71 1.77 -6	2.65 2.71 -6	4.19 4.06 13	3.75 3.68 7	2.47 2.51 -4	1.14 1.13 1		
12	.21 .24 -3	.29 .32 -3	.47 .50 -3	.69 .72 -3	1.37 1.38 -1	2.10 2.08 2	4.19 4.07 12	8.00 7.20 80	8.39 7.52 87	4.09 3.96 13	1.47 1.42 5		
10	.25 .28 -3	.30 .33 -3	.41 .44 -3	.66 .70 -4	1.34 1.32 2	2.18 2.15 3	3.77 3.70 7	8.35 7.50 85	8.64 7.94 70	3.95 3.99 -4	1.42 1.42 0		
08	.21 .24 -3	.24 .27 -3	.37 .40 -3	.55 .58 -3	1.00 1.03 -3	1.46 1.51 -5	2.49 2.54 -5	4.10 3.99 11	3.89 3.96 -7	2.72 2.81 -9			
06	.14 .17 -3	.18 .21 -3	.25 .28 -3	.39 .43 -4	.58 .63 -5	.96 1.01 -5	1.24 1.24 0	1.57 1.52 5	1.48 1.48 0				
04	.12 .13 -1	.14 .15 -1	.18 .20 -2	.25 .28 -3	.28 .32 -4	.43 .51 -8							
02	.05 .06 -1	.06 .07 -1	.08 .09 -1	.10 .12 -2	.11 .14 -3								

PRESTO
PDQ
DELTA * 100

KEFF(PRESTO-B)=1.01280
KEFF(PDQ) =1.00906

FIGURE 5.2.2
COMPARISON OF PRESTO-B NODAL AND
PDQ07 FINE MESH POWER DISTRIBUTION
FOR B2C5 COLD CRITICAL CASE SR02

	27	29	31	33	35	37	39	41	43	45	47	49	51
26	.44 .49 -5	.56 .62 -6	.70 .76 -6	.90 .96 -6	1.20 1.23 -3	1.53 1.52 1	1.34 1.37 -3	1.18 1.22 -4	1.15 1.18 -3	.85 .89 -4	.50 .55 -5	.35 .37 -2	.15 .17 -2
24	.51 .56 -5	.63 .68 -5	.86 .92 -6	1.15 1.19 -4	1.62 1.65 -3	1.81 1.79 2	1.89 1.87 2	1.50 1.52 -2	1.24 1.29 -3	.81 .85 -4	.53 .57 -4	.37 .38 -1	.16 .16 0
22	.57 .61 -4	.81 .86 -5	1.04 1.08 -4	1.65 1.68 -3	2.11 2.13 -2	2.94 2.87 7	2.82 2.75 7	2.24 2.24 0	1.39 1.41 -2	.96 .98 -2	.56 .58 -2	.37 .38 -1	.16 .17 -1
20	.59 .63 -4	.81 .84 -3	1.31 1.33 -2	1.79 1.77 2	3.14 3.04 10	5.20 4.69 51	5.62 5.01 61	2.80 2.71 9	1.62 1.60 2	.99 .99 0	.61 .63 -2	.38 .38 0	.16 .16 0
18	.65 .69 -4	.88 .91 -3	1.17 1.19 -2	1.97 1.92 5	2.90 2.82 8	5.65 5.07 58	5.21 4.67 54	3.20 3.08 12	1.94 1.84 10	1.12 1.09 3	.58 .58 0	.31 .32 -1	.13 .14 -1
16	.67 .71 -4	.73 .77 -1	1.04 1.08 -4	1.44 1.47 -3	2.22 2.24 -2	2.80 2.73 7	2.92 2.85 7	2.03 2.05 -2	1.46 1.47 -1	.84 .86 -2	.53 .54 -1	.29 .30 -1	
14	.49 .54 -5	.62 .67 -5	.77 .82 -5	1.12 1.17 -5	1.38 1.40 -2	1.71 1.69 2	1.64 1.64 0	1.47 1.49 -2	.99 1.02 -3	.65 .68 -3	.33 .35 -2		
12	.38 .43 -5	.46 .51 -5	.63 .67 -4	.71 .76 -5	1.04 1.06 -2	1.04 1.05 -1	1.13 1.14 -1	1.01 1.03 -2	.81 .84 -3	.54 .56 -2	.23 .24 -1		
10	.37 .40 -3	.39 .43 -4	.41 .45 -4	.49 .53 -4	.69 .71 -2	.71 .74 -3	.66 .69 -3	.70 .72 -2	.59 .63 -4	.38 .41 -3	.16 .17 -1		
08	.27 .30 -3	.25 .29 -4	.31 .33 -2	.33 .36 -3	.43 .45 -2	.40 .43 -3	.40 .43 -3	.42 .44 -2	.34 .37 -3	.25 .27 -2			
06	.16 .19 -3	.17 .20 -3	.18 .21 -3	.21 .24 -3	.23 .24 -1	.25 .27 -2	.21 .22 -1	.18 .19 -1	.14 .15 -1				
04	.12 .13 -1	.12 .13 -1	.13 .14 -1	.13 .14 -1	.11 .12 -1	.13 .14 -1							
02	.05 .06 -1	.05 .06 -1	.05 .06 -1	.05 .06 -1	.05 .06 -1								

PRESTO
PDQ
DELTA * 100

KEFF(PRESTO-B)=1.00450
KEFF(PDQ) =1.00170

FIGURE 5.2.3
COMPARISON OF PRESTO-B NODAL AND
PDQ07 FINE MESH POWER DISTRIBUTION
FOR B2C5 COLD CRITICAL CASE A50

	27	29	31	33	35	37	39	41	43	45	47	49	51
26	.85 .89 -4	1.27 1.26 1	1.32 1.32 0	1.04 1.10 -6	1.16 1.21 -5	1.74 1.69 5	1.49 1.49 0	1.02 1.07 -5	1.11 1.11 0	1.24 1.18 6	.87 .85 2	.51 .49 2	.21 .22 -1
24	1.26 1.26 0	1.02 1.06 -4	1.13 1.19 -6	1.61 1.58 3	1.76 1.73 3	1.22 1.26 -4	1.19 1.25 -6	1.42 1.39 3	1.43 1.37 6	.82 .85 -3	.62 .63 -1	.63 .59 4	.32 .29 3
22	1.37 1.36 1	1.26 1.31 -5	1.27 1.31 -4	1.93 1.90 3	1.75 1.72 3	1.30 1.36 -6	1.17 1.22 -5	1.55 1.51 4	1.27 1.23 4	.82 .83 -1	.56 .58 -2	.58 .55 3	.30 .28 2
20	1.08 1.14 -6	1.68 1.64 4	1.97 1.94 3	1.35 1.41 -6	1.46 1.51 -5	1.72 1.70 2	1.75 1.71 4	1.08 1.12 -4	.87 .91 -4	.94 .93 1	.74 .73 1	.41 .41 0	.17 .17 0
18	1.26 1.30 -4	1.86 1.83 3	1.80 1.77 3	1.48 1.53 -5	1.34 1.40 -6	1.85 1.82 3	1.62 1.59 3	1.21 1.25 -4	1.00 1.02 -2	1.00 .97 3	.65 .64 1	.28 .29 -1	.11 .12 -1
16	1.85 1.79 6	1.28 1.32 -4	1.35 1.41 -6	1.73 1.71 2	1.81 1.79 2	1.22 1.27 -5	1.18 1.23 -5	1.34 1.32 2	1.21 1.19 2	.64 .66 -2	.41 .43 -2	.21 .23 -2	
14	1.55 1.54 1	1.23 1.29 -6	1.20 1.24 -4	1.73 1.70 3	1.60 1.57 3	1.15 1.20 -5	1.03 1.08 -5	1.36 1.33 3	1.06 1.04 2	.59 .60 -1	.29 .29 0		
12	1.03 1.07 -4	1.45 1.42 3	1.57 1.52 5	1.05 1.09 -4	1.20 1.24 -4	1.34 1.32 2	1.36 1.33 3	.94 .96 -2	.79 .81 -2	.75 .70 5	.37 .34 3		
10	1.13 1.13 0	1.45 1.39 6	1.29 1.24 5	.87 .91 -4	1.01 1.02 -1	1.24 1.21 3	1.07 1.05 2	.79 .81 -2	.68 .69 -1	.65 .60 5	.33 .29 4		
08	1.26 1.19 7	.84 .86 -2	.84 .85 -1	.95 .94 1	1.02 .98 4	.65 .68 -3	.59 .61 -2	.75 .71 4	.64 .60 4	.37 .38 -1			
06	.89 .86 3	.63 .64 -1	.57 .59 -2	.75 .74 1	.66 .64 2	.42 .45 -3	.31 .32 -1	.41 .36 5	.35 .31 4				
04	.52 .50 2	.65 .59 6	.60 .56 4	.41 .41 0	.26 .27 -1	.22 .24 -2							
02	.21 .21 0	.31 .29 2	.30 .27 3	.17 .17 0	.11 .12 -1								

PRESTO
PDQ
DELTA * 100

KEFF(PRESTO-B)=1.06710
KEFF(PDQ) =1.06455

FIGURE 5.2.4
COMPARISON OF PRESTO-B NODAL AND
PDQ07 FINE MESH POWER DISTRIBUTION
FOR B2C5 COLD CRITICAL CASE A25

	27	29	31	33	35	37	39	41	43	45	47	49	51
26	.87 .92 -5	1.50 1.44 6	1.51 1.47 4	1.01 1.07 -6	1.16 1.21 -5	2.05 1.94 11	1.77 1.73 4	1.04 1.10 -6	1.10 1.13 -3	1.45 1.37 8	1.05 1.04 1	.54 .55 -1	.21 .21 0
24	.87 .94 -7	1.06 1.10 -4	1.13 1.19 -6	1.00 1.08 -8	1.14 1.22 -8	1.25 1.29 -4	1.24 1.30 -6	.93 1.01 -8	.91 .97 -6	.81 .86 -5	.66 .70 -4	.45 .47 -2	.18 .20 -2
22	.98 1.05 -7	1.38 1.42 -4	1.33 1.37 -4	1.28 1.37 -9	1.16 1.24 -8	1.37 1.42 -5	1.25 1.30 -5	1.04 1.12 -8	.80 .86 -6	.81 .84 -3	.60 .64 -4	.41 .44 -3	.17 .19 -2
20	1.20 1.25 -5	2.12 2.00 12	2.46 2.33 13	1.45 1.49 -4	1.56 1.60 -4	2.13 2.04 9	2.19 2.08 11	1.16 1.20 -4	.89 .94 -5	1.13 1.10 3	.95 .93 2	.47 .48 -1	.18 .18 0
18	1.36 1.38 -2	2.33 2.21 12	2.24 2.12 12	1.59 1.62 -3	1.44 1.48 -4	2.30 2.20 10	2.03 1.94 9	1.33 1.36 -3	1.06 1.07 -1	1.24 1.17 7	.89 .86 3	.38 .40 -2	.15 .16 -1
16	1.27 1.32 -5	1.37 1.39 -2	1.45 1.48 -3	1.18 1.26 -8	1.24 1.32 -8	1.31 1.35 -4	1.30 1.34 -4	.95 1.01 -6	.81 .87 -6	.68 .70 -2	.54 .56 -2	.30 .33 -3	
14	1.03 1.09 -6	1.30 1.33 -3	1.25 1.28 -3	1.15 1.21 -6	1.06 1.12 -6	1.21 1.25 -4	1.11 1.15 -4	.94 .99 -5	.69 .73 -4	.61 .61 0	.37 .37 0		
12	1.09 1.10 -1	1.78 1.66 12	1.93 1.78 15	1.10 1.11 -1	1.26 1.28 -2	1.65 1.57 8	1.70 1.60 10	1.02 1.02 0	.84 .83 1	.93 .81 12	.51 .43 8		
10	1.24 1.20 4	1.82 1.65 17	1.63 1.49 14	.96 .98 -2	1.12 1.10 2	1.57 1.48 9	1.38 1.31 7	.91 .91 0	.75 .75 0	.83 .71 12	.48 .38 10		
08	.87 .87 0	.90 .90 0	.92 .90 2	.68 .70 -2	.72 .74 -2	.71 .72 -1	.66 .68 -2	.55 .57 -2	.43 .46 -3	.40 .40 0			
06	.55 .56 -1	.64 .62 2	.59 .58 1	.48 .50 -2	.40 .41 -1	.41 .42 -1	.31 .31 0	.23 .24 -1	.17 .19 -2				
04	.50 .46 4	.75 .63 12	.70 .60 10	.40 .37 3	.23 .22 1	.21 .22 -1							
02	.25 .23 2	.40 .33 7	.38 .32 6	.19 .19 0	.12 .11 1								

PRESTO
PDQ
DELTA * 100

KEFF(PRESTO-B)=1.03160
KEFF(PDQ) =1.02808

FIGURE 5.2.5
COMPARISON OF PRESTO-B NODAL AND
PDQ07 FINE MESH POWER DISTRIBUTION
FOR B2C5 COLD CRITICAL CASE ARI

	27	29	31	33	35	37	39	41	43	45	47	49	51
26	.96 1.00 -4	1.11 1.12 -1	1.12 1.15 -3	1.15 1.19 -4	1.27 1.29 -2	1.44 1.43 1	1.21 1.24 -3	1.15 1.16 -1	1.27 1.23 4	1.06 1.03 3	.70 .71 -1	.55 .52 3	.26 .25 1
24	1.11 1.13 -2	1.18 1.20 -2	1.28 1.31 -3	1.32 1.34 -2	1.47 1.48 -1	1.35 1.36 -1	1.34 1.36 -2	1.20 1.20 0	1.20 1.18 2	.91 .91 0	.70 .70 0	.55 .52 3	.25 .24 1
22	1.18 1.21 -3	1.44 1.45 -1	1.41 1.43 -2	1.63 1.64 -1	1.47 1.49 -2	1.48 1.49 -1	1.33 1.35 -2	1.33 1.33 0	1.07 1.07 0	.93 .92 1	.65 .66 -1	.51 .49 2	.24 .23 1
20	1.22 1.25 -3	1.40 1.41 -1	1.67 1.69 -2	1.56 1.57 -1	1.71 1.71 0	1.49 1.51 -2	1.51 1.51 0	1.25 1.26 -1	1.04 1.05 -1	.84 .85 -1	.65 .65 0	.48 .46 2	.22 .21 1
18	1.41 1.42 -1	1.58 1.59 -1	1.53 1.55 -2	1.73 1.72 1	1.58 1.59 -1	1.64 1.65 -1	1.41 1.42 -1	1.46 1.44 2	1.24 1.20 4	.93 .91 2	.59 .59 0	.38 .37 1	.18 .17 1
16	1.58 1.57 1	1.45 1.45 0	1.55 1.56 -1	1.51 1.52 -1	1.61 1.62 -1	1.43 1.45 -2	1.41 1.42 -1	1.22 1.23 -1	1.10 1.10 0	.77 .77 0	.57 .56 1	.35 .34 1	
14	1.30 1.32 -2	1.42 1.43 -1	1.38 1.39 -1	1.51 1.51 0	1.40 1.40 0	1.38 1.40 -2	1.25 1.27 -2	1.24 1.24 0	.95 .96 -1	.71 .71 0	.40 .39 1		
12	1.17 1.18 -1	1.24 1.25 -1	1.37 1.36 1	1.22 1.23 -1	1.45 1.43 2	1.22 1.23 -1	1.25 1.25 0	1.16 1.14 2	1.01 1.00 1	.71 .70 1	.32 .31 1		
10	1.32 1.28 4	1.25 1.22 3	1.10 1.09 1	1.04 1.05 -1	1.25 1.21 4	1.12 1.12 0	.96 .97 -1	1.01 1.00 1	.88 .89 -1	.58 .59 -1	.25 .25 0		
08	1.09 1.06 3	.94 .94 0	.97 .95 2	.86 .86 0	.95 .93 2	.79 .79 0	.73 .73 0	.72 .71 1	.58 .59 -1	.44 .43 1			
06	.73 .73 0	.73 .72 1	.68 .68 0	.67 .67 0	.61 .60 1	.60 .59 1	.44 .43 1	.35 .34 1	.27 .27 0				
04	.58 .54 4	.57 .53 4	.54 .51 3	.49 .47 2	.36 .35 1	.37 .36 1							
02	.26 .25 1	.25 .24 1	.24 .23 1	.22 .21 1	.18 .18 0								

PRESTO
PDQ
DELTA * 100

KEFF(PRESTO-B)=0.97841
KEFF(PDQ) =0.97816

FIGURE 5.2.6
COMPARISON OF PRESTO-B NODAL AND
PDQ07 FINE MESH POWER DISTRIBUTION FOR B2C5
BOC HOT POWER OPERATION
AXIAL PLANE 03; VOID=0.6%

	27	29	31	33	35	37	39	41	43	45	47	49	51
26	.45 .48 -6.3	.78 .76 2.6	.85 .83 2.4	.47 .51 -7.8	.53 .57 -7.0	1.00 .98 2.0	1.09 1.09 0.0	.64 .70 -8.6	.91 .97 -6.2	1.52 1.49 2.0	1.38 1.38 0.0	.77 .80 -3.8	.29 .33 -12.1
24	.82 .79 3.8	.96 .93 3.2	.99 .95 4.2	.93 .92 1.1	.97 .95 2.1	1.19 1.17 1.7	1.25 1.22 2.5	1.28 1.27 0.8	1.47 1.45 1.4	1.60 1.60 0.0	1.66 1.62 2.5	1.21 1.16 4.3	.51 .50 2.0
22	.86 .84 2.4	1.01 .97 4.1	1.03 1.00 3.0	.96 .94 2.1	1.05 1.04 1.0	1.23 1.20 2.5	1.34 1.32 1.5	1.36 1.34 1.5	1.39 1.38 0.7	1.61 1.58 1.9	1.55 1.56 -0.6	1.28 1.27 0.8	.58 .59 -1.7
20	.49 .52 -5.8	.93 .91 2.2	.95 .93 2.2	.56 .60 -6.7	.70 .74 -5.4	1.17 1.17 0.0	1.31 1.29 1.6	.73 .78 -6.4	.74 .80 -7.5	1.39 1.40 -0.7	1.54 1.54 0.0	1.17 1.17 0.0	.52 .53 -1.9
18	.51 .54 -5.6	.95 .93 2.2	1.02 1.01 1.0	.68 .73 -6.9	.61 .66 -7.6	1.12 1.11 0.9	1.23 1.23 0.0	.85 .91 -6.6	.91 .96 -5.2	1.36 1.34 1.5	1.19 1.22 -2.5	.71 .74 -4.1	.40 .41 -2.4
16	.97 .95 2.1	1.14 1.13 0.9	1.14 1.11 2.7	1.14 1.14 0.0	1.13 1.12 0.9	1.29 1.29 0.0	1.27 1.25 1.6	1.26 1.27 -0.8	1.31 1.30 0.8	1.22 1.21 0.8	.89 .90 -1.1	.55 .54 1.9	
14	1.07 1.07 0.0	1.18 1.15 2.6	1.30 1.29 0.8	1.30 1.28 1.6	1.22 1.22 0.0	1.25 1.23 1.6	1.35 1.35 0.0	1.29 1.28 0.8	1.15 1.15 0.0	1.16 1.11 4.5	.65 .62 4.8		
12	.67 .72 -6.9	1.28 1.27 0.8	1.34 1.31 2.3	.72 .77 -6.5	.84 .90 -6.7	1.24 1.26 -1.6	1.30 1.29 0.8	.75 .80 -6.3	.65 .69 -5.8	.84 .80 5.0	.46 .46 0.0		
10	.93 .98 -5.1	1.56 1.53 2.0	1.40 1.40 0.0	.73 .79 -7.6	.89 .95 -6.3	1.29 1.28 0.8	1.14 1.13 0.9	.65 .69 -5.8	.53 .56 -5.4	.62 .58 6.9	.32 .31 3.2		
08	1.62 1.58 2.5	1.65 1.65 0.0	1.65 1.62 1.9	1.39 1.39 0.0	1.32 1.31 0.8	1.20 1.19 0.8	1.12 1.07 4.7	.75 .73 2.7	.57 .55 3.6	.35 .32 9.4			
06	1.43 1.44 -0.7	1.71 1.67 2.4	1.57 1.58 -0.7	1.52 1.53 -0.7	1.16 1.19 -2.5	.93 .93 0.0	.62 .59 5.1	.40 .40 0.0	.28 .28 0.0				
04	.81 .84 -3.6	1.23 1.18 4.2	1.31 1.30 0.8	1.14 1.13 0.9	.62 .65 -4.6	.51 .50 2.0							
02	.29 .33 -12.1	.53 .51 3.9	.59 .59 0.0	.50 .51 -2.0	.36 .38 -5.3								

PRESTO-B
PDQ
% DIFF

KEFF(PRESTO-B) = 1.02360
KEFF(PDQ07) = 1.01993

FIGURE 5.2.7
COMPARISON OF PRESTO-B NODAL AND
PDQ07 FINE MESH POWER DISTRIBUTION FOR B2C5
BOC HOT POWER OPERATION
AXIAL PLANE 12; VOID=48.3%

	27	29	31	33	35	37	39	41	43	45	47	49	51
26	.66 .70 -5.7	.97 .95 2.1	1.10 1.10 0.0	1.04 1.05 -1.0	1.07 1.09 -1.8	1.16 1.17 -0.9	1.13 1.12 0.9	.76 .80 -5.0	.83 .84 -3.5	1.15 1.14 0.9	1.12 1.14 -1.8	1.05 1.03 1.9	.63 .63 0.0
24	.97 .96 1.0	1.08 1.06 1.9	1.10 1.10 0.0	1.14 1.15 -0.9	1.16 1.17 -0.9	1.21 1.21 0.0	1.20 1.19 0.8	1.18 1.17 0.9	1.21 1.20 0.8	1.20 1.21 -0.8	1.21 1.20 0.8	1.02 1.00 2.0	.59 .60 -1.7
22	1.09 1.09 2.4	1.13 1.13 4.1	1.12 1.10 3.0	1.10 1.09 2.1	1.13 1.11 1.0	1.20 1.19 2.5	1.29 1.28 1.5	1.34 1.35 1.5	1.30 1.31 0.7	1.28 1.29 1.9	1.16 1.17 -0.6	1.01 1.00 0.8	.57 .58 -1.7
20	1.01 1.03 -1.9	1.12 1.12 0.0	1.08 1.07 0.9	.74 .77 -3.9	.83 .87 -4.6	1.19 1.18 0.9	1.35 1.37 -1.5	1.30 1.32 -1.5	1.28 1.30 -1.5	1.28 1.30 -1.5	1.19 1.21 -1.7	.94 .94 0.0	.52 .53 -1.9
18	1.03 1.04 -1.0	1.11 1.12 -0.9	1.09 1.07 1.9	.82 .85 -3.5	.78 .81 -3.7	1.18 1.17 0.9	1.33 1.34 -0.8	1.46 1.47 -0.7	1.46 1.46 0.0	1.30 1.32 -1.5	1.06 1.08 -1.9	.75 .77 -2.6	.47 .48 -2.1
16	1.11 1.11 0.0	1.15 1.14 0.9	1.12 1.11 0.9	1.13 1.12 0.9	1.15 1.14 0.9	1.23 1.22 0.8	1.24 1.24 0.0	1.32 1.33 -0.8	1.33 1.34 -0.8	1.15 1.15 0.0	.90 .92 -2.2	.62 .62 0.0	
14	1.05 1.04 1.0	1.10 1.09 0.9	1.19 1.18 0.9	1.25 1.25 0.0	1.25 1.25 0.0	1.20 1.20 0.0	1.22 1.21 0.8	1.19 1.18 0.9	1.10 1.08 1.9	1.06 1.03 2.9	.67 .66 1.5		
12	.69 .73 -5.5	1.08 1.06 1.9	1.22 1.22 0.0	1.15 1.15 0.0	1.30 1.30 0.0	1.23 1.23 0.0	1.14 1.13 0.9	.77 .81 -4.9	.73 .76 -4.0	.84 .81 3.7	.51 .51 0.0		
10	.74 .77 -3.9	1.10 1.08 1.9	1.17 1.16 0.9	1.11 1.13 -1.8	1.27 1.26 0.8	1.20 1.21 -0.8	1.03 1.01 2.0	.70 .72 -2.8	.64 .66 -3.0	.70 .66 6.1	.41 .41 0.0		
08	1.04 1.02 2.0	1.08 1.07 0.9	1.13 1.13 0.0	1.13 1.14 -0.9	1.14 1.15 -0.9	1.04 1.04 0.0	.98 .94 4.3	.78 .75 4.0	.69 .64 7.8	.45 .43 4.7			
06	1.01 1.01 0.0	1.08 1.07 0.9	1.03 1.03 0.0	1.06 1.07 -0.9	.95 .95 0.0	.84 .85 -1.2	.62 .61 1.6	.48 .48 0.0	.40 .39 2.6				
04	.95 .92 3.2	.93 .90 3.3	.90 .88 2.3	.84 .83 1.2	.65 .65 0.0	.55 .55 0.0							
02	.56 .55 1.8	.54 .53 1.9	.52 .52 0.0	.47 .47 0.0	.42 .43 -2.3								

PRESTO-B
PDQ
% DIFF

KEFF(PRESTO-B) = 1.00070
KEFF(PDQ07) = 0.99974

FIGURE 5.2.8
COMPARISON OF PRESTO-B NODAL AND
PDQ07 FINE MESH POWER DISTRIBUTION FOR B2C5
BOC HOT POWER OPERATION
AXIAL PLANE 22; VOID=66.1%

	27	29	31	33	35	37	39	41	43	45	47	49	51
26	.68 .69 -1.5	1.07 1.01 5.9	1.13 1.10 2.7	1.21 1.19 1.7	1.29 1.27 1.6	1.45 1.43 1.4	1.40 1.39 0.7	1.48 1.48 0.0	1.52 1.51 0.7	1.40 1.40 0.0	1.09 1.11 -1.8	.99 .98 1.0	.64 .66 -3.0
24	1.05 1.00 5.0	1.11 1.05 5.7	1.19 1.16 2.6	1.19 1.16 2.6	1.33 1.31 1.5	1.30 1.27 2.4	1.42 1.43 -0.7	1.38 1.37 0.7	1.45 1.46 -0.7	1.22 1.23 -0.8	1.09 1.11 -1.8	.95 .94 1.1	.61 .63 -3.2
22	1.14 1.11 2.7	1.28 1.24 3.2	1.16 1.10 5.5	1.23 1.18 4.2	1.14 1.10 3.6	1.29 1.27 1.6	1.28 1.27 0.8	1.41 1.41 0.0	1.26 1.26 0.0	1.22 1.24 -1.6	.99 1.00 -1.0	.89 .89 0.0	.57 .59 -3.4
20	1.20 1.19 0.8	1.20 1.17 2.6	1.23 1.19 3.4	.76 .79 -3.8	.81 .83 -2.4	1.13 1.09 3.7	1.30 1.30 0.0	1.24 1.25 -0.8	1.19 1.21 -1.7	1.06 1.07 -0.9	.96 .99 -3.0	.80 .81 -1.2	.51 .53 -3.8
18	1.32 1.30 1.5	1.35 1.33 1.5	1.15 1.10 4.6	.81 .83 -2.4	.76 .78 -2.6	1.17 1.14 2.6	1.15 1.14 0.9	1.23 1.24 -0.8	1.17 1.17 0.0	1.04 1.06 -1.9	.81 .83 -2.4	.62 .67 -7.5	.45 .48 -6.3
16	1.46 1.44 1.4	1.30 1.27 2.4	1.30 1.28 1.6	1.12 1.08 3.7	1.14 1.12 1.8	1.09 1.06 2.8	1.15 1.14 0.9	1.04 1.04 0.0	1.04 1.05 -1.0	.84 .85 -1.2	.73 .77 -5.2	.56 .57 -1.8	
14	1.38 1.38 0.0	1.41 1.42 -0.7	1.27 1.25 1.6	1.27 1.27 0.0	1.13 1.12 0.9	1.12 1.12 0.0	.99 .98 1.0	.96 .94 2.1	.80 .79 1.3	.73 .73 0.0	.55 .56 -1.8		
12	1.43 1.43 0.0	1.36 1.35 0.7	1.38 1.38 0.0	1.20 1.20 0.0	1.22 1.23 0.8	1.03 1.02 1.0	.94 .93 1.1	.59 .62 -4.8	.53 .56 -5.4	.60 .59 1.7	.40 .42 -4.8		
10	1.50 1.49 0.7	1.41 1.41 0.0	1.23 1.22 0.8	1.16 1.18 -1.7	1.16 1.16 0.0	1.03 1.04 -1.0	.79 .78 1.3	.53 .56 -5.4	.44 .48 -8.3	.46 .46 0.0	.32 .34 -5.9		
08	1.36 1.36 0.0	1.19 1.20 -0.8	1.19 1.21 -1.7	1.04 1.05 -1.0	1.04 1.05 -1.0	.84 .85 -1.2	.74 .73 1.4	.60 .60 0.0	.46 .47 -2.1	.35 .36 -2.8			
06	1.06 1.08 -1.9	1.07 1.09 -1.8	.96 .98 -2.0	.94 .97 -3.1	.80 .82 -2.4	.74 .78 -5.1	.59 .59 0.0	.43 .45 -4.4	.34 .35 -2.9				
04	.95 .94 1.1	.92 .92 0.0	.85 .86 -1.2	.78 .79 -1.3	.58 .63 -7.9	.57 .57 0.0							
02	.61 .63 -3.2	.58 .59 -1.7	.54 .56 -3.6	.49 .52 -5.8	.45 .47 -4.3								

PRESTO-B
PDQ
% DIFF

KEFF(PRESTO-B) = 1.02980
KEFF(PDQ07) = 1.02975

5.3 Cold Critical and Shutdown Margin Analysis

The PRESTO cold zero-power model has been benchmarked extensively against a variety of cold critical state-point data for Brunswick Units 1 and 2, and Quad-Cities Unit 1. The criticals presented cover a range of 0 to 15 GWD/T core average exposure and 310° to 414°K moderator temperature. Critical eigenvalues presented are adjusted for temperature and period defect, with the temperature effect determined by interpolation between the results of calculations performed at 292° and 392°K.

Tables 5.3.1, 5.3.2, and 5.3.3 contain the results of in-sequence critical comparisons for Brunswick Units 1 and 2 and Quad-Cities Unit 1, respectively. The combined average critical eigenvalue for the two Brunswick units is 0.99387, with a standard deviation of .00234. With the Quad-Cities criticals factored in, the combined average critical eigenvalue becomes 0.99373, with a standard deviation of .00277.

Figure 5.3.1 is a composite plot of the critical eigenvalues accumulated for all three units. Initial cycles of Brunswick 1 and Quad-Cities 1 both show lower average critical eigenvalue than is exhibited in subsequent cycles. Likewise, this bias is not observed for any of the Brunswick 2, Cycles 4 and 5, criticals. We believe that this anomaly is peculiar to initial cycle cores and may be due to a slight overprediction of the worth of the gadolinia in the fresh fuel. In subsequent cycles, with a much smaller inventory of gadolinia bearing fuel, the effect of this gadolinia over-prediction is much less, resulting in a step jump in critical eigenvalue. In Quad-Cities Cycle 2, this jump in critical eigenvalue was much greater than that for Brunswick 1,

Cycle 2, due to the fact that only 64 fresh gadolinia bearing assembly were added to a 724-assembly core; whereas, in Brunswick 1, Cycle 2, 176 fresh assemblies were added to a 560-assembly core.

Since CP&L's design efforts for the Brunswick units will involve cores with a fairly homogeneous mix of irradiated fuel of varying exposures and fresh gadolinia-bearing fuel, the cold critical results for all but the initial cycles best represent CP&L's ability to perform these analyses. When the results of the Brunswick 1, Cycle 1, and Quad-Cities 1, Cycle 1, in-sequence criticals are factored out, the combined average critical eigenvalue for all other cycles (both Brunswick and Quad-Cities) is 0.99496, with a standard deviation of 0.00205. It should be noted that these statistics are very consistent with those presented in Section 5.4 and Table 5.4.1 for hot, full-power reactivity.

In order to determine PRESTO's ability to perform shutdown margin calculations, a series of ten local (clumped) criticals from Cycle 1 of Quad-Cities 1 (taken at three separate exposure points) were analyzed. Since nine of the ten local criticals were clustered about two exposure points, rather than being equally distributed throughout cycle one, as were the in-sequence criticals, it was appropriate to present the eigenvalue differences between the local and in-sequence criticals at corresponding points in the cycle. These results are presented in Table 5.3.4. Table 5.3.4 shows that there is no appreciable bias between local and in-sequence criticals at corresponding exposures. The standard deviation of the differences is 0.00146.

TABLE 5.3.1

BRUNSWICK 1 CYCLES 1-3 COLD CRITICAL COMPARISONS

DATE	CORE AVG MWD/MT	TEMPERATURE (°K)	PERIOD (SEC.)	CORRECTED KEFF
CYCLE 1				
12/01/76	0.0	323	61	0.99544
06/28/77	1703	340	150	0.99164
02/26/78	4893	358	300	0.99110
05/03/78	6117	368	130	0.99247
05/23/78	6451	363	160	0.99354
09/30/78	9042	368	130	0.98881
CYCLE 2				
04/16/79	6978	350	63	0.99504
06/08/79	7647	374	150	0.99508
12/19/79	10462	364	100	0.99448
04/12/80	12569	382	109	0.99292
CYCLE 3				
08/27/80	7783	378	193	0.99626
01/06/81	10225	369	76	0.99375
04/08/81	11644	389	115	0.99207
07/06/81	11772	361	350	0.99415
02/11/82	14591	369	113	0.99669
06/04/82	16260	387	151	0.99731
10/25/82	16915	361	100	0.99923

	CYCLE 1	CYCLE 2	CYCLE 3	TOTAL
AVERAGE:	0.99217	0.99438	0.99564	0.99412
STANDARD DEVIATION:	0.00225	0.00101	0.00244	0.00254

TABLE 5.3.2

BRUNSWICK 2 CYCLES 4-5 COLD CRITICAL COMPARISONS

DATE	CORE AVG MWD/MT	TEMPERATURE (°K)	PERIOD (SEC.)	CORRECTED KEFF
CYCLE 4				
09/17/80	9193	333	68	0.99361
01/10/81	10617	414	200	0.99043
04/09/81	11344	355	140	0.99345
07/27/81	11808	365	163	0.99300
10/29/81	13683	394	250	0.99319
01/28/82	15131	389	159	0.99545
CYCLE 5				
09/29/82	10215	354	114	0.99586
10/01/82	10215	400	311	0.99569
10/16/82	10299	355	400	0.99551

	CYCLE 4	CYCLE 5	TOTAL
AVERAGE:	0.99319	0.99569	0.99402
STANDARD DEVIATION:	0.00161	0.00018	0.00179

TABLE 5.3.3

QUAD CITIES 1 CYCLES 1-2 COLD CRITICAL COMPARISONS

IN-SEQUENCE CRITICALS

DATE	CORE AVG MWD/MT	TEMPERATURE (°K)	PERIOD (SEC.)	CORRECTED KEFF
CYCLE 1				
04/05/72	0.0	337	230	0.99147
02/08/73	2866	344	300	0.98634
05/07/73	3749	322	300	0.99127
08/07/73	4938	322	45	0.99125
01/06/74	6911	355	300	0.99529
CYCLE 2				
10/06/74	8296	358	100	0.99556
12/16/74	9138	344	45	0.99816
05/04/75	10603	361	130	0.99724

	CYCLE 1	CYCLE 2	TOTAL
AVERAGE:	0.99112	0.99699	0.99332
STANDARD DEVIATION:	0.00318	0.00132	0.00393

TABLE 5.3.4

QUAD CITIES 1 CYCLE 1 LOCAL CRITICAL COMPARISONS

DATE	RODS FULLY WITHDRAWN	CRITICAL ROD POS.	CORE AVG MWD/MT	TEMPERATURE (°K)	PERIOD (SEC.)	DELTA KEFF (IN-SEQ.-LOCAL)
03/15/72	46-19	46-23 @ 44	0.0	344	50	0.00012
03/15/72	18-35 22-35	18-31 @ 06	0.0	343	238	0.00032
03/15/72	30-43 30-47	26-43 @ 06	0.0	342	160	-0.00066
03/16/72	18-11	22-11 @ 46	0.0	342	65	-0.00083
03/16/72	26-27 30-27	30-31 @ 08	0.0	343	245	-0.00298
05/03/73	50-27	50-23 @ 22	3749	315	54	0.00193
05/03/73		26-11 @ 38 22-11 @ 20	3749	294	75	0.00036
05/03/73	22-11	22-15 @ 18	3749	298	280	0.00201
05/03/73	26-11	22-11 @ 20	3749	297	65	0.00030
01/06/74	22-11 22-15	26-11 @ 06	6911	356	100	-0.00109
					AVERAGE	-0.00005
					STANDARD DEVIATION	0.00146

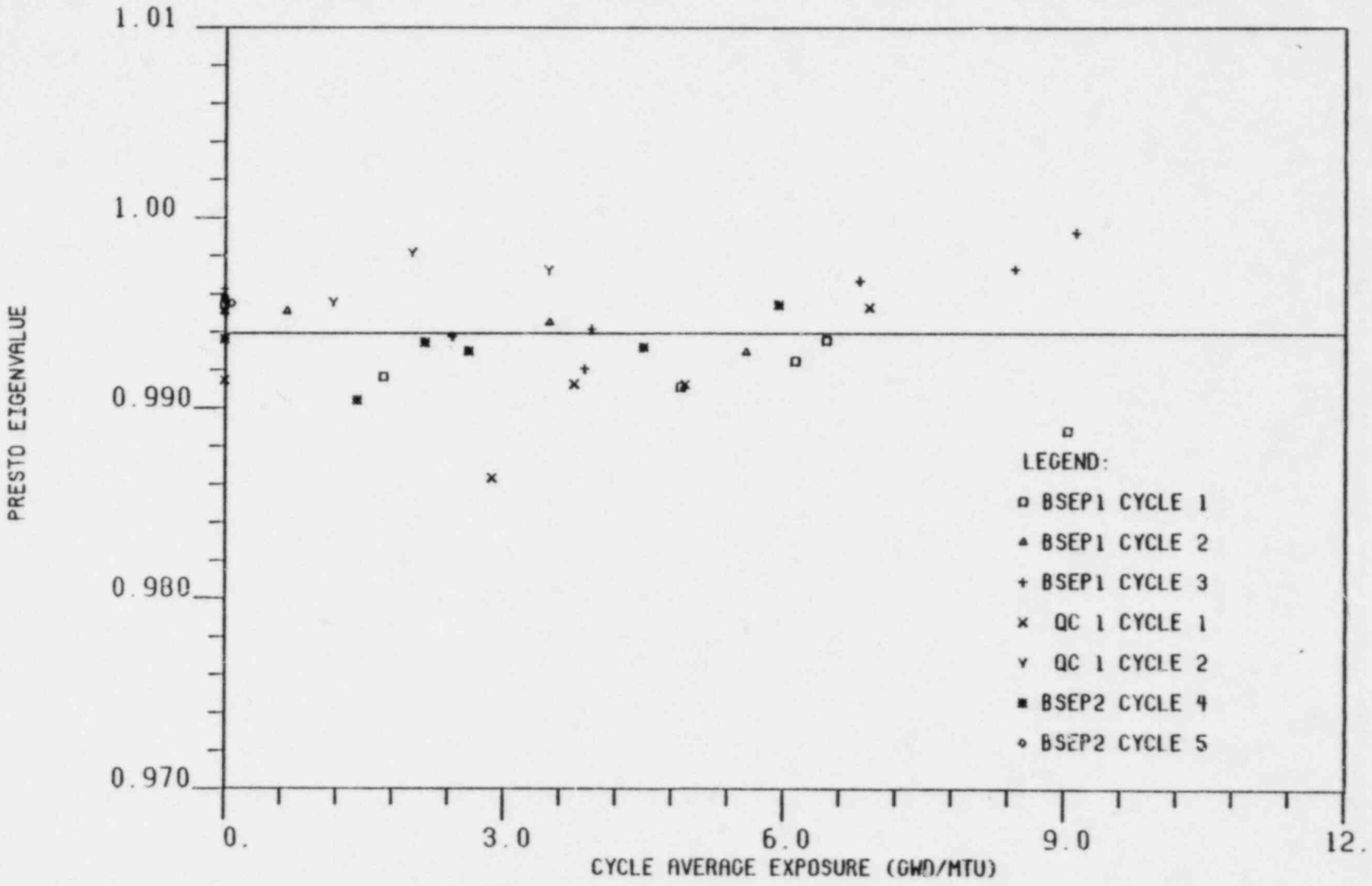

PRESTO-B ZERO-POWER CRITICAL EIGENVALUE VS. EXPOSURE

Figure 5.3.1

5.4 Hot Reactivity Calculations

PRESTO-B core-follow calculations were conducted for Brunswick 1, Cycles 1 through 3; Brunswick 2, Cycles 4 and 5; and Quad-Cities Unit 1, Cycles 1 and 2. This resulted in 159 different projections of core effective eigenvalue for a variety of hot operating conditions. The cumulative average eigenvalue for seven cycles of three separate reactors is K_{ave} = 0.99565, with a standard deviation of σ = 0.00199. The maximum standard deviation for any one cycle was 0.00251. The minimum standard deviation for any one cycle was 0.00040. Figure 5.4.1 is a composite plot of the hot operating eigenvalues for all of the points analyzed versus cycle average exposure.

This figure shows a slight trend of increasing eigenvalue with cycle exposure. It is possible that, as is suspected in the case of the cold critical comparisons, this trend is due to a basic over-prediction of the worth of gadolinia in the fresh fuel. Figures 5.4.2 through 5.4.6 plot the PRESTO hot eigenvalue versus core average power density, bundle average mass flux, control-rod density, average coolant density, and inlet sub-cooling, respectively. Of these, Figure 5.4.5 is the only plot that shows any discernible trend; i.e., that of increasing eigenvalue with core average coolant density. It is not at all evident, however, whether this is a cause or an effect, since average coolant density tends to increase near end of cycle when the reactor is operated with a more top-peaked power distribution. In any event, the trends in the PRESTO hot eigenvalue data are very slight, and the overall standard deviation is quite small.

As a further check on the quality of the hot reactivity projections, a limited sensitivity study was conducted for Brunswick 2, Cycle 5, using vendor-quoted heat balance uncertainties. These uncertainties were translated into equivalent reactor power, core flow, steam dome pressure, and feed enthalpy variations. Several PRESTO-B simulations were performed for a rated condition in which the heat balance was perturbed. The results of this study are shown in Table 5.4.2. The study addresses the major heat balance components of the eigenvalue uncertainty. A vector summation of the expected eigenvalue differences for one standard deviation in power, flow, pressure, and feedwater enthalpy is a conservative estimate of the heat balance uncertainty in eigenvalue. The result was σ_{Heat} = 0.00114 Δk, which represents the smallest standard deviation one could expect from simulation of a large number of conditions. PRESTO-B predictions of hot reactivity for the 159 cases analyzed by CP&L show variations about an average which are only twice the theoretical minimum.

TABLE 5.4.1

SUMMARY OF PRESTO KEFFECTIVES

BY UNIT AND CYCLE

UNIT/ CYCLE	NUMBER DATAPTS.	MEAN KEFF	STANDARD DEVIATION
B1C1	32	0.99522	0.00147
B1C2	24	0.99449	0.00070
B1C3	33	0.99522	0.00251
B2C4	37	0.99706	0.00171
B2C5	4	0.99541	0.00035
Q1C1	16	0.99601	0.00224
Q1C2	13	0.99560	0.00153
B1C1-3	89	0.99503	0.00183
B2C4-5	41	0.99690	0.00172
B1C1-3/ B2C4-5	130	0.99562	0.00199
Q1C1-2	29	0.99583	0.00196
B1C1-3/ B2C4-5/ Q1C1-2	159	0.99565	0.00199

TABLE 5.4.2

BRUNSWICK 2 CYCLE 5 HEAT BALANCE

SENSITIVITY STUDY

INITIAL CONDITIONS:

POWER	2436 MWTH		
CORE FLOW	77 MLB/HR	(9.7E+3	Kg/SEC)
DHS	21.9 BTU/LBM	(51.0	KJ/Kg)
FEED ENTHALPY	393 BTU/LBM	(913.0	KJ/Kg)
PRESSURE	1035 PSIA	(7.14	MPa)

VARIABLE	HEAT BALANCE UNCERTAINTY*	EIGENVALUE VARIATION DUE TO PERTURBATION
POWER	1.76%	.00088
CORE FLOW	2.50%	.00066
PRESSURE	0.75%	.00030
FEED ENTHALPY	0.20%	.00004

EIGENVALUE UNCERTAINTY DUE TO COMBINED
HEAT BALANCE UNCERTAINTY

$$\sigma_{heat} = 0.00114$$

* REFERENCE 17

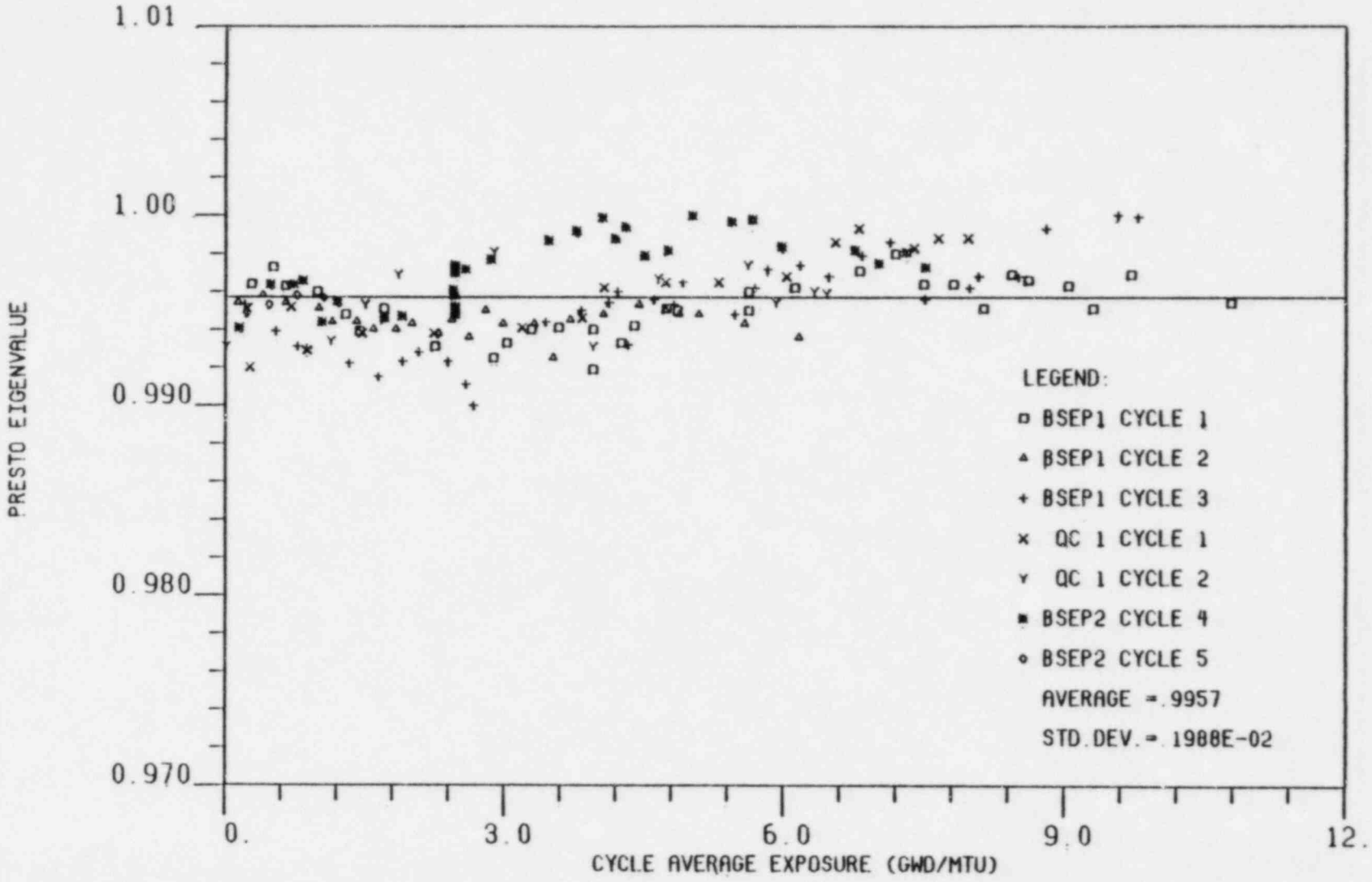

PRESTO-B HOT EIGENVALUE VS. CYCLE AVERAGE EXPOSURE

Figure 5.4.1

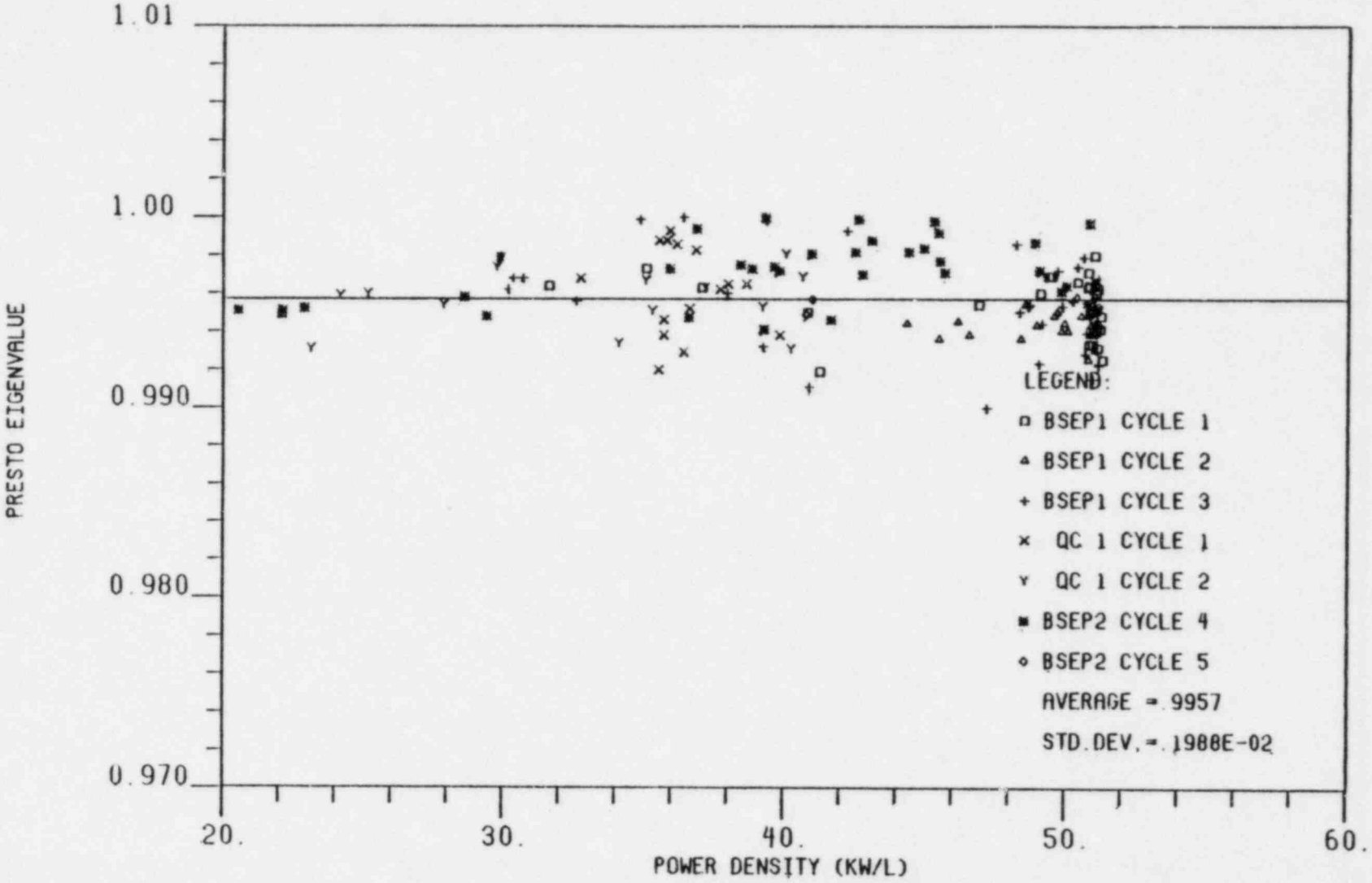

PRESTO-B HOT EIGENVALUE VS. CORE AVERAGE POWER DENSITY

Figure 5.4.2

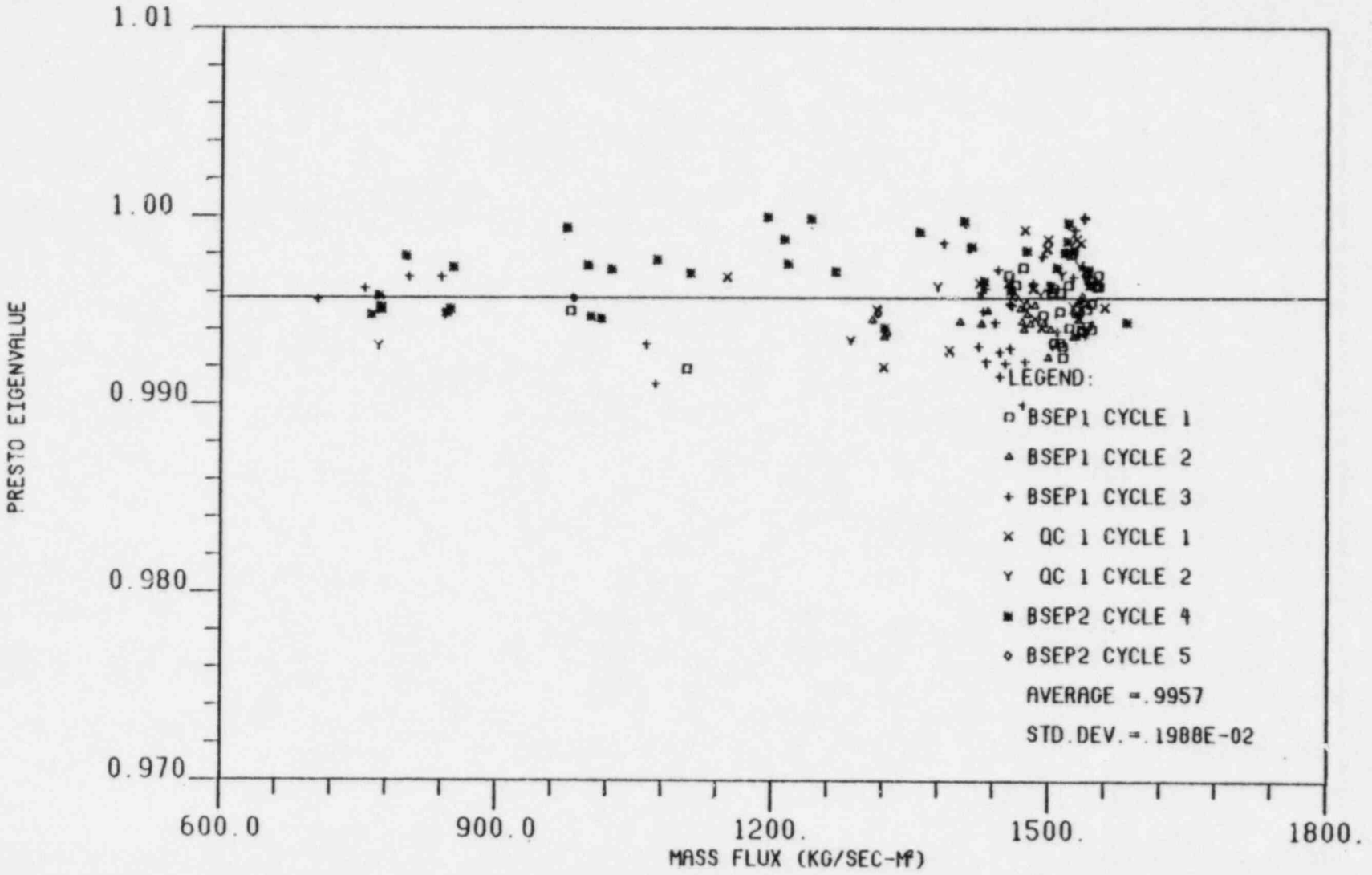

PRESTO-B HOT EIGENVALUE VS. BUNDLE AVERAGE MASS FLUX

Figure 5.4.3

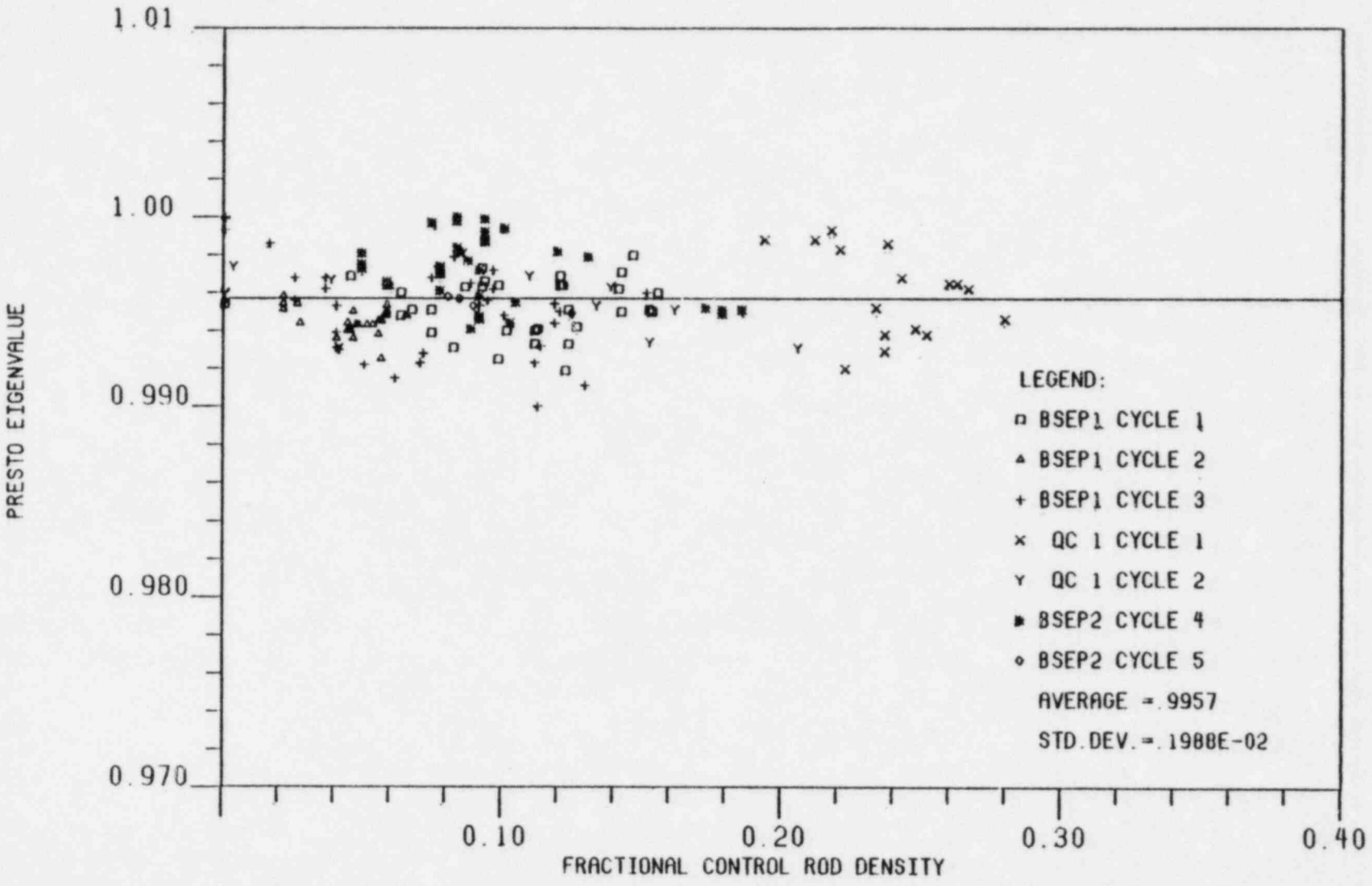

PRESTO-B HOT EIGENVALUE VS. CONTROL ROD DENSITY

Figure 5.4.4

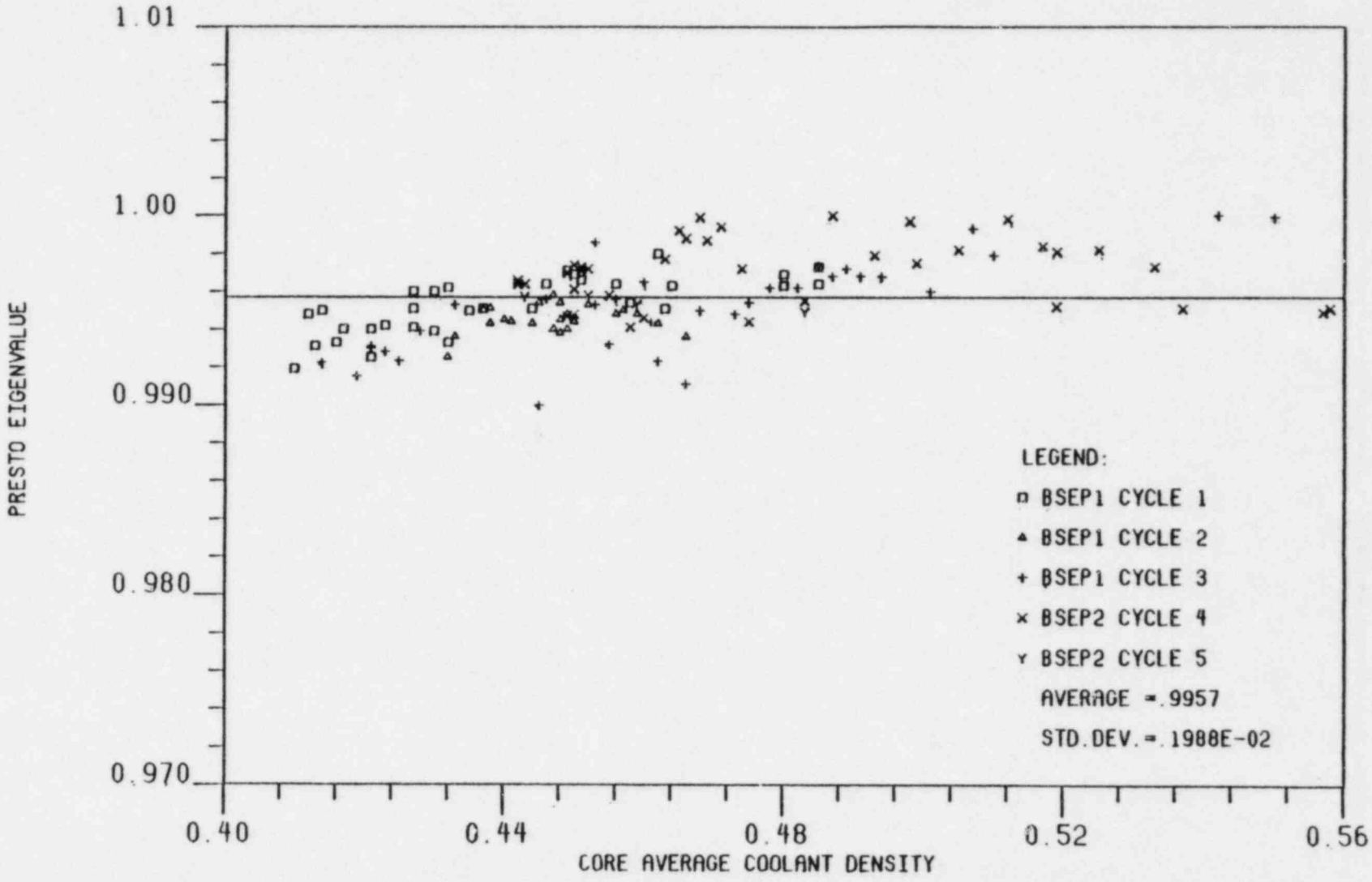

PRESTO-B HOT EIGENVALUE VS. AVERAGE COOLANT DENSITY

Figure 5.4.5

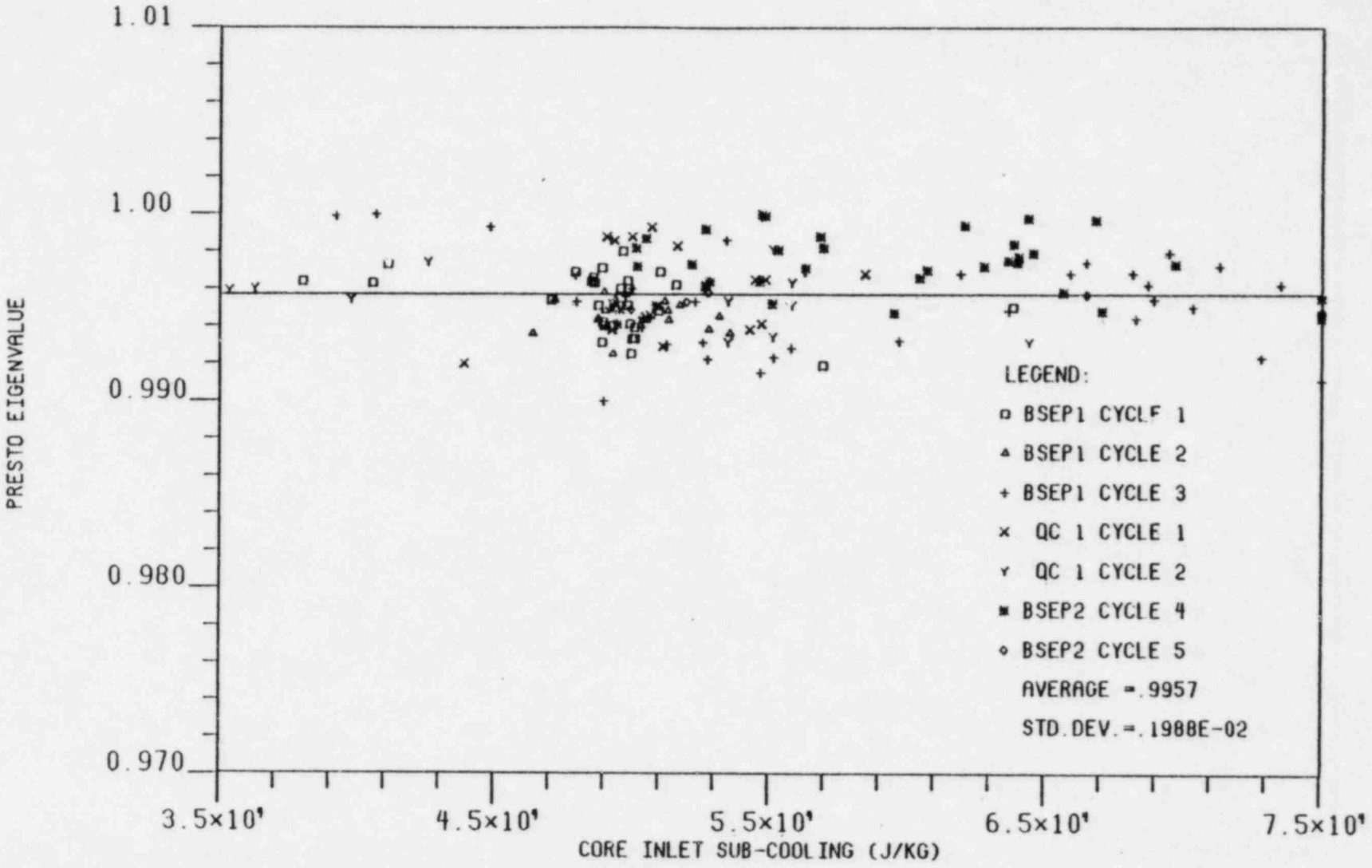

PRESTO-B HOT EIGENVALUE VS. INLET SUB-COOLING

Figure 5.4.6

5.5 Hot Power Distribution Comparisons

The ability of the PRESTO-B nodal method to predict the power distribution for a fixed set of cross sections was demonstrated in Section 5.1. The purpose of this section is to justify the use of RECORD and PRESTO-B simulation capability to predict three-dimensional reactor operations.

The ability of a nodal simulator to predict the Traveling In-core Probe (TIP) signal distribution provides implicit justification for power distribution predictions of statepoints during the reactor cycle. Under normal operating conditions, the TIP distribution provides the reference from which all other power distribution measurements are generated. TIP comparisons provide evidence of a simulator's ability to predict the cumulative response of four-bundle cells within a core.

Table 5.5.1 presents the results of PRESTO-B TIP simulations for Brunswick 1, Cycles 1, 2, and 3, and Brunswick 2, Cycle 4. For these cases, the measured TIP data was reconstructed from LPRM's using the standard process computer method. This approach results in some additional uncertainty over the direct TIP measurements due to drifting LPRM's; however, it is the best data available for the Brunswick units. Reference 17 indicates an expected TIP measurement uncertainty of 5.0 percent for initial cores and 6.7 percent for reload cores.

Figure 5.5.1 through Figure 5.5.12 show axial TIP distribution comparisons for the beginning, middle, and end of cycle for each of the Brunswick cycles modeled.

Table 5.5.1 reports comparisons of the total standard deviation, standard deviation of the TIP integrals, and ratio of PRESTO-B to measured maximum TIP readings. The total standard deviation and maximum TIP ratios relate to the ability of PRESTO-B to predict nodal power peaking. The standard deviation of the TIP integrals indirectly confirms the ability of PRESTO-B to predict total bundle power for the purpose of CPR evaluations. The results of these analyses give overall standard deviations of 8.65 percent and 4.85 percent, respectively, for total and integral. The peak predictions show a bias of -2.9 percent and standard deviation of 4.4 percent.

Table 5.5.2 presents the results of the PRESTO-B TIP simulations for Quad-Cities, Unit 1, Cycles 1 and 2. These data are presented in the form of Table 5.5.1, with additional entries showing comparisons between measured symmetric TIPS. The large differences between symmetric measurements account for the slightly larger standard deviations (9.3 percent and 5.3 percent, respectively, for total and integral) obtained for the Quad-Cities comparisons.

Figure 5.5.13 through 5.5.18 show axial TIP distribution comparisons for the beginning, middle, and end of cycle for both cycles of Quad-Cities Unit 1.

Additional information relating to power distribution predictive capability can be inferred by comparing PRESTO-B and the process computer predicted nodal peaking factors. Figure 5.5.19 presents composite plot of the ratio of PRESTO-B to process computer predicted most limiting Maximum Average Planar Linear Heat Generation Rate (MAPLHGR) as a function of core average exposure for the Brunswick units. The average ratio of PRESTO-B MAPLHGR to plant data

is 1.008, with a standard deviation of 5.7 percent. The standard deviation is consistent with the variations in the prediction of maximum local TIP factor noted previously, although the bias in MAPLHGR prediction is +0.8 percent. The uncertainty is the process computer power projections has components in addition to the previously quoted TIP measurement uncertainty.

Figures 5.5.20 through 5.5.26 show typical comparisons of PRESTO-B and process computer power distributions for various points in each cycle of the Brunswick units. The points chosen are intended to show comparisons for a variety of combination of core power and flow. The most direct justification for power distribution projections will be presented in the following section concerning PRESTO-B's predictions of Quad-Cities gamma scans.

Table 5.5.1 BSEP TIPS COMPARISON SUMMARY

	CASE NO.	DATE	STD.DEV TOTAL	STD.DEV INTEGRAL	PEAK RATIO CALC/P.C.
B1C1	7	04/01/77	0.0497	0.0251	1.005
	17	10/23/77	0.0657	0.0264	0.965
	23	02/09/78	0.0691	0.0315	1.032
	28	06/08/78	0.0563	0.0386	0.975
	35	09/24/78	0.0613	0.0382	1.011
	42	01/12/79	0.0490	0.0351	0.993
	AVERAGE		0.0590	0.0329	0.997
B1C2	3	05/24/79	0.0974	0.0694	0.992
	7	07/25/79	0.1022	0.0628	0.933
	13	10/04/79	0.1107	0.0589	0.918
	17	12/27/79	0.0866	0.0504	0.926
	21	02/11/80	0.0709	0.0491	0.920
	23	02/26/80	0.0706	0.0487	0.961
	27	05/08/80	0.0779	0.0439	0.973
	AVERAGE		0.0893	0.0554	0.946
B1C3	1	09/07/80	0.0881	0.0465	1.027
	4	10/05/80	0.0816	0.0468	1.019
	8	11/27/80	0.0758	0.0452	0.975
	22	04/16/81	0.0701	0.0378	0.918
	30	12/13/81	0.0602	0.0383	0.975
	42	05/30/82	0.0819	0.0441	0.947
	43	06/24/82	0.0978	0.0402	0.985
	46	11/28/82	0.0912	0.0435	0.960
	AVERAGE		0.0816	0.0429	0.976
B2C4	1	10/05/80	0.0810	0.0545	0.970
	2	10/25/80	0.0757	0.0483	0.989
	5	11/27/80	0.0880	0.0533	1.073
	9	02/05/81	0.0909	0.0596	0.961
	11	04/30/81	0.0975	0.0582	1.027
	16	08/26/81	0.1107	0.0596	0.968
	22	11/12/81	0.1091	0.0538	1.014
	27	01/04/82	0.1193	0.0580	0.939
	29	03/11/82	0.1120	0.0553	0.936
	31	04/12/82	0.1256	0.0601	0.849
	AVERAGE		0.1022	0.0562	0.973
B2C5	3	12/16/82	0.0719	0.0327	0.922
	OVERALL		0.0865	0.0485	0.971±0.044

Table 5.5.2 QUAD CITIES TIP COMPARISON SUMMARY

	CASE NO.	DATE	STD.DEV TOTAL	STD.DEV INTEGRAL	SYM. MEAS. STD. DEV. (TOTAL)
Q1C1	1	06/29/72	0.0886	0.0547	0.1073
	2	08/30/72	0.1076	0.0576	0.1204
	3	09/11/72	0.0979	0.0586	0.1244
	4	11/01/72	0.1132	0.0588	----
	5	12/26/72	0.0911	0.0586	----
	6	03/08/73	0.0954	0.0634	0.1250
	7	05/16/73	0.1203	0.0621	----
	8	06/06/73	0.1207	0.0619	----
	9	07/19/73	0.1113	0.0591	----
	10	08/30/73	0.1017	0.0608	----
	11	11/01/73	0.0798	0.0547	----
	12	12/11/73	0.1077	0.0603	0.1216
	13	12/29/73	0.0907	0.0560	0.1305
	14	02/13/74	0.0831	0.0544	----
	15	03/05/74	0.0882	0.0561	0.1089
	16	03/26/74	------	------	----
	AVERAGE		0.0998	0.0585	0.1197
Q1C2	17	07/26/74	0.0966	0.0443	0.1125
	18	08/15/74	0.1129	0.0489	0.1233
	19	09/12/74	0.0921	0.0453	0.1088
	20	10/23/74	0.0930	0.0488	----
	21	11/18/74	0.0861	0.0472	----
	22	12/11/74	0.0860	0.0469	----
	23	04/03/75	0.0701	0.0462	0.1011
	24	06/19/75	0.0678	0.0425	----
	25	08/08/75	0.0846	0.0469	----
	26	10/20/75	------	------	----
	27	11/13/75	0.0649	0.0461	0.0974
	28	12/19/75	0.0733	0.0432	0.0918
	29	12/31/75	0.0864	0.0485	0.0923
	AVERAGE		0.0845	0.0462	0.1039
	OVERALL		0.0930	0.0530	0.1118

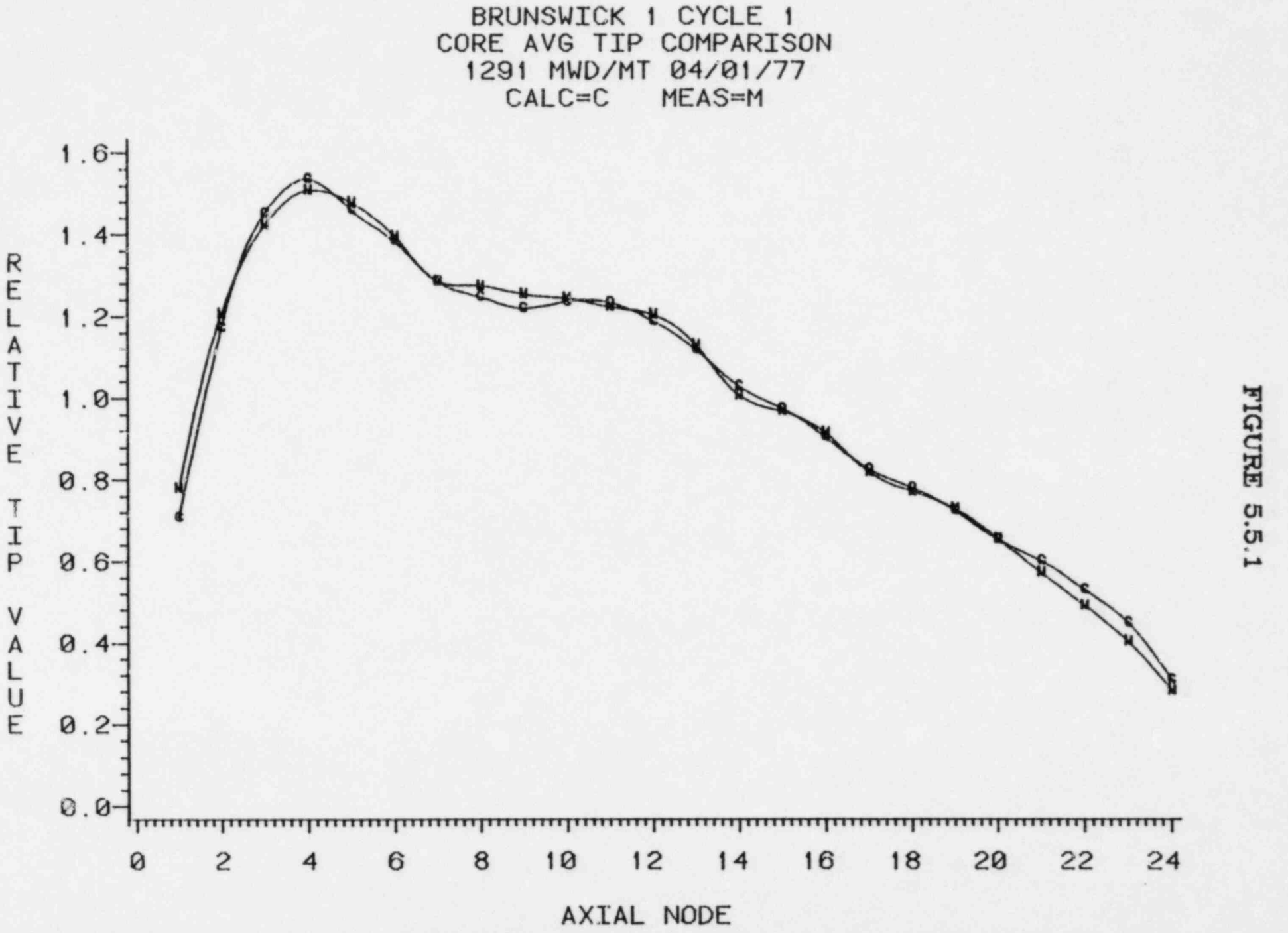
BRUNSWICK 1 CYCLE 1
CORE AVG TIP COMPARISON
1291 MWD/MT 04/01/77
CALC=C MEAS=M
RELATIVE TIP VALUE
1.6
1.4
1.2
1.0
0.8
0.6
0.4
0.2
0.0
0
2
4
6
8
10
12
14
16
18
20
22
24
AXIAL NODE

FIGURE 5.5.1

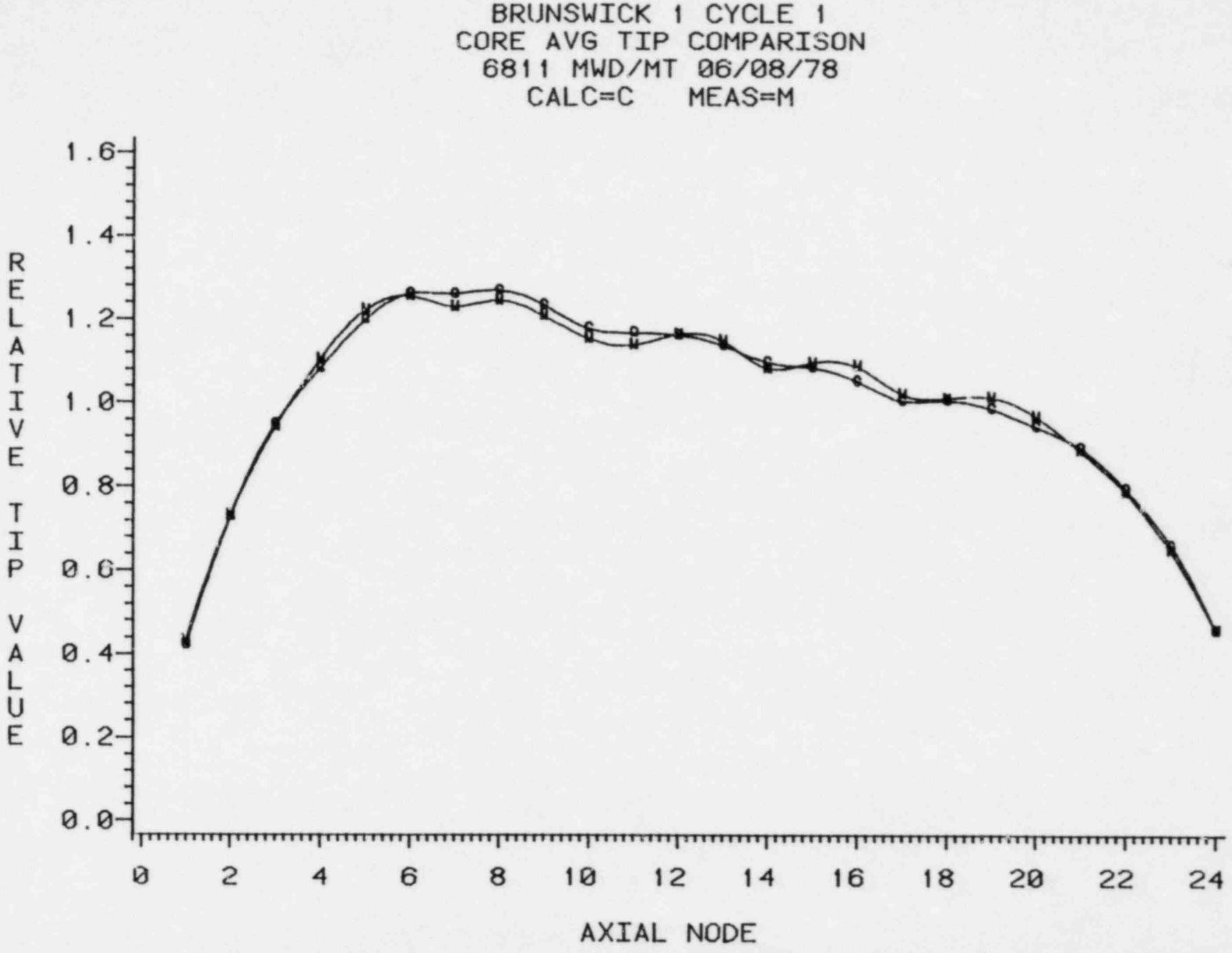
BRUNSWICK 1 CYCLE 1
CORE AVG TIP COMPARISON
6811 MWD/MT 06/08/78
CALC=C MEAS=M
RELATIVE TIP VALUE
1.6
1.4
1.2
1.0
0.8
0.6
0.4
0.2
0.0
0
2
4
6
8
10
12
14
16
18
20
22
24
AXIAL NODE

FIGURE 5.5.2

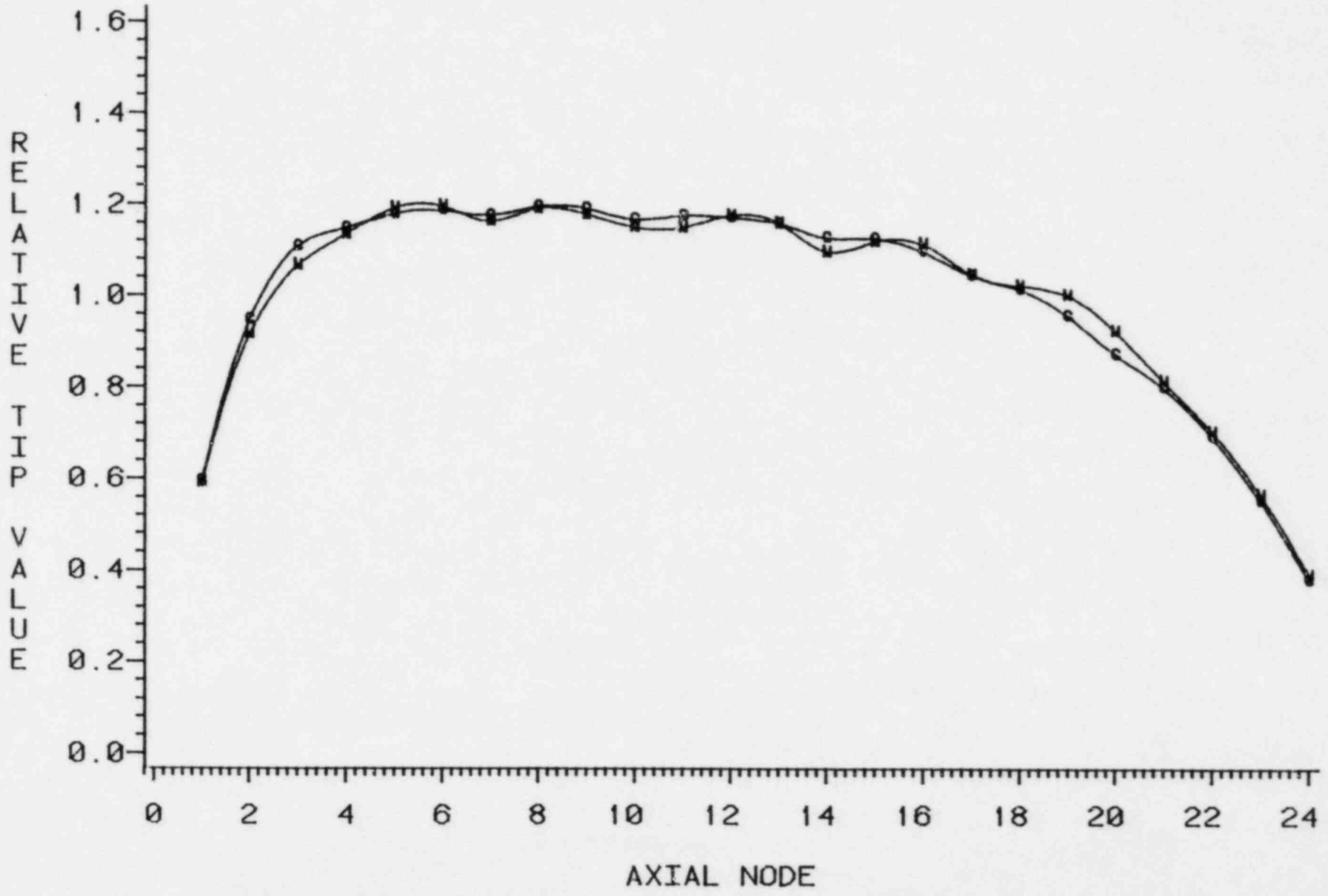
BRUNSWICK 1 CYCLE 1
CORE AVG TIP COMPARISON
10783 MWD/MT 01/12/79
CALC=C MEAS=M
RELATIVE TIP VALUE
1.6
1.4
1.2
1.0
0.8
0.6
0.4
0.2
0.0
0
2
4
6
8
10
12
14
16
18
20
22
24
AXIAL NODE

FIGURE 5.5.3

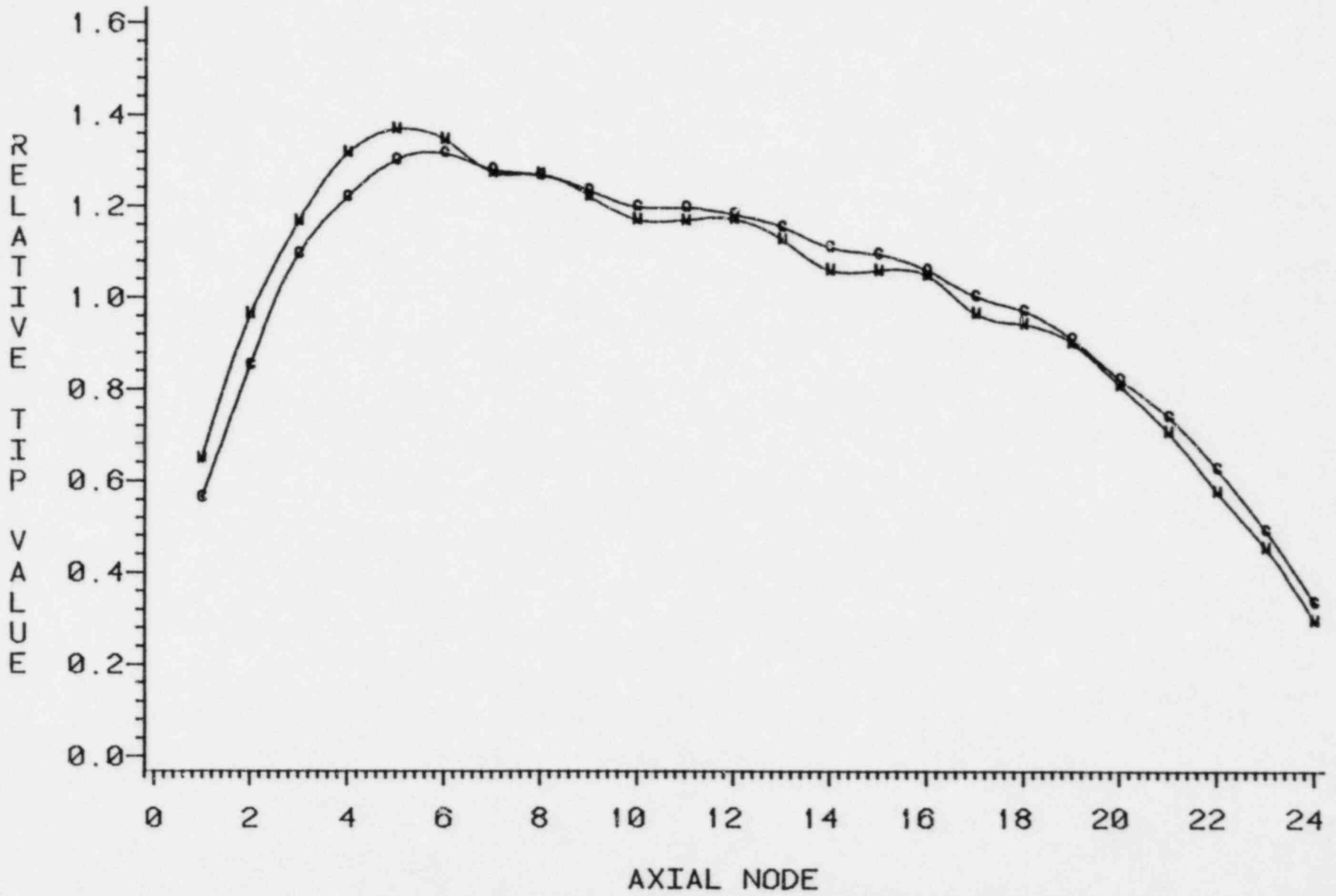
BRUNSWICK 1 CYCLE 2
CORE AVG TIP COMPARISON
7589 MWD/MT 05/24/79
CALC=C MEAS=M
RELATIVE TIP VALUE
1.6
1.4
1.2
1.0
0.8
0.6
0.4
0.2
0.0
0
2
4
6
8
10
12
14
16
18
20
22
24
AXIAL NODE

FIGURE 5.5.4

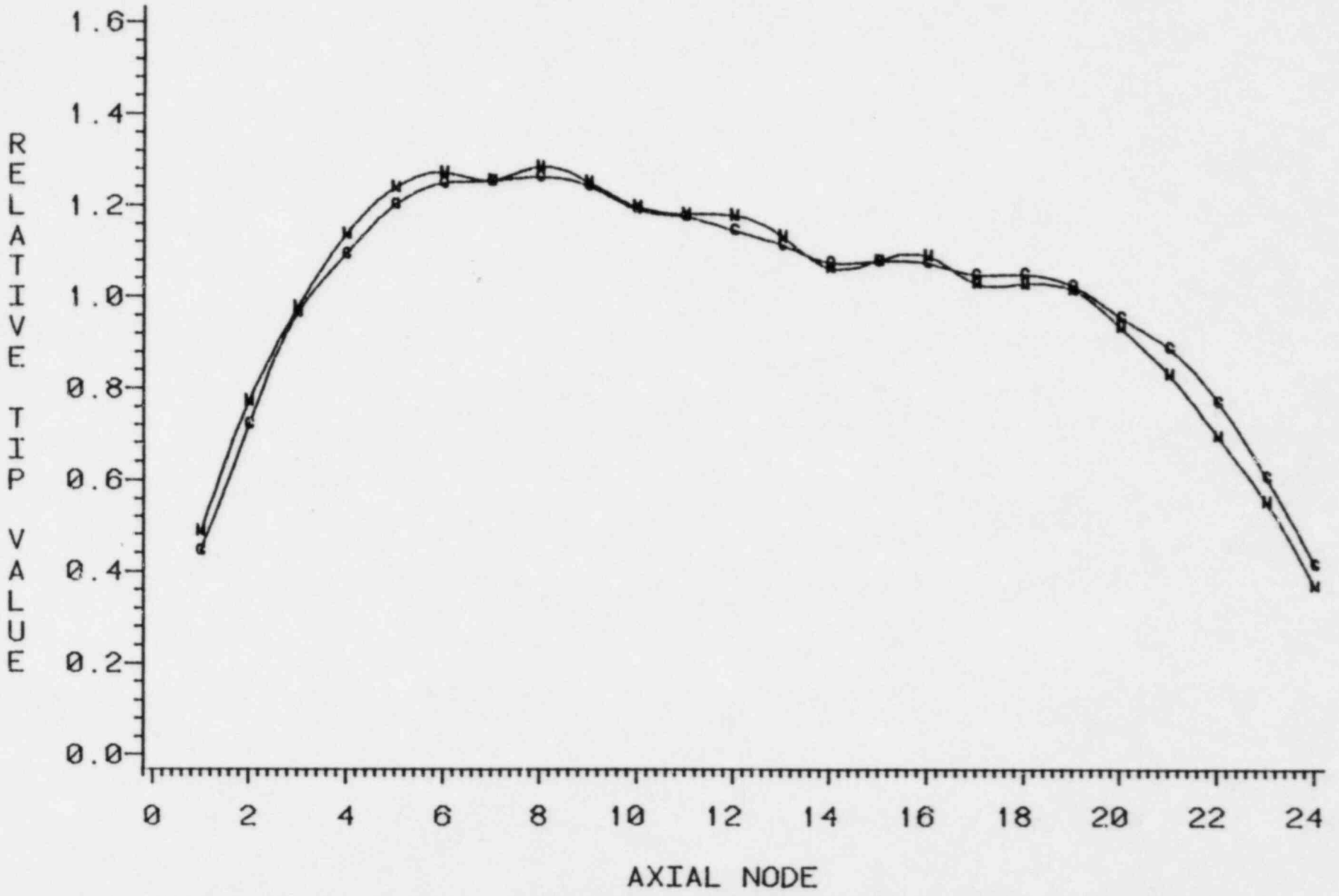
BRUNSWICK 1 CYCLE 2
CORE AVG TIP COMPARISON
11668 MWD/MT 02/11/80
CALC=C MEAS=M
RELATIVE TIP VALUE
1.6
1.4
1.2
1.0
0.8
0.6
0.4
0.2
0.0
0
2
4
6
8
10
12
14
16
18
20
22
24
AXIAL NODE

FIGURE 5.5.5

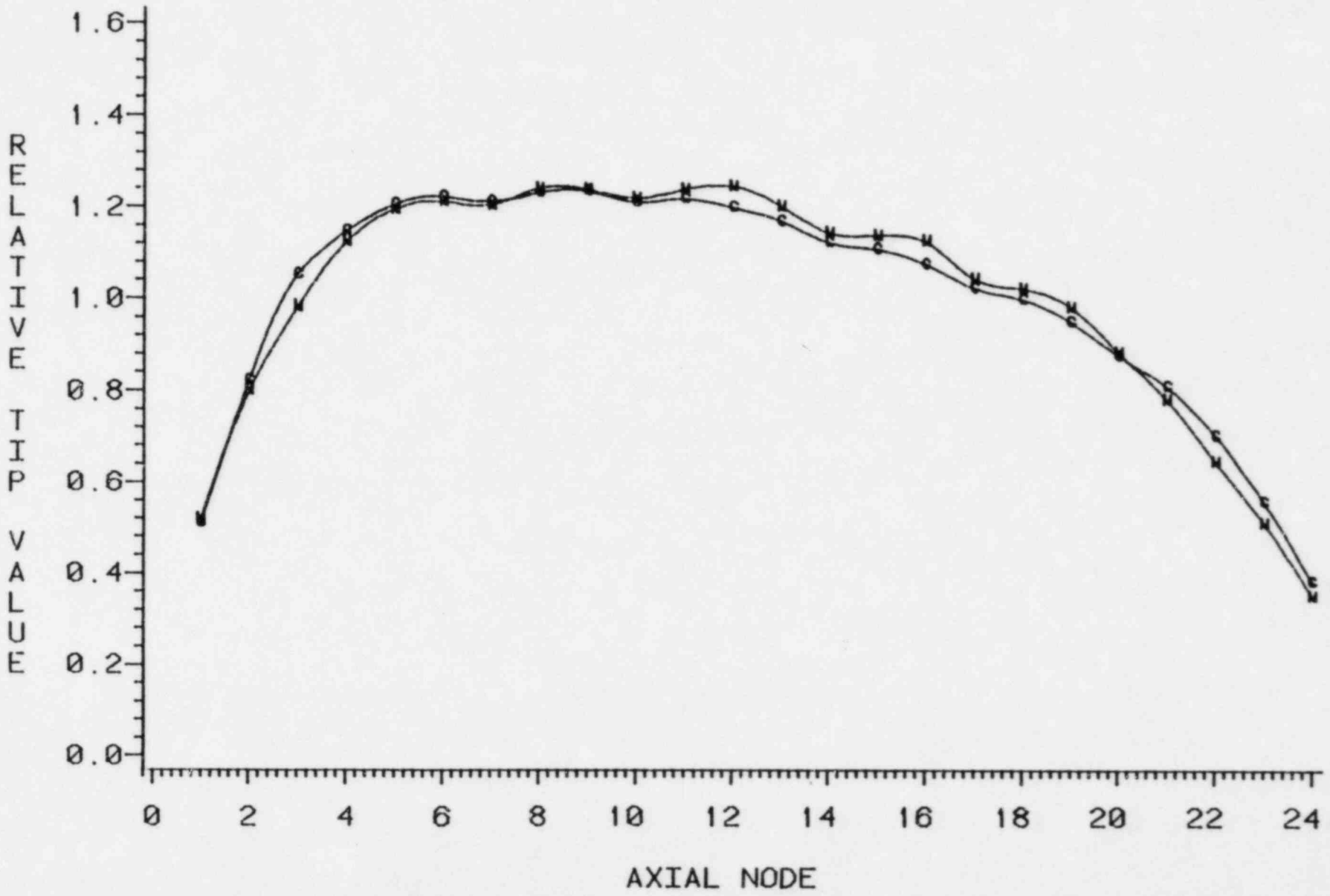
BRUNSWICK 1 CYCLE 2
CORE AVG TIP COMPARISON
13099 MWD/MT 05/08/80
CALC=C MEAS=M
RELATIVE TIP VALUE
1.6
1.4
1.2
1.0
0.8
0.6
0.4
0.2
0.0
0
2
4
6
8
10
12
14
16
18
20
22
24
AXIAL NODE

FIGURE 5.5.6

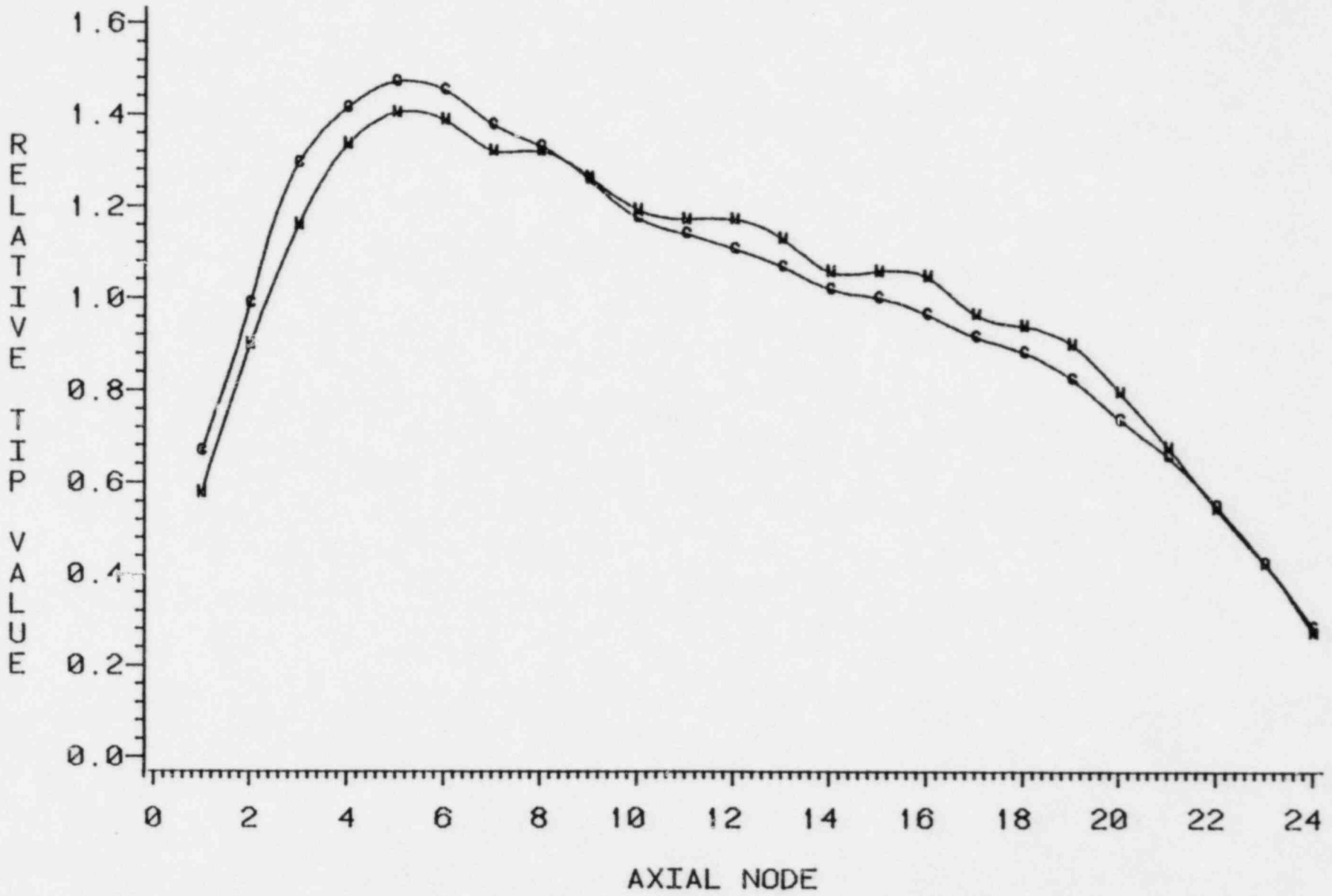
BRUNSWICK 1 CYCLE 3
CORE AVG TIP COMPARISON
8151 MWD/MT 09/07/80
CALC=C MEAS=M
RELATIVE TIP VALUE
1.6
1.4
1.2
1.0
0.8
0.6
0.4
0.2
0.0
0
2
4
6
8
10
12
14
16
18
20
22
24
AXIAL NODE

FIGURE 5.5.7

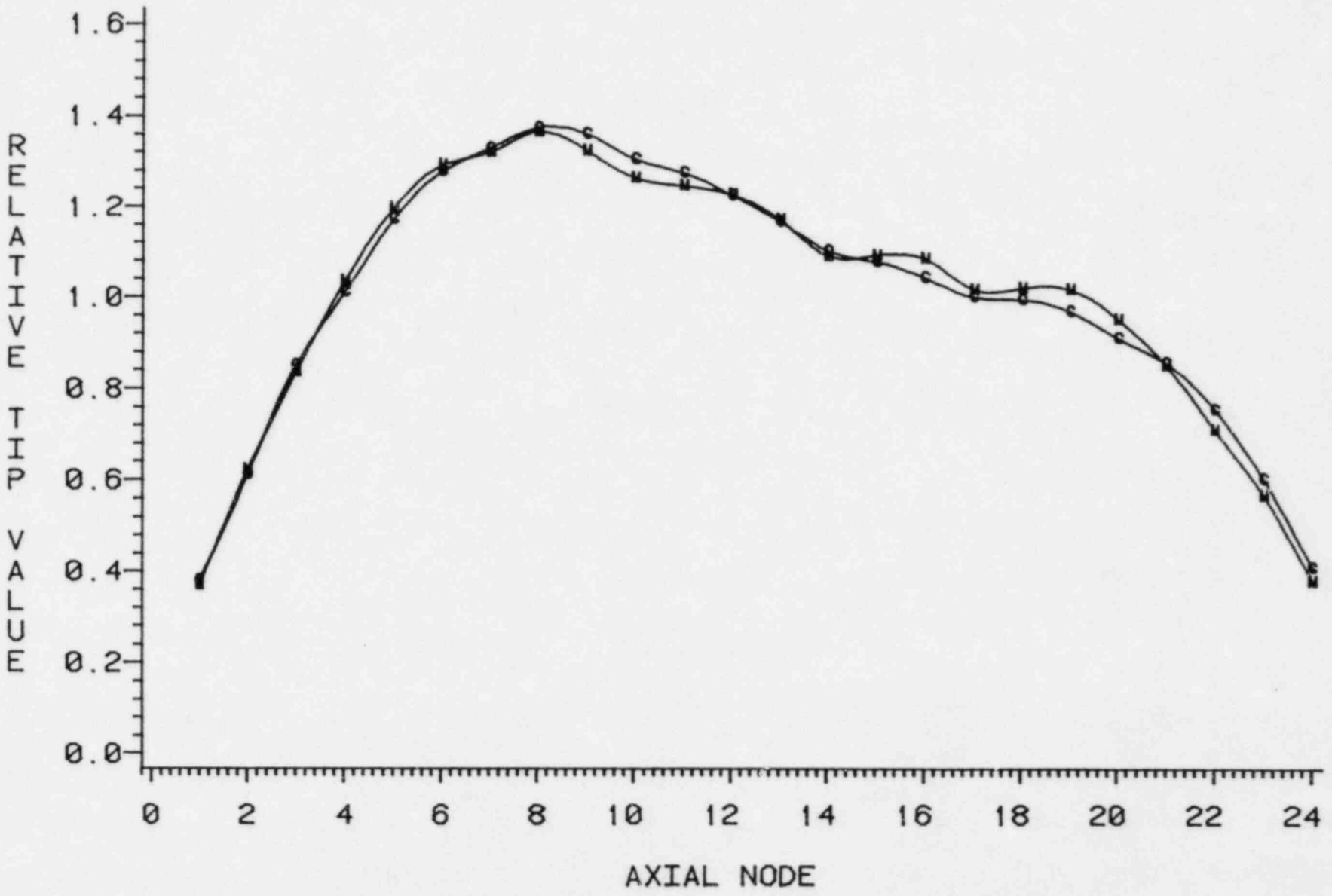
BRUNSWICK 1 CYCLE 3
CORE AVG TIP COMPARISON
13622 MWD/MT 12/13/81
CALC=C MEAS=M
RELATIVE TIP VALUE
1.6
1.4
1.2
1.0
0.8
0.6
0.4
0.2
0.0
0
2
4
6
8
10
12
14
16
18
20
22
24
AXIAL NODE

FIGURE 5.5.8

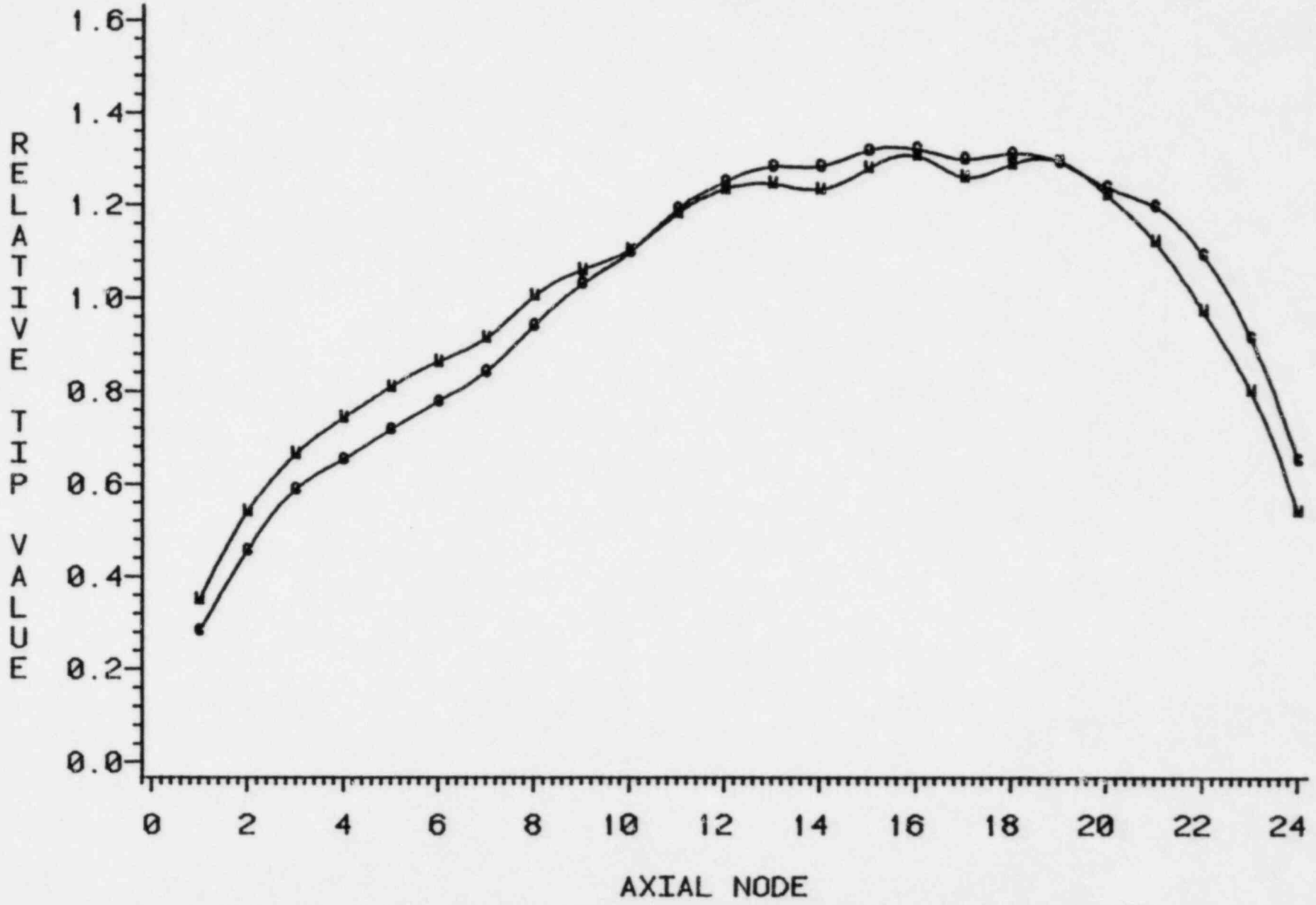
BRUNSWICK 1 CYCLE 3
CORE AVG TIP COMPARISON
17721 MWD/MT 11/28/82
CALC=C MEAS=M
RELATIVE TIP VALUE
1.6
1.4
1.2
1.0
0.8
0.6
0.4
0.2
0.0
0
2
4
6
8
10
12
14
16
18
20
22
24
AXIAL NODE

FIGURE 5.5.9

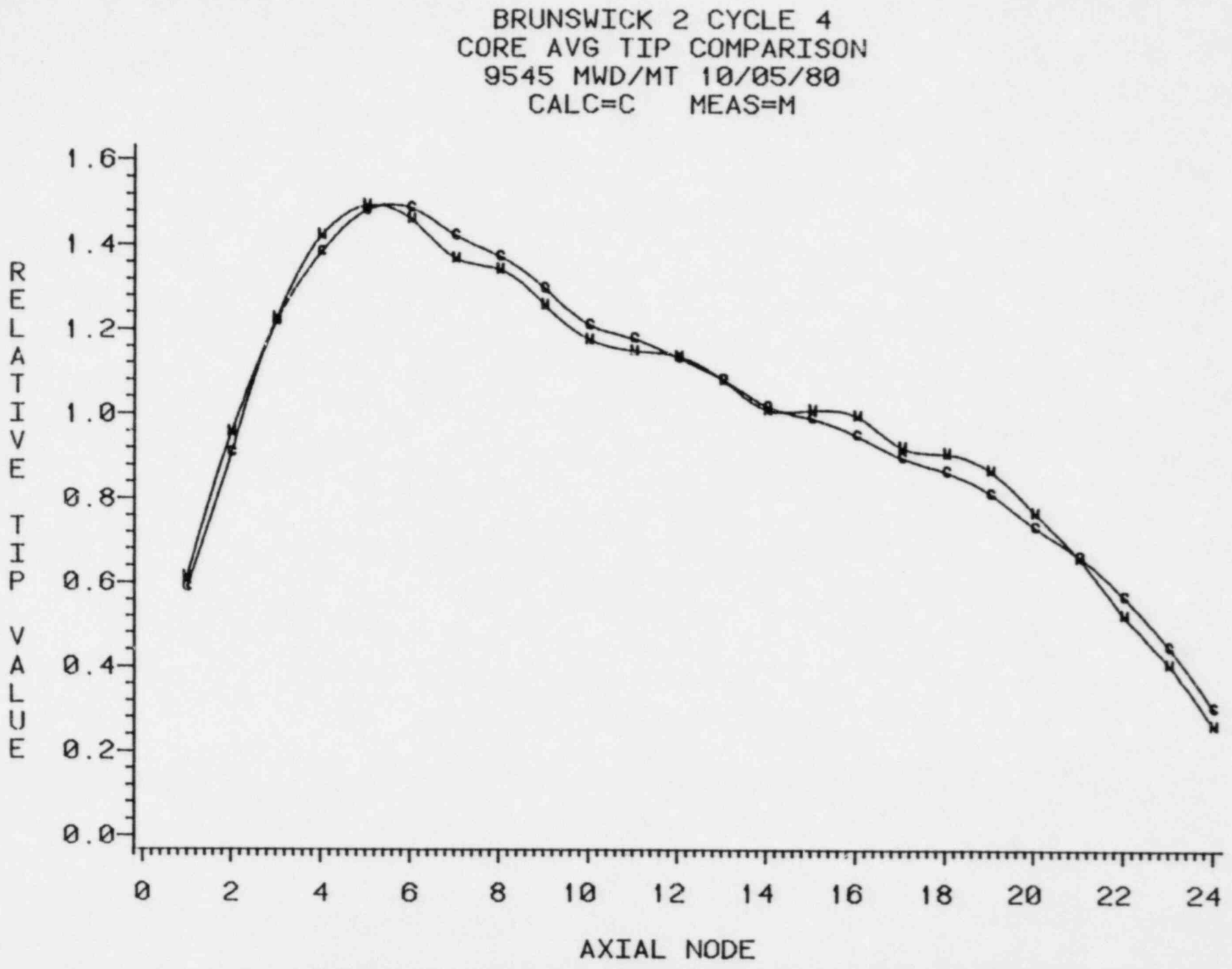
BRUNSWICK 2 CYCLE 4
CORE AVG TIP COMPARISON
9545 MWD/MT 10/05/80
CALC=C MEAS=M
RELATIVE TIP VALUE
1.6
1.4
1.2
1.0
0.8
0.6
0.4
0.2
0.0
0
2
4
6
8
10
12
14
16
18
20
22
24
AXIAL NODE

FIGURE 5.5.10

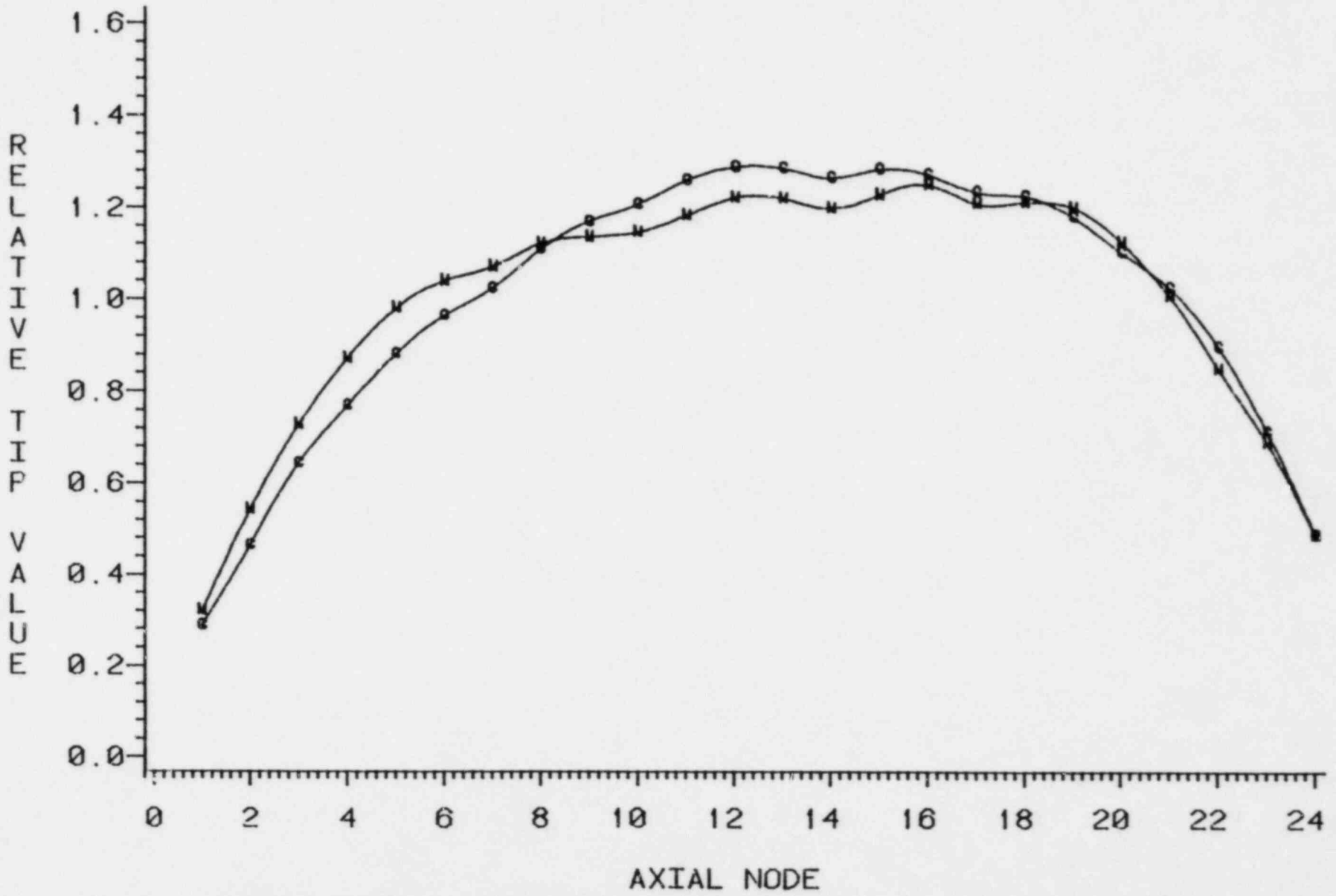
BRUNSWICK 2 CYCLE 4
CORE AVG TIP COMPARISON
14149 MWD/MT 11/12/81
CALC=C MEAS=M
RELATIVE TIP VALUE
1.6
1.4
1.2
1.0
0.8
0.6
0.4
0.2
0.0
0
2
4
6
8
10
12
14
16
18
20
22
24
AXIAL NODE

FIGURE 5.5.11

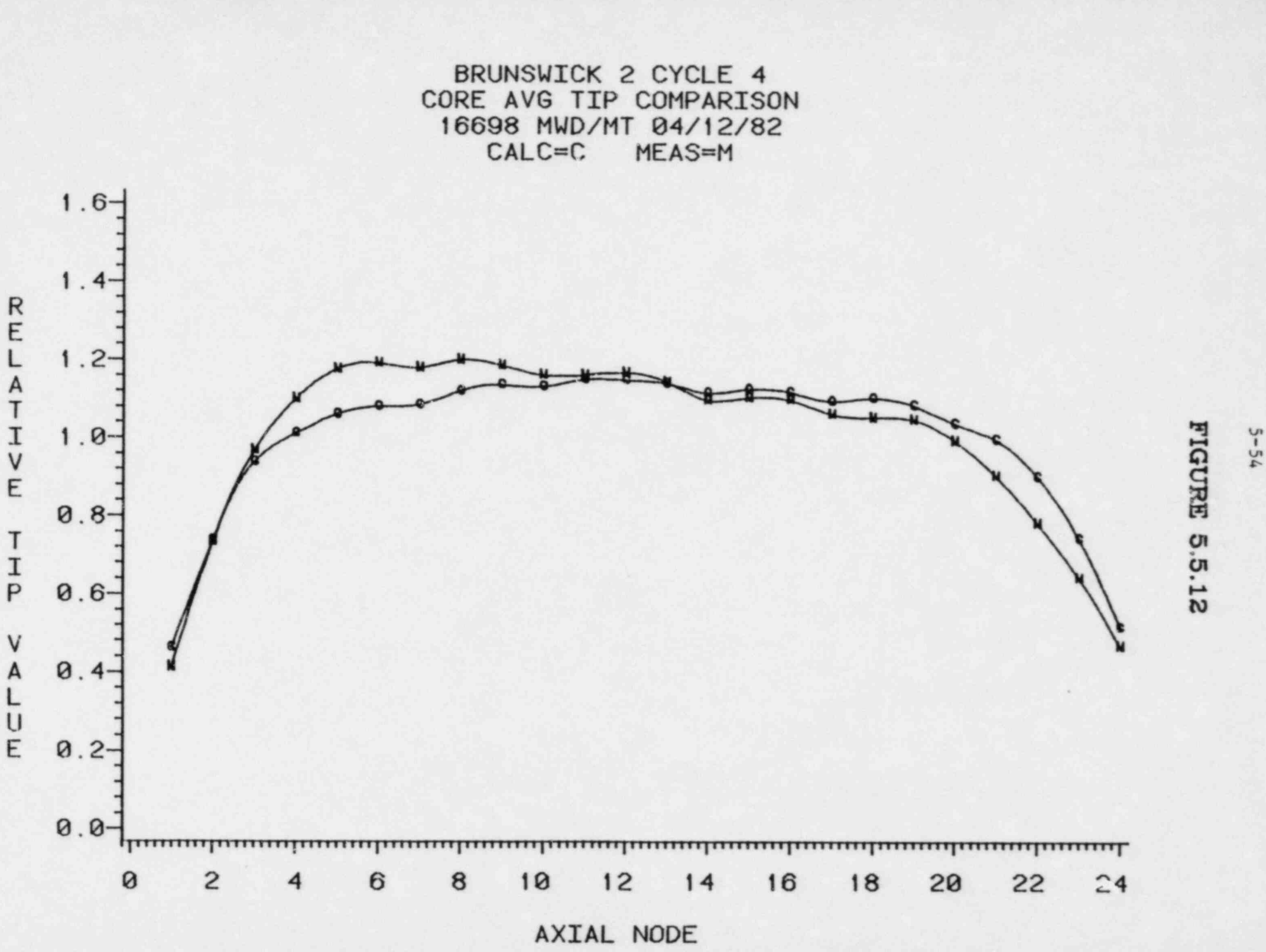
BRUNSWICK 2 CYCLE 4
CORE AVG TIP COMPARISON
16698 MWD/MT 04/12/82
CALC=C MEAS=M
RELATIVE TIP VALUE
1.6
1.4
1.2
1.0
0.8
0.6
0.4
0.2
0.0
0
2
4
6
8
10
12
14
16
18
20
22
24
AXIAL NODE

FIGURE 5.5.12

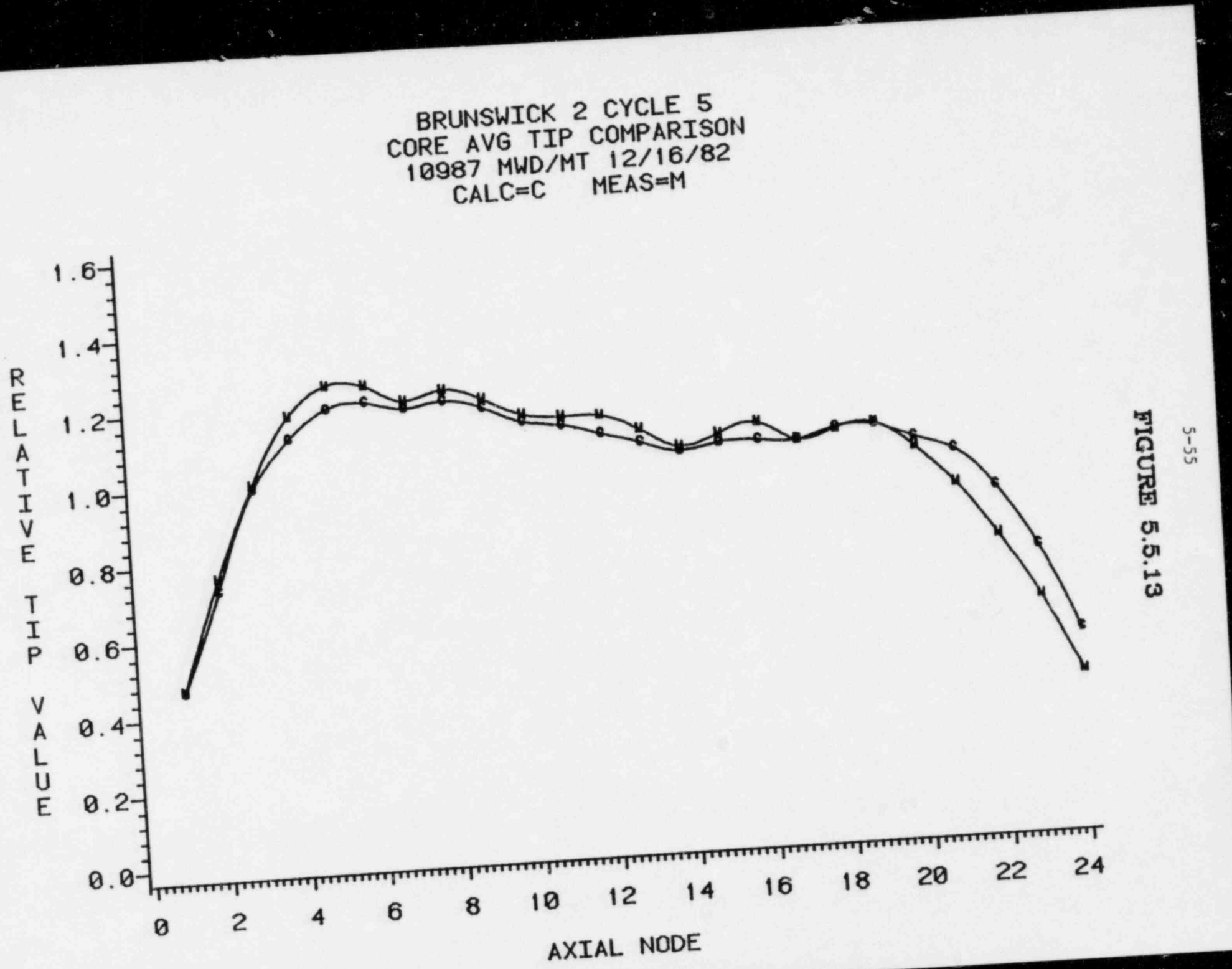
BRUNSWICK 2 CYCLE 5
CORE AVG TIP COMPARISON
10987 MWD/MT 12/16/82
CALC=C MEAS=M
RELATIVE TIP VALUE
1.6
1.4
1.2
1.0
0.8
0.6
0.4
0.2
0.0
0
2
4
6
8
10
12
14
16
18
20
22
24
AXIAL NODE

FIGURE 5.5.13

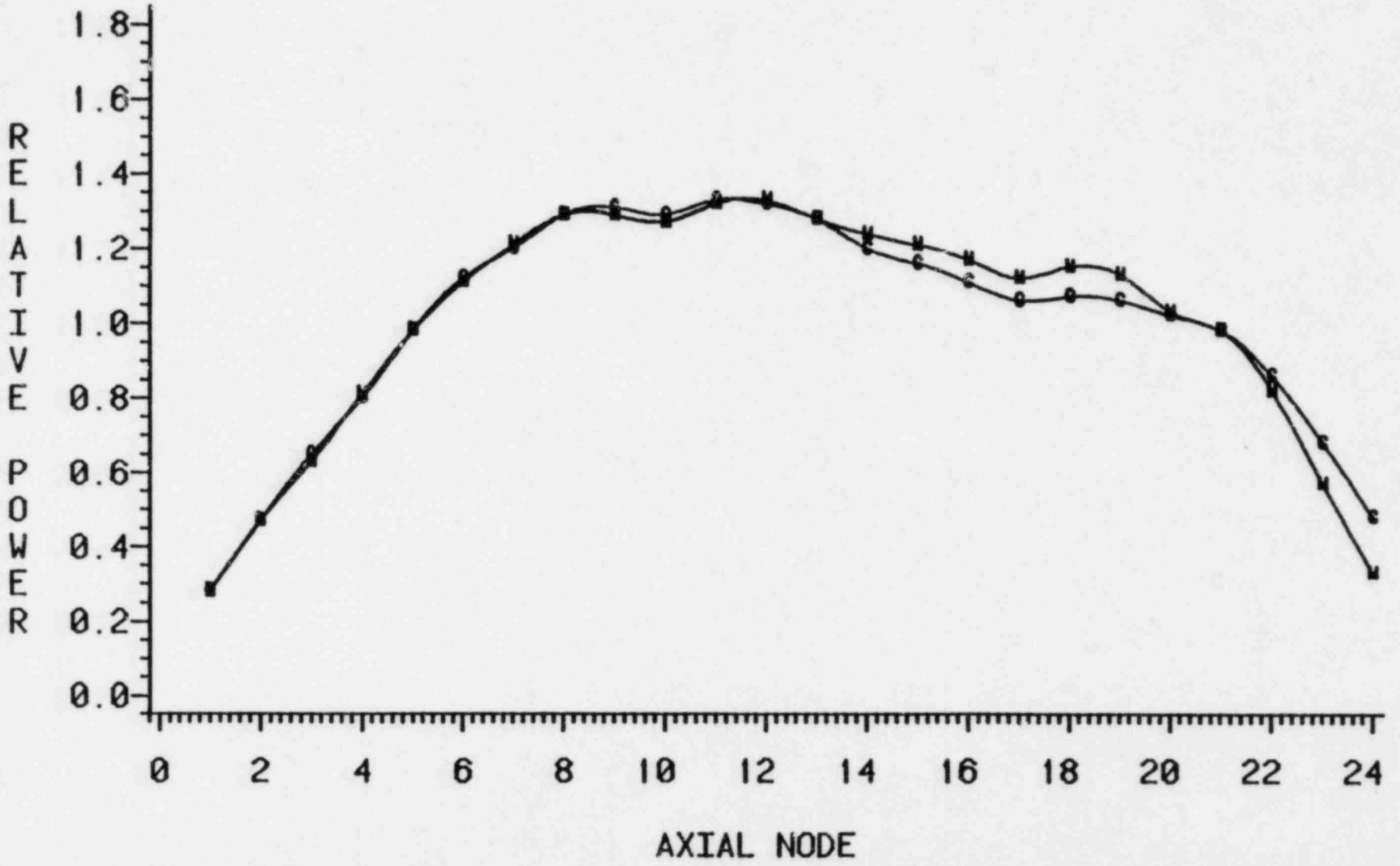
QUAD CITIES 1 CYCLE 1
CORE AVG TIP COMPARISON
272 MWD/MT 06/29/72
CALC=C MEAS=M
RELATIVE POWER
1.8
1.6
1.4
1.2
1.0
0.8
0.6
0.4
0.2
0.0
0
2
4
6
8
10
12
14
16
18
20
22
24
AXIAL NODE

FIGURE 5.5.14

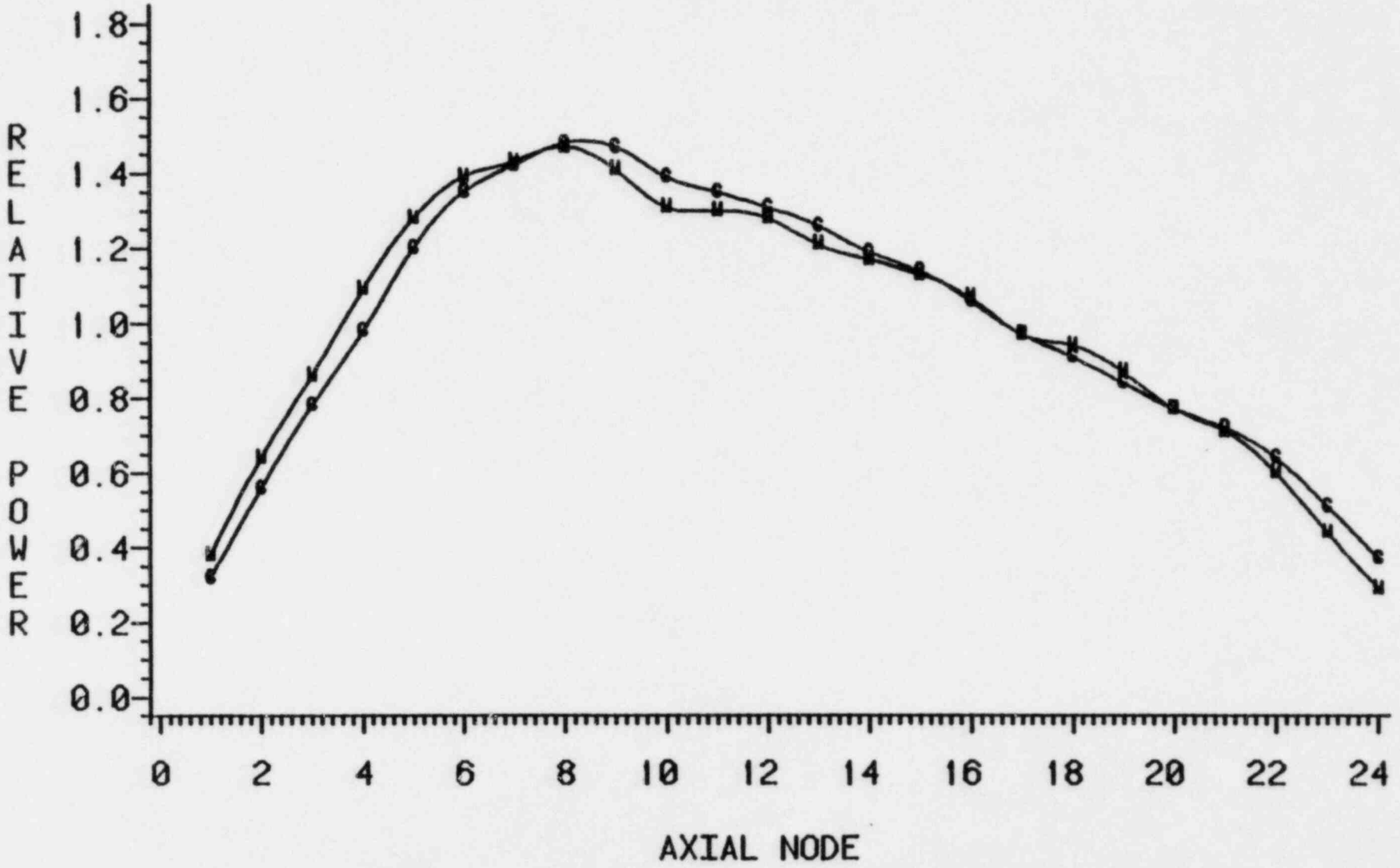
QUAD CITIES 1 CYCLE 1
CORE AVG TIP COMPARISON
3190 MWD/MT 03/08/73
CALC=C MEAS=M
RELATIVE POWER
1.8
1.6
1.4
1.2
1.0
0.8
0.6
0.4
0.2
0.0
0
2
4
6
8
10
12
14
16
18
20
22
24
AXIAL NODE

FIGURE 5.5.15

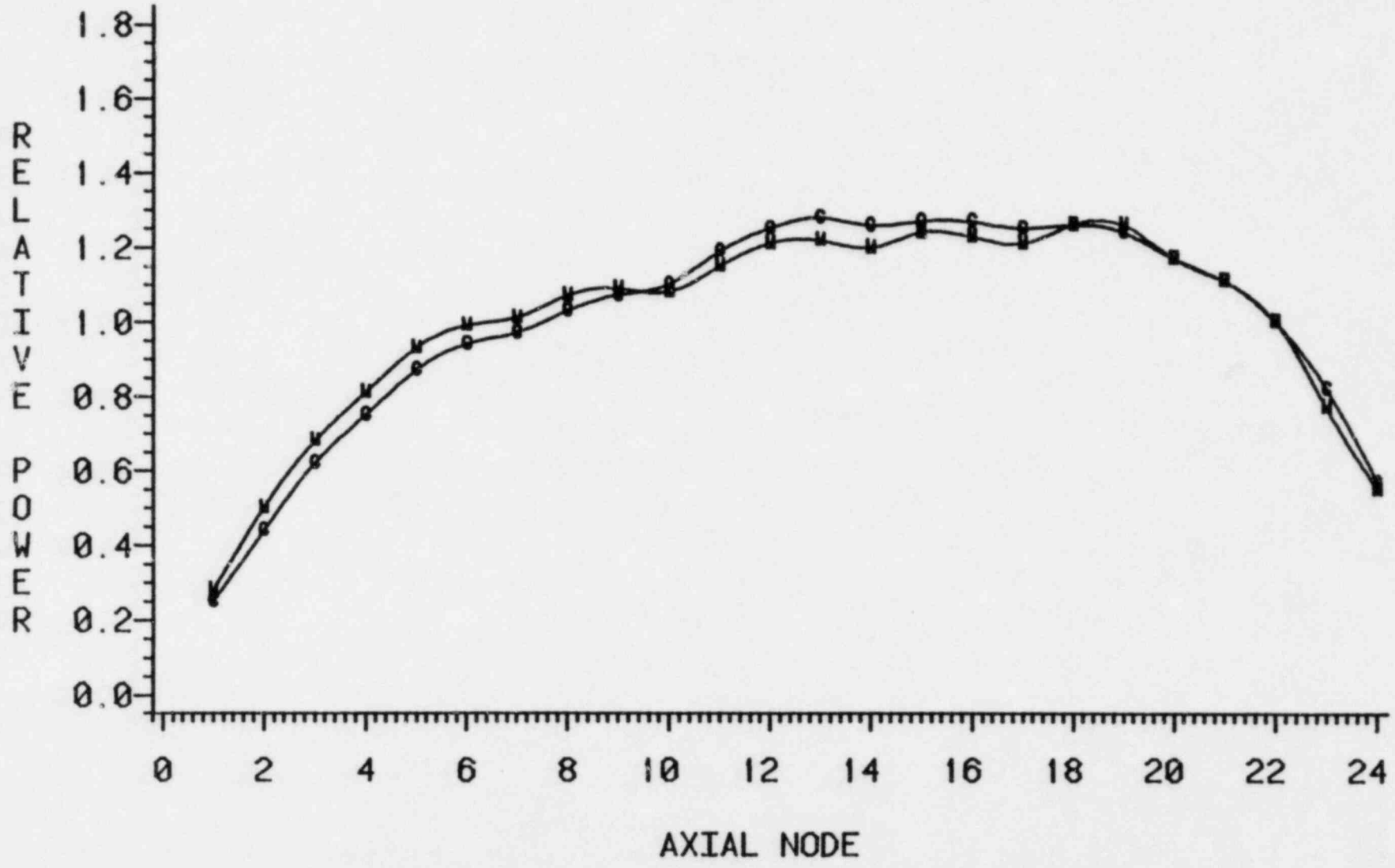
QUAD CITIES 1 CYCLE 1
CORE AVG TIP COMPARISON
7659 MWD/MT 03/05/74
CALC=C MEAS=M
RELATIVE POWER
1.8
1.6
1.4
1.2
1.0
0.8
0.6
0.4
0.2
0.0
0
2
4
6
8
10
12
14
16
18
20
22
24
AXIAL NODE

FIGURE 5.5.16

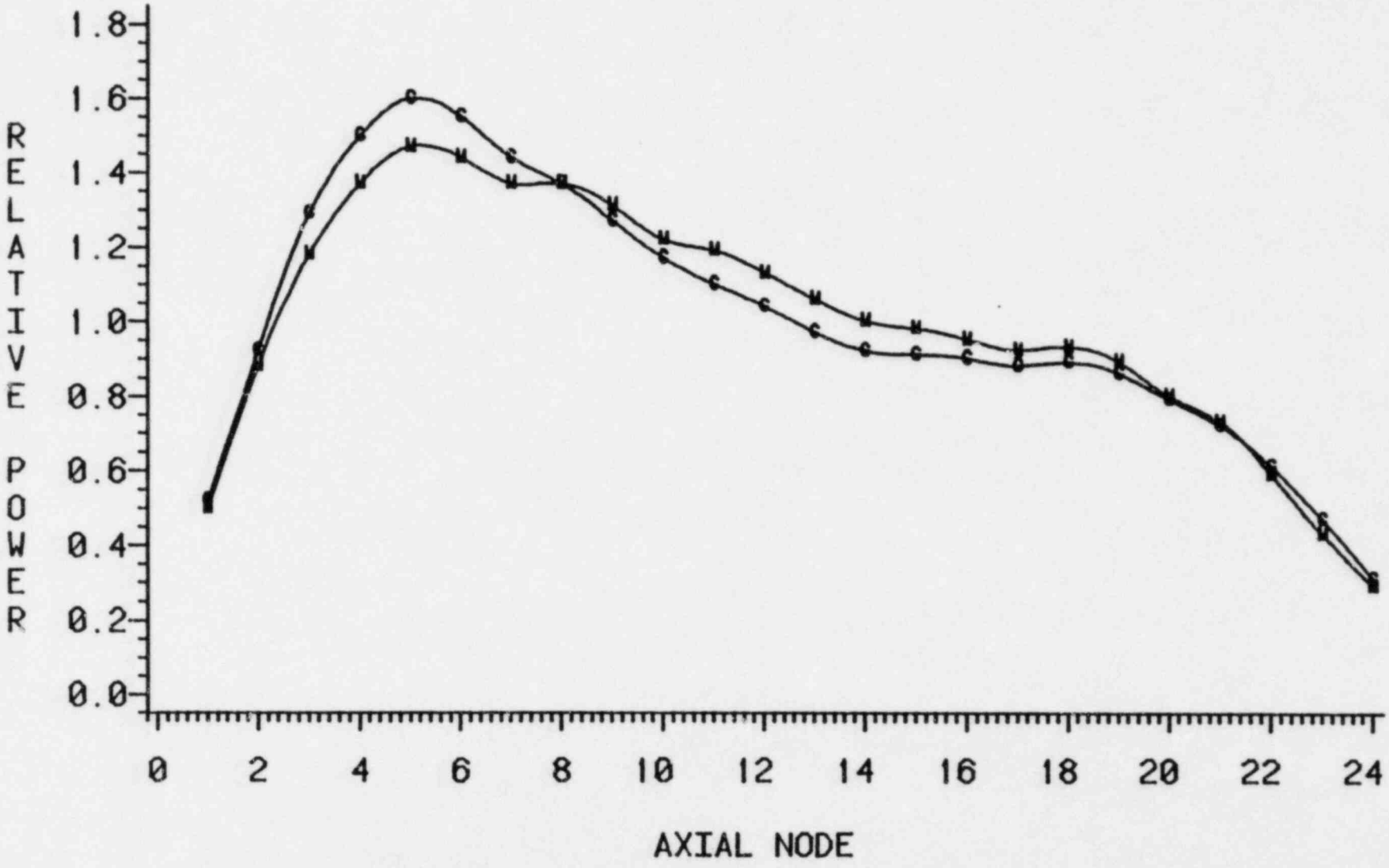
QUAD CITIES 1 CYCLE 2
CORE AVG TIP COMPARISON
7303 MWD/MT 07/26/74
CALC=C MEAS=M
RELATIVE POWER
1.8
1.6
1.4
1.2
1.0
0.8
0.6
0.4
0.2
0.0
0
2
4
6
8
10
12
14
16
18
20
22
24
AXIAL NODE

FIGURE 5.5.17

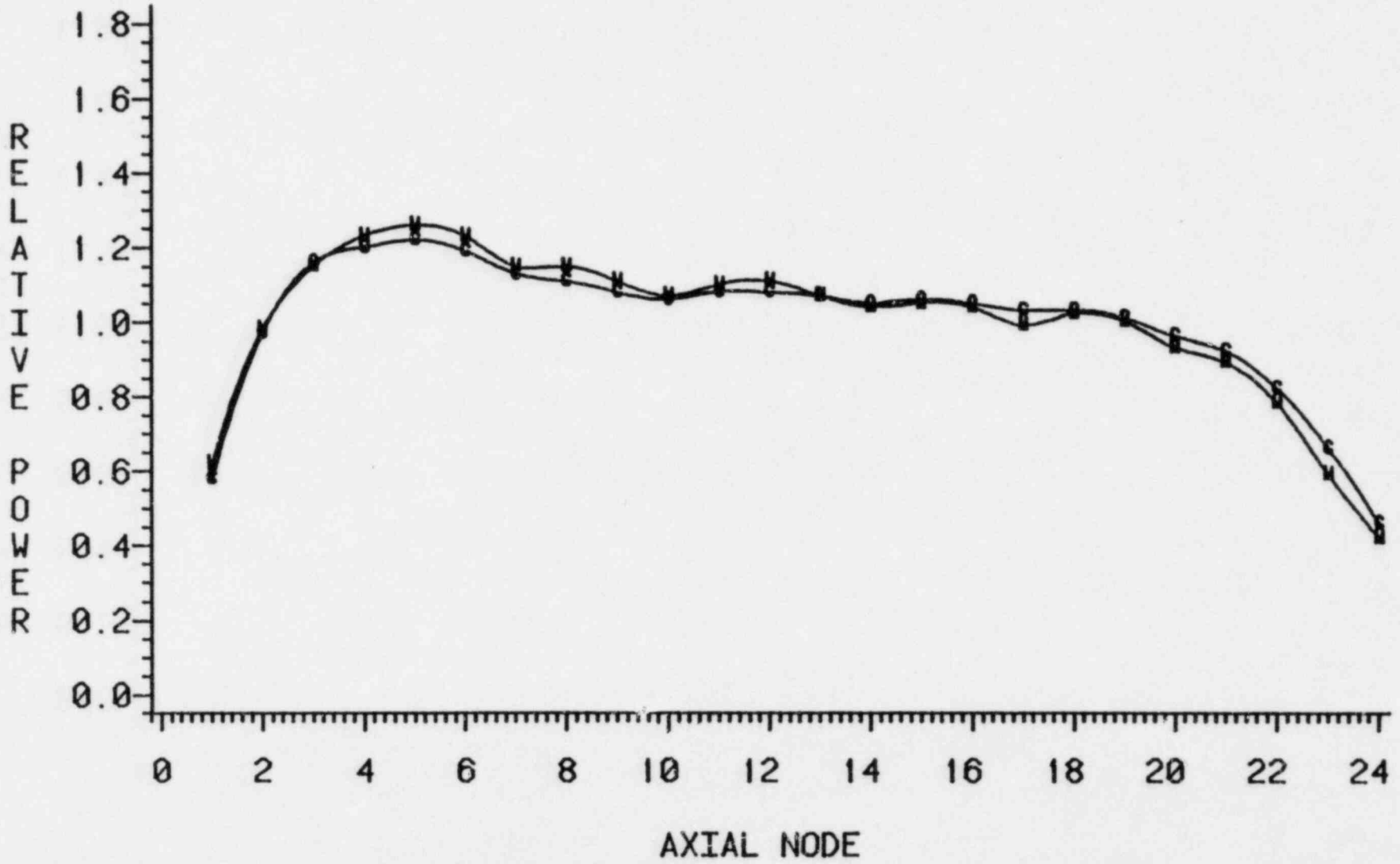
QUAD CITIES 1 CYCLE 2
CORE AVG TIP COMPARISON
10173 MWD/MT 04/03/75
CALC=C MEAS=M
RELATIVE POWER
1.8
1.6
1.4
1.2
1.0
0.8
0.6
0.4
0.2
0.0
0
2
4
6
8
10
12
14
16
18
20
22
24
AXIAL NODE

FIGURE 5.5.18

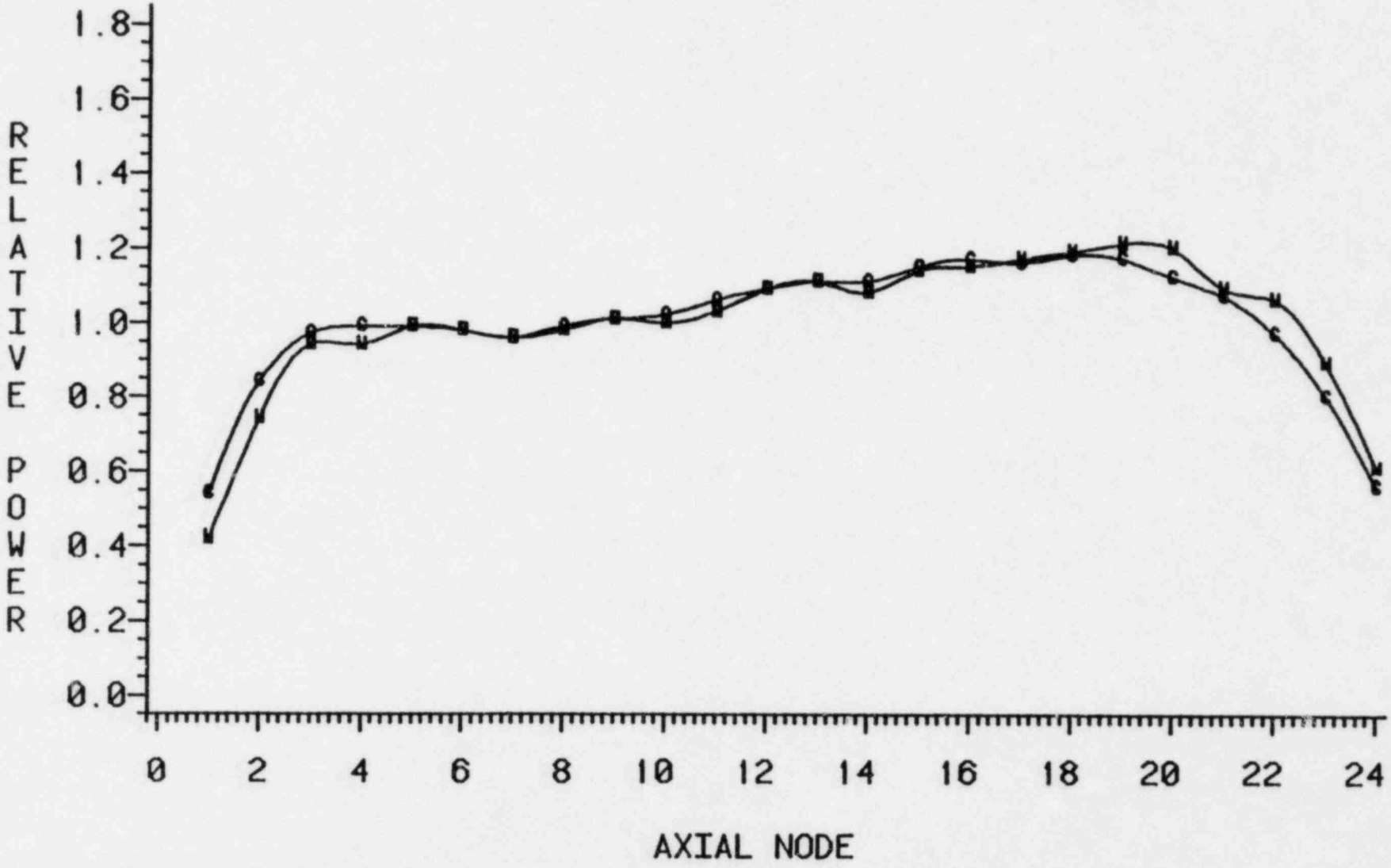
QUAD CITIES 1 CYCLE 2
CORE AVG TIP COMPARISON
13741 MWD/MT 12/31/75
CALC=C MEAS=M
RELATIVE POWER
1.8
1.6
1.4
1.2
1.0
0.8
0.6
0.4
0.2
0.0
0
2
4
6
8
10
12
14
16
18
20
22
24
AXIAL NODE

FIGURE 5.5.19

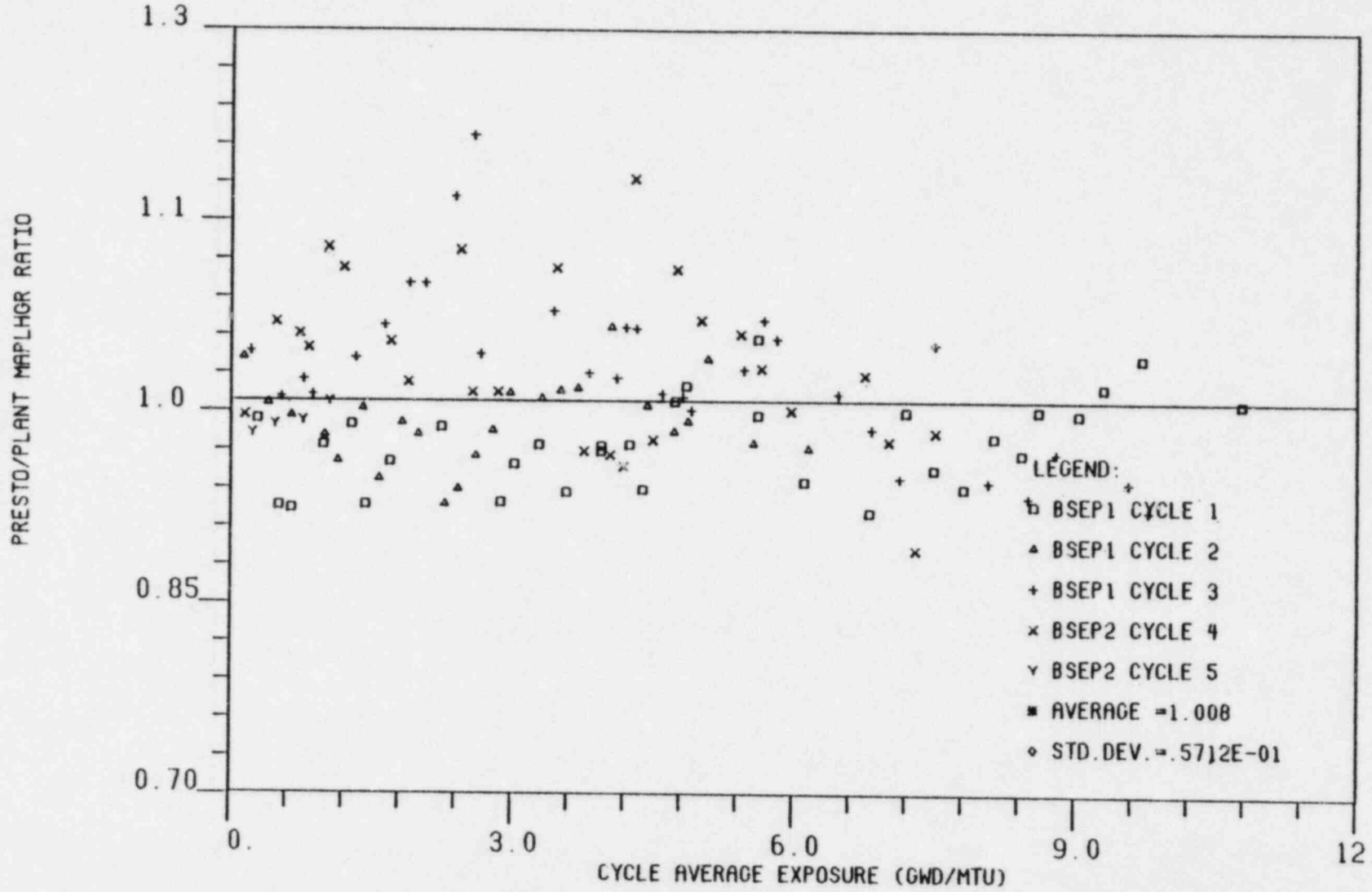

RATIO OF PRESTO/PLANT MAPLHGR VS. CYCLE AVERAGE EXPOSURE

Figure 5.5.20

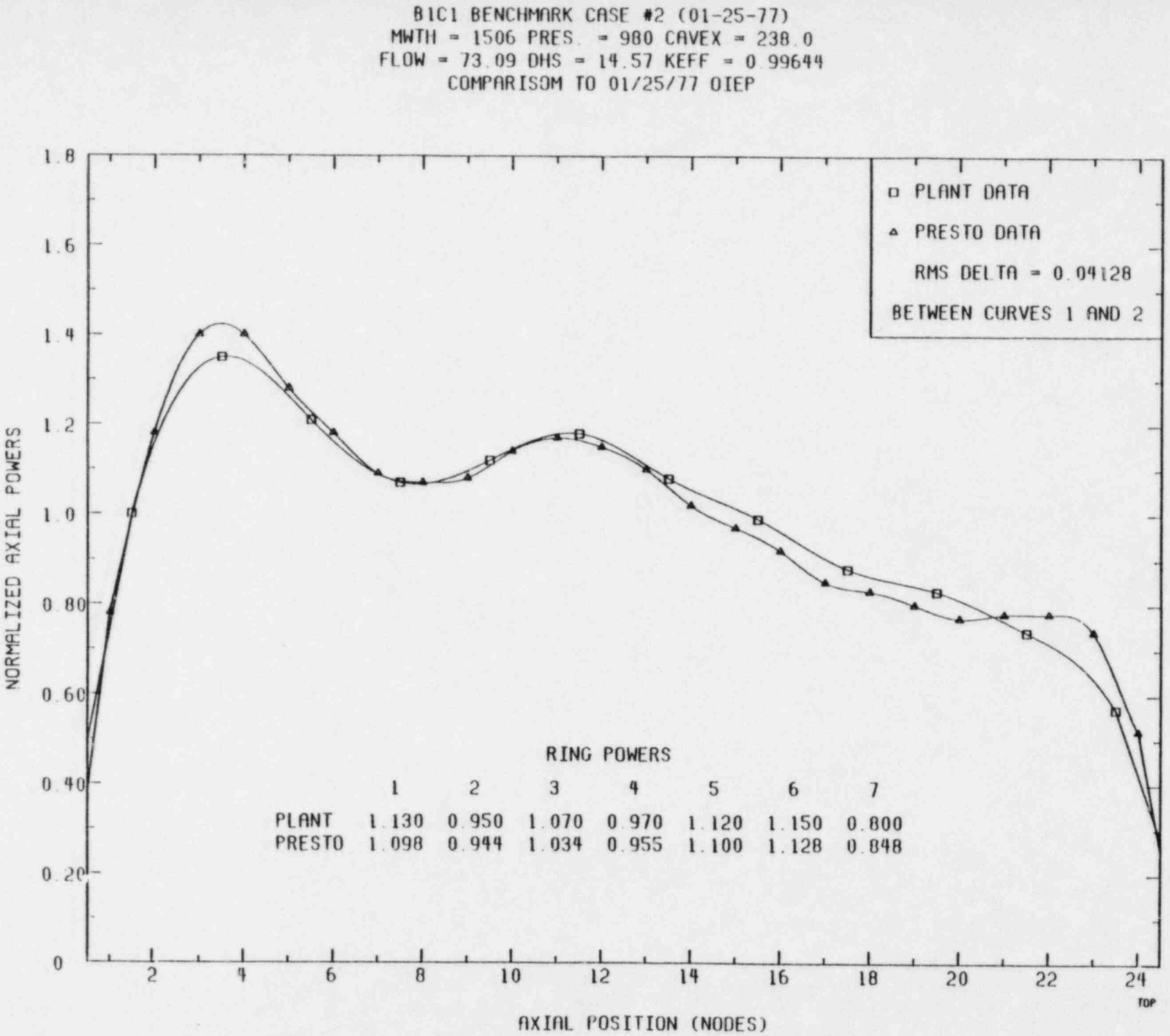
B1C1 BENCHMARK CASE #2 (01-25-77)
MWTH = 1506 PRES. = 980 CAVEX = 238.0
FLOW = 73.09 DHS = 14.57 KEFF = 0.99644
COMPARISOM TO 01/25/77 OIEP
PLANT DATA
PRESTO DATA
RMS DELTA = 0.04128
BETWEEN CURVES 1 AND 2
NORMALIZED AXIAL POWERS
AXIAL POSITION (NODES)
TOP
RING POWERS
1 2 3 4 5 6 7
PLANT 1.130 0.950 1.070 0.970 1.120 1.150 0.800
PRESTO 1.098 0.944 1.034 0.955 1.100 1.128 0.848

Figure 5.5.21

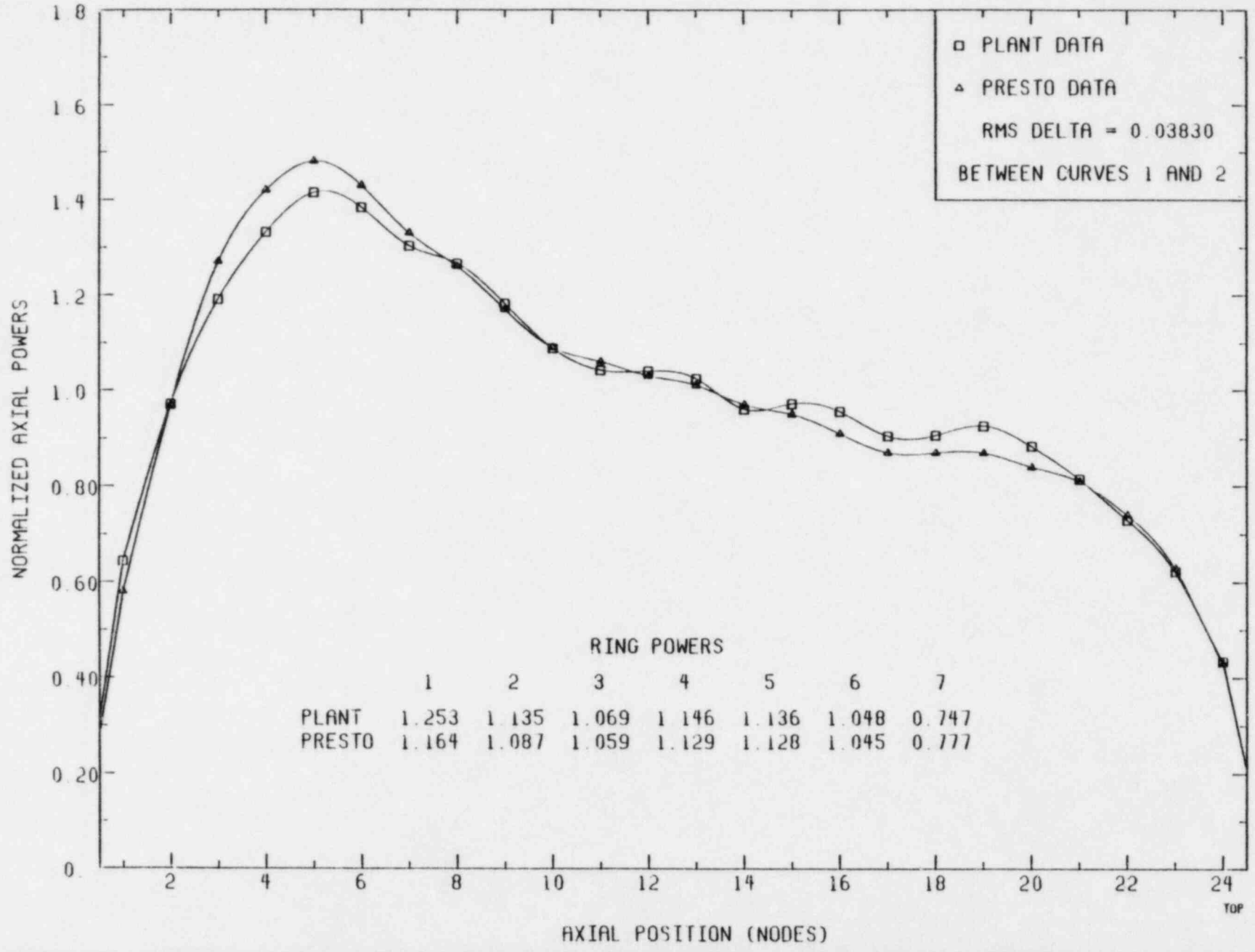
B1C1 BENCHMARK LOW FLOW/POWER CASE #2 (04-14-78)
MWTH = 1943.73 PRES = 986.32 CAVEX = 5222.7
FLOW = 40.02 DHS = 26.20 KEFF = 0.99496
COMPARISON TO 04/14/78 DATA
PLANT DATA
PRESTO DATA
RMS DELTA = 0.03830
BETWEEN CURVES 1 AND 2
NORMALIZED AXIAL POWERS
AXIAL POSITION (NODES)
TOP
RING POWERS
1 2 3 4 5 6 7
PLANT 1.253 1.135 1.069 1.146 1.136 1.048 0.747
PRESTO 1.164 1.087 1.059 1.129 1.128 1.045 0.777

Figure 5.5.22

B1C2 BENCHMARK CASE #12 (09-26-79)
MWTH = 2304.53 PRES. = 1008.07 CAVEX = 8640.6
FLOW = 66.00 DHS = 21.17 KEFF = 0.99359
COMPARISON TO 9/26/79 OIEP DATA

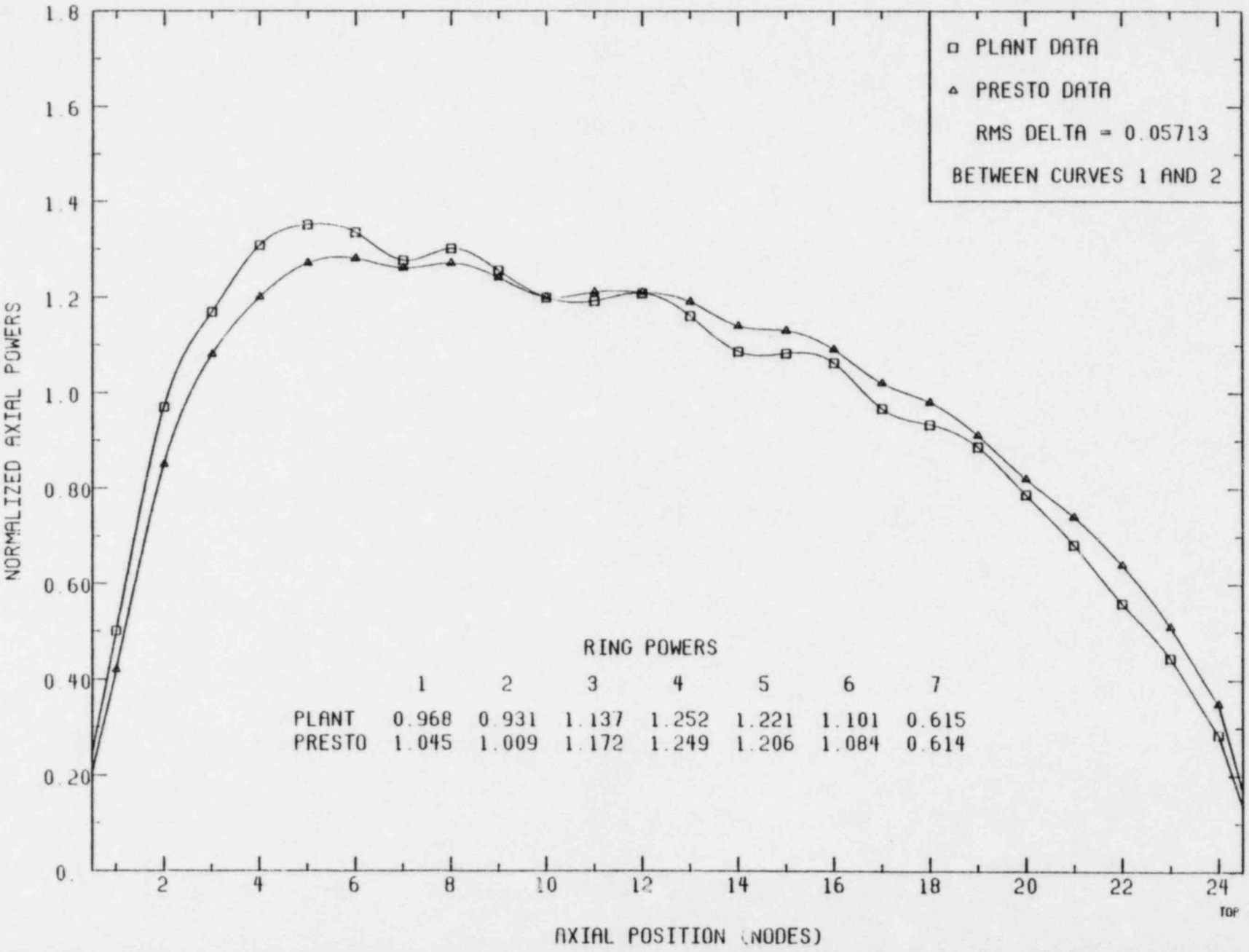

RING POWERS

	1	2	3	4	5	6	7
PLANT	0.968	0.931	1.137	1.252	1.221	1.101	0.615
PRESTO	1.045	1.009	1.172	1.249	1.206	1.084	0.614

Figure 5.5.23

B1C3 BENCHMARK CASE #22 (04-16-81)
MWTH = 1807.93 PRES. = 1017.45 CAVEX = 10667.0
FLOW = 71.24 DHS = 19.73 KEFF = 0.99597
COMPARISON TO 04/16/81 OIEP DATA

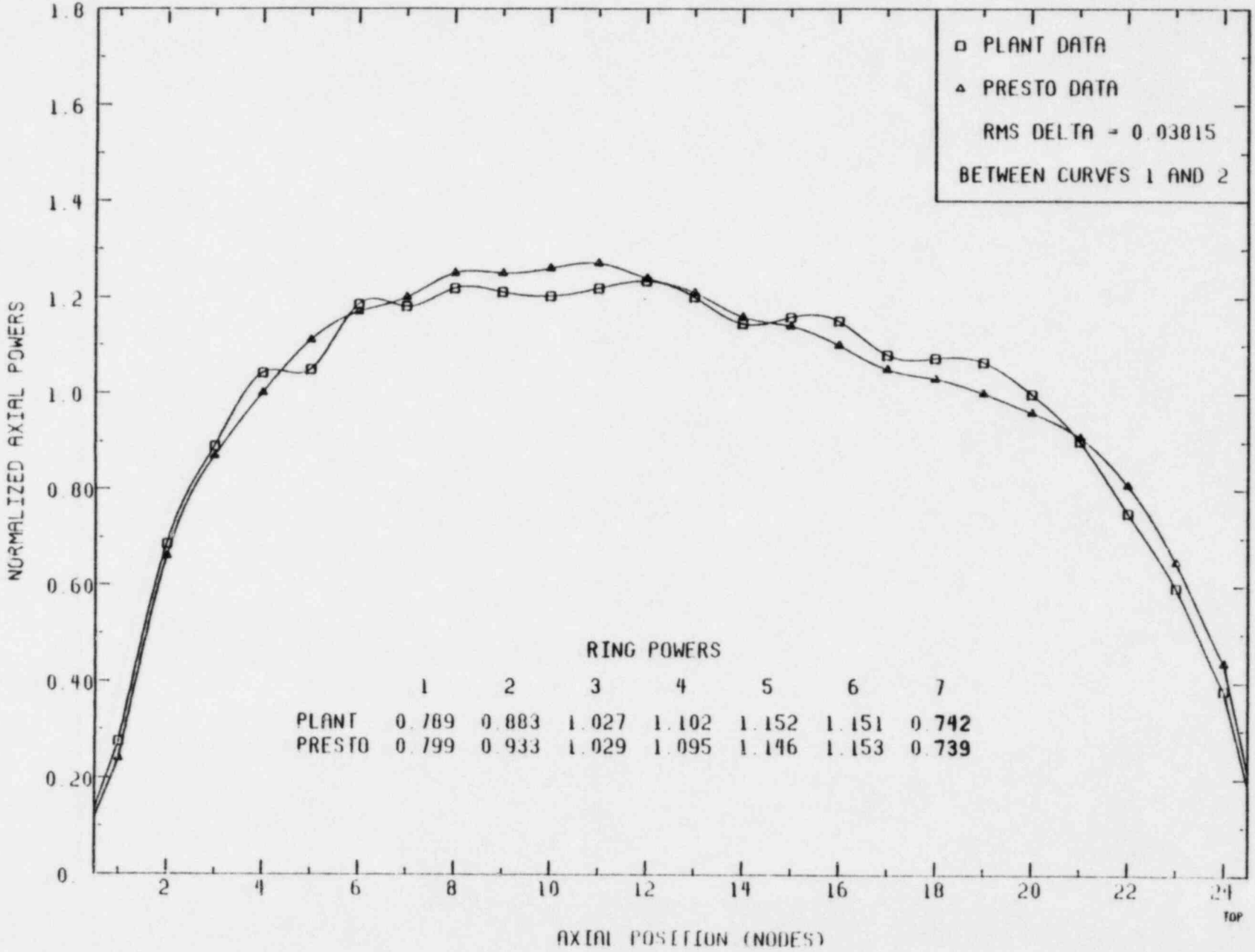

RING POWERS

	1	2	3	4	5	6	7
PLANT	0.789	0.883	1.027	1.102	1.152	1.151	0.742
PRESTO	0.799	0.933	1.029	1.095	1.146	1.153	0.739

Figure 5.5.24

Figure 5.5.25

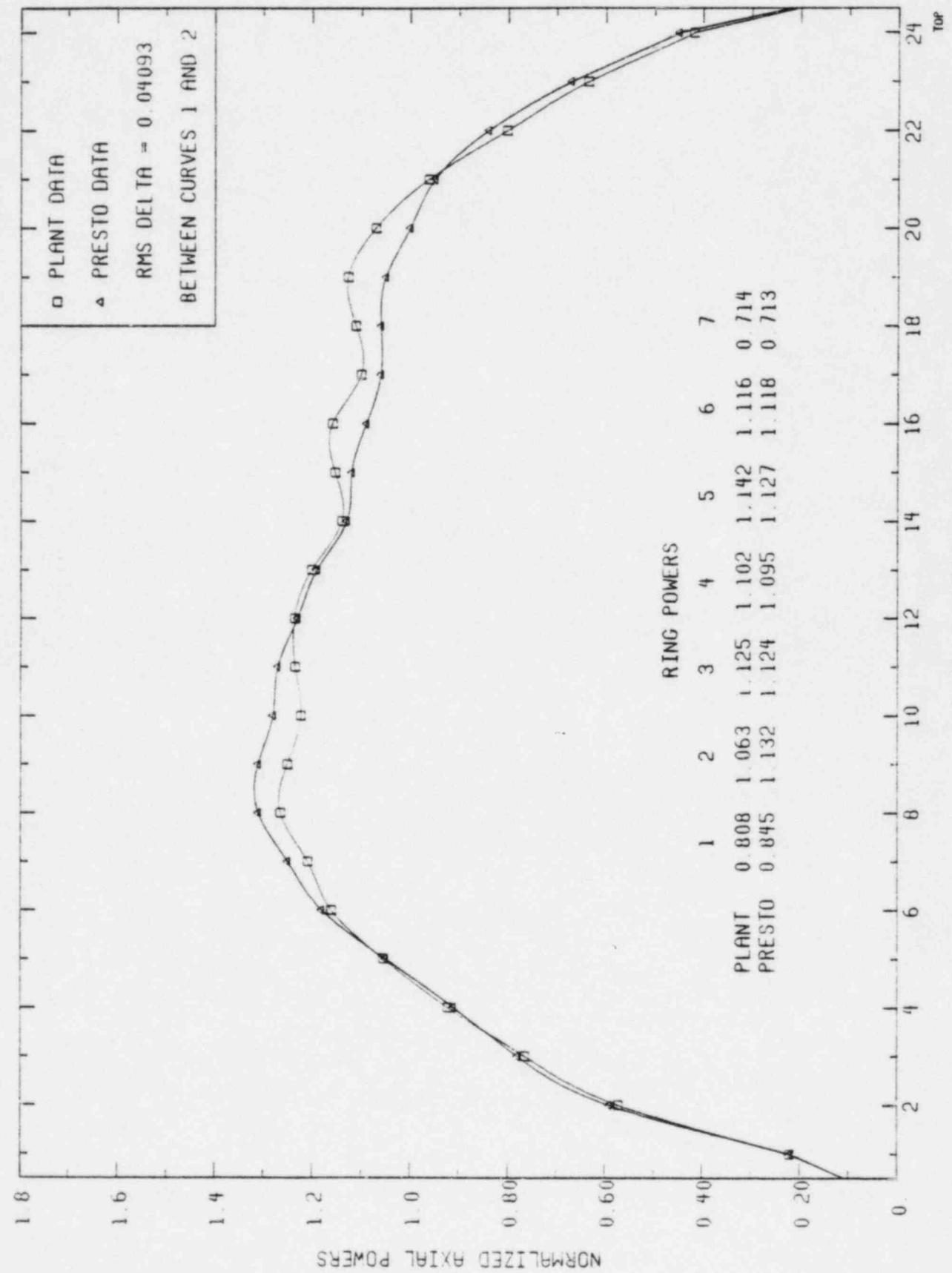
B1C3 BENCHMARK CASE #30 (12-13-81)
MWTH = 2421.75 PRES. = 1012.95 CAVEX = 11940.0
FLOW = 71.43 DHS = 29.64 KEFF = 0.99622
COMPARISON TO 12/13/81 OIEP DATA
PLANT DATA
PRESTO DATA
RMS DELTA = 0.04093
BETWEEN CURVES 1 AND 2
RING POWERS
1 2 3 4 5 6 7
PLANT 0.808 1.063 1.125 1.102 1.142 1.116 0.714
PRESTO 0.845 1.132 1.124 1.095 1.127 1.118 0.713
NORMALIZED AXIAL POWERS
AXIAL POSITION (NODES)
TOP

B1C3 BENCHMARK CASE #39 (04-25-82)
MWTH = 1437.34 PRES = 968.70 CAVEX = 14142.7
FLOW = 37.78 DHS = 28.70 KEFF = 0.99624
COMPARISON TO 04/25/82 OIEP DATA

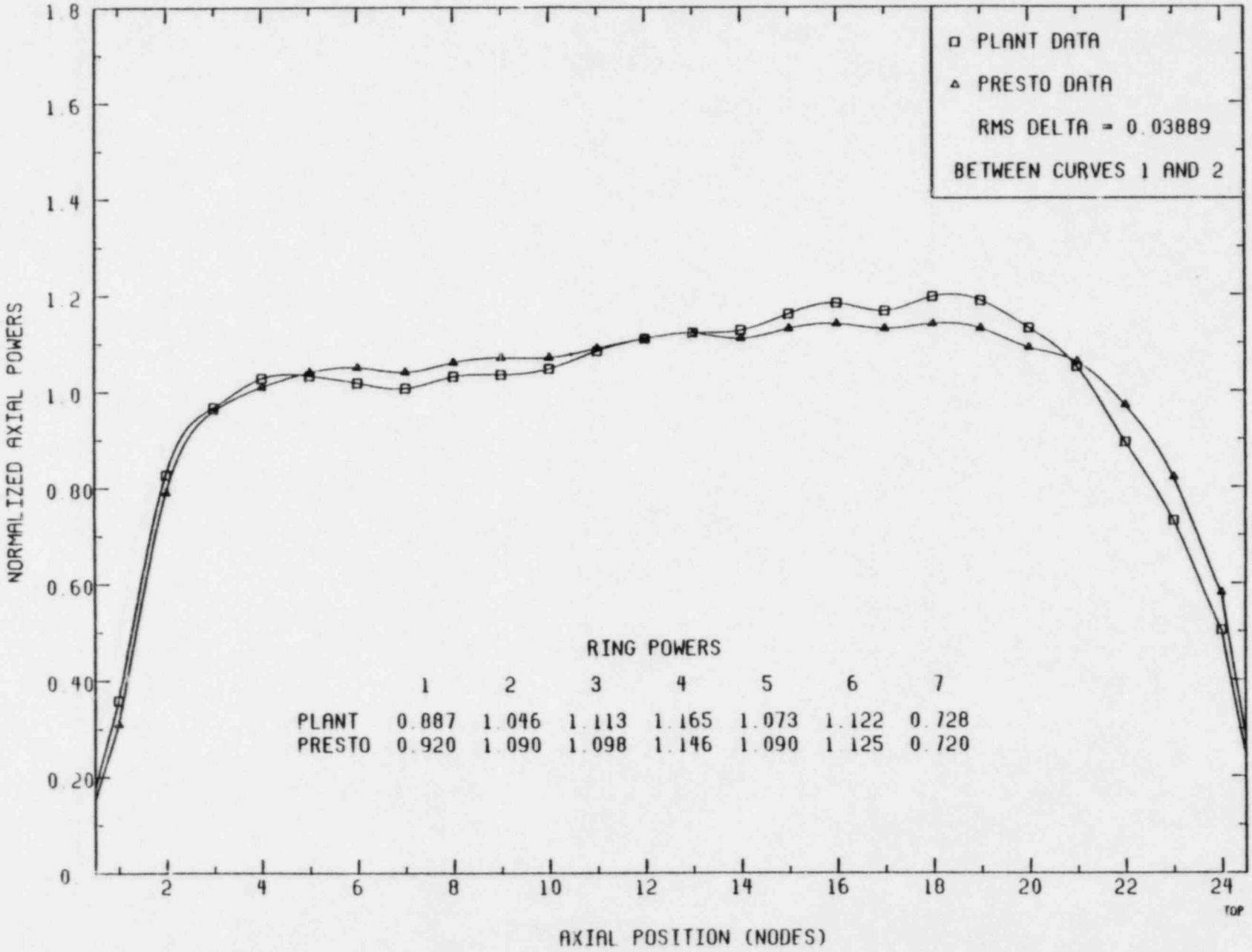

Figure 5.5.26

B1C3 BENCHMARK CASE #46 (11-28-82)
MWTH = 1660.51 PRES. = 1000.57 CAVEX = 15702.1
FLOW = 76.80 DHS = 14.95 KEFF = 0.99991
COMPARISON TO 11/28/82 OIEP DATA

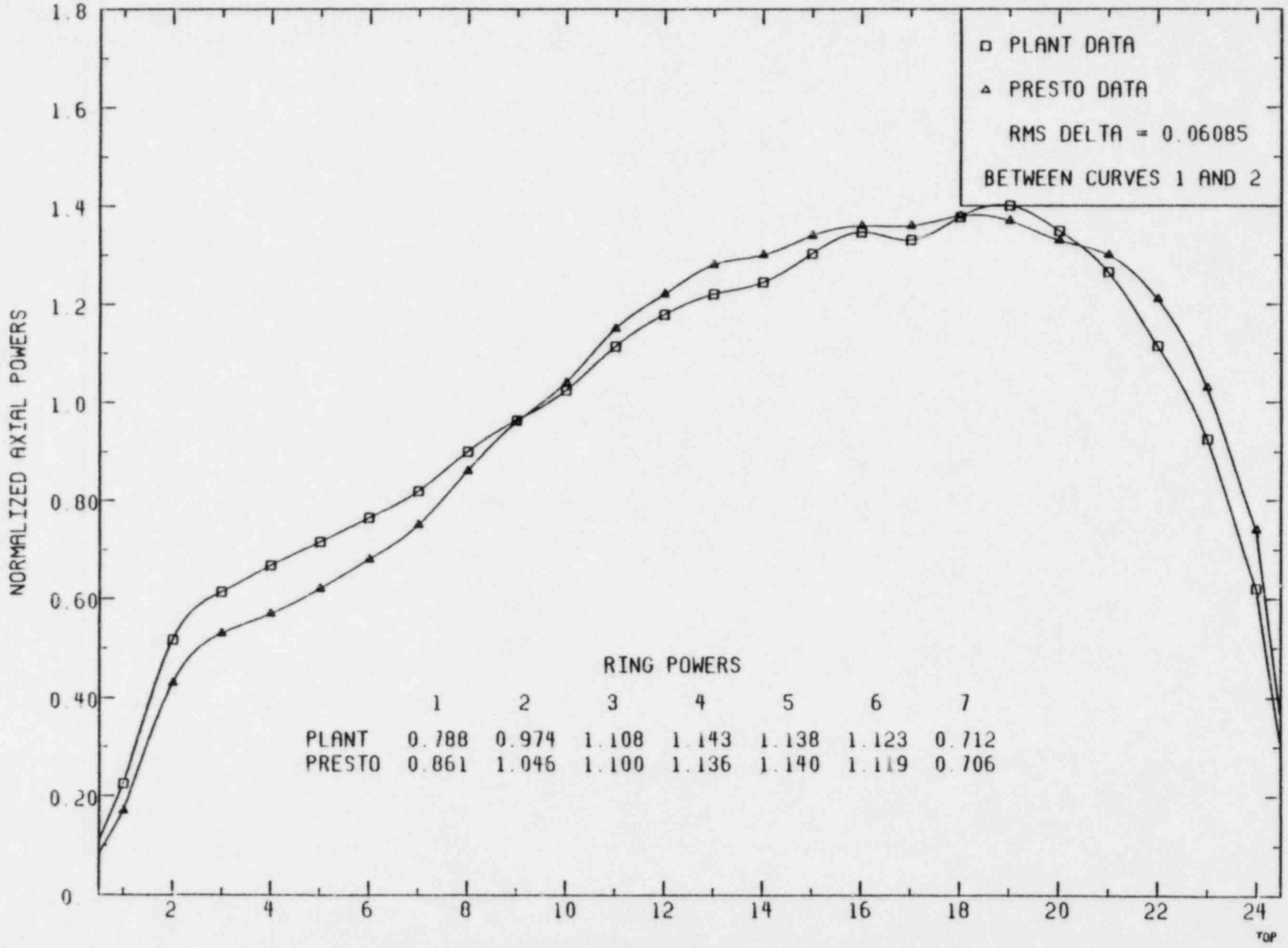

RING POWERS

	1	2	3	4	5	6	7
PLANT	0.788	0.974	1.108	1.143	1.138	1.123	0.712
PRESTO	0.861	1.046	1.100	1.136	1.140	1.119	0.706

Figure 5.5.27

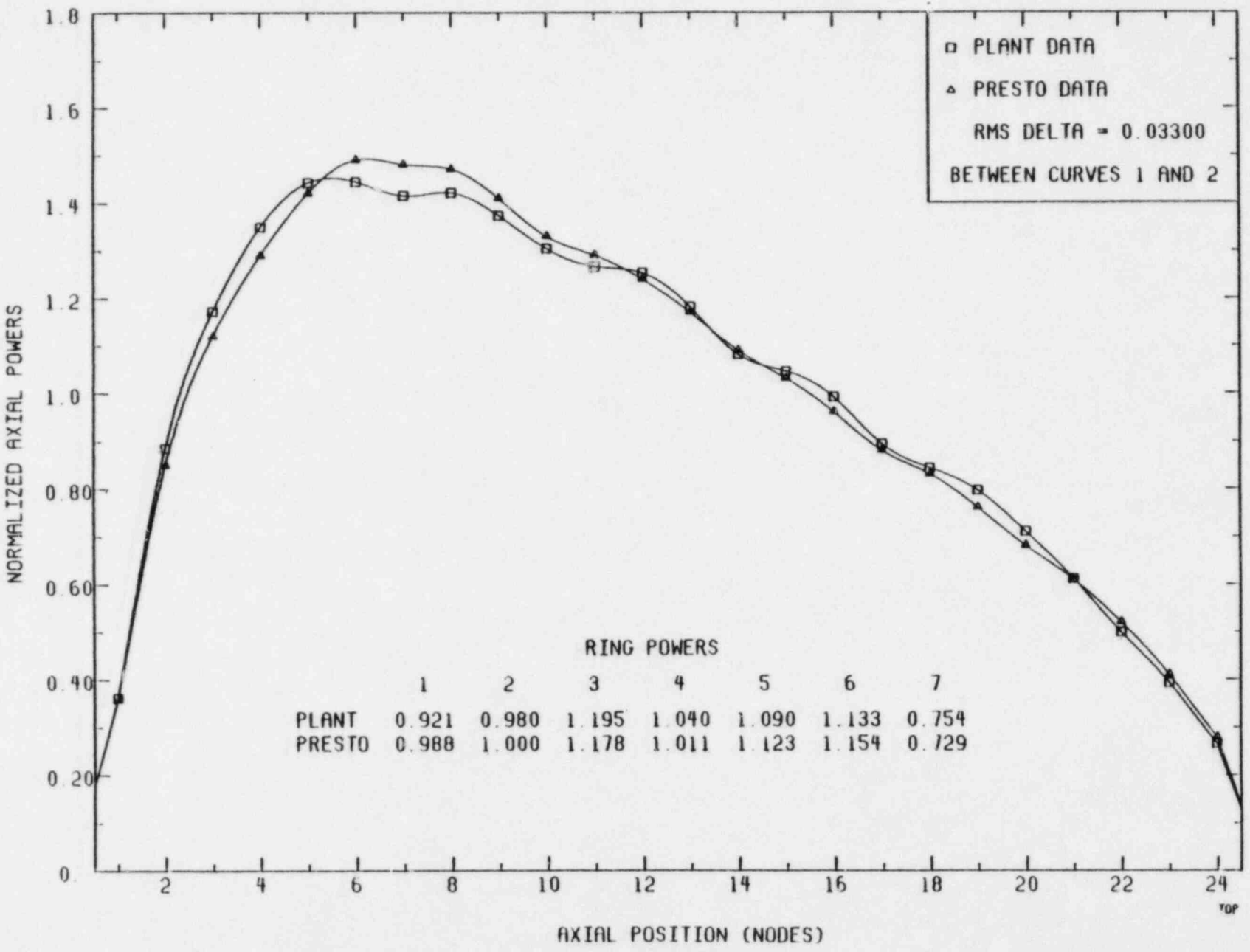
B2C4 BENCHMARK CASE #08 (01-25-81)
MWTH = 1983.80 PRES. = 0993.50 CAVEX = 9975.9
FLOW = 47.10 DHS = 40.30 KEFF = 0.99461
COMPARISON TO 01/25/81 OIEP DATA
PLANT DATA
PRESTO DATA
RMS DELTA = 0.03300
BETWEEN CURVES 1 AND 2
NORMALIZED AXIAL POWERS
AXIAL POSITION (NODES)
TOP
RING POWERS
1 2 3 4 5 6 7
PLANT 0.921 0.980 1.195 1.040 1.090 1.133 0.754
PRESTO 0.988 1.000 1.178 1.011 1.123 1.154 0.729

Figure 5.5.28

Figure 5.5.29

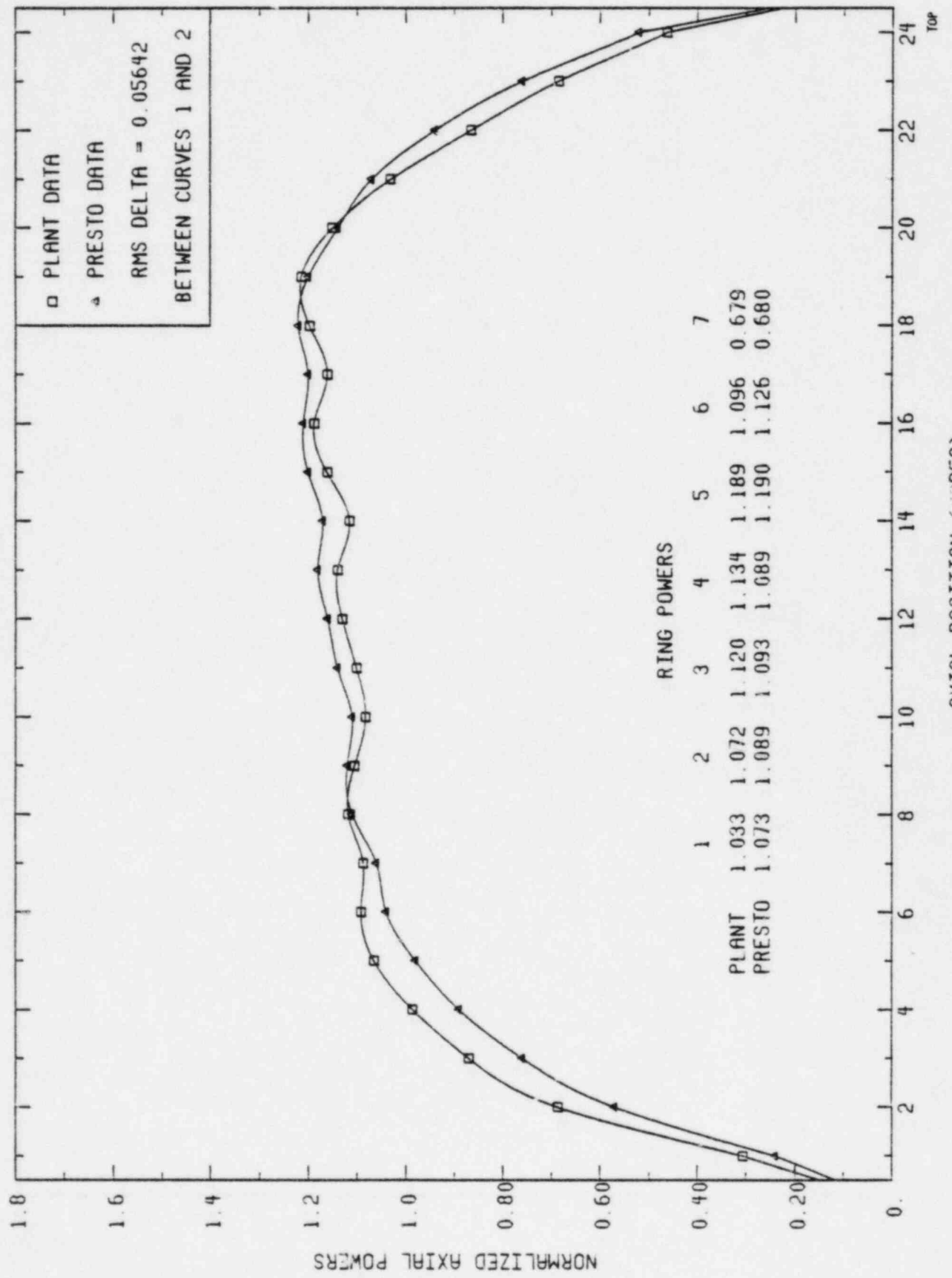
B2C4 BENCHMARK CASE #21 (10-22-81)
MWTH = 1424.11 PRES. = 978.07 CAVEX = 12467.1
FLOW = 40.00 DHS = 26.87 KEFF = 0.99790
COMPARISON TO 10/22/81 OIEP DATA
PLANT DATA
PRESTO DATA
RMS DELTA = 0.05642
BETWEEN CURVES 1 AND 2
RING POWERS
1 2 3 4 5 6 7
PLANT 1.033 1.072 1.120 1.134 1.189 1.096 0.679
PRESTO 1.073 1.089 1.093 1.089 1.190 1.126 0.680
NORMALIZED AXIAL POWERS
AXIAL POSITION (NODES)
TOP
0. 0.20 0.40 0.60 0.80 1.0 1.2 1.4 1.6 1.8
2 4 6 8 10 12 14 16 18 20 22 24

Figure 5.5.30

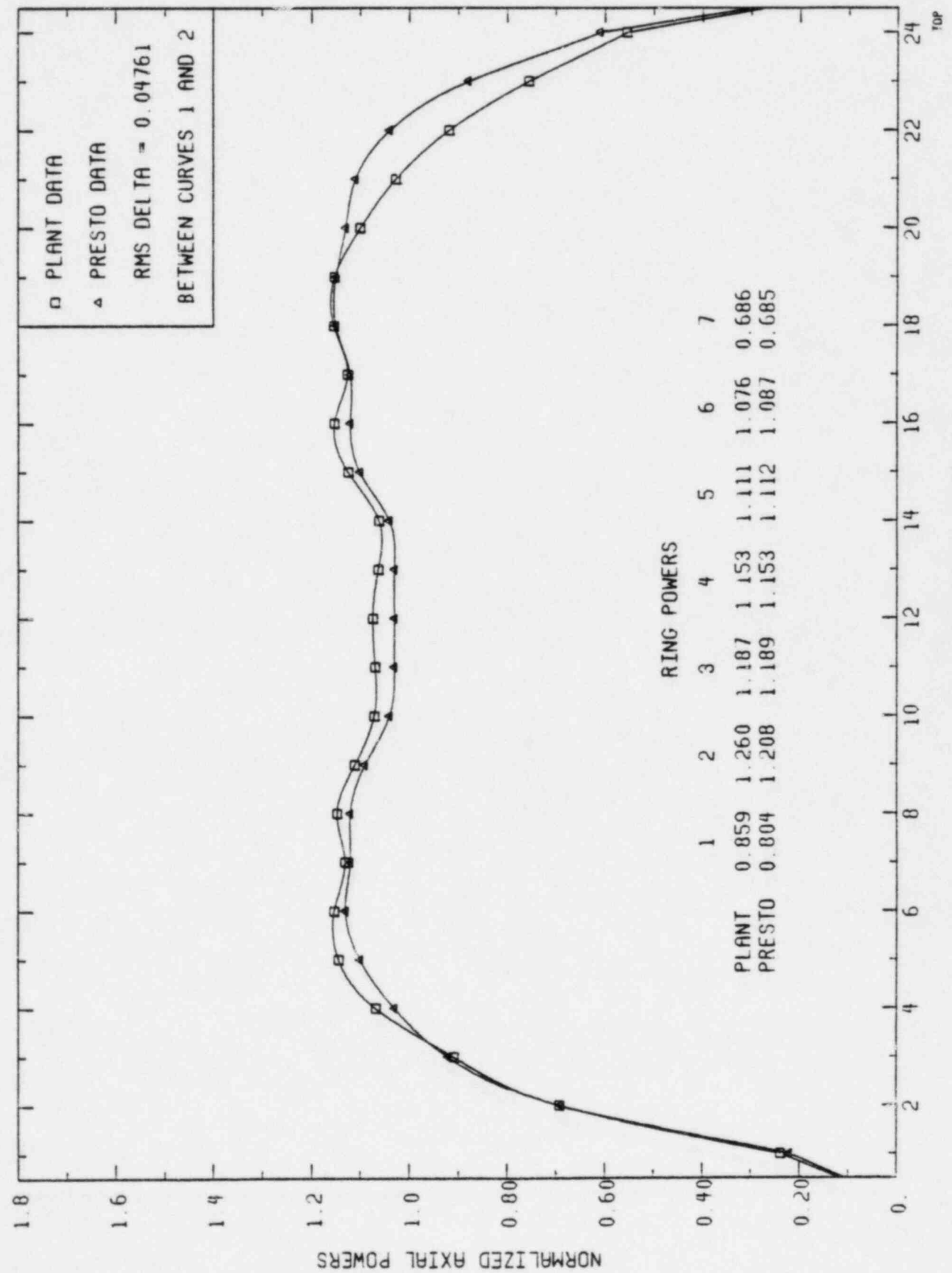
B2C5 BENCHMARK CASE #02 (10-27-82)
MWTH = 1942.06 PRES. = 990.82 CAVEX = 9478.9
FLOW = 67.39 DHS = 19.33 KEFF = 0.99490
COMPARISON TO 10/27/82 OIEP DATA
□ PLANT DATA
△ PRESTO DATA
RMS DELTA = 0.04761
BETWEEN CURVES 1 AND 2
RING POWERS
1 2 3 4 5 6 7
PLANT 0.859 1.260 1.187 1.153 1.111 1.076 0.686
PRESTO 0.804 1.208 1.189 1.153 1.112 1.087 0.685
NORMALIZED AXIAL POWERS
AXIAL POSITION (NODES)
TOP

5.6 Quad-Cities Unit 1 Gamma Scan Analysis

The 1974 and 1976 Quad-Cities Unit 1 gamma scan measurements provide an opportunity to test the PRESTO-B hot full-power model against data more directly related to power distribution than TIPs or process computer extrapolations. The 1976 measurements are considered particularly excellent since the reactor operated near steady conditions for the final month of Cycle 2.

Table 5.6.1 summarizes the results of PRESTO comparisons to the 1974 gamma scan measurements performed at End-of-Cycle 1. Measured data for this table was taken from Reference 13. Since instrument calibration was only performed between readings of symmetric assemblies, this data is only useful in comparing relative axial La-140 activities. For the 17 uncontrolled assemblies scanned, the average difference in peak-to-average La-140 activity (calculated - measured) was 3.62 percent, with a standard deviation of 2.94 percent. Fourteen controlled assemblies showed a 3.51 percent average difference with a 3.32 percent standard deviation. For the entire population of 31 data points, the average difference was 3.57 percent, with a 3.07 percent standard deviation. The formulas used for computing the differences and standard deviations are as follows:

$$\text{Percent Difference} = 200 \times (C - M)/(C + M), \text{ and}$$

$$\text{Standard Deviation} = \left[\frac{\sum^{n} (Di - \bar{D})^2}{n-1}\right]^{1/2}.$$

These results show very good agreement between calculated and measured peak-to-average values, with essentially no difference between rodded and unrodded conditions.

Figures 5.6.1, 5.6.2, and 5.6.3 show calculated versus measured axial La-140 activities for the average of all 31 assemblies scanned, a typical partially controlled assembly (location 55-40), and a typical uncontrolled assembly (location 23-10), respectively. Again, very good agreement is seen, although PRESTO tends to overpredict the power level by 4 to 8 percent near the top of the core.

The combined measurement uncertainty quoted in Reference 8 is approximately 3.0 percent.

Table 5.6.2 summarizes the results of PRESTO peak-to-average comparisons to the 1976 gamma scan measurements, performed at end of Cycle 2. Since PRESTO simulations were performed assuming quarter-core mirror symmetry, Table 5.6.2 includes only the 71 assemblies actually in the octant that was scanned, with symmetric assemblies in other octants deleted. Table 5.6.2 shows that, on the average, PRESTO underpredicted assembly peak-to-average powers by 2.06 percent, with a standard deviation of 1.49 percent. This excellent agreement is illustrated in Figures 5.6.4 through 5.6.9.

Figure 5.6.4 is an eighth core map showing calculated versus measured bundle average La-140 activities for the 71 assemblies within the octant that was scanned at EOC2. Figure 5.6.4 shows that PRESTO has a tendency to overpredict

the radial power level near the core periphery, and to underpredict by two to three percent in the interior. The 1976 gamma scan comparisons yielded a nodal standard deviation (71 assemblies times 12 nodes) of 3.77 percent. The integral standard deviation (71 assembly average differences) was only 2.52 percent. These comparisons are within the range of measurement uncertainties quoted in Reference 8.

Figure 5.6.5 is an axial plot of calculated versus measured average La-140 activity for the 71 assemblies in the octant. Figure 5.6.6 is an axial plot of the best individual assembly, Figure 5.6.7 shows the worst assembly, and Figures 5.6.8 and 5.6.9 give the axial comparisons for the four mixed-oxide assemblies at the center of the core, and for the nine peripheral assemblies that were scanned. All of these figures show excellent agreement between calculated and measured values.

TABLE 5.6.1

MEASURED VS. CALCULATED ASSEMBLY La-140 ACTIVITIES
PEAK-TO-AVERAGE VALUES; QUAD CITIES 1 1974 GAMMA SCAN

ROD NOTCH	LOCATION XX-YY	FRESTO CALCULATED	GAMMA SCAN	PERCENT DIFFERENCE
48	39-58	1.2722	1.2712	0.0786
48	41-58	1.2194	1.2125	0.5675
48	41-56	1.2169	1.2236	-0.5491
48	17-48	1.3483	1.2870	4.6522
48	55-42	1.2527	1.1854	5.5207
48	57-42	1.2256	1.1913	2.8383
48	57-40	1.2645	1.2452	1.5380
48	07-34	1.2575	1.1763	6.6727
48	09-32	1.2220	1.1476	6.2795
48	07-26	1.2446	1.1696	6.2132
48	09-24	1.2549	1.1859	5.6539
48	31-26	1.4868	1.3543	9.3274
48	47-18	1.3159	1.2498	5.1526
48	23-10	1.1956	1.1784	1.4490
48	25-08	1.2292	1.2390	-0.7941
48	31-10	1.2285	1.1718	4.7244
48	33-08	1.2482	1.2212	2.1868
38	39-56	1.2748	1.2815	-0.5242
14	17-50	1.6603	1.6087	3.1569
38	15-48	1.3457	1.2800	5.0044
38	55-40	1.2763	1.2688	0.5894
08	09-34	1.5157	1.4180	6.6605
28	07-32	1.3374	1.3225	1.1203
08	09-26	1.5135	1.3660	10.2448
38	07-24	1.2709	1.2313	3.1652
14	49-18	1.6420	1.6017	2.4848
38	47-16	1.3247	1.2829	3.2060
08	25-10	1.4647	1.3579	7.5675
38	23-08	1.2430	1.2512	-0.6575
08	33-10	1.4813	1.3851	6.7123
28	31-08	1.3744	1.3693	0.3718

17 UNCONTROLLED ASSEMBLIES:	AVERAGE DIFFERENCE =	3.62
	STANDARD DEVIATION =	2.94
14 CONTROLLED ASSEMBLIES:	AVERAGE DIFFERENCE =	3.51
	STANDARD DEVIATION =	3.32
TOTAL, 31 ASSEMBLIES:	AVERAGE DIFFERENCE =	3.57
	STANDARD DEVIATION =	3.07

TABLE 5.6.2

MEASURED VS. CALCULATED ASSEMBLY La-140 ACTIVITIES
PEAK-TO-AVERAGE VALUES; QUAD CITIES 1 1976 GAMMA SCAN

BUNID	PRESTO CALCULATED	GAMMA SCAN	PERCENT DIFFERENCE	BUNID	PRESTO CALCULATED	GAMMA SCAN	PERCENT DIFFERENCE
CX546	1.32081	1.35893	-2.84833	CX297	1.18040	1.19822	-1.49813
CX719	1.34758	1.33283	1.10071	CX523	1.33624	1.34679	-0.78713
CX191	1.29855	1.29333	0.40270	CX198	1.27422	1.28750	-1.03621
GEB162	1.28352	1.35306	-5.27460	GEH022	1.16841	1.19437	-2.19716
CX494	1.35150	1.34991	0.11763	CX393	1.18701	1.20281	-1.32229
CX286	1.30822	1.32657	-1.39279	GEH002	1.14227	1.16192	-1.70534
GEH008	1.17635	1.21071	-2.87916	CX672	1.16960	1.19837	-2.43023
CX490	1.28620	1.34999	-4.83918	GEB132	1.12943	1.15886	-2.57148
CX174	1.31855	1.33070	-0.91709	CX585	1.16139	1.21026	-4.12152
CX617	1.27485	1.30858	-2.61096	CX281	1.15273	1.18437	-2.70774
CX100	1.19639	1.22246	-2.15595	GEB105	1.12358	1.16733	-3.81948
CX024	1.17730	1.18724	-0.84109	CX643	1.29898	1.33571	-2.78890
CX553	1.28734	1.35829	-5.36298	CX044	1.23500	1.24454	-0.76962
CX332	1.18638	1.21691	-2.54075	CX327	1.22046	1.22849	-0.65625
GEH029	1.14494	1.16596	-1.81932	CX362	1.19401	1.21441	-1.69379
GEB123	1.14107	1.16641	-2.19661	CX306	1.17888	1.20064	-1.82919
CX662	1.33241	1.38273	-3.70682	CX660	1.15821	1.18565	-2.34096
CX150	1.27216	1.31081	-2.99299	CX287	1.14954	1.17168	-1.90717
CX440	1.20243	1.25861	-4.56567	CX498	1.16156	1.18920	-2.35200
CX015	1.16745	1.18937	-1.86006	CX310	1.16448	1.18664	-1.88499
CX378	1.18281	1.20615	-1.95347	CX683	1.29290	1.33110	-2.91175
CX186	1.19405	1.20394	-0.82474	CX520	1.32297	1.31161	0.86305
CX682	1.33218	1.41602	-6.10161	CX137	1.27929	1.27854	0.05824
CX611	1.37258	1.39245	-1.43754	CX420	1.25103	1.24201	0.72351
CX351	1.23996	1.27142	-2.50547	CX106	1.24149	1.23413	0.59499
GEH023	1.16697	1.20080	-2.85792	CX394	1.22994	1.22626	0.29968
CX396	1.17773	1.20543	-2.32473	CX057	1.21021	1.22331	-1.07701
CX093	1.17529	1.21868	-3.62455	CX052	1.18127	1.19901	-1.49042
CX316	1.19355	1.21730	-1.97007	CX162	1.15264	1.17772	-2.15235
CX723	1.18680	1.20279	-1.33885	CX717	1.14334	1.15633	-1.12925
GEB149	1.15273	1.18611	-2.85499	CX225	1.15292	1.18645	-2.86616
CX631	1.30078	1.32629	-1.94173	CX453	1.16273	1.19577	-2.80157
CX399	1.19515	1.25477	-4.86645	CX165	1.17451	1.19319	-1.57797
CX397	1.17472	1.21031	-2.98418	CX482	1.16187	1.18022	-1.56760
CX231	1.17915	1.21806	-3.24590	GEB161	1.13020	1.13318	-0.26354
CX161	1.19065	1.22372	-2.73927				

AVERAGE DIFFERENCE = -2.06299

STANDARD DEVIATION = 1.49187

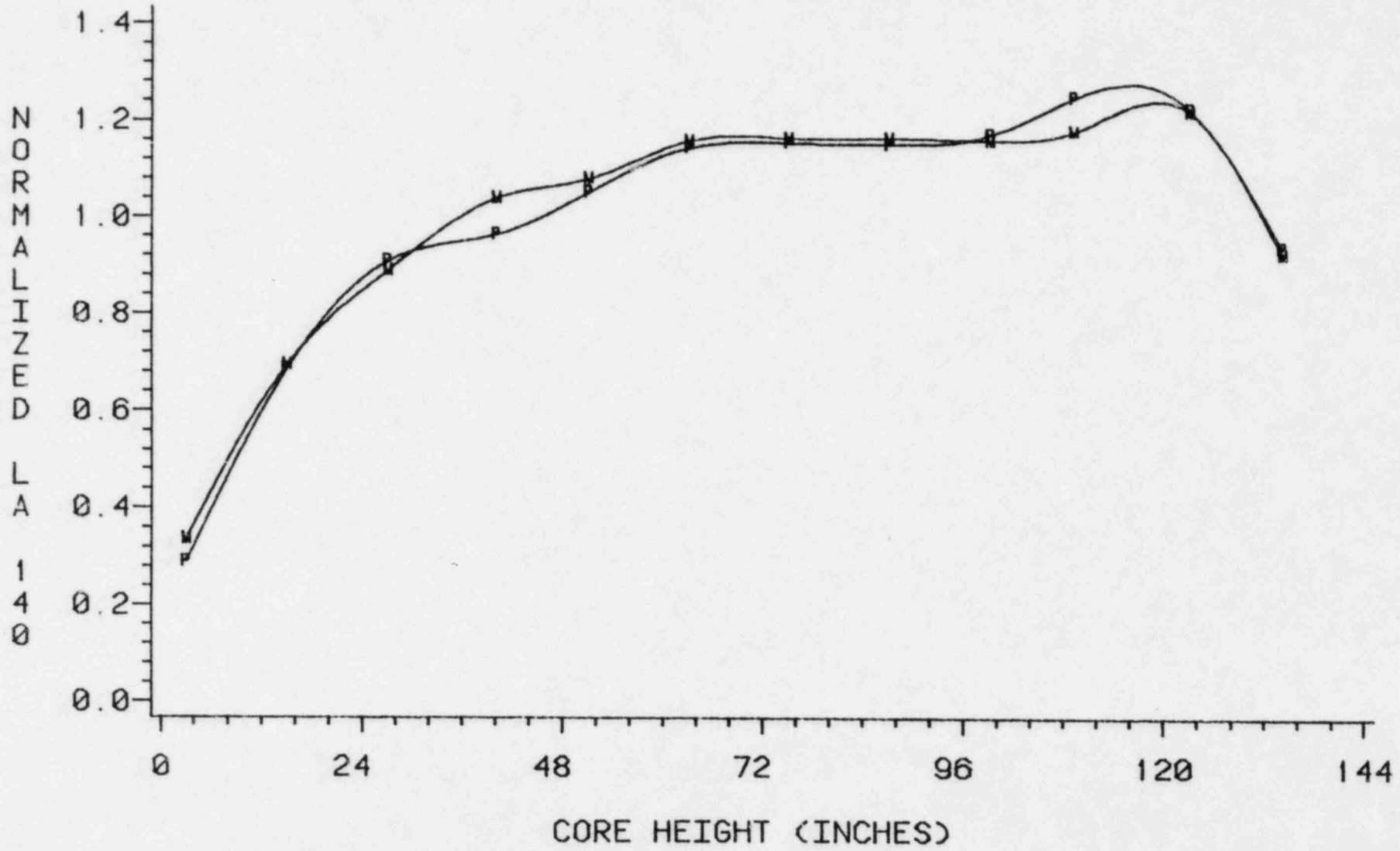
QUAD CITIES 1 1974 GAMMA SCAN
CALC. VS. MEAS. LA-140 ACTIVITY
31 ASSEMBLY AVERAGE
P=PRESTO M=MEASURED
NORMALIZED LA 140
1.4
1.2
1.0
0.8
0.6
0.4
0.2
0.0
0
24
48
72
96
120
144
CORE HEIGHT (INCHES)

FIGURE 5.6.1

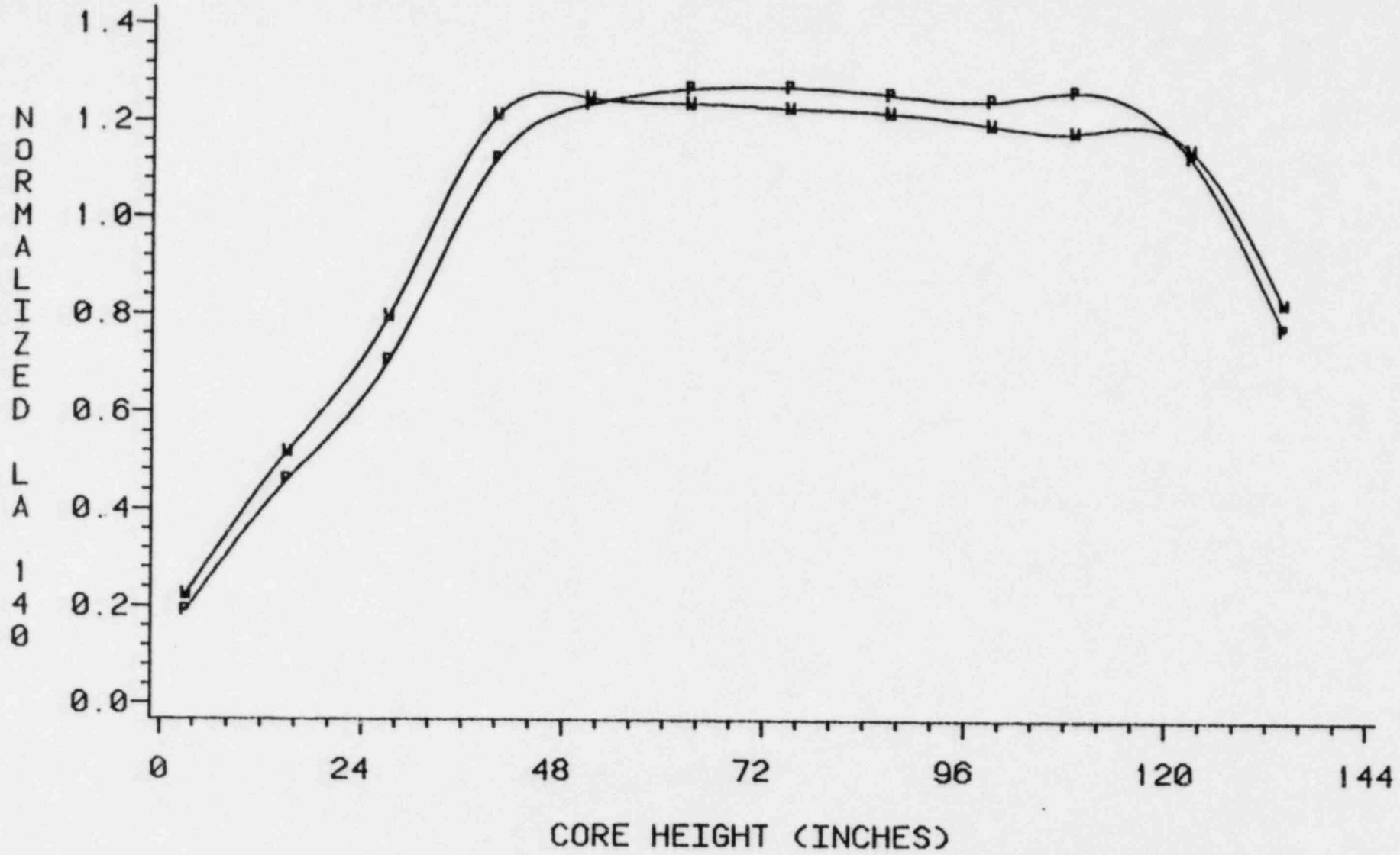
QUAD CITIES 1 1974 GAMMA SCAN
CALC. VS. MEAS. LA-140 ACTIVITY
TYPICAL PARTIALLY CONTROLLED ASSEMBLY
P=PRESTO M=MEASURED
NORMALIZED LA 140
1.4
1.2
1.0
0.8
0.6
0.4
0.2
0.0
0
24
48
72
96
120
144
CORE HEIGHT (INCHES)

FIGURE 5.8.2

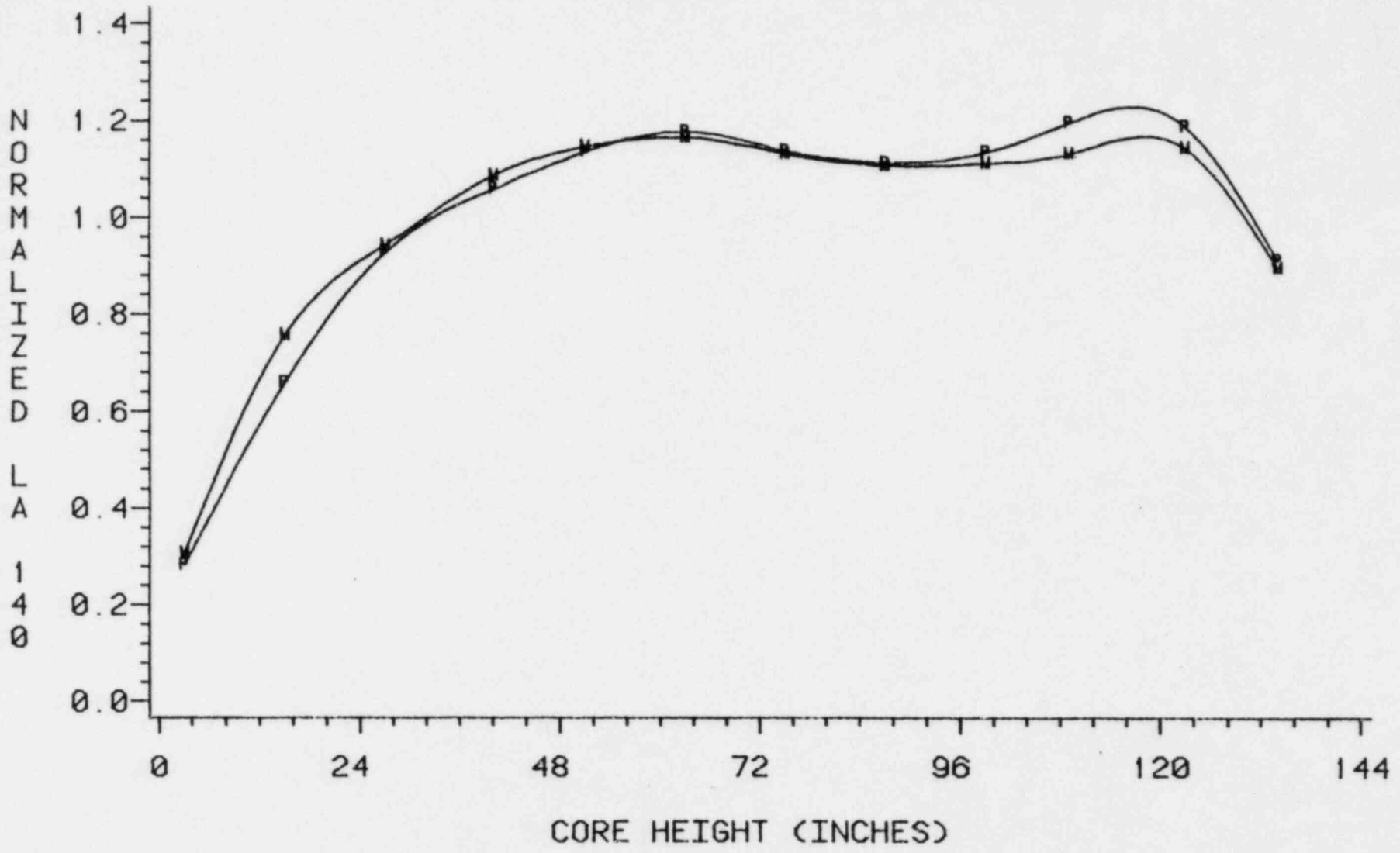
QUAD CITIES 1 1974 GAMMA SCAN
CALC. VS. MEAS. LA-140 ACTIVITY
TYPICAL UNCONTROLLED ASSEMBLY
P=PRESTO M=MEASURED
NORMALIZED LA 140
1.4
1.2
1.0
0.8
0.6
0.4
0.2
0.0
0
24
48
72
96
120
144
CORE HEIGHT (INCHES)

FIGURE 5.6.3

FIGURE 5.6.4

QUAD CITIES 1 CYCLE 2 GAMMA-SCAN RESULTS

PRESTO CALCULATED VS. MEASURED La-140 ACTIVITIES

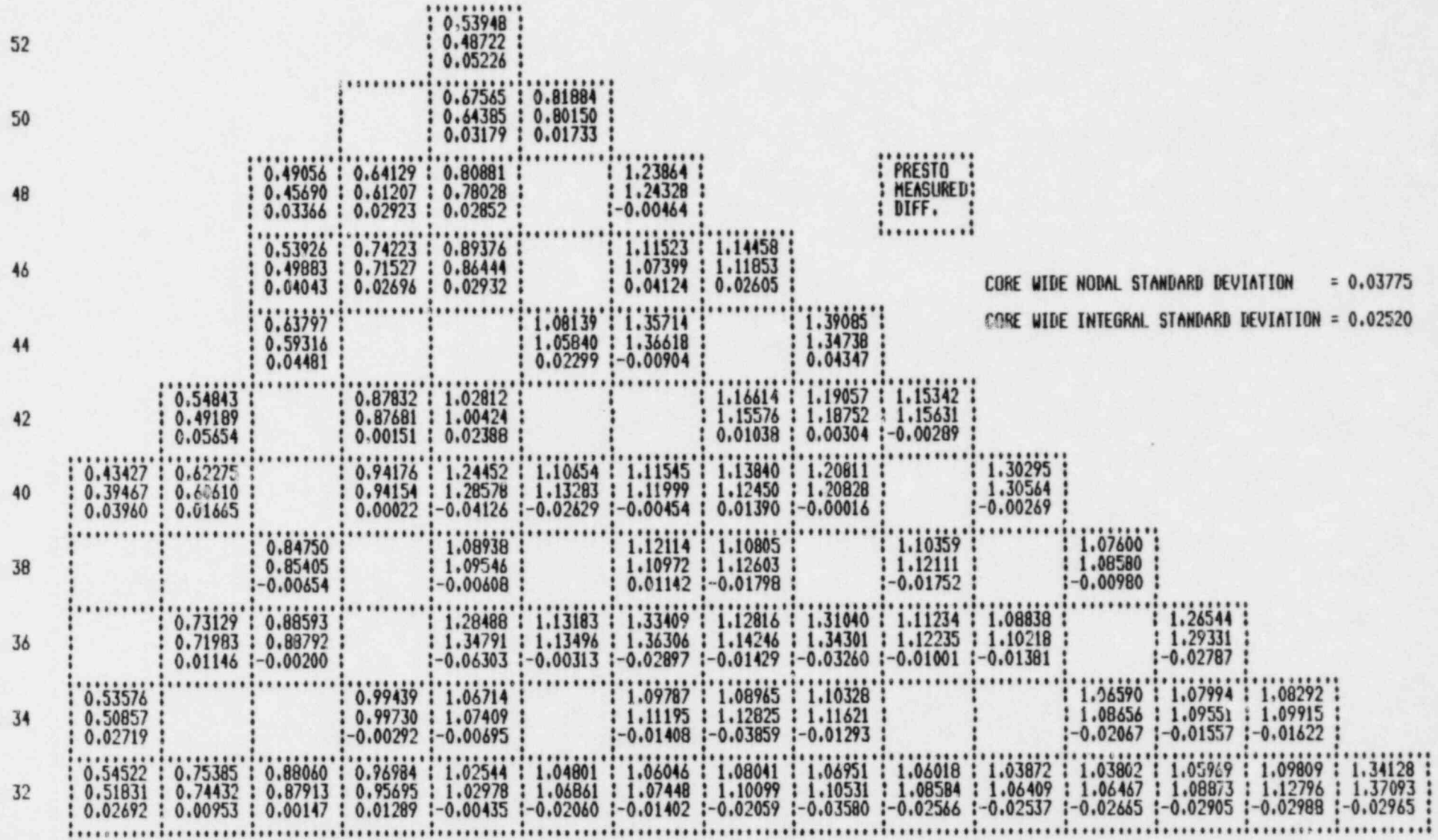

CORE WIDE NODAL STANDARD DEVIATION = 0.03775

CORE WIDE INTEGRAL STANDARD DEVIATION = 0.02520

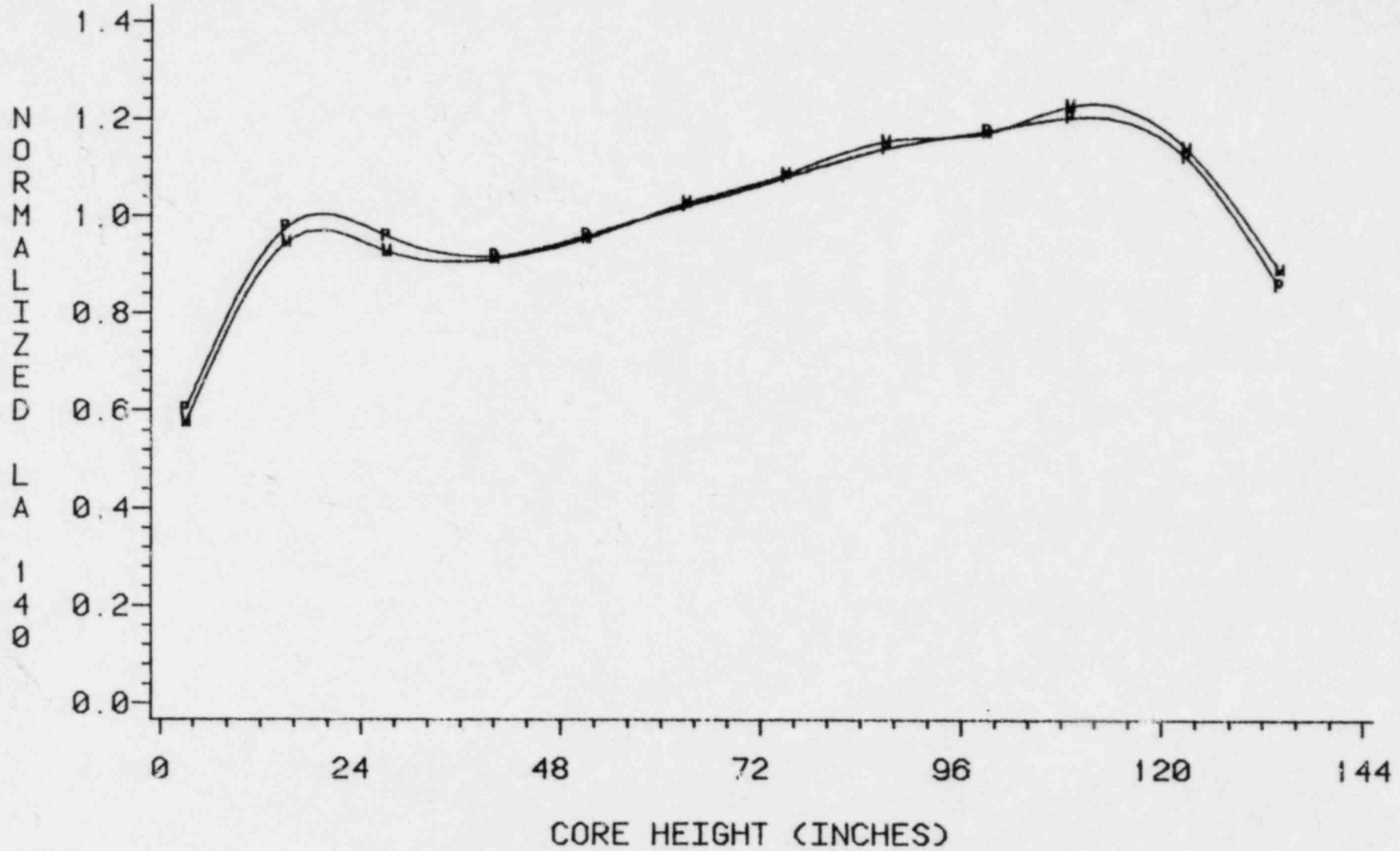
QUAD CITIES 1 1976 GAMMA SCAN
CALC. VS. MEAS. LA-140 ACTIVITY
OCTANT AVERAGE (71 ASSEMBLIES)
P=PRESTO M=MEASURED
NORMALIZED LA 140
1.4
1.2
1.0
0.8
0.6
0.4
0.2
0.0
0
24
48
72
96
120
144
CORE HEIGHT (INCHES)

FIGURE 5.6.5

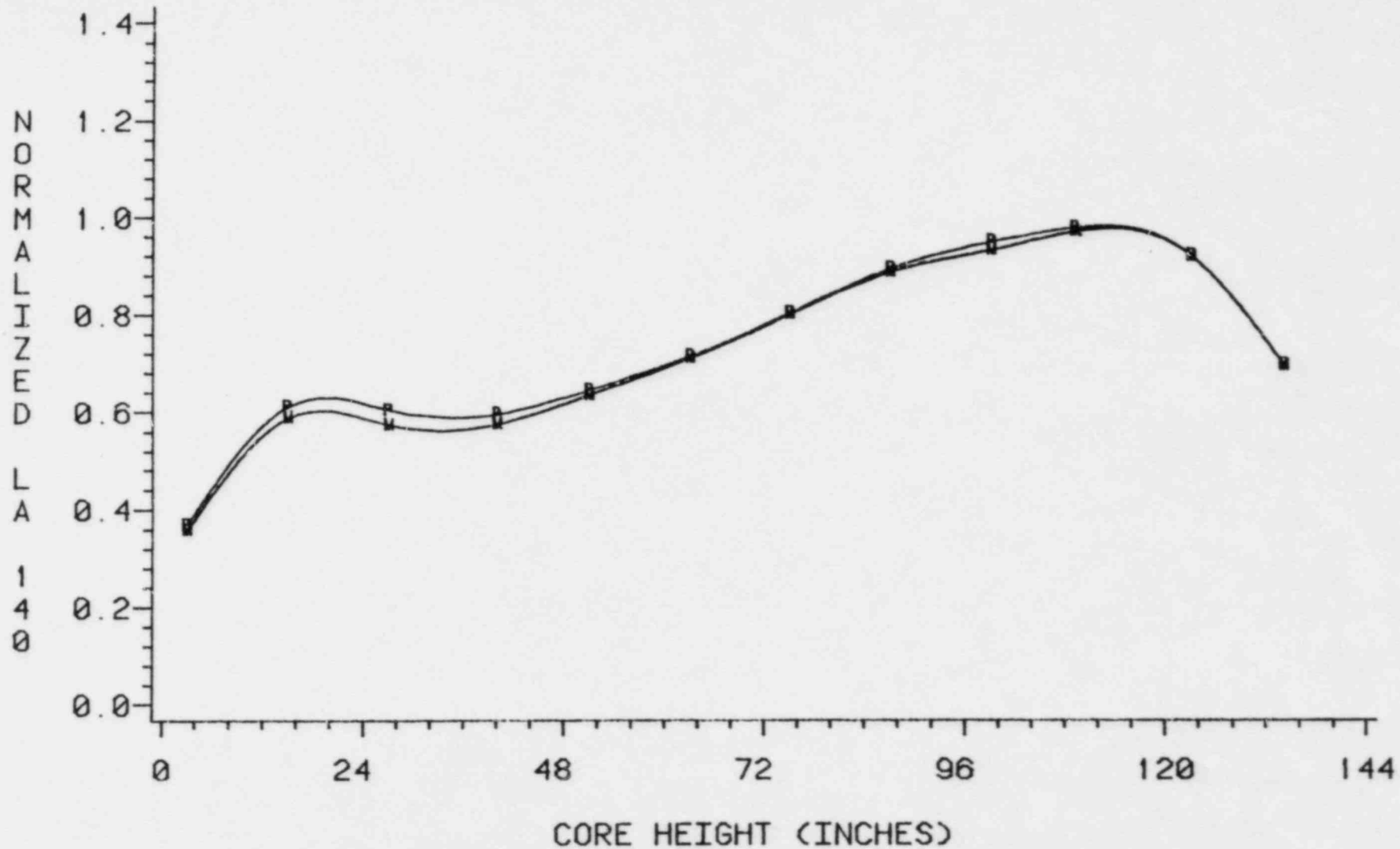
QUAD CITIES 1 1976 GAMMA SCAN
CALC. VS. MEAS. LA-140 ACTIVITY
ASSEMBLY CX 523 (BEST CASE)
P=PRESTO M=MEASURED
NORMALIZED LA 140
1.4
1.2
1.0
0.8
0.6
0.4
0.2
0.0
0
24
48
72
96
120
144
CORE HEIGHT (INCHES)

FIGURE 5.8.8

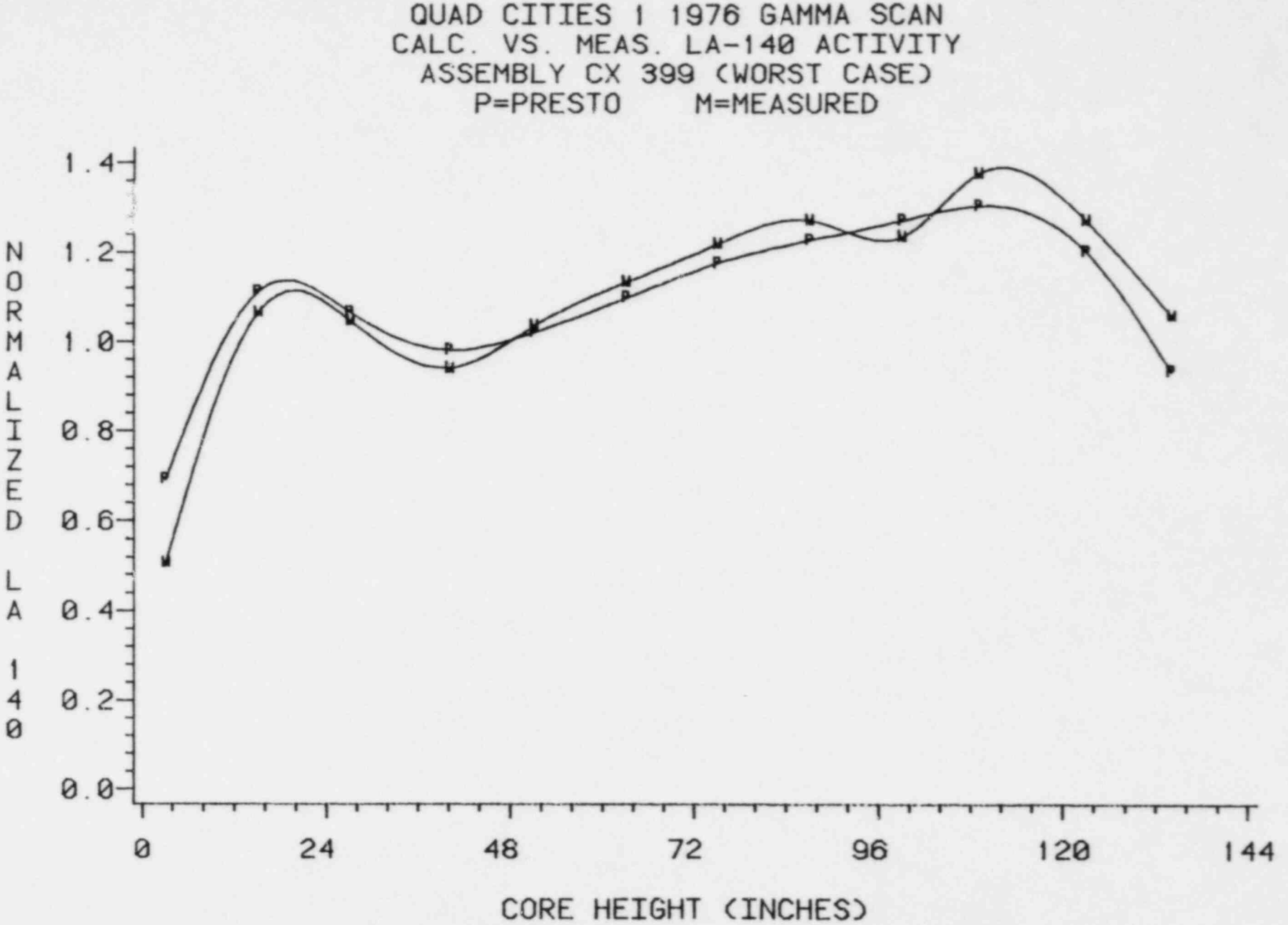
QUAD CITIES 1 1976 GAMMA SCAN
CALC. VS. MEAS. LA-140 ACTIVITY
ASSEMBLY CX 399 (WORST CASE)
P=PRESTO M=MEASURED
NORMALIZED LA 140
1.4
1.2
1.0
0.8
0.6
0.4
0.2
0.0
0
24
48
72
96
120
144
CORE HEIGHT (INCHES)

FIGURE 5.8.7

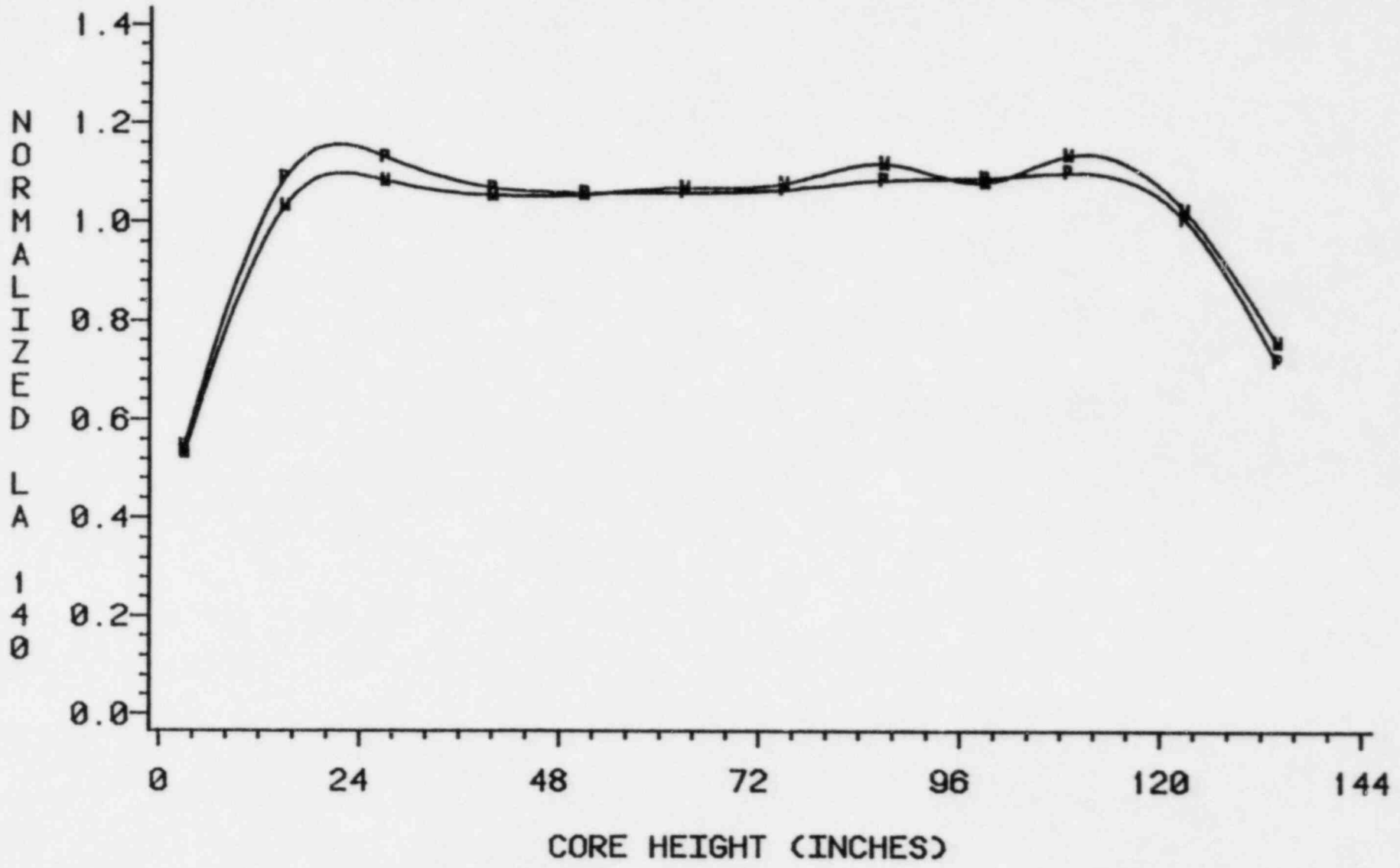
QUAD CITIES 1 1976 GAMMA SCAN
CALC. VS. MEAS. LA-140 ACTIVITY
FOUR CENTER M02 ASSEMBLIES
P=PRESTO M=MEASURED
NORMALIZED LA 140
1.4
1.2
1.0
0.8
0.6
0.4
0.2
0.0
0
24
48
72
96
120
144
CORE HEIGHT (INCHES)

FIGURE 5.8.8

FIGURE 5.6.9

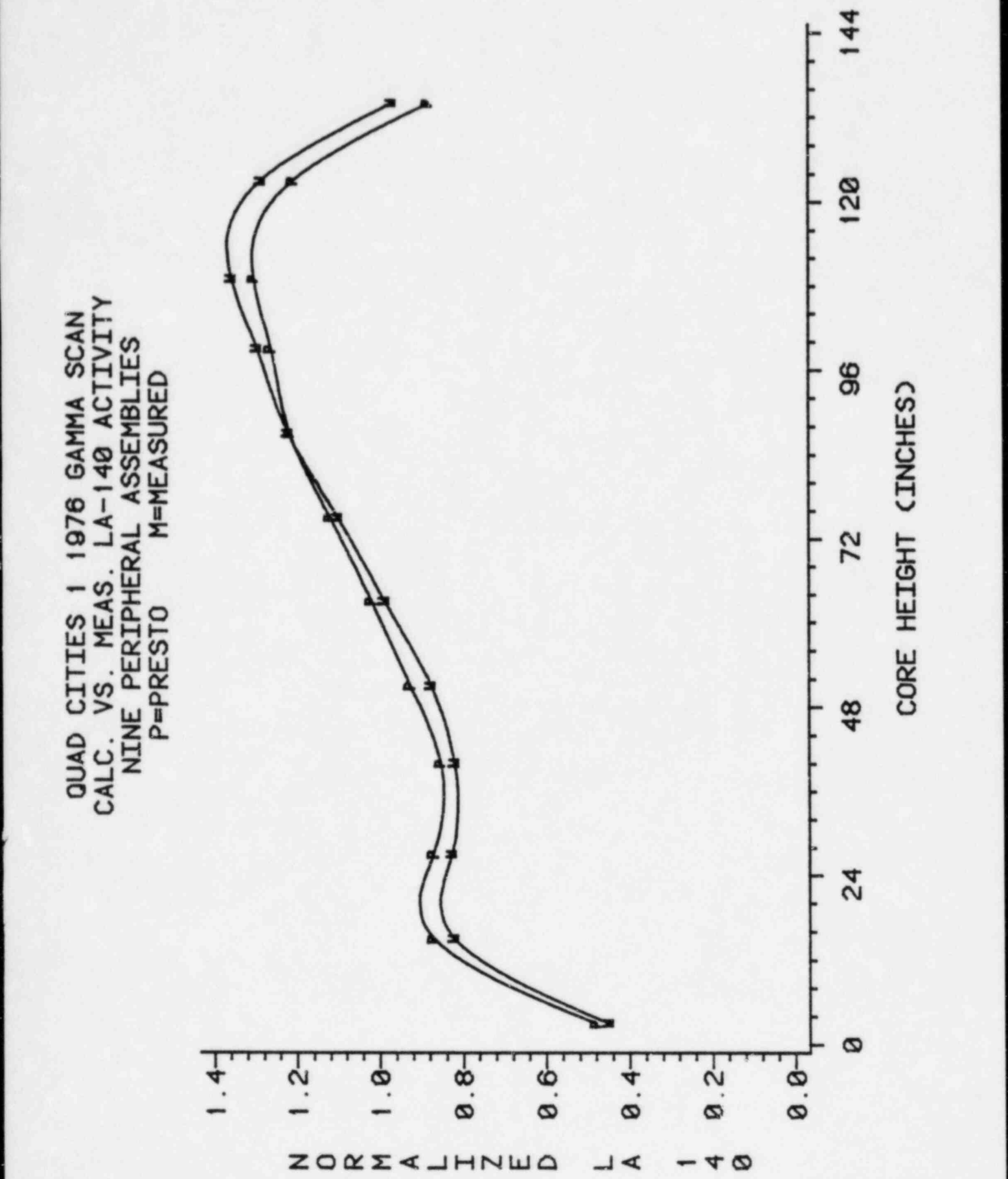
QUAD CITIES 1 1976 GAMMA SCAN
CALC. VS. MEAS. LA-140 ACTIVITY
NINE PERIPHERAL ASSEMBLIES
P=PRESTO M=MEASURED
NORMALIZED LA 140
1.4
1.2
1.0
0.8
0.6
0.4
0.2
0.0
0
24
48
72
96
120
144
CORE HEIGHT (INCHES)

5.7 Core Flow Distribution and Pressure Drop

Justification for the PRESTO-B core flow model is given by comparison with process computer results. Figure 5.7.1 presents a composite plot of the ratio of PRESTO-B to process computer core pressure drop for the Brunswick Units. The average value of this ratio is 1.002, with a standard deviation of .035.

Figure 5.7.2 through 5.7.5 show comparisons of the PRESTO-B and process computer core flow distribution for Brunswick 1, Cycle 3, for a variety of combinations of average power and flow. These states range from (100/100) percent power/flow to (50/45) percent power/flow. These four cases show an average RMS difference between PRESTO and process computer calculations of three percent of full flow. Interior and exterior orificed bundles are predicted equally well. The hot bundle flows are in good agreement with the process computer results.

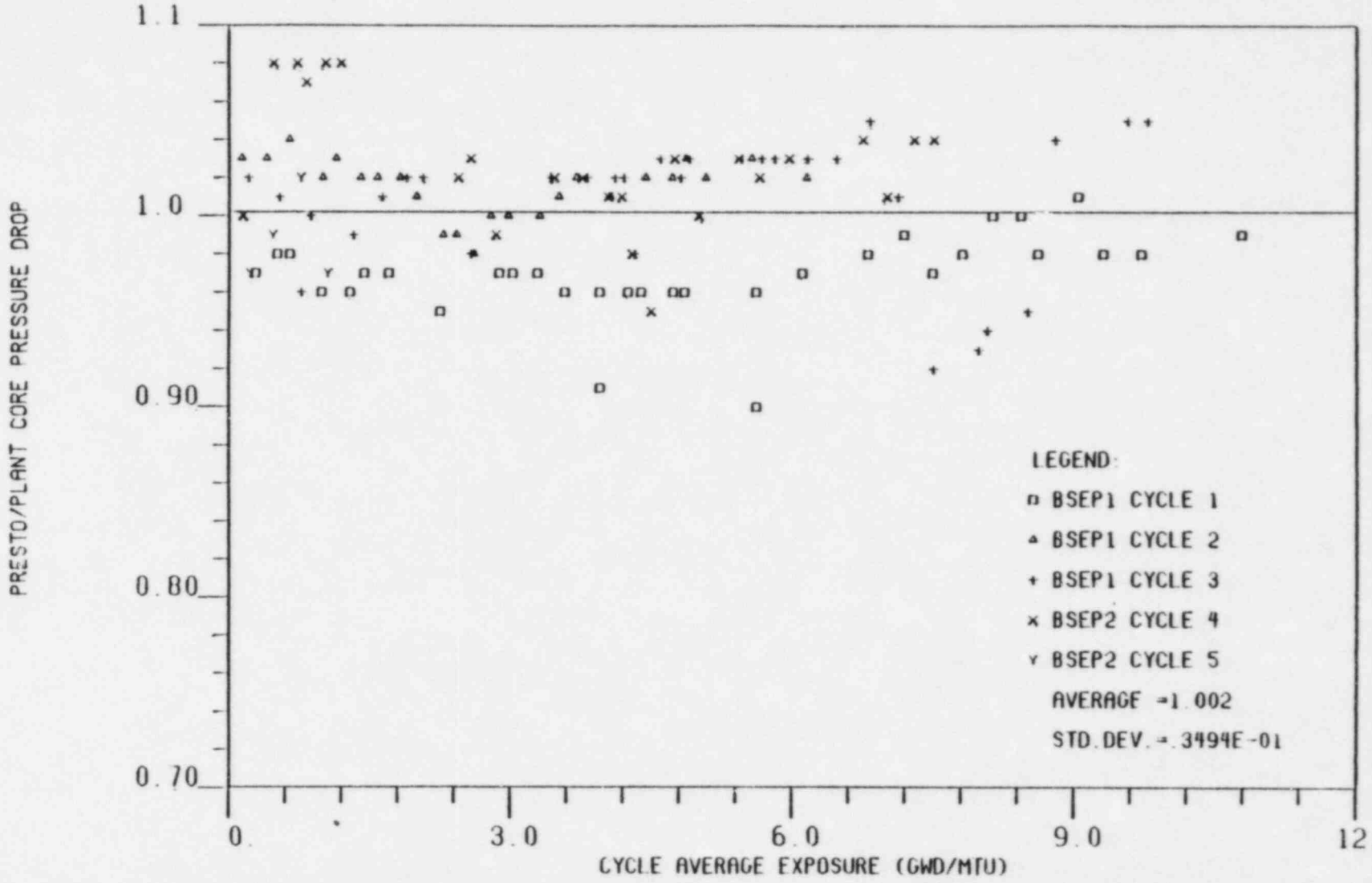

RATIO PRESTO/PLANT CORE PRESSURE DROP VS. CYCLE EXPOSURE

FIGURE 5.7.2
BRUNSWICK UNIT 1 CYCLE 3
COMPARISON OF PRESTO-B AND PROCESS COMPUTER
BUNDLE FLOW DISTRIBUTION (KG/SEC)
11-26-81; POWER=99.4%; FLOW=99.4%

	27	29	31	33	35	37	39	41	43	45	47	49	51
26	17.1 17.5 -.4	16.3 16.9 -.6	15.3 15.9 -.6	16.1 16.4 -.3	15.7 16.0 -.3	15.9 16.0 -.1	15.3 15.3 .0	17.2 17.0 .2	16.9 17.3 .6	16.6 16.5 .1	15.8 15.9 -.1	16.9 16.6 .3	8.8 8.7 .1
24	16.3 16.9 -.6	15.7 16.4 -.7	16.0 16.1 -.1	15.6 15.7 -.1	16.1 16.1 .0	15.5 15.6 -.1	15.7 15.4 .3	15.8 15.3 .5	16.3 16.3 .0	15.9 15.9 .0	16.2 16.0 .2	16.9 16.6 .3	8.8 8.7 .1
22	15.4 16.2 -.8	16.0 16.3 -.3	15.4 16.0 -.6	16.4 16.4 .0	15.7 16.4 -.7	16.1 16.5 -.4	15.1 15.6 -.5	15.9 16.0 -.1	15.3 15.1 .2	16.2 15.9 .3	15.7 15.8 -.1	16.9 16.6 .3	8.8 8.7 .1
20	16.4 16.8 -.4	15.7 15.9 -.2	16.4 16.5 -.1	17.6 17.7 -.1	17.6 17.8 -.2	16.0 16.1 -.1	16.0 16.1 -.1	15.8 15.9 -.1	15.8 15.7 .1	15.4 15.5 -.1	16.2 16.0 .2	16.9 16.7 .2	8.8 8.7 .1
18	16.0 16.4 -.4	16.2 16.2 .0	15.8 16.0 -.2	17.6 17.6 .0	17.3 17.9 -.6	16.4 16.8 -.4	15.3 * 15.1 * .2 *	16.2 15.9 .3	15.5 15.7 -.2	16.4 16.4 .0	16.3 16.5 -.2	17.6 17.4 .2	8.9 8.9 .0
16	16.1 16.1 .0	15.6 15.8 -.2	16.2 16.2 .0	16.0 15.8 .2	16.4 16.8 -.4	16.2 16.7 -.5	15.8 15.4 .4	15.4 15.2 .2	16.1 15.9 .2	16.0 16.1 -.1	17.2 16.9 .3	8.7 8.6 .1	
14	15.4 15.7 -.3	15.7 15.7 .0	15.2 15.6 -.4	16.0 16.1 -.1	15.3 15.7 -.4	15.8 15.9 -.1	15.4 15.5 -.1	16.6 16.3 .3	16.2 16.3 -.1	17.0 16.7 .3	8.7 8.7 .0		
12	17.2 17.2 .0	15.9 15.7 .2	16.0 16.1 -.1	15.8 16.0 -.2	16.2 16.4 -.2	15.4 15.9 -.5	16.6 16.3 .3	17.5 17.5 .0	18.1 18.2 -.1	17.7 17.4 .3	8.9 8.8 .1		
10	16.9 17.7 -.8	16.3 16.7 -.4	15.4 15.1 .3	15.9 15.7 .2	15.5 15.9 -.4	16.1 16.0 .1	16.2 16.5 -.3	18.2 18.3 -.1	18.5 19.2 .3	18.7 18.9 -.2	8.9 9.0 -.1		
08	16.6 16.9 -.3	16.0 16.3 -.3	16.2 15.8 .4	15.4 15.5 -.1	16.4 16.4 .0	16.1 16.3 -.2	17.0 16.9 .1	17.7 17.6 .1	18.7 18.9 -.2	8.9 8.9 .0			
06	15.8 16.0 -.2	16.2 16.0 .2	15.7 15.7 .0	16.2 15.9 .3	16.3 16.6 -.3	17.3 17.0 .3	8.7 8.7 .0	8.9 8.8 .1	8.9 9.0 -.1				
04	16.9 16.6 .3	16.9 16.5 .4	16.9 16.5 .4	16.9 16.5 .4	17.7 17.4 .3	8.8 8.6 .2							
02	8.8 8.7 .1	8.8 8.7 .1	8.8 8.7 .1	8.8 8.7 .1	8.9 8.9 .0								

PRESTO-B
P.C.
DIFF.

RMS DIFFERENCE = 0.35 KG/SEC

* MOST LIMITING CPR

FIGURE 5.7.3
BRUNSWICK UNIT 1 CYCLE 3
COMPARISON OF PRESTO-B AND PROCESS COMPUTER
BUNDLE FLOW DISTRIBUTION (KG/SEC)
12-28-80; POWER=79.9%; FLOW=69.6%

	27	29	31	33	35	37	39	41	43	45	47	49	51
26	11.3 11.7 -.4	11.6 12.2 -.6	11.3 12.0 -.7	11.1 11.2 -.1	10.8 11.0 -.2	12.0 12.3 -.3	12.0 12.2 -.2	11.4 11.1 .3	11.0 11.2 -.2	11.8 12.1 -.3	11.8 12.4 -.6	11.8 11.9 -.1	6.2 6.3 -.1
24	11.2 11.7 -.5	10.9 11.3 -.4	11.1 11.3 -.2	10.6 10.7 -.1	11.1 11.3 -.2	11.0 11.1 -.1	11.1 10.8 .3	10.8 10.5 .3	11.1 11.2 -.1	11.0 11.1 -.1	11.3 11.5 -.2	11.7 11.9 -.2	6.2 6.3 -.1
22	10.9 11.5 -.6	11.3 11.6 -.3	11.1 11.3 -.2	11.1 11.2 -.1	10.8 11.2 -.4	11.3 11.4 -.1	10.9 11.3 -.4	11.0 11.2 -.2	10.7 # 10.6 # .1	11.3 11.2 .1	11.2 11.6 -.4	11.7 11.9 -.2	6.2 6.3 -.1
20	11.4 11.6 -.2	12.0 12.3 -.3	12.2 12.3 -.1	11.2 11.1 .1	11.3 11.4 -.1	11.8 12.0 -.2	11.9 12.3 -.4	10.9 11.0 -.1	10.9 10.8 .1	11.3 11.6 -.3	11.6 11.9 -.3	12.1 12.3 -.2	6.2 6.3 -.1
18	11.1 11.0 .1	12.2 12.4 -.2	12.2 12.4 -.2	11.4 11.4 .0	11.2 11.6 -.4	12.0 12.5 -.5	11.8 12.1 -.3	11.3 11.2 .1	10.8 11.0 -.2	11.7 11.9 -.2	11.9 12.3 -.4	12.3 12.5 -.2	6.3 6.4 -.1
16	11.3 11.3 .0	11.2 11.1 .1	11.5 11.5 .0	11.0 10.8 .2	11.2 11.7 -.5	11.3 11.7 -.4	11.1 10.9 .2	10.8 10.9 -.1	11.0 10.8 .2	11.3 11.5 -.2	12.0 11.9 .1	6.2 6.2 .0	
14	11.0 11.3 -.3	11.3 11.3 .0	11.2 11.5 -.3	11.2 11.5 -.3	10.8 11.1 -.3	11.0 11.1 -.1	10.9 10.8 .1	11.3 11.0 .3	11.0 10.9 .1	11.4 11.0 .4	6.2 6.3 -.1		
12	11.6 11.6 .0	12.2 12.4 -.2	12.3 12.6 -.3	11.2 11.3 -.1	11.3 11.4 -.1	11.3 11.8 -.5	11.6 11.5 .1	11.1 10.9 .2	11.4 11.0 .4	11.8 11.6 .2	6.3 6.3 .0		
10	11.4 11.6 -.2	12.3 12.6 -.3	12.2 12.3 -.1	11.3 11.0 .3	11.1 11.2 -.1	11.5 11.6 -.1	11.6 11.9 -.3	11.5 11.5 .0	11.7 12.0 -.3	12.3 12.3 .0	6.3 6.4 -.1		
08	11.6 11.6 .0	11.4 11.3 .1	11.7 11.4 .3	11.2 11.2 .0	11.6 11.6 .0	11.4 11.6 -.2	11.7 11.6 .1	12.0 12.0 .0	12.4 12.3 .1	6.3 6.3 .0			
06	11.2 11.2 .0	11.3 11.1 .2	11.3 11.3 .0	11.4 11.2 .2	11.6 11.8 -.2	12.0 11.9 .1	6.2 6.3 -.1	6.3 6.3 .0	6.3 6.4 -.1				
04	11.7 11.4 .3	11.7 11.4 .3	11.8 11.7 .1	12.0 11.9 .1	12.3 12.3 .0	6.2 6.2 .0							
02	6.3 6.3 .0	6.3 6.3 .0	6.3 6.3 .0	6.3 6.3 .0	6.3 6.4 -.1								

PRESTO-B
P.C.
DIFF.

RMS DIFFERENCE = 0.51 KG/SEC

MOST LIMITING CPR

FIGURE 5.7.4
BRUNSWICK UNIT 1 CYCLE 3
COMPARISON OF PRESTO-B AND PROCESS COMPUTER
BUNDLE FLOW DISTRIBUTION (KG/SEC)
04-16-81; POWER=74.2%; FLOW=92.5%

	27	29	31	33	35	37	39	41	43	45	47	49	51
26	15.9 16.0 -.1	15.5 15.9 -.4	15.0 15.4 -.4	15.3 15.4 -.1	15.0 15.0 .0	14.9 15.1 -.2	14.4 14.5 -.1	15.1 14.8 .3	14.7 14.7 .0	15.0 14.9 .1	14.5 14.7 -.2	15.3 15.1 .2	8.0 7.9 .1
24	16.4 16.6 -.2	15.4 15.6 -.2	15.4 15.4 .0	15.9 15.9 .0	15.9 16.0 -.1	14.9 15.0 -.1	14.9 14.6 .3	15.6 15.5 .1	15.7 15.8 -.1	14.8 14.6 .2	14.9 14.7 .2	15.5 15.2 .3	8.0 7.9 .1
22	16.2 16.5 -.3	15.5 15.6 -.1	15.1 15.3 -.2	16.0 16.0 .0	15.8 16.1 -.3	15.1 15.1 .0	14.6 14.9 -.3	15.6 15.7 -.1	15.5 15.5 .0	15.1 14.9 .2	14.7 14.7 .0	15.5 15.3 .2	8.0 7.9 .1
20	15.5 15.5 .0	15.0 15.2 -.2	15.2 15.2 .0	15.3 15.1 .2	15.2 15.1 .1	14.7 14.6 .1	14.8 14.9 -.1	14.7 14.6 .1	14.8 14.5 .3	14.5 14.6 -.1	14.9 14.7 .2	15.5 15.4 .1	8.0 7.9 .1
18	15.2 15.1 .1	15.2 15.2 .0	14.9 15.0 -.1	15.3 15.1 .2	15.0 15.3 -.3	14.9 15.2 -.3	14.3 14.1 .2	14.8 14.3 .5	14.3 14.3 .0	15.0 14.8 .2	15.1 15.1 .0	16.0 15.6 .4	8.0 8.0 .0
16	16.1 16.1 .0	15.1 15.0 .1	15.3 15.1 .2	16.1 15.9 .2	16.1 16.2 -.1	15.2 15.3 -.1	14.7 14.2 .5	14.4 14.2 .2	14.8 14.4 .4	14.9 14.8 .1	15.7 15.3 .4	8.0 7.8 .2	
14	15.8 16.0 -.2	15.1 14.8 .3	14.8 15.2 .4	16.0 16.1 -.1	15.9 16.1 -.2	15.1 15.0 .1	14.6 14.5 .1	15.3 15.0 .3	15.1 15.0 .1	15.5 15.2 .3	7.9 7.9 .0		
12	15.2 15.0 .2	14.7 14.6 .1	14.9 15.1 -.2	15.0 15.0 .0	15.2 15.2 .0	14.7 15.1 -.4	15.4 15.0 .4	16.2 16.0 .2	16.6 16.4 .2	16.2 15.9 .3	8.0 7.9 .1		
10	14.6 15.1 -.5	14.8 15.0 -.2	14.4 14.3 .1	14.8 14.5 .3	14.6 14.8 -.2	15.0 14.9 .1	15.2 15.4 -.2	16.6 16.6 .0	16.9 17.3 -.4	16.9 16.9 .0	8.1 8.1 .0		
08	15.4 15.7 -.3	14.7 15.0 -.3	15.0 14.8 .2	14.9 15.2 -.3	15.5 15.5 .0	15.1 15.3 -.2	15.7 15.6 .1	16.3 16.1 .2	16.9 17.0 -.1	8.1 8.0 .1			
06	15.3 15.8 -.5	15.0 15.2 -.2	14.8 15.2 -.4	15.4 15.5 -.1	15.6 15.9 -.3	15.9 15.8 .1	7.9 7.9 .0	8.0 8.0 .0	8.1 8.1 .0				
04	15.6 15.6 .0	15.5 15.5 .0	15.6 15.5 .1	15.7 15.8 -.1	16.2 16.2 .0	8.0 7.9 .1							
02	8.0 7.9 .1	8.0 7.9 .1	8.0 7.9 .1	8.0 7.9 .1	8.0 8.0 .0								

PRESTO-B
P.C.
DIFF.

RMS DIFFERENCE = 0.30 KG/SEC

* MOST LIMITING CPR

FIGURE 5.7.5
BRUNSWICK UNIT 1 CYCLE 3
COMPARISON OF PRESTO-B AND PROCESS COMPUTER
BUNDLE FLOW DISTRIBUTION (KG/SEC)
09-27-81; POWER=50.4%; FLOW=44.7%

	27	29	31	33	35	37	39	41	43	45	47	49	51
26	7.5 7.8 -.3	7.4 7.7 -.3	7.3 7.7 -.4	7.4 7.6 -.2	7.4 7.5 -.1	7.3 7.5 -.2	7.1 7.3 -.2	7.3 7.4 -.1	7.2 7.3 -.1	7.3 7.3 .0	7.1 7.3 -.2	7.4 7.4 .0	4.2 4.2 .0
24	7.6 8.1 -.5	7.4 7.7 -.3	7.4 7.7 -.3	7.7 8.0 -.3	7.6 7.9 -.3	7.3 7.5 -.2	7.3 7.3 .0	7.6 7.7 -.1	7.5 7.7 -.2	7.2 7.3 -.1	7.2 7.3 -.1	7.4 7.5 -.1	4.2 4.2 .0
22	7.7 8.1 -.4	7.4 7.6 -.2	7.4 7.6 -.2	7.6 7.9 -.3	7.7 8.0 -.3	7.4 7.5 -.1	7.2 7.4 -.2	7.5 7.7 -.2	7.5 7.8 -.3	7.3 7.4 -.1	7.2 7.3 -.1	7.5 7.5 .0	4.2 4.2 .0
20	7.4 7.6 -.2	7.3 7.5 -.2	7.3 7.5 -.2	7.4 7.5 -.1	7.4 7.5 -.1	7.2 7.3 -.1	7.2 7.4 -.2	7.3 7.4 -.1	7.3 7.3 .0	7.1 7.4 -.3	7.3 7.3 .0	7.5 7.6 -.1	4.2 4.2 .0
18	7.4 7.5 -.1	7.3 7.5 -.2	7.2 7.5 -.3	7.4 7.5 -.1	7.3 7.6 -.3	7.3 7.6 -.3	7.1 7.3 -.2	7.3 7.4 -.1	7.2 7.4 -.2	7.3 7.5 -.2	7.4 7.6 -.2	7.7 7.8 -.1	4.1 4.2 -.1
16	7.6 7.9 -.3	7.3 7.4 -.1	7.4 7.5 -.1	7.6 7.8 -.2	7.6 7.9 -.3	7.3 7.6 -.3	7.3 7.3 .0	7.5 7.7 -.2	7.6 7.8 -.2	7.4 7.6 -.2	7.6 7.7 -.1	4.2 4.2 .0	
14	7.6 7.9 -.3	7.3 7.4 -.1	7.2 7.5 -.3	7.6 7.9 -.3	7.6 8.0 -.4	7.3 7.5 -.2	7.2 7.3 -.1	7.5 7.7 -.2	7.6 7.9 -.3	7.5 7.6 -.1	4.2 4.2 .0		
12	7.4 7.5 -.1	7.2 7.3 -.1	7.2 7.5 -.3	7.3 7.4 -.1	7.3 7.5 -.2	7.1 7.5 -.4	7.3 7.3 .0	7.3 7.3 .0	7.5 7.6 -.1	7.6 7.8 -.2	4.2 4.2 .0		
10	7.2 7.5 -.3	7.2 7.5 -.3	7.1 # 7.3 # -.2 #	7.2 7.4 -.2	7.1 7.4 -.3	7.2 7.4 -.2	7.1 7.3 -.2	7.4 7.4 .0	7.5 7.8 -.3	7.7 7.9 -.2	4.1 4.2 -.1		
08	7.5 7.9 -.4	7.3 7.5 -.2	7.3 7.4 -.1	7.4 7.7 -.3	7.4 7.7 -.3	7.3 7.6 -.3	7.4 7.4 .0	7.5 7.5 .0	7.7 7.9 -.2	4.2 4.2 .0			
06	7.6 8.1 -.5	7.4 7.7 -.3	7.3 7.7 -.4	7.5 7.9 -.4	7.6 8.0 -.4	7.6 7.8 -.2	4.2 4.2 .0	4.2 4.2 .0	4.1 4.2 -.1				
04	7.6 7.9 -.3	7.6 7.8 -.2	7.6 7.8 -.2	7.6 7.9 -.3	7.7 8.0 -.3	4.1 4.2 -.1							
02	4.1 4.2 -.1	4.1 4.2 -.1	4.1 4.2 -.1	4.1 4.2 -.1	4.0 4.2 -.2								

PRESTO-B
P.C.
DIFF.

RMS DIFFERENCE = 0.41 KG/SEC

MOST LIMITING CPR

5.8 Simulation of a Brunswick 2, Cycle 4, Xenon Transient

On May 1, 1981, Brunswick Unit 2 underwent a planned power reduction for the purpose of a control rod sequence exchange. Plant personnel provided detailed measurements during this exchange, which is representative of a planned non-equilibrium maneuver. Figure 5.8.1 illustrates the percent core power, flow, and Xenon concentration during a 5.5-hour transient period. This controlled transient is particularly good for demonstrating the ability of PRESTO to predict off-nominal conditions because the rod sequence exchange was initiated from an equilibrium xenon, high-power, nominal condition. The data taken by the plant staff during the maneuver includes the process computer OD-3 heat balance, OD-7 control rod configuration, and OD-8 measured LPRM distribution. The process computer P1 power distribution projection was also supplied at the initial condition.

The transient was modeled in PRESTO by entering the heat balance and control rod patterns as a function of time. From this, PRESTO predicted the critical eigenvalues and power shapes. The total core flows were calculated by FIBWR, based on measured core support plate pressure drop. This was done to provide consistency over the range of operations.

The power distribution was analyzed on a local basis by comparing predicted to measured LPRM's. In order to perform the LPRM analysis, local gain adjustment factors had to be generated to intercalibrate the initial PRESTO and plant data. The PRESTO-predicted LPRM's were forced to agree with plant

measurements at time zero by normalizing the initial PRESTO predictions to the plant data. This was necessary because the LPRM system can only provide a relative measure of local power. Figure 5.8.2 is a comparison of the PRESTO predicted and process computer measured power distributions at the initial condition.

Figure 5.8.3 presents the PRESTO-predicted axial power shapes at various times during the transient. Figures 5.8.4 through 5.8.10 show the PRESTO-predicted and plant-measured LPRM maps at various times during the transient. Table 5.8.1 is a summary of the relevant state parameters in the PRESTO prediction for those times in which the control rod patterns were quarter-core symmetric.

In summary, the transient demonstrated PRESTO-predictive capability over the following range of conditions:

Power: 97 to 40 percent of rated

Core Flow: 94 to 50 percent of rated

Subcooling: 94 to 133 percent of rated

Xenon Concentration: Equilibrium at 97 percent power to 1.7 times equilibrium at 43 percent power

Control Rod Density: 7.8 to 17.9 percent control. This includes a sequence exchange at T = 3.4 hours.

Void Fraction: 41 to 26 percent core average voids.

The average eigenvalue for those cases listed on Table 5.8.1 is 0.99613, with a standard deviation of .00105. The average value compares well with the initial value, and the standard deviation is consistent with that expected from the heat balance uncertainty.

The PRESTO prediction of LPRM's during the transient compares well with the plant measurements. The maximum RMS difference in local power density as compared with the initial prediction is 3.5 percent of rated power density. PRESTO predicts slightly greater power in the bottom of the core than is measured for the low-power conditions. One should observe that there is very little change in the predictive capability for the T = 3.15-hour and the T = 5.13-hour LPRM comparisons. This is significant because the two comparisons are made for completely different control rod patterns. This indicates that PRESTO has the capacity to predict the local power changes associated with the control rod withdrawal error transient.

Table 5.8.1

Summary of the Brunswick 2, Cycle 4
Xenon Transient Prediction Using PRESTO-B

Time (Hrs)	% Rated Power	% Rated Flow	% Rated Subcooling	% Initial Xenon	% Control Density	% Void Fraction	K_{eff}	% RMS* Local Power Difference	% Average* Local Power Difference
0.00	97.1	94.4	101.1	100.0	7.8	41.0	0.99662	0.0	0.0
0.15	89.3	82.3	107.6	100.2	7.8	41.0	0.99714	-	-
0.22	83.6	77.0	116.0	100.3	7.8	41.2	0.99701	-	-
0.37	77.5	64.8	122.3	101.0	7.8	41.2	0.99741	-	-
0.97	77.9	66.5	120.0	103.5	7.8	40.9	0.99715	2.0	-.1
1.12	70.2	55.3	133.2	104.2	7.8	41.4	0.99725	2.0	+.1
1.52	57.4	49.5	128.2	106.4	9.2	41.1	0.99483	-	-
1.63	55.9	50.1	125.5	107.4	9.2	40.4	0.99580	3.5	+.2
2.27	44.7	50.2	105.3	112.8	17.3	31.4	0.99525	2.9	-1.2
3.15	40.1	50.2	97.2	119.8	18.6	28.9	0.99508	3.4	-1.6
5.13	43.2	54.8	94.7	127.7	17.9	26.0	0.99491	3.4	-0.9
5.48	43.2	55.1	94.3	128.1	17.9	25.9	0.99513	-	-

*The % difference in local power (PRESTO-Plant) represents percent of rated power density as calculated by the LPRM system. The PRESTO-predicted LPRM's were forced to agree with the plant measurements at time = 0.0.

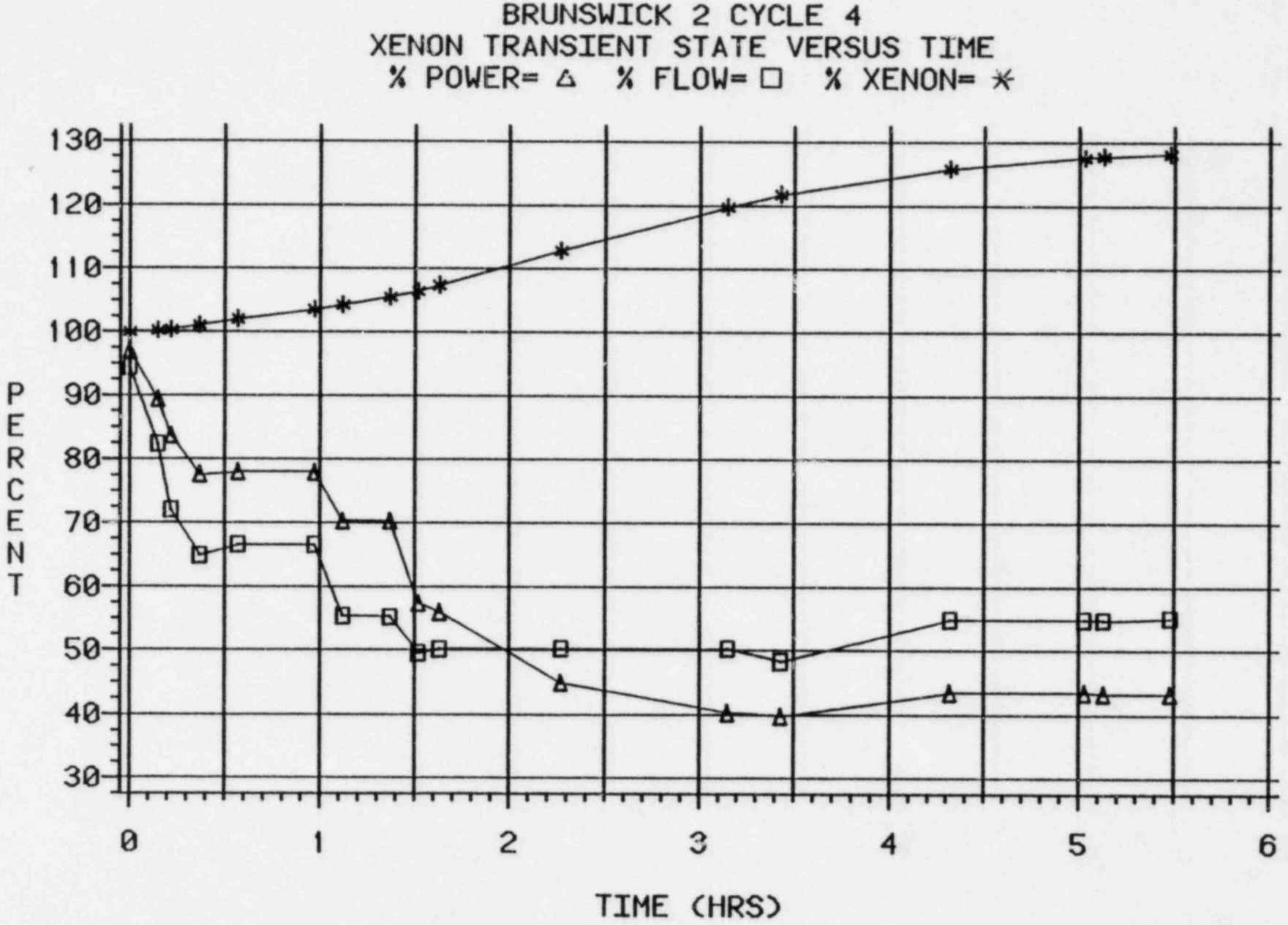
BRUNSWICK 2 CYCLE 4
XENON TRANSIENT STATE VERSUS TIME
% POWER= △ % FLOW= □ % XENON= *
PERCENT
130
120
110
100
90
80
70
60
50
40
30
0
1
2
3
4
5
6
TIME (HRS)

FIGURE 5.8.1

B2C4 XENON TRANSIENT INITIAL CONDITIONS
MWTH = 2365 PRES. = 1018 CAVEX = 11861
FLOW = 72.70 DHS = 19.70 KEFF = 0.99662
COMPARISON TO 05/01/81 OIEP P-1 DATA

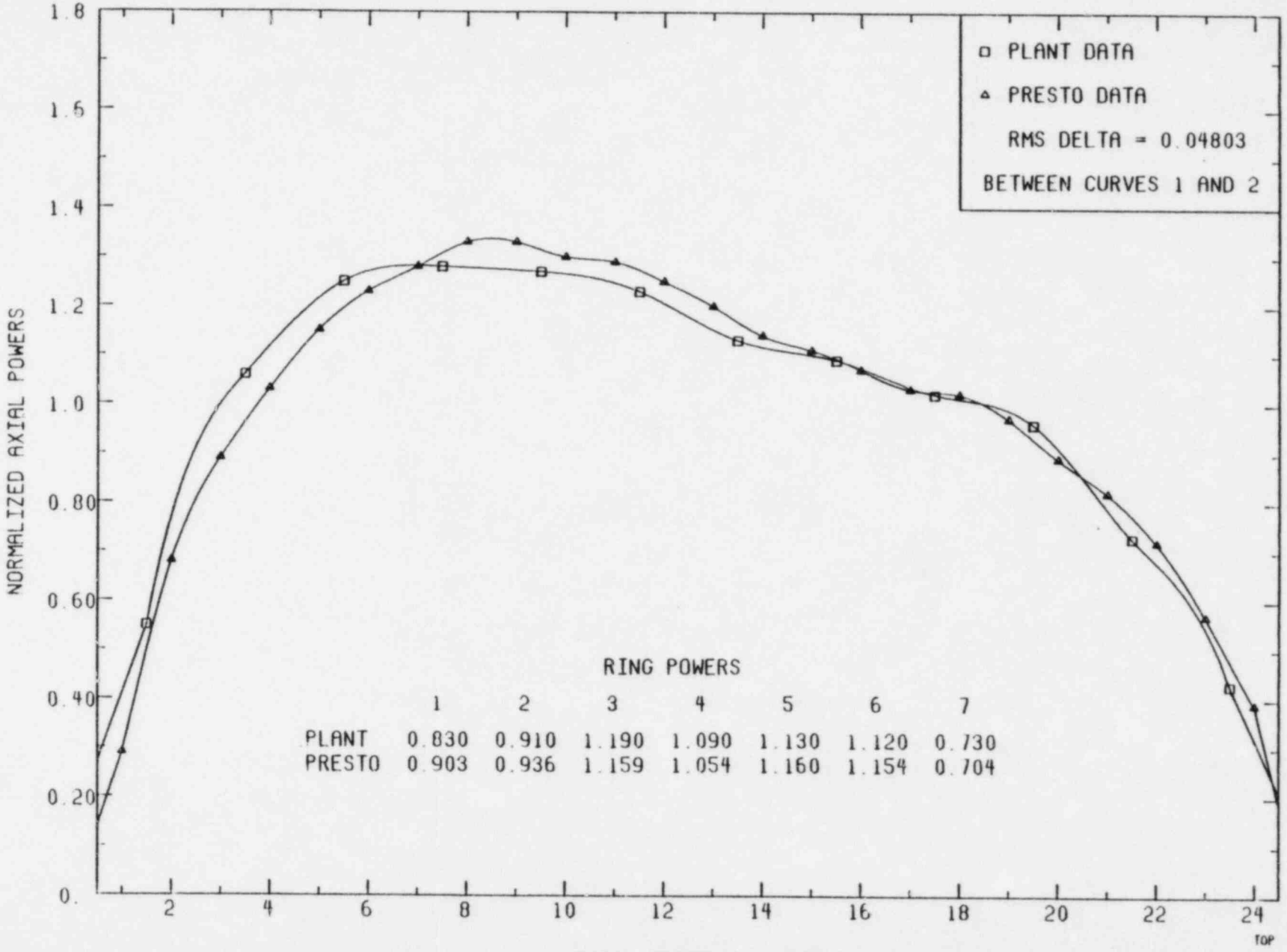

RING POWERS

	1	2	3	4	5	6	7
PLANT	0.830	0.910	1.190	1.090	1.130	1.120	0.730
PRESTO	0.903	0.936	1.159	1.054	1.160	1.154	0.704

Figure 5.8.2

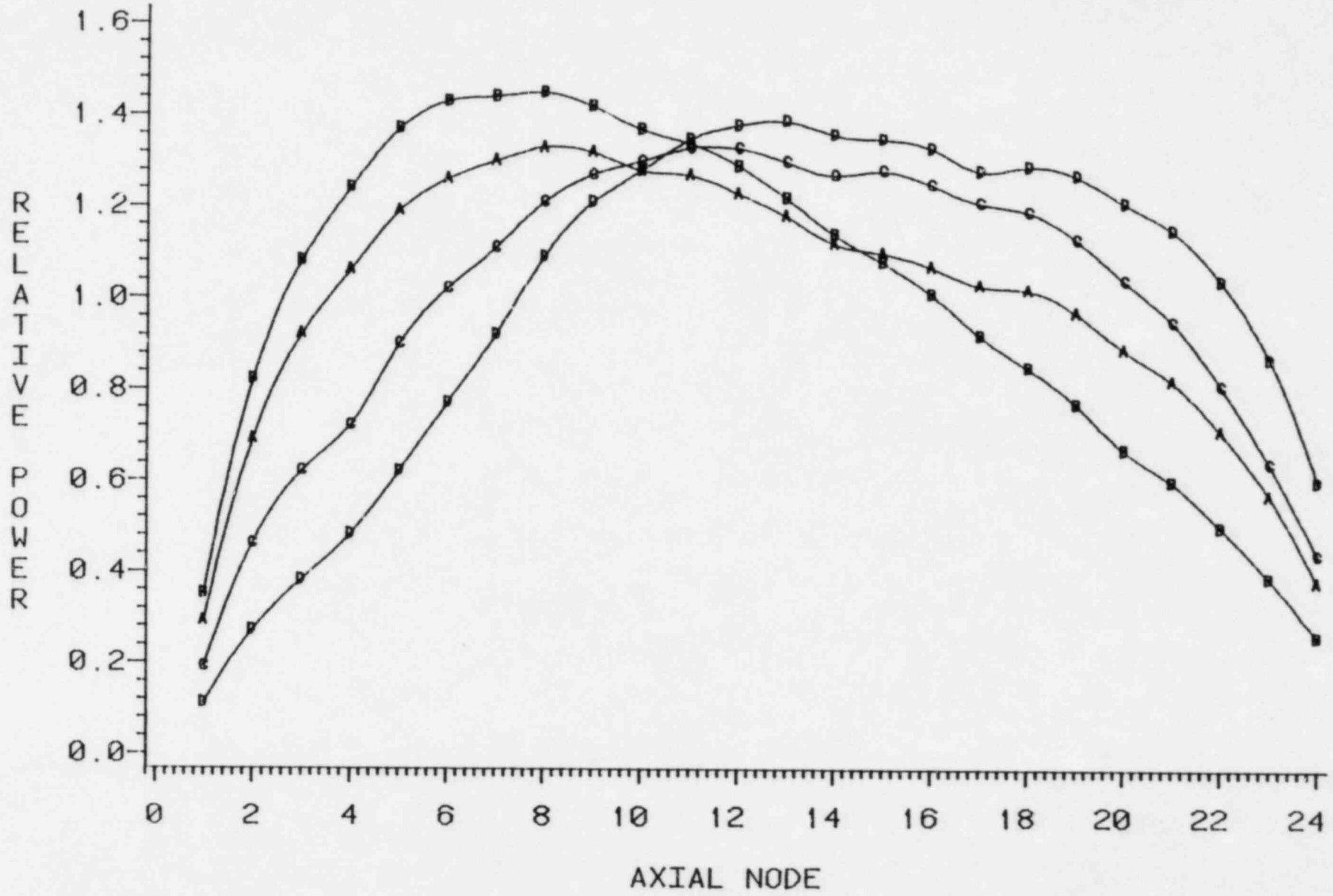
BRUNSWICK 2 CYCLE 4 XENON TRANSIENT
PRESTO PREDICTED AXIAL POWER SHAPES AT VARIOUS TIMES
A(T=0.97 HR) B(T=1.63 HR) C(T=3.15 HR) D(T=5.13 HR)
RELATIVE POWER
1.6
1.4
1.2
1.0
0.8
0.6
0.4
0.2
0.0
0
2
4
6
8
10
12
14
16
18
20
22
24
AXIAL NODE

FIGURE 5.8.3

BRUNSWICK 2 CYCLE 4
XENON TRANSIENT
PRESTO PREDICTED AND PLANT MEASURED LPRMS

PLANT LPRMS TIME = 0.00 HR

		04	*12*	*20*	*28*	*36*	*44*
45	D		23	29	30	26	19
	C		38	43	51	40	34
	B		49	57	67	56	47
	A		53	68	63	60	37
37	D	21	28	45	43	45	26
	C	36	47	60	57	56	45
	B	50	56	60	0	65	67
	A	35	49	62	53	54	47
29	D	27	30	37	38	31	30
	C	41	50	50	42	44	54
	B	58	0	60	46	53	65
	A	0	40	0	33	54	56
21	D	22	30	40	41	36	26
	C	45	50	54	43	59	50
	B	58	65	62	45	66	64
	A	54	51	0	48	60	58
13	D		27	35	38	31	24
	C		45	45	49	48	49
	B		61	52	59	55	75
	A		54	57	65	60	60
05	D			0	26	16	
	C			41	45	0	
	B			57	59	41	
	A			64	0	40	
		04	*12*	*20*	*28*	*36*	*44*

PRESTO LPRMS TIME = 0.00 HR

		04	*12*	*20*	*28*	*36*	*44*
45	D		23	29	30	26	19
	C		38	43	51	40	34
	B		49	57	67	56	47
	A		53	68	63	60	37
37	D	21	28	45	43	45	26
	C	36	47	60	57	56	45
	B	50	56	60	0	65	67
	A	35	49	62	53	54	47
29	D	27	30	37	38	31	30
	C	41	50	50	42	44	54
	B	58	0	60	46	53	65
	A	0	40	0	33	54	57
21	D	22	30	40	41	36	26
	C	45	50	54	43	59	50
	B	58	65	62	45	66	64
	A	54	51	0	48	61	59
13	D		27	35	38	31	24
	C		45	45	49	48	49
	B		61	52	59	55	75
	A		54	57	65	60	60
05	D			0	26	16	
	C			41	45	0	
	B			57	59	41	
	A			64	0	40	
		04	*12*	*20*	*28*	*36*	*44*

Figure 5.8.4

BRUNSWICK 2 CYCLE 4
XENON TRANSIENT
PRESTO PREDICTED AND PLANT MEASURED LPRMS

PLANT LPRMS TIME = 0.97 HR

		04	*12*	*20*	*28*	*36*	*44*
45	D		19	24	25	21	16
	C		31	35	40	32	27
	B		39	45	52	44	38
	A		44	55	52	49	31
37	D	17	23	37	35	36	21
	C	29	38	48	45	45	36
	B	40	45	48	0	51	53
	A	29	40	51	43	44	39
29	D	22	24	30	31	25	24
	C	32	40	40	33	35	43
	B	46	0	47	37	41	51
	A	0	33	0	28	44	46
21	D	17	25	32	34	29	21
	C	35	40	44	35	46	39
	B	45	52	49	36	51	50
	A	44	42	0	40	49	47
13	D		22	29	32	26	19
	C		35	36	39	38	40
	B		48	41	47	44	60
	A		44	47	54	49	49
05	D			0	21	12	
	C			32	36	0	
	B			45	47	33	
	A			53	0	33	
		04	*12*	*20*	*28*	*36*	*44*

PRESTO LPRMS TIME = 0.97 HR

		04	*12*	*20*	*28*	*36*	*44*
45	D		18	23	24	21	15
	C		30	34	40	32	26
	B		38	45	53	44	37
	A		45	58	53	51	31
37	D	16	22	36	34	36	21
	C	28	37	47	45	44	36
	B	40	44	47	0	51	53
	A	29	41	52	44	45	39
29	D	21	24	29	30	25	24
	C	32	40	39	33	35	43
	B	46	0	47	37	42	51
	A	0	34	0	27	46	47
21	D	17	24	32	33	29	21
	C	35	40	43	34	47	40
	B	45	51	49	36	52	50
	A	45	43	0	40	51	49
13	D		21	28	30	25	19
	C		36	35	39	38	39
	B		48	41	46	43	59
	A		46	48	55	51	50
05	D			0	21	13	
	C			32	35	0	
	B			45	47	32	
	A			54	0	33	
		04	*12*	*20*	*28*	*36*	*44*

Figure 5.8.5

BRUNSWICK 2 CYCLE 4
XENON TRANSIENT
PRESTO PREDICTED AND PLANT MEASURED LPRMS

PLANT LPRMS TIME = 1.12 HR

		04	*12*	*20*	*28*	*36*	*44*
45	D		17	22	22	19	14
	C		28	31	36	29	25
	B		35	40	47	40	34
	A		40	50	47	45	28
37	D	15	21	33	32	33	19
	C	26	34	43	40	40	32
	B	36	40	43	0	46	48
	A	26	37	46	39	40	35
29	D	21	22	27	28	23	21
	C	28	35	35	30	31	38
	B	41	0	42	33	37	45
	A	0	30	0	25	40	41
21	D	15	23	29	31	26	19
	C	31	36	39	31	42	35
	B	40	46	44	32	46	44
	A	40	38	0	36	45	43
13	D		20	26	29	23	17
	C		32	32	35	34	36
	B		43	36	42	39	54
	A		40	42	49	45	44
05	D			0	19	11	
	C			29	32	0	
	B			40	42	30	
	A			48	0	30	
		04	*12*	*20*	*28*	*36*	*44*

PRESTO LPRMS TIME = 1.12 HR

		04	*12*	*20*	*28*	*36*	*44*
45	D		16	21	22	19	13
	C		27	31	36	28	24
	B		34	40	47	39	33
	A		41	53	49	46	28
37	D	15	20	32	31	32	19
	C	25	34	42	40	40	32
	B	36	39	43	0	46	47
	A	26	38	47	40	41	36
29	D	19	22	27	27	22	21
	C	29	36	36	30	31	38
	B	41	0	42	33	37	46
	A	0	30	0	25	41	43
21	D	16	22	29	30	26	19
	C	32	36	38	30	42	36
	B	41	46	44	32	46	45
	A	41	39	0	36	46	45
13	D		19	25	27	22	17
	C		32	32	35	34	35
	B		43	37	42	39	53
	A		42	44	50	46	46
05	D			0	19	11	
	C			29	32	0	
	B			40	42	29	
	A			49	0	30	
		04	*12*	*20*	*28*	*36*	*44*

Figure 5.8.6

BRUNSWICK 2 CYCLE 4
XENON TRANSIENT
PRESTO PREDICTED AND PLANT MEASURED LPRMS

PLANT LPRMS TIME = 1.63 HR

		04	*12*	*20*	*28*	*36*	*44*
45	D		11	12	12	11	10
	C		21	23	26	22	19
	B		30	35	40	34	29
	A		35	44	41	39	24
37	D	11	13	15	14	16	14
	C	21	26	31	28	30	26
	B	31	35	36	0	40	42
	A	23	32	40	34	35	31
29	D	17	16	16	15	15	16
	C	23	29	27	23	25	31
	B	36	0	37	28	32	39
	A	0	26	0	23	35	36
21	D	12	18	16	15	16	14
	C	26	29	30	23	32	28
	B	34	40	38	28	40	39
	A	35	33	0	31	39	37
13	D		12	12	12	12	12
	C		25	23	25	25	30
	B		37	32	36	34	48
	A		35	37	43	39	38
05	D			0	12	6	
	C			22	24	0	
	B			35	36	25	
	A			42	0	26	
		04	*12*	*20*	*28*	*36*	*44*

PRESTO LPRMS TIME = 1.63 HR

		04	*12*	*20*	*28*	*36*	*44*
45	D		10	11	11	10	9
	C		21	22	26	21	19
	B		29	34	40	33	28
	A		37	48	44	42	26
37	D	11	13	14	12	16	13
	C	21	26	30	28	30	26
	B	30	34	36	0	39	40
	A	24	34	43	37	38	33
29	D	15	15	15	13	14	16
	C	24	29	27	22	24	32
	B	35	0	36	28	32	39
	A	0	28	0	23	38	39
21	D	12	15	15	13	16	14
	C	26	28	28	22	32	29
	B	35	39	37	27	40	38
	A	38	36	0	34	42	41
13	D		12	11	11	11	12
	C		25	22	24	25	27
	B		37	31	35	33	45
	A		38	40	45	42	42
05	D			0	11	7	
	C			21	23	0	
	B			34	35	25	
	A			45	0	28	
		04	*12*	*20*	*28*	*36*	*44*

Figure 5.8.7

BRUNSWICK 2 CYCLE 4
XENON TRANSIENT
PRESTO PREDICTED AND PLANT MEASURED LPRMS

PLANT LPRMS TIME = 2.27 HR

		04	*12*	*20*	*28*	*36*	*44*
45	D		12	14	13	12	11
	C		18	23	26	21	15
	B		21	32	37	29	17
	A		20	34	32	27	10
37	D	14	18	18	16	20	18
	C	19	24	32	30	30	22
	B	21	23	29	0	29	27
	A	11	17	23	21	18	16
29	D	22	20	23	20	21	20
	C	22	30	33	26	29	32
	B	27	0	24	20	21	33
	A	0	11	0	11	10	17
21	D	15	21	21	19	22	18
	C	23	30	33	25	36	28
	B	24	31	26	22	26	31
	A	14	16	0	16	15	18
13	D		16	13	14	14	16
	C		20	23	25	24	24
	B		24	28	33	27	29
	A		21	26	31	25	19
05	D			0	12	6	
	C			22	24	0	
	B			31	34	22	
	A			33	0	19	
		04	*12*	*20*	*28*	*36*	*44*

PRESTO LPRMS TIME = 2.27 HR

		04	*12*	*20*	*28*	*36*	*44*
45	D		11	12	12	11	10
	C		17	22	26	19	14
	B		20	30	36	27	16
	A		19	35	33	28	10
37	D	14	16	17	14	20	17
	C	18	23	31	29	28	22
	B	21	23	29	0	29	27
	A	11	18	24	23	20	16
29	D	19	19	21	18	19	20
	C	21	29	31	25	28	30
	B	26	0	25	21	22	33
	A	0	12	0	9	12	18
21	D	16	18	20	17	20	17
	C	23	28	31	24	34	27
	B	26	30	27	22	29	30
	A	15	17	0	17	17	19
13	D		14	12	12	12	15
	C		20	22	24	23	21
	B		24	27	32	26	27
	A		21	27	32	26	20
05	D			0	11	7	
	C			21	23	0	
	B			30	32	21	
	A			33	0	19	
		04	*12*	*20*	*28*	*36*	*44*

5-104
Figure 5.8.8

BRUNSWICK 2 CYCLE 4
XENON TRANSIENT
PRESTO PREDICTED AND PLANT MEASURED LPRMS

PLANT LPRMS TIME = 3.15 HR

		04	*12*	*20*	*28*	*36*	*44*
45	D		12	14	14	13	11
	C		18	20	20	20	15
	B		19	27	26	26	15
	A		16	27	25	22	8
37	D	12	17	18	17	20	17
	C	19	23	31	29	29	21
	B	20	22	26	0	27	25
	A	9	14	18	16	15	13
29	D	18	19	23	20	21	18
	C	21	30	33	26	29	31
	B	25	0	22	19	19	32
	A	0	9	0	9	8	14
21	D	12	20	21	19	22	17
	C	22	29	33	25	35	28
	B	23	29	24	21	24	30
	A	11	13	0	12	12	15
13	D		16	13	14	14	15
	C		20	21	23	23	24
	B		22	24	27	24	27
	A		17	21	24	20	16
05	D			0	13	7	
	C			19	17	0	
	B			25	21	18	
	A			26	0	15	
		04	*12*	*20*	*28*	*36*	*44*

PRESTO LPRMS TIME = 3.15 HR

		04	*12*	*20*	*28*	*36*	*44*
45	D		11	12	12	11	10
	C		16	18	19	18	14
	B		19	25	26	24	15
	A		15	28	26	22	8
37	D	12	16	17	14	20	16
	C	17	22	29	27	27	21
	B	19	21	27	0	27	25
	A	9	15	20	18	16	13
29	D	14	18	20	17	19	18
	C	20	28	31	24	27	29
	B	25	0	23	19	21	31
	A	0	10	0	8	10	15
21	D	12	17	19	16	20	15
	C	22	27	31	23	34	26
	B	24	28	25	20	27	29
	A	12	14	0	14	13	16
13	D		14	12	12	12	14
	C		19	20	20	21	21
	B		22	23	26	23	25
	A		17	22	25	21	16
05	D			0	12	7	
	C			17	16	0	
	B			24	21	17	
	A			26	0	15	
		04	*12*	*20*	*28*	*36*	*44*

BRUNSWICK 2 CYCLE 4
XENON TRANSIENT
PRESTO PREDICTED AND PLANT MEASURED LPRMS

PLANT LPRMS TIME = 5.13 HR

		04	*12*	*20*	*28*	*36*	*44*
45	D		17	17	15	18	14
	C		23	23	23	24	21
	B		19	24	25	23	19
	A		9	11	12	9	7
37	D	14	21	26	25	29	19
	C	17	32	38	35	42	25
	B	15	24	30	0	31	26
	A	5	11	14	13	11	11
29	D	18	21	32	34	24	17
	C	18	30	33	31	31	26
	B	19	0	28	22	28	27
	A	0	8	0	9	8	11
21	D	13	22	31	33	26	17
	C	20	32	36	30	41	26
	B	18	34	29	24	34	28
	A	7	11	0	11	10	11
13	D		20	19	20	21	18
	C		31	28	28	36	30
	B		24	25	28	26	31
	A		11	11	15	12	14
05	D			0	14	10	
	C			19	19	0	
	B			17	17	12	
	A			8	0	5	
		04	*12*	*20*	*28*	*36*	*44*

PRESTO LPRMS TIME = 5.13 HR

		04	*12*	*20*	*28*	*36*	*44*
45	D		17	15	14	17	14
	C		22	21	22	22	20
	B		19	23	25	23	19
	A		9	12	13	10	7
37	D	15	19	26	23	28	18
	C	16	30	38	34	39	23
	B	15	24	31	0	32	26
	A	6	12	16	15	13	11
29	D	15	20	30	32	23	18
	C	18	28	32	29	28	25
	B	20	0	30	23	29	27
	A	0	9	0	8	10	12
21	D	13	20	29	30	25	16
	C	20	29	34	29	38	24
	B	20	32	31	24	36	27
	A	8	12	0	13	12	13
13	D		19	18	18	19	18
	C		29	26	25	32	27
	B		25	25	28	26	27
	A		12	13	17	13	14
05	D			0	12	10	
	C			18	18	0	
	B			19	18	13	
	A			9	0	5	
		04	*12*	*20*	*28*	*36*	*44*

Figure 5.8.10

5.9 Simulation of a Brunswick 1 Loss of Feedwater Heater Startup Test

A loss of feedwater heater transient was performed as part of the Brunswick 1 startup and operations testing program. The feedwater temperature reduction was a result of a partial bypass of normal feedwater heater extraction steam. Approximately 95 percent of the 63°F reduction in feedwater temperature occurred within two minutes. Table 5.9.1 shows the heat balance data obtained from the plant process computer (OD-3) just before the transient and at the approximate peak power condition. Figure 5.9.1 shows the distribution of measured LPRM (Local Power Range Monitor) readings at initial and peak power conditions.

This transient was modeled with PRESTO-B by simulating the conditions before and after the test as a xenon transient. Seventeen hours prior to the test, the plant was operating at 97 percent power and 91 percent flow. The plant operators reduced power and moved rods over this time period in order to establish initial conditions according to the test procedure. The PRESTO-B predicted eigenvalue at the initiation of the test (after 17 hours of xenon transient) was 0.99300. This value is only about 0.003 lower than the K_{eff} resulting from core follow calculations at the same point in Cycle 1.

The actual loss of feedwater heater transient was simulated by entering the OD-3 heat balance data at the initial and peak conditions. The PRESTO-B critical power search option was then employed to establish a power level which would yield the initial eigenvalue of 0.99300. This simulation resulted in a calculated ratio of peak to initial power of 1.092 versus a measured ratio of 1.098.

The LPRM distribution was simulated by PRESTO-B in the same manner as was indicated in Section 5.8. The measured LPRM distribution was input to PRESTO-B at the test initial conditions. From this, PRESTO-B generated calibration constants to be applied to the later projection. The PRESTO-B LPRM projections at the transient peak have relevance in that they show the predicted extent of the power increase and effects of redistribution caused by this cold water event. Figure 5.9.2 shows the PRESTO-B predicted LPRM distribution along with the difference between calculated and measured LPRMs at the peak power condition.

The re-distribution of axial power during this transient provides significant negative reactivity which assists in limiting the peak power rise. This effect is not routinely modeled when the loss of feedwater heater transient is analyzed with point kinetics methods. The use of PRESTO-B in three dimensions has reduced the change in core power by greater than 20 percent as compared with a point kinetics analysis.

The overall results of this simulation are considered to be excellent. The PRESTO-B slight underprediction of the core power increase is well within the heat balance measurement uncertainty. This simulation shows the ability of PRESTO-B to predict the composite effects of void collapse, power re-distribution, and Doppler feedback caused by a change in core inlet enthalpy.

Table 5.9.1

Brunswick 1 Loss of Feedwater
Heat Startup Test
Heat Balance Data

Item	Units	Initial	Peak
Time	HR	16:51	16:57
Power	MWTH	1774.	1948.
Core Flow	MLB/HR	76.18	76.85
	KG/SEC	9596.	9681.
Steam Dome Pressure	PSIA	990.7	992.2
	MPA	6.831	6.841
Feedwater Temperature	DEG-F	392.0	329.0
	DEG-C	200.0	165.0
Core Inlet Subcooling	BTU/LBM	17.4	23.9
	KJ/Kg	40.4	55.7
Core Plate Pressure Drop	PSI	17.11	17.46
	MPA	0.118	0.120

BRUNSWICK 1 CYCLE 1
LOSS OF FEEDWATER HEAT
STARTUP TEST
LPRM SUMMARY

MEASURED LPRMS BEFORE TRANSIENT

		04	*12*	*20*	*28*	*36*	*44*
45	D		20	27	29	24	0
	C		33	40	43	37	23
	B		37	44	47	0	27
	A		43	56	60	44	30
37	D	18	25	35	36	30	24
	C	27	37	40	41	34	37
	B	32	39	38	38	37	42
	A	38	44	38	38	40	52
29	D	23	36	30	28	37	27
	C	40	40	39	39	40	38
	B	45	39	37	0	0	47
	A	0	47	34	33	38	61
21	D	22	32	32	29	37	27
	C	35	40	39	32	37	0
	B	41	42	37	45	37	45
	A	43	47	35	34	38	57
13	D		23	32	36	25	0
	C		0	38	41	36	31
	B		38	39	41	38	36
	A		44	51	49	43	43
05	D			22	23	17	
	C			36	36	28	
	B			42	43	33	
	A			52	54	39	
		04	*12*	*20*	*28*	*36*	*44*

MEASURED LPRMS AT PEAK POWER

		04	*12*	*20*	*28*	*36*	*44*
45	D		21	28	30	25	0
	C		35	42	45	39	25
	B		42	48	51	0	31
	A		50	65	69	51	34
37	D	19	26	37	38	32	25
	C	28	39	42	43	36	39
	B	36	43	43	43	42	47
	A	44	51	44	44	47	60
29	D	24	37	31	29	38	28
	C	42	41	41	41	43	39
	B	50	44	42	0	0	51
	A	0	54	39	38	44	71
21	D	23	34	33	30	38	29
	C	37	42	42	37	40	0
	B	46	47	42	48	41	49
	A	50	55	41	40	44	66
13	D		24	34	38	26	0
	C		0	40	43	37	34
	B		43	43	45	43	41
	A		51	58	57	49	50
05	D			23	24	18	
	C			38	38	30	
	B			46	47	37	
	A			60	63	45	
		04	*12*	*20*	*28*	*36*	*44*

5-110
Figure 5.9.1

BRUNSWICK 1 CYCLE 1
LOSS OF FEEDWATER HEAT
STARTUP TEST
SUMMARY OF PRESTO-B PREDICTED LPRMS

PRESTO PREDICTED LPRMS AT PEAK POWER

		04	*12*	*20*	*28*	*36*	*44*
45	D		20	[illegible]	29	24	0
	C		34	[illegible]	44	38	24
	B		41	[illegible]	51	0	30
	A		50	[illegible]	69	51	35
37	D	18	26	36	37	31	24
	C	28	39	42	43	36	38
	B	35	43	43	43	41	46
	A	44	51	44	44	46	60
29	D	23	37	31	29	38	27
	C	41	42	42	42	42	39
	B	49	43	42	0	0	51
	A	[illegible]	54	39	38	44	70
21	D	22	33	33	30	38	27
	C	36	42	42	34	39	0
	B	45	47	42	51	42	49
	A	50	54	40	39	44	66
13	D		24	33	37	26	0
	C		0	40	43	38	32
	B		42	43	45	42	40
	A		51	59	56	50	50
05	D			22	23	17	
	C			37	37	29	
	B			46	47	36	
	A			60	62	45	
		04	*12*	*20*	*28*	*36*	*44*

DIFFERENCE BETWEEN CALCULATED AND MEASURED LPRMS

		04	*12*	*20*	*28*	*36*	*44*
45	D		-1	-1	-1	-1	0
	C		-1	-1	-1	-1	-1
	B		-1	0	0	0	-1
	A		0	0	0	0	+1
37	D	-1	0	-1	-1	-1	-1
	C	0	0	0	0	0	-1
	B	-1	0	0	0	-1	-1
	A	0	0	0	0	-1	0
29	D	-1	0	0	0	0	-1
	C	-1	+1	+1	+1	-1	0
	B	-1	-1	0	0	0	0
	A	0	0	0	0	0	-1
21	D	-1	-1	0	0	0	-2
	C	-1	0	0	-3	-1	0
	B	-1	0	0	+3	-1	0
	A	0	-1	-1	-1	0	0
13	D		0	-1	-1	0	0
	C		0	0	0	+1	-2
	B		-1	0	0	-1	-1
	A		0	+1	-1	+1	0
05	D			-1	-1	-1	
	C			-1	-1	-1	
	B			0	0	-1	
	A			0	-1	0	
		04	*12*	*20*	*28*	*36*	*44*

Figure 5.9.2

6.0 Summary and Conclusions

The system of computer codes presented in Section 1.0 has been extensively benchmarked against data from Brunswick Units 1 and 2 and Quad-Cities Unit 1. The operational data has been supplemented by higher order simulations and separate effects testing.

The following summaries and conclusions relate to the use of CP&L steady-state BWR analysis methods. The uncertainties quoted in this document contain a combination of analysis and measurement uncertainties which are unique to the data base presented in this report.

6.1 Lattice Physics Summary

The lattice code RECORD is used in CP&L's steady-state BWR analysis methods to provide cross sections, peaking factors, delayed neutron parameters, and detector response factors for the nodal simulation in PRESTO. The bulk of our verification effort has consequently gone into qualifying PRESTO results against the operating and experimental data from a number of cycles of different reactors. Although these comparisons provide estimates of the overall accuracy of the RECORD-PRESTO system, additional work has been done to provide independent qualification of RECORD.

Scandpower's comparisons of RECORD - MD1 calculated k-effectives for 55 cold, clean criticals, reported in Section 10.0 of Reference 1, show that RECORD can be expected to give reasonable predictions of reactivity for clean UO_2

lattices; some bias is shown for clean MO_2 lattices. CP&L's comparisons of RECORD and CPM calculated hot, exposure-dependent K-effectives for a range of Gd_2O_3 loadings in typical BWR assemblies (Section 3.1), show relatively small calculational differences, especially at BOL; but some divergence, dependent on void and Gd_2O_3 loading, occurs during depletion. For our design and analysis purposes, reactivity bias and uncertainty will be determined from the PRESTO results (discussed below).

Comparisons of RECORD-calculated fuel isotopes with mass spectrograph measurements of twice-burned pellet samples from CP&L's PWR, and of once-burned pellet samples from Quad-Cities 1, Cycle 2, a BWR, show RECORD consistently underpredicts the production of Pu-240 with exposure. A consequent perturbation is seen in calculations of higher isotopes. This anomaly is explained in part by the fact that only U-238 resonances are temperature broadened in computing resonance integrals. The approximation is acceptable, since the reactivity and reaction rate effect of Pu-240 is relatively small for assemblies that are initially all UO_2.

Comparisons of RECORD-calculated pin-relative fission densities with pin-relative La-140 gamma intensities measured for four assemblies from QC1, Cycle 2, show excellent agreement over a range of assembly types, exposure, and void history. RECORD's predictions of local peaking factors for three UO_2 assemblies averaged only 0.2 percent low, with standard deviation of 1.6 percent. The standard deviation of measured calculated differences for all measured pins (including the MO_2 assembly) averaged only 2.7 percent, and for pins initially bearing Gd_2O_3, 2.8 percent.

These results confirm the conclusions that RECORD-THERMOS adequately calculates the parameters of interest in commercially available fuel assemblies. A bias in treating Pu-240 becomes significant only for high Pu loadings in MO_2 fuel. Predictions of pin fission densities were particularly excellent for initially UO_2 assemblies and form a sound basis for predicting power distributions and peaking factors.

6.2 Core Simulations

6.2.1 Hot Eigenvalue and Rodworth

Qualification of PRESTO's ability to predict hot operating reactivity is derived through comparison with fine-mesh diffusion theory analyses and through the modeling of a large number of actual plant operating statepoints.

The fine-mesh comparisons include modeling of the IAEA standard 3-D benchmark, presented in Reference 2; and comparisons with 2-D PDQ07 calculations, performed at three different axial planes for a reference core condition in Cycle 5 of Brunswick Unit 2. These analyses were presented in Section 5.2.

Comparisons with actual operating conditions make up the majority of the data available for qualification of PRESTO's ability to calculate hot reactivity. Table 5.4.1 summarizes the PRESTO hot comparisons. For 159 data points over seven cycles of three reactors, the combined average hot eigenvalue is 0.99565, with a standard deviation of 0.00199. The hot eigenvalue results are also presented as a function of core average exposure, power density, mass flux, control rod density, coolant density, and inlet subcooling in Figures 5.4.1 through 5.4.6. A reactivity study was performed using vendor-quoted uncertainties in core power, core flow, pressure, and feedwater enthalpy. The resultant heat balance related uncertainty in eigenvalue is 0.00114. The PRESTO comparisons show a standard deviation that is somewhat less than twice the theoretical minimum.

6.2.2 Cold Critical Eigenvalue and Rodworth

The ability of the PRESTO-B model to accurately perform a variety of cold-critical analyses was demonstrated in Sections 5.2 and 5.3. In Section 5.2, PRESTO results for a number of core configurations consistent with in-sequence critical and local critical (i.e., shutdown margin) problems were compared with results from fine mesh 3-D PDQ07 analyses. Tables 5.2.1 and 5.2.2 both show that for either ARI or ARO calculations, there is very little bias between PRESTO and PDQ07 results. In cases where the calculation of cold zero-power rodworths is important, however, PRESTO consistently overpredicts core reactivity, relative to PDQ07, by an average of .00282.

In addition to comparisons with fine mesh PDQ07, PRESTO-B has been benchmarked against a large number of cold critical statepoints for both Brunswick units as well as for Quad-Cities Unit 1. Section 5.3 shows that for reload cores, the mean PRESTO critical eigenvalue for in-sequence criticals is 0.99496, with a standard deviation of 0.00205, which is in good agreement with the results achieved in the hot full-power reactivity calculations. Also, comparisons for Quad-Cities 1, Cycle 1, showed no bias between the local and in-sequence critical eigenvalue, and a standard deviation for the local/in-sequence differences of 0.00146.

Based on the above data, conservative lower bound eigenvalues for cold shutdown margin design evaluations have been determined using one-sided tolerance factors, which will give 95 percent assurance that 95 percent of the cases actually encountered would fall at or above the lower bound eigenvalue

tolerance limit. The design cold shutdown eigenvalue tolerances for reload cores are 0.00477 in the case of in-sequence or distributed criticals, and 0.00639 in the case of local, or shutdown-margin-related criticals; both are to be applied to a mean critical eigenvalue of 0.99496.

6.2.3 Power Distribution

The evaluation of PRESTO's ability to calculate power distributions was based on comparisons with four types of data:

1. Fine mesh, higher order calculations,

2. Measured TIPs from operating reactors,

3. Gamma scan measurements from operating reactors, and

4. Process computer evaluations of MAPLHGR for operating reactors.

The results of these comparisons are summarized in Table 6.2.1.

The Quad Cities' EOC2 gamma scans constitute the most accurate measurement of power distributions included in CP&L's benchmarking. The statistical combination of standard deviations of the PRESTO/gamma scan differences and the measurement uncertainties gives a conservative estimate of the 1σ uncertainty in PRESTO power predictions. Figure 6.2.1 illustrates this

process, and the estimates between "reactor power" and "PRESTO power" represent the uncertainty to be attached to PRESTO power when plant measurement uncertainties are not to be accounted for.

The standard deviations of differences in PRESTO calculated and plant-measured TIPs is representative of the uncertainty in PRESTO power when measurement uncertainties are included. The relationship is also shown in Figure 6.2.1. Combining the nodal 1σ for PRESTO power inferred from gamma-scan comparisons with GE's estimated LPRM-measured TIPs uncertainty gives the expected 1σ in TIPs comparisons. The result, 8.1 percent, agrees well with 8.9 percent actually observed for the combined Quad Cities and BSEP comparisons.

The following table is a composite of estimates derived for the 1σ uncertainties in PRESTO power predictions:

	Measurement Uncertainty Included	Measurement Uncertainty Removed
Nodal Power	8.9%	4.5%
Assembly Power	5.1%	3.2%
Peak Nodal Power	4.4%	3.5%

Use of these uncertainties must be consistent with the intended use of a given calculation. For example, measurement uncertainties must be retained in calculations for operations support or process monitoring since results are compared to measurements. For analyses whose results are compared to a limit which includes the plant measurement uncertainties, only the calculational uncertainty is used. Similarly, in perturbation studies to determine changes in power, only the calculational uncertainty needs to be included.

Table 6.2.1

SUMMARY POWER DISTRIBUTION COMPARISONS

Std. Dev. (per cent) of Calculated/Reference Differences

Comparison	Performed By	Nodal Power	Assembly Power	Peak Power	Measurement Std. Dev.
Higher Order Calculations					
IAEA 2-D Benchmark	ScP	1.0	1.0		
IAEA 3-D Benchmark	ScP	4.8	1.2		
4-Bundle (Flux Option 1)	ScP	1.6	1.6		
4-Bundle (Flux Option 2)	ScP	1.2	1.2		
PDQ07 Quarter-Core	CP&L	3.9	3.9		
TIPs					
BSEP 1 and 2	CP&L	8.65	4.85	4.4	6.7 *
QC 1	CP&L	9.3	5.3		11.2 **
Assembly Gamma Scans					
Hatch 1	ScP	6.4	2.5		1.7
QC 1 EOC 1	CP&L			3.07	2.5
QC 1 EOC 2	CP&L	3.77	2.52	1.49	2.5
MAPLHGR					
BSEP 1 and 2	CP&L	6.1			6.3
Pin Gamma Scans					
QC 1 EOC2	CP&L	2.6		2.8	1.3

* NEDO-20340 GE's estimate for reload cores

** Std. Dev. of differences between symmetric locations

Figure 6.3.1

Basis For Estimating PRESTO Power Distribution Uncertainties

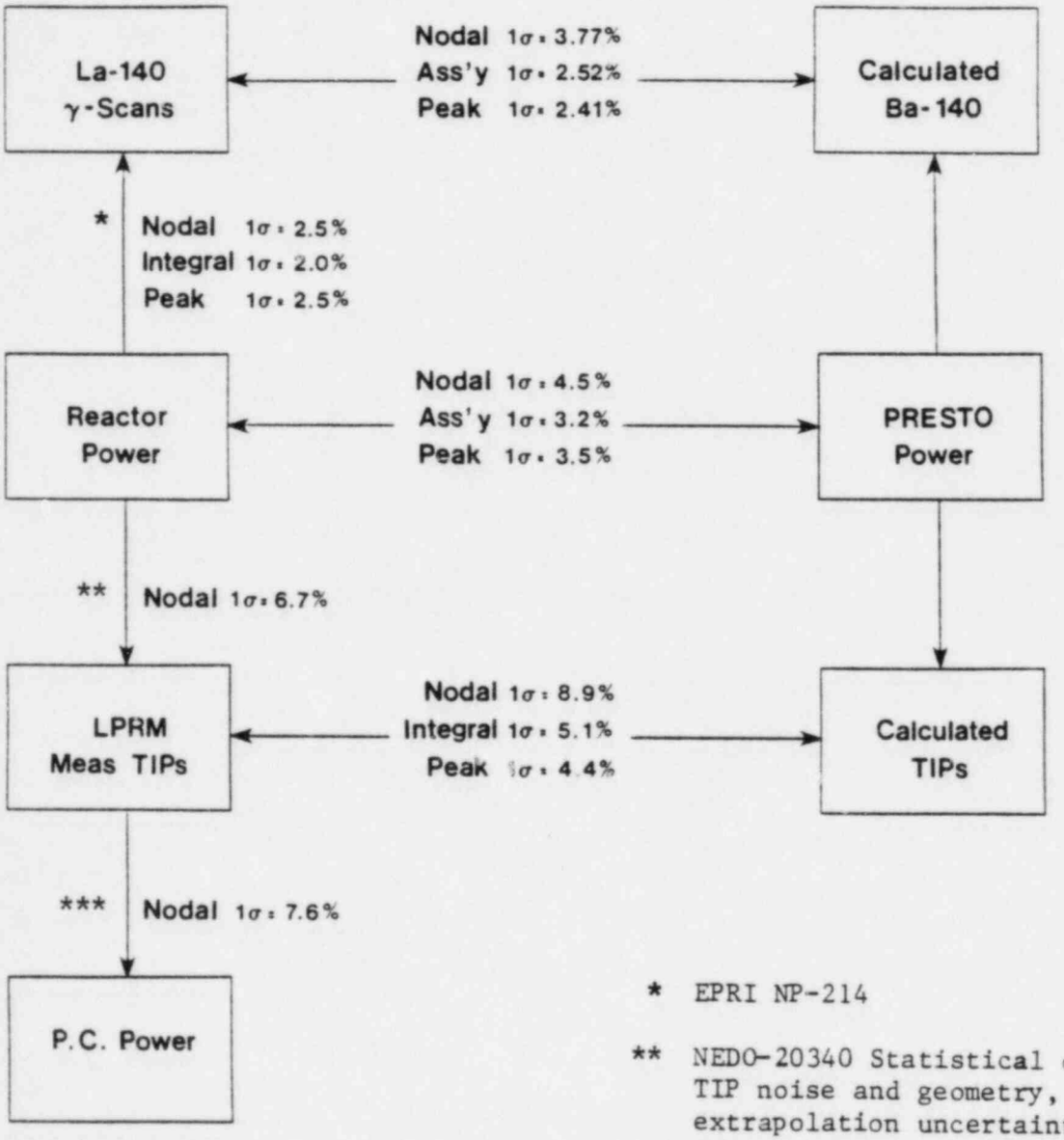

* EPRI NP-214

** NEDO-20340 Statistical combination of TIP noise and geometry, and LPRM extrapolation uncertainties for reloads

*** NEDO-20340 Statistical combination of P.C. power, diffusion theory, void and exposure uncertainties for reloads

6.2.4 LPRM Predictions

The Local Power Range Monitors (LPRM) System provides continuous information proportional to the local power distribution within the core of a BWR. The LPRM's provide safety-related information to the reactor protection system through the Average Power Range Monitor (APRM) System and the Rod Block Monitor (RBM) System. In Sections 5.8 and 5.9, PRESTO-B projections of LPRM's have been compared with several plant measurements. The range of simulations include large changes in control rod pattern, power, flow, inlet sub-cooling, and xenon.

These results show that PRESTO-B can be used to accurately predict LPRM's, APRM's, and RBM instrumentation. A typical application would be the analysis of the continuous rod withdrawal transient in the power range.

6.2.5 Hydraulic Modeling

Section 5.7 presents comparisons of PRESTO-B and process computer predicted pressure drop and bundle flows. The average ratio of PRESTO-B to process computer pressure drop was 1.002, with a standard deviation of 0.035. The average RMS difference between PRESTO and process computer flows was three percent of rated flows. These are considered to be excellent comparisons to vendor calculations.

The PRESTO-B void model was compared with FRIGG Loop data. The correlation used by CP&L shows an average bias and standard deviation of -1.13 percent and 2.21 percent voids, respectively, as compared with 31 measured distributions.

These previous results support the conclusion that the PRESTO-B hydraulic model provides an accurate simulation of the reactor's hydraulic environment.

6.2.6 Integral Simulations

Probably the most useful application of a nodal simulation system is to provide pre-predictions of the complete reactor environment for operations guidance and licensing. PRESTO-B has been tested against 159 hot operating conditions for the Brunswick Units and Quad-Cities Cycles 1 and 2. These cases cover a wide range of power/flow conditions (rated conditions to less than 50 percent power/50 percent flow). PRESTO-B has been extensively tested for warm zero power and cold conditions. These results show that PRESTO-B is capable of providing high-quality simulations of the Brunswick reactor cores.

Capability was also demonstrated for PRESTO-B simulation of various transient conditions in which the core is expected to establish a new stable power level. In particular, evidence was presented to show that PRESTO-B can be used to predict the core response to the Loss of Feedwater Heater (LFWH) and continuous control Rod Withdrawal Error (RWE) transients.

7.0 References

(1) H. K. Naess and T. Skardhamar, "Methods of RECORD: An LWR Fuel Assembly Burnup Code," Scandpower Inc., Topical Report, December 1982. CP&L File NF-1583.02.

(2) S. Borresen, L. Moberg, and J. Rasmussen, "Methods of PRESTO-B, A Three-Dimensional, BWR Core Simulation Code," Scandpower Inc., Topical Report, December 1982. CP&L File NF-1583.03.

(3) EPRI, "FIBWR: A Steady-State Core Flow Distribution Code for Boiling Water Reactors, Code Verification and Qualification Report," EPRI-NP-1923, July 1981.

(4) M. A. Pope, "Verification of CP&L Reference BWR Thermal-Hydraulic Methods Using the FIBWR Computer Code," Carolina Power & Light Company, February 1983. CP&L File NF-1583.04.

(5) A. Ahlin, M. Edenius, "The Collision Probability Module CPM," Chapter 6, Part II, of ARMP System Documentation, CCM-3, EPRI, September 1977.

(6) A. A. Bauer, et. al., "Progress on Evaluating Strength and Ductility of Irradiated Zircaloy," BMI-1938, Battelle Columbus Laboratories, September 1975 (Prepared for NRC Under Contract W-7405-eng-92).

(7) EPRI, "Burnup and Transuranium Element Composition in Irradiated UO_2, UO_2-Gd_2O_3, and UO_2-PUO_2, Rods From the Quad-Cities 1 Reactor," EPRI-NP-2307-LD, March 1982.

(8) EPRI, "Gamma Scan Measurements at Quad-Cities Nuclear Power Station Unit 1 Following Cycle 2," EPRI NP-214, July 1976.

(9) EPRI, "Light Water Reactor Fuel Rod Modeling Code Evaluation," EPRI-NP-369, March 1977.

(10) R. K. Haling, "Operating Strategy for Maintaining an Optimum Power Distribution Through Life," ANS Topical Meeting, TID 7672, 1963.

(11) D. M. Ver Plank, "Methods for the Analysis of Boiling Water Reactors Steady-State Core Physics," Yankee Atomic Electric Company, YAEC-1238, March 1981.

(12) T. D. Beu, et. al., "Verification of TVA Steady-State BWR Physics Methods," Tennessee Valley Authority, TVA-TR79-01A, January 1979.

(13) G. R. Parkos, "BWR Simulator Methods Verification," General Electric, NEDO-20946, May 1976.

(14) EPRI, "Core Design and Operating Data for Cycles 1 and 2 of Quad-Cities 1," EPRI-NP-240, November 1976.

(15) H. E. Bliss, letter to K. E. Karcher, Commonwealth Edison, NFS:BPS:82-047, May 1982.

(16) D. M. Ver Plank, letter to K. E. Karcher, Yankee Atomic Electric Company, April 1982.

(17) J. F. Carew, "Process Computer Performance Evaluation Accuracy," General Electric, NEDO-20340, June 1974.

(18) W. K. Bertram, et. al., "A Fission Product Group Cross Section Library," AAEC/E214 (1971).

(19) R. J. J. Stamm'ler, "K-7 THERMOS, Neutron Thermalization in a Heterogeneous Cylindrically Symmetric Reactor Cell," Kjeller Report KR-47 (1963).

(20) S. Borresen, letter to K. E. Karcher, Scandpower A/S, T15/6.15.01, January 1983.

(21) S. Borresen, "A Simplified, Coarse Mesh, Three-Dimensional Diffusion Scheme for Calculating the Gross Power Distribution in a Boiling Water Reactor," NUCL Sci. & Eng., 1971, page 37.